UNIVERSITÀ DI SIENA 1240

Dipartimento di Biotecnologie, Chimica e Farmacia

Dottorato in Scienze Chimiche e Farmaceutiche

XXXIII Ciclo

Coordinatore: Prof. Maurizio Taddei

Design and development of new organic molecules as alternative fluorophores for LSC application

Settore scientifico disciplinare: Fotovoltaico

Candidato/a
Costanza Papucci
Università di Siena - CNR-ICCOM Firenze

Tutore
Maurizio Taddei
Università di Siena
Dipartimento di Biotecnologie, Chimica e Farmacia

Anno accademico 2020-2021

SOMMARIO

Abstract

Presently, Luminescent Solar Concentrators (LSCs) are considered promising alternative optical devices for the sunlight harvest and production of energy. A LSC is composed by a thin transparent polymer slab, doped with a fluorophore able to absorb solar radiation and concentrate it, at a specific wavelength, at the edges of the slab, where a thin PV cell can capture and use to produce electricity. Due to the low-priced materials and their innovative aesthetic properties, LSCs find an easy integration in architectural systems, such as roofs, windows, canopies and greenhouse. The heart of LSC device remains fluorophore, which needs to follow several optoelectronic properties: broad absorption range, long-wavelength emission maximum, large Stokes shift, high fluorescence quantum yield, low-priced materials and production, good optical efficiency and good dispersion in the host materials. The organic molecules are more versatile class of luminophores, which can largely satisfy LSC requirements, due to their close relationship between molecular design and optoelectronic tunability.

During this Ph.D., keeping in mind all these targets, a careful and specific molecular design supported by computational analysis have been accomplished. Three classes of new organic fluorophores characterized by D-A-D structure have been planned and executed. The synthetic optimization and the employment of sustainable procedures have been carried out when possible, favoring cross-coupling reactions and more eco-friendly approaches. All organic chromophores have spectroscopically characterized in solution and polymer dispersion, designing a common prototype of LSC device for all chromophores. Alternative matrices have been tested to evaluate their impact on optoelectronic properties of the various fluorophores.

LSC performances of each chromophore have been assessed and compared with those of literature reference Lumogen F Red 305 (**LR305**).

Riassunto

Oggigiorno, i Concentratori Solari Luminescenti (LSCs) sono considerati degli alternativi e promettenti dispositivi fotovoltaici. Un LSC è costituito da una sottile lastra polimerica trasparente, drogata con un fluoroforo, ad una specifica concentrazione, in grado di assorbire la radiazione solare e concentrarla, ad una specifica lunghezza d'onda, sui bordi della lastra. Qui, uno strato sottile di cella fotovoltaica a base, generalmente di silicio, cattura la radiazione emessa e la impiega per produrre energia elettrica. Grazie all'utilizzo di materiali a basso costo e alle loro proprietà estetiche innovative, gli LSC possono essere impiegati come dispositivi integrabili in sistemi architettonici quali tetti, finestre, serre, pensiline o barriere stradali.

Il fulcro di un dispositivo LSC è il fluoroforo. Questo deve rispondere a specifiche caratteristiche sia chimiche che ottiche, quali ampio intervallo di assorbimento e di emissione di fluorescenza, ampio Stokes shift, elevate rese quantiche di fluorescenza, un processo di produzione a basso costo e una buona dispersione e compatibilità con la matrice polimerica. In questo contesto, le molecole organiche risultano essere una delle classi di cromofori più versatili, in quanto possono soddisfare questi requisiti, grazie alla possibilità di modificarne le proprietà tramite un opportuno design molecolare.

Durante questo progetto di dottorato, sono stati realizzati vari specifici design molecolari, tramite uno studio preliminare basato su analisi computazionali. Sono state progettate e preparate tre differenti classi di nuovi cromofori organici caratterizzati da una struttura D-A-D. L'ottimizzazione sintetica e l'impiego di procedure sostenibili sono state utilizzate quando possibile, favorendo reazioni di accoppiamento C-C (cross coupling) e approcci più eco-compatibili. Tutti i composti organici sono stati caratterizzati spettroscopicamente in soluzione e in matrici polimeriche, attraverso la caratterizzazione di un tipico prototipo di dispositivo LSC (5x5 cm^2), per ogni fluoroforo.

Sono inoltre state testate matrici alternative, valutandone l'impatto che avevano sulle proprietà optoelettroniche dei vari cromofori. Le prestazioni dei singoli composti organici sono state valutate e confrontate con quelle di riferimento in letteratura, Lumogen F Red 305 (**LR305**).

CHAPTER 1:

INTRODUCTION

1 THE ENERGY ISSUE

Each generation is called to face new challenges and opportunities. However, in a closed system like Earth, some opportunities discovered and developed by a generation could imply important challenges for the followed ones.

An important challenge for the 20th century generation was to satisfy energy demand in the world.
In this scenario, population growth plays a crucial role as it strongly impacts on socio-economic processes, spatial distribution and policy implications.
In the last sixty years, the growth of the world's population was increased from 2.5 billion of people in 1950 to 7 billion in 2015, with a global population growth of 1.24% per year, in the last ten years. The estimations of the world's population developments, show a slight increase in people more than one billion in the next ten years, reaching 8.3 billion in 2030 and 9.8 billion in 2050[1].
The increase in the global population rate and the higher life expectancy leads to a huge increase in energy demand. Energy is embedded in all types of goods and is at the base of any kind of service, required by people's needs. All basic human necessities, such as food and water supply, environment requirements, urbanization, health, are strictly dependent on energy availability[2].
On the other side, while energy demand increases with economical and social requirements, energy distribution affects several aspects of life worldwide, such as disparities among states, generated by the unfair distribution of energy sources, with consequent enhances inequities (about half of the primary energy supply is consumed by the 10% of the population, living in wealthy countries, while the poorest 25% of mankind consumes less than 3%)[3] .
The energy demand is closely correlated to the availability of natural capital. The amount of natural reserves, produced by Earth (oxygen, water, etc.), determines human's quality of life and economy.
In a sustainable and close system, like our planet, the consumption of natural capital over one year should not overcome the produced one in the same timescale.
Unfortunately, this is not the case. Since 1976, resources produced by Earth in the whole year have been consumed in less time than one year. It's possible to calculate the day within the year when one annual natural capital was consumed. Such day is called Overshooting Day.

---

[1] United Nations, Department of Economic and Social Affairs, Population Division (2017). World Population Prospects: The 2017 Revision, Key Findings and Advance Tables. Working Paper No. ESA/P/WP/248.
[2] N. Armaroli, V. Balzani, *Angew. Chem. Int. Ed.*, **2007**, *46*, 52-66.
[3] N. Armaroli, V. Balzani, *Chem. Sus. Chem*. **2011**, *4*, 21–36.

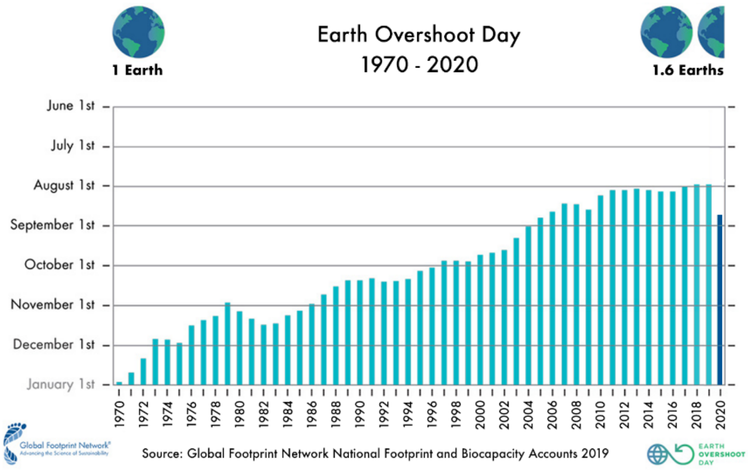

Fig. 1: *The Overshooting Day trend from 1970 to 2020*[4]*.*

For 2020, the Overshooting Day was the 22nd of August; that means that in 2020, the human being consumes 1.6 Earth (Fig.1).

Even if part of the natural capital can be regenerated by direct or indirect action of sunlight on the biosphere, the Earth's regenerative capacity has not been sufficient to balance the depletion of the natural capital, accumulated over the past year. In 1961, the humanity requirements covered 70% of the capital; in the '80s was 100% and in 1999 was 120%[5]. That means we are now living at the edge of our planet's possibilities. In the last 50 years, other than consuming all annual production of the natural capital, the resources that Earth has stored during the last centuries have already been depleted. Furthermore, some resources such as metals and fossil fuels cannot be regenerated according to the human timescale.

The main energy source of the 20th century was fossil fuels. Nowadays, they represent 80% of the global energy supply. However, their progressive exploitation had left mankind with a loss of energy resources and harmful effects to the Earth's atmosphere such as pollution, global warming and increasing of the greenhouse effect. Furthermore, their costs increased depending on social, political and economical choices of countries, indirectly contributing to disparities and inequities in human society[6].
For example, the top three oil consumers in the world of 2016 were United States (20%), China (13%) and India (3%); among them, only United States was the major oil producer. Those three countries together consumed more than the third of the world's consumptions.
The Energy Information Administration (EIA) estimated the world oil consumption, in 2016, 96.92 million barrels per day: 60% of this consumption was due to the first ten consumers of oil, which not corresponded to the ten world producers (Fig. 2).

---

[4] https://www.overshootday.org/
[5] Mathis Wackernagel, Niels B Schulz, Diana Deumling, Alejandro Callejas Linares, Martin Jenkins, Valerie Kapos, Chad Monfreda, Jonathan Loh, Norman Myers, Richard Norgaard, Jørgen Randers, *Proc. Natl. Acad. Sci. USA*, **2002**, *99*, 9266-71.
[6] N. Armaroli, V. Balzani, *Chem. Sus. Chem*. **2011**, *4*, 21–36.

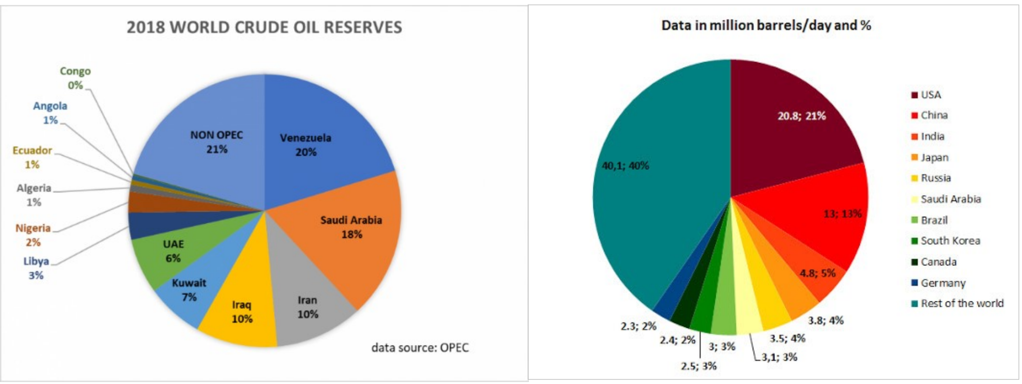

Fig 2: *World oil reserves (on the left) and world oil consumers (on the right) relative to 2018*[7].

In 2019, World's demand amounted to 1.1 million oil barrels per day, 3987 Bcm of natural gas and 5437 Mtce of coal[8].

However, there are alternative energy sources that can become successful when they will reach competitive prices compared with fossil fuels: the real challenge of the 21st century is to face an energy transition by the exploitation of renewable alternative resources.
Renewable energies (REs) such as biomass, hydropower, wind, bio-heat and solar energy are the alternative, since they are inexhaustible (in terms of human timescale) and their environmental impact is lower than that, due to fossil sources. Currently, the contribution of REs to the global energy demand is 26.5%, where the hydropower provides 16.4%[9]. On the other hand, the energy demand will rise by 37% in 2040 and the electricity consumption in the world will increase by 80%[10] (for forecasts for 2050, see figure 3).

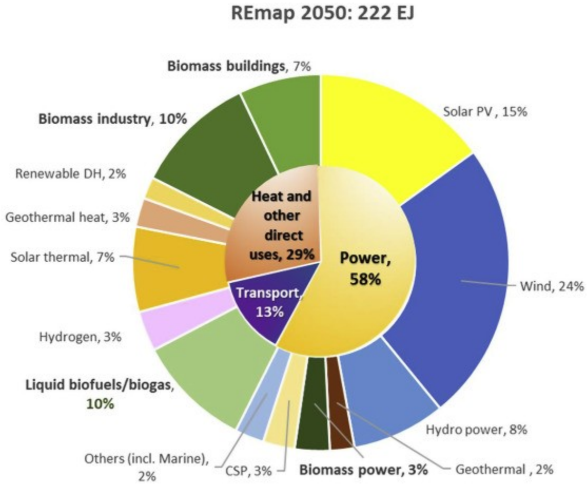

Fig. 3: *Forecasts of REs employment in 2050, in total final energy consumption terms*[11].

---

[7] a) https://oilprice.com/Energy/Crude-Oil/How-Much-Crude-Oil-Has-The-World-Really-Consumed.html; b) World Oil and Gas Review **2019**

[8] https://IEA.org/reports.

[9] Hydropower Status Report, International hydropower association (**2018**), 5th ed2018.

[10] MS Javed, T Ma, J Jurasz, MY Amin, *Renewable Energy*, **2020**, *148*, 176-192.

[11] Dolf Gielen, Francisco Boshell, Deger Saygin, Morgan D.Bazilian, Nicholas Wagner, Ricardo Gorini, *Energy Strategy Reviews*, **2019**, 24, 38–50.

Hydropower, solar and wind are the most abundant REs and the technologies for their exploitation are the most developed and economically viable.

Hydropower covered around 70% of such sources[12], providing reliable energy generation and opportunities for economic development[13] . However, the scale and type of hydropower projects, as well as the social, economic and environmental impacts of its plants,[14] can be a limitation for future employment as it may disrupt natural flowing water and harm ecosystem balance[15].

The second and third renewable sources employed for energy production are wind and solar power, in particular for electrical energy supply.

Wind power supply covered 4% of global electricity production in 2016. In 2018, the global installed wind capacity was 591 GW for total installed wind power; in 2019, this value increased by 1.17% in one year, reaching 651 GW[16]. It is expected that in 2050, the wind power supply will be strongly increased[17].

Solar energy reaches Earth in different forms, two of them are light and heat which can be employed in heating processes and production of electricity. The availability of solar energy is inexhaustible for the human timescale. Solar photovoltaic (PV) is the state of the art in active solar electricity generation. PV share in global electricity generation was almost 3% in 2019, with 720 TWh produced and is estimated to increase from 720 TWh in 2019 to almost 3300 TWh in 2030[18]. The PV capacity factor increased from 20% in 2010 to 24% in 2019[19].

Despite from 2015 to now the installed capacity of wind power has been higher than PV, it is expected that PV installed capacity will soon overtake the wind one[20]. Indeed, the PV market increased to around 115 GW installed solar power in 2019, compared to 100 GW in 2018, with an improvement of 1.15% in only one year (Fig. 4).

---

[12] International Energy Agency, Tracking clean energy progress, (**2017**), https://www.iea.org/publications/freepublications/publication/TrackingCleanEnergyProgress2017.pdf.

[13] ShouYi Li, XingBo Zhou, YuJie Wang, JianPing Zhou, XiaoHu Du, ZuYu Che, *Sci. China Technol. Sci.,***2015**, 58, 1263-71.

[14] International Energy AgencyTechnology roadmap: hydropower, (**2012**), https://www.iea.org/publications/freepublications/publication/2012_Hydropower_Roadmap.pdf.

[15] Maria Snoussi, Johnson Kitheka, Yohanna Shaghude, Alioune Kane, Russell, Arthurton, Martin Le Tissier, Hassan Virji, *Environ. Manag.,* **2007,** *39*, 587-600.

[16] REN21, Renewable 2019 Global Status Report 2019, **2019**.

[17] IRENA (**2019**), Future of wind: Deployment, investment, technology, grid integration and socio-economic aspects (A Global Energy Transformation paper), International Renewable Energy Agency, Abu Dhabi.

[18] International Energy Agency (IEA), https://www.iea.org/reports/solar-pv.

[19] Energy Information Administration (EIA), https://www.eia.gov/electricity/monthly.

[20] REN21, Renewables 2018 Global Status Report. 2018, **2018**.

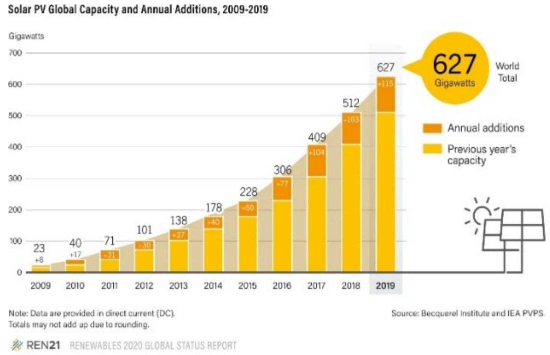

Solar PV Global Capacity and Annual Additions, 2009-2019

Note: Data are provided in direct current (DC).
Totals may not add up due to rounding.

Source: Becquerel Institute and IEA PVPS.

REN21 RENEWABLES 2020 GLOBAL STATUS REPORT

Solar PV Global Capacity, by Country and Region, 2009-2019

Note: Data are provided in direct current (DC).

REN21 RENEWABLES 2020 GLOBAL STATUS REPORT

Fig.4: *Solar PV Global Capacity and Annual Additions 2009-2019 (on the left) and solar PV Global Capacity by countries 2009-2019 (on the right)*[16].

In 2019, in most countries, the support schemes to PV, adequate regulatory frameworks and political choices on-grid connections have been necessary to make competitive large-scale systems. At the same time, competition drove declining prices and opening new markets; the pressure of lower prices and expectations of rising global demand encouraged the entry of new companies into the sector and the ongoing pursuit of innovation[21].

1.1 THE ENERGY OF SUN

An inexhaustible source of energy comes from the Sun. Comparing to the other renewable sources, solar energy is far larger, being estimated at ~ 15.2×10^5 TWh[22], namely 3.8×10^{23} kW of energy every hour, and 170,000 TW of tat strike Earth every moment.

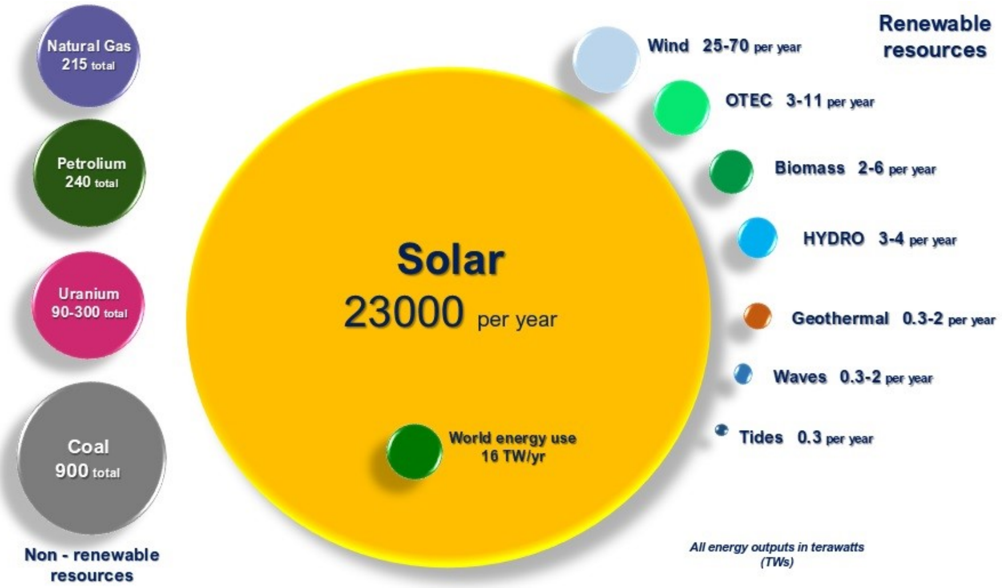

Fig. 5: *Solar energy from Sun and the world energy distribution of all resources.*

The huge amount of energy from the Sun could widely cover the power demand of the world, every hour, Earth's surface receives 1.08×10^{14} kW, more energy than that demanded by

---

[21] REN21, Renewables 2019 Global Status Report. 2019, **2019**.

[22] R. Perez, M. Perez, **n.d.**, DOI 10.1016/j.eneco.2008.12.011.

humans in a year (about 16 TW per year) (Fig. 5). If 0.1% of this energy would be converted at an efficiency of 10%, it would produce four times the world's generating capacity of 3000 GW[23].

1.2 PHOTOVOLTAICS: FROM SUN TO ELECTRICITY

Sunlight can be employed for the production of electricity, through the harvesting of solar radiation. The conversion of sunlight into electricity can be achieved indirectly, using concentrated solar power (CSP), or directly, through photovoltaics (PVs).
The first one is based on the concentration of sunlight to solar towers, thanks to the employment of collectors. Light concentrated can be involved to produce high-temperature fluids, which generate electricity through a large-scale turbines system. CSP is a cheap method for electricity production; however, its economic operation conditions are strictly dependent on the wide sunbelt extended between the 35th northern and 35th southern latitude[24]. Thus, the major part of wealthy countries are ruled out and its market diffusion is not supported by them. The most promising devices, which harness solar power appear to be the photovoltaic devices (PV). In this case, sunlight is directly transformed into electricity.
The story of PV devices begins in 1839 when the French physicist A.-E. Becquerel, while he was working on metal electrodes in an electrolyte solution, noticed small electrical current production as a result of their light exposure. In 1940, R. Shoemarker Ohl, investigating some silicon samples with some cracks, noticed a current flow through that material after light exposition that was the first p-n junction. Thirty years later, in 1954, a group of scientists, working on silicon with some impurities of gallium, produced the first silicon solar cell[25]. This solar cell showed 6% of the efficiency of conversion of sunlight to electricity. However, the first device was expensive and was unsuccessful. From that day, the interest in silicon-based solar cells grow up leading to the drop in costs and the improvement of new technologies and advanced materials that have made possible to reach around 29% of efficiency[26]: the photovoltaic industry was born.

To produce electricity, a PV cell requires three basic conditions:

- the capability of absorbing light, with the generation of electron-hole pairs;
- the separation of charge of opposite types;
- the extraction of charge and carry to an external circuit.

Due to these requirements, three classes of PV were developed and employed in the last decades for the production of electricity, named as PV generations[27].

---

[23] M. Thirugnanasambandam, S.Iniyan, R. Goic, *Renewable and Sustainable Energy Reviews*, **2010**, *14*, 312–322.
[24] Fundamental Study of Cross Linear Concentration System and Solar Power System in Tokyo Tech, **2017**.
[25] APS News, **2009**, *18*,4.
[26] Andrew Blakers, Ngwe Zin, Keith R. McIntosh, Kean Fong, *Energy Procedia*, **2013**, 33, 1 – 10.
[27] American Journal of Optics and Photonics, 2015, *3*(*5*), 94-113.

1.2.1 First generation: Silicon solar cell

Silicon solar cells have remained the dominant commercial material for solar energy devices in the last twenty years. Their efficiencies turn around 22-23% for monocrystalline silicon solar cells to 18-19% for polycrystalline one, with a consistent lifetime of 30 years[28] (Fig. 6).

Fig. 6: *Silicon-based PV module of first-generation: monocrystalline module (on left) and polycrystalline panels (on right)*[29].

Mono and polycrystalline cells are based on silicon wafers. The first ones are formed on silicon crystal in a homogenous structure, with a thickness of 0.3 mm; the second is based on many small silicon grains. These wafers of 200-300 µm of thickness are obtained from doping Silicon with 0.1% atom of group III (B or Al for positive junction, p-type junction), as acceptor element, or of group V (P or As for negative junction, n-type junction), as donor one.

Usually, silicon wafers are p-type doped; therefore, a doped n-type surface is employed on the front side of the wafers. That generates a p-n junction system. When light impacts the p-n junction, photons with equal or higher energy than semiconductor one involves the excitation of an electron from the valence band to the conduction one. Charge separation is generated and a hole, formed from the excitation of electrons, move on the valence band.

The condition to create a photovoltaic phenomenon is to separate these pairs of charges, before their recombination. To avoid the recombination process, an internal electric field is required. A strong electric field exists in p-n junction due to spatial cargo. Due to the generation of electron-hole pairs, the negative charges (electrons) move from p-type to n-type conductor and the positive ones (holes) from n-type conductor to p-type, until reaching electrostatic balance. Thus, a depletion region between p-type and n-type conductor is generated, producing an internal electric field (*built-in* electric field) (Fig. 7)[30]. In this balance, if a charged particle is placed in the depletion region, it will move from one side to the other, under a *built-in* electric field.

---

[28] B. O'Regan, M. Grätzel, *Nature*, **1991**, *353*, 737–740.

[29] Adapted image from: 1) https://www.futurasun.com/dt_gallery/monocristallino-5bb/; 2) http://www.neofos.it/lavorazioni/pannelli-solari-fotovoltaici/.

[30] a) R. F. Pierret (**1996**), *Semiconductor Device Fundamentals*; b) R. H. Bishop (**2002**), *The Mechatronics Handbook.*

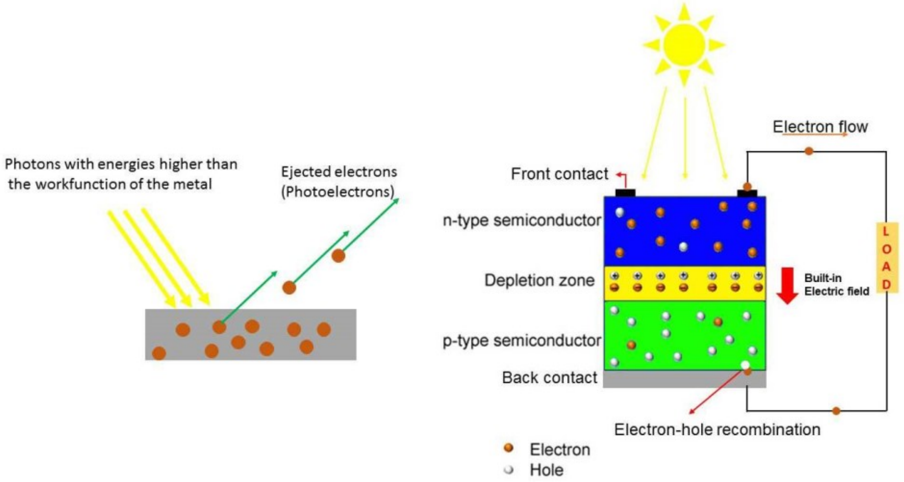

Fig. 7: *Schematic representation of photoelectric effect (left) and Si-based PV cell mechanism (right)*[31].

In a PV cell, the excitation induced by sunlight absorption of n-type semiconductor can generate an electron-hole pair, which moves in p-n junction and is separated due to *built-in* electric field. Hence, a DC electric current is registered in the external circuit.

Crystalline silicon has been a success from laboratory to commercial availability and makes up 90% of the global PV market[32]. At the moment, such devices remain the principal choice for PV. Due to the abundance and non-toxicity of Silicon, the high and stable efficiency, the improvement in manufacturing and production infrastructures.. However, large-scale production is still labeled by the high costs of materials and installation.

1.2.2 Second generation: Thin-film solar cell

The high costs of large-scale silicon-based solar cells -induced the investigation of other cheaper materials or technologies for energy production.

In the late 1970s, the first thin-film cells appeared on the market: a small strip of amorphous silicon was tested powering solar calculators.

A thin-film system consists of a slab of glass covered with a thin layer of photoactive material; three main materials are used: amorphous silicon (a-Si), cadmium telluride (CdTe) and copper indium gallium selenide (CIGS)[33] (Fig. 8).

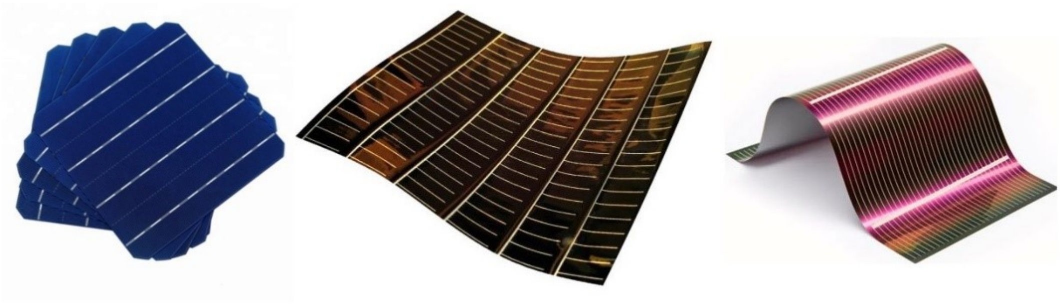

Fig. 8: *Second generation PV prototypes: a-Si(left), CdTe (central) and CIGS (right) films.*

---

[31] https://asdn.net/asdn/energy/solar.

[32] K. L. Chopra, P. D. Paulson, V. Dutta, *Res. Appl.,***2004**, 69-92.

[33] T. D.Lee, A. U. Ebong, *Renewable and Sustainable Energy Reviews*, **2017**, *70*, 1286–97.

The main advantage of this technology is the reduced cost because thanks to the low direct band gaps of the photoactive source it is possible to use a very thin layer (Table 1), requiring less amount of material.

Table 1: *Energetical, physical and chemical features comparison between the three principal photoactive materials in a common PV system of second generation.*

	a-Si	**CdTe**	**CISG**
Band Gap (eV)	1.75	1.44	1.0-1.6
Thickness (μm)	1	3-5	1-2
Toxicity	None	Cd	None

Furthermore, thin-film cells can be incorporated as building-integrated photovoltaics (BIPVs) or everyday electronics (watches, calculators, etc.).

The principal disadvantage is the lower efficiencies recovered, if compared with crystalline silicon cells, both in lab scale (about 12% for a-Si, 20-21% for CdTe and CIGS) and for module (17% for CdTe, 15% for CIGS).[34, 35,36] Moreover, in some cases primary materials are toxic, affecting the chemical disposal, at the end of cells life.

1.2.3 Third generation: A bridge through the PV generation cells

Recently, a novel class of photovoltaics has emerged which employs a multi-junction energy production approach. Single *p-n* junction systems are confined in the Shockley-Queisser limit, which sets a maximum efficiency that cannot be overcome. The semiconductor involved in these devices can absorb only photons with specific energy compared to, or higher than, the energy of their own bandgap. Electrons absorbing photons with higher energy relax to the band edge, thermally releasing the surplus of energy (thermalization loss). Therefore, their limit depends on the semiconductor energy bandgap and can move from 31% to 40%[37].

To overcome the Shockley-Queisser limit, emerging new semiconductors need to be developed.

---

[34] H.S. Ullal, *Proc. 28th IEEE PVSC,* **2000**, 418–423.

[35] H. Ye, H.S. Park, V.A. Akhavan, B.W. Goodfellow, M.G. Panthani, B.A. Korgel, A.J. Bard, *J. Phys. Chem. C,* **2011**, 115, 234–240.

[36] F. Dimroth, M. Grave, P. Beutel, U. Fiedeler, C. Karcher, T.N.D. Tibbits, E. Oliva, G. Siefer, M. Schachtner, A. Wekkeli et al., *Prog. Photovoltaics Res. Appl.* **2014**, *22*, 277–282.

[37] J.J. Wysocki, P. Rappaport, *Cit. J. Appl. Phys* **1961**, *32*, 510.

The third generation of PVs is based on wide innovative harvesting technologies, starting from multi-junction cells. The employment of several layers coated with a wide range of photoactive materials determines a broad extended absorption range, as a consequence of the sum of different components band gaps. In this regard, remarkable results have been obtained for Ga-As-In-based four-junction cells, showing a record of 46% efficiency. However, the high costs of their production limit their applications[38].

A less costly alternative based similarly on the same architectural model of the multiple energy levels systems, is Organic Photovoltaics (OPVs).

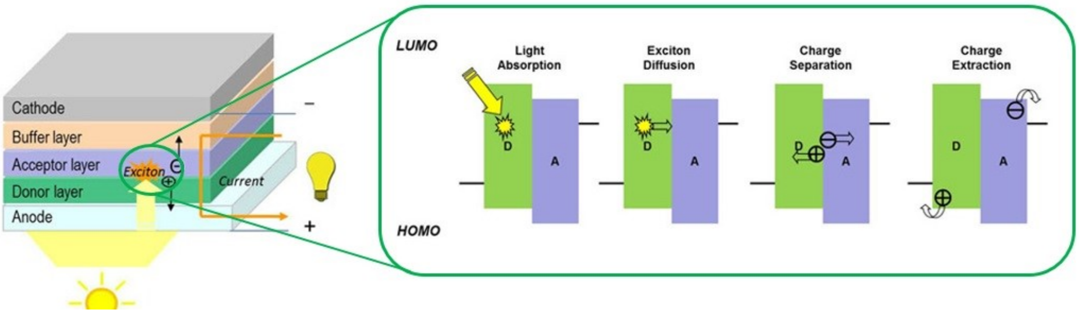

Fig. 9: *OPVs: general structure of a bilayer cell and its mechanism*[39].

Similar to multi *p-n* junctions, OPVs are composed of two or more layers of photoactive organic compounds, sandwiched between two electrodes (see Fig. 9). After sunlight excitation, the donor unit (D) absorbs the solar radiation, promoting an electron from the ground state (HOMO) to the first excited state at lower energy (LUMO). Due to contact of donor D and acceptor A materials and to appropriate energy levels between conduction and valence bands, the excited electron diffuses from the donor material to the acceptor one. On the donor moiety, a hole is formed and charge separation is observed (free holes and electrons). A photocurrent is generated when the holes and the electrons move to the corresponding electrode through donor and acceptor compounds[40].

The simple structure, the low costs of the materials and the simple production are excellent advantages for such devices. However, their performances are strictly bound by a specific design and fabrication of the molecule[41]. Practically, at the moment, the current low efficiency (17% in tandem polymer/NFA[42,43]) and some problems of long term stability circumscribe their diffusion.

In the last two decades, alternative PV cell types have been considered, especially for their new concept approach: dye-sensitizer solar cells (DSSCs) and Perovskite solar cells (PSCs). Both of them are based on different mechanisms to convert solar energy into electricity.

---

[38] F. Dimroth, T.N.D. Tibbits, M. Niemeyer, F. Predan, P. Beutel, C. Karcher, E. Oliva, *IEEE J. Photovoltaics,* **2016**, *6*, 343-349.

[39] Organic photovoltaic (OPV) tutorial, Organic and printed electronics, Sigma Aldrich.

[40] J. Niklas, O.G. Poluektov, *Adv. Energy Mater*., **2017**, *7*, 1602226.

[41] V. Savikhin, M. Babics, M. Neophytou, S. Liu, S.D. Oosterhout, H. Yan, X. Gu, P.M. Beaujuge, M. F. Toney, *Chem. Mater*., **2018**, *30*, 7872–84.

[42] L. Meng, Y. Zhang, X. Wan, C. Li, X. Zhang, Y. Wang, X. Ke, Z. Xiao, L. Ding, R. Xia, H.-L. Yip, Y. Cao, Y. Chen, *Science,* **2018**, *361*, 1094–98.

[43] D. Di Carlo Rasi, R.A.J. Janssen, *Adv. Mater.* **2019**, *31*, DOI 10.1002/adma.201806499.

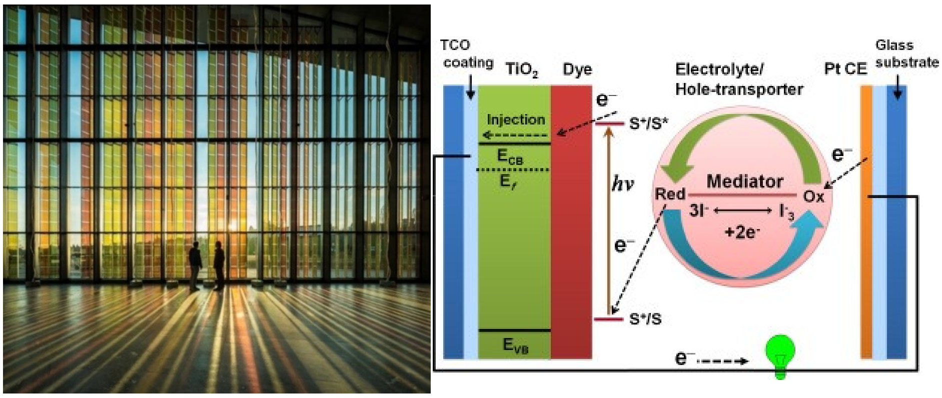

Fig. 10: *Dye-sensitizer solar cell (DSSC), actually employed in PV market*[44] *and its schematic mechanism*[45].

Dye-sensitizer solar cell (DSSC) technology was reported for the first time in 1991 from M. Grätzel and B. O'Regan[46]. The new mechanism, introduced by the two chemists, was based on the imitation of the photosynthetic process (Fig. 10). While in the typical PV cell Si-based the semiconductor acts as photoreceptor and charge transfer, in DSSC system (called also "Grätzel's cell") the semiconductor (e.g. TiO_2) is linked with full organic or hybrid metallic-organic sensitizer, which works such as chlorophyll pigment in a leaf.

The dye absorbs photons at a specific wavelength causing the transfer of electrons from the dye to the semiconductor and from this to the external circuit. The cycle is closed through a redox pair that regenerates the dye and which is in turn regenerated by the electrons coming from the external cycle. The abundance and the moderate or low costs of materials make DSSC technology an interesting alternative; however, the power conversion in electricity reaches, for the moment, only 14% of efficiency at lab-scale and 5-6% for large-scale modules[47].

---

[44] Assessment and exploitation of the inherent value of waste electrical and electronic equipment (WEEE) for circular economy, **2018**, doi: 10.23889/SUthesis.39601.

[45] S. Yun, J.N. Freitas, A.F. Nogueira, Y. Wang, S. Ahmad, Z.-S. Wang, *Progress in Polymer Science*, **2016**, *59*, 1-40.

[46] B. O'Regan, M. Grätzel, *Nature* **1991**, *353*, 737–740.

[47] K. Kakiage, Y. Aoyama, T. Yano, K. Oya, J. Fujisawa, M. Hanaya, *Chem. Commun.,* **2015**, *51*, 15894–97.

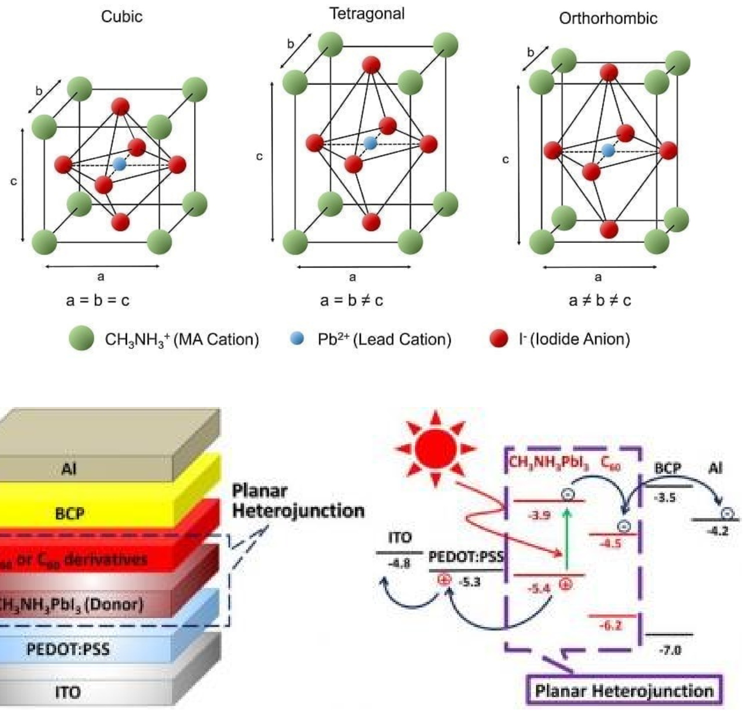

Fig. 11: *A common Perovskite solar cell composition in its possible crysalline conformations (up)*[48] *and the schematic structure and mechanism of a typical PSC*[49].

Perovskite solar cells (PSCs) have received great attention from the research community due to the interesting improvement of their efficiency, from 3.8% to 22.1%, since 2009[50,51].

The first photoactive material used in a PSC was calcium titanate, discovered by G. Rose and named by the mineralogist L. Perovski. Since that, the term "perovskite" was attributed to all compounds which present the same crystal structure as calcium titanate, with a general formula ABX_3, where A is an organic cation (such as ammonium organic salt), B a metal cation (e.g. Pb^{2+}) and X is a halide anion (e.g. I^-) [52] (Fig. 11).

The first structure model was inspired to the DSSC device, where the electrolyte covers both mesoporous TiO_2 particles and the perovskite material takes the place of the dye-sensitizer. Hole-transporting material (HTM) is necessary to transport the hole from the perovskite to the cathode.

The design of PSC, the choice of halide in the perovskite material, the thickness of TiO_2, the structural features of HTM contribute to affect the photovoltaic efficiency of the device.

Perovskite material is cheap, soluble, easy to synthesize and to assemble; however, some drawbacks restrain PSC development and their access to the global market. The high solubility makes the perovskite material sensible to moisture; the crystalline structure could be lost at high temperature, easily reached in a solar panel, for long-time exposure; finally, during the

---

[48] https://www.perovskite-info.com/perovskite-solar.

[49] App. Note, AN_P45 Affiliation: Edimburgh Instruments Ltd., **2018**, Stuart Thomson.

[50] A. Kojima, K. Teshima, Y. Shirai, T. Miyasaka, *J. Am. Chem. Soc.*, **2009**, *131*, 6050–51.

[51] M. Saliba, T. Matsui, J.-Y. Seo, K. Domansk, J.-P. Correa-Baena, M. K. Nazeeruddin, S. M. Zakeeruddin, W. Tress, A. Abate, A. Hagfeldt and M. Grätzel, *Energy Environ. Sci.*, **2016**, *9*, 1989–97.

[52] Z. Shi, A.H. Jayatissa, *Materials*, **2018**, *11*, 729.

production of electricity, from the degradation of perovskite material, PbI_2 is generated, that is a carcinogen substance.

1.3 LUMINESCENT SOLAR CONCENTRATORS

The progress made in PV technology leads the modern module costs near 1-2 Euro/Wp, bringing the electricity costs close to 2 Euro/kWh. This price is still far from the large-scale electricity generation costs for conventional fossil fuels (0.02-0.04 Euro/kWh)[53] and further improvement are needed.

It is well known that the high performances of silicon-based PV modules depend on several geographic and structural parameters. The losses of power for a module can be due to temperature loss (L_{ct}) and capture losses (L_{cm}). Indeed, temperature plays a crucial role in PV performances as the rising of temperature could have a negative effect on the efficiency of the module. Such parameter depends on several conditions such as the weather data, solar source, thermal and physical properties of the module, heat transfer coefficient due to the wind[54]. The capture losses collect all the other loss mechanisms associated with engineering parameters such as the joule effect of the wiring, diodes, shading effect, and with geographic conditions as latitude, low irradiance, snow covering, exposure[55] .

Southern exposure with a specific angle of inclination could maximize PV module performances. The inclination (*Tilt angle*) depends on the angle with which the solar radiation reaches the Earth (Fig.12 and 13).

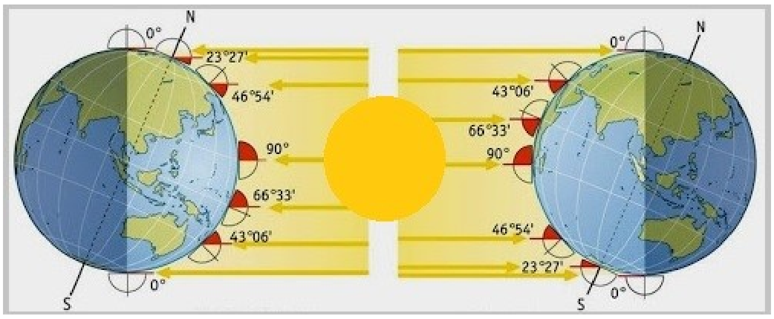

Fig. 12: *Effect of incident solar radiation to the incident angles at different latitude*[56]*.*

---

[53] W. G.J.H.M.van Sark, *Renewable Energy*, **2013**, *49*, 207–210.

[54] E. Skoplaki, J.A.Palyvos, *Renewable Energy*, **2009**, *34*, 23–29.

[55] I. Santiago, D. Trillo-Montero, I.M. Moreno-Garcia V. Pallarés-López, J.J. Luna-Rodríguez, *Renewable and Sustainable Energy Reviews*, **2018**, *90*, 70–89.

[56] Lupia Palmieri Parotto – La Terra, Zanichelli editore, **2009**.

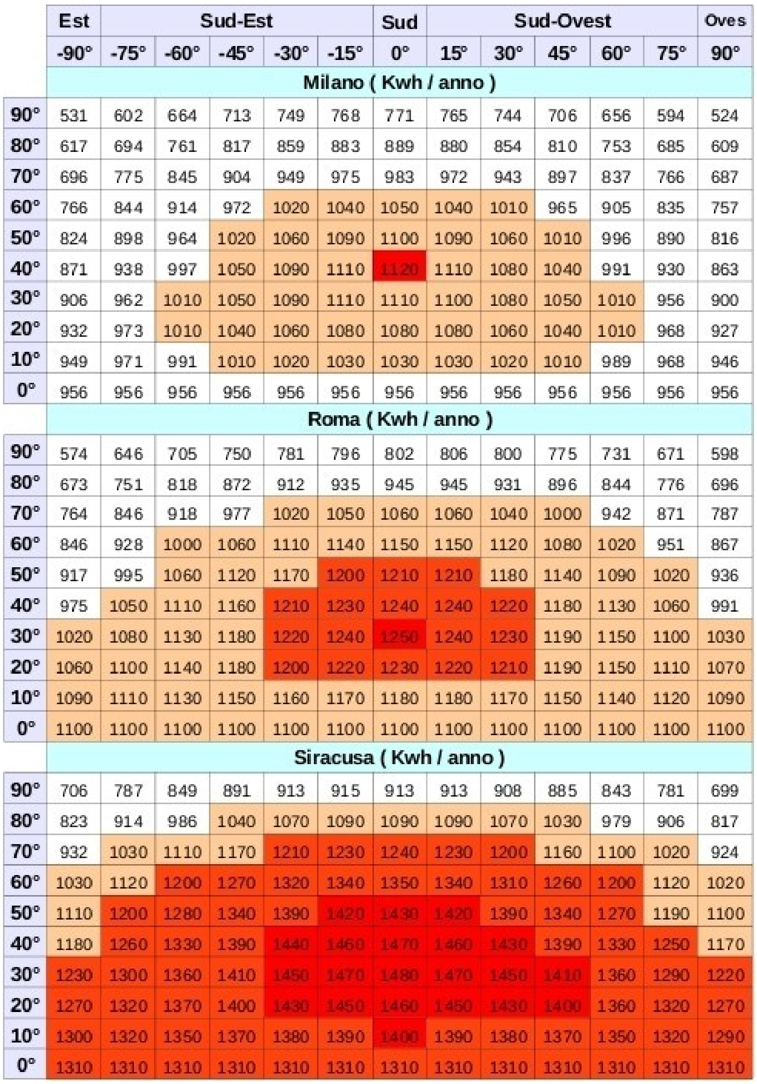

	Est	Sud-Est					Sud	Sud-Ovest					Oves
	-90°	-75°	-60°	-45°	-30°	-15°	0°	15°	30°	45°	60°	75°	90°
	Milano (Kwh / anno)												
90°	531	602	664	713	749	768	771	765	744	706	656	594	524
80°	617	694	761	817	859	883	889	880	854	810	753	685	609
70°	696	775	845	904	949	975	983	972	943	897	837	766	687
60°	766	844	914	972	1020	1040	1050	1040	1010	965	905	835	757
50°	824	898	964	1020	1060	1090	1100	1090	1060	1010	996	890	816
40°	871	938	997	1050	1090	1110	1120	1110	1080	1040	991	930	863
30°	906	962	1010	1050	1090	1110	1110	1100	1080	1050	1010	956	900
20°	932	973	1010	1040	1060	1080	1080	1080	1060	1040	1010	968	927
10°	949	971	991	1010	1020	1030	1030	1030	1020	1010	989	968	946
0°	956	956	956	956	956	956	956	956	956	956	956	956	956
	Roma (Kwh / anno)												
90°	574	646	705	750	781	796	802	806	800	775	731	671	598
80°	673	751	818	872	912	935	945	945	931	896	844	776	696
70°	764	846	918	977	1020	1050	1060	1060	1040	1000	942	871	787
60°	846	928	1000	1060	1110	1140	1150	1150	1120	1080	1020	951	867
50°	917	995	1060	1120	1170	1200	1210	1210	1180	1140	1090	1020	936
40°	975	1050	1110	1160	1210	1230	1240	1240	1220	1180	1130	1060	991
30°	1020	1080	1130	1180	1220	1240	1250	1240	1230	1190	1150	1100	1030
20°	1060	1100	1140	1180	1200	1220	1230	1220	1210	1190	1150	1110	1070
10°	1090	1110	1130	1150	1160	1170	1180	1180	1170	1150	1140	1120	1090
0°	1100	1100	1100	1100	1100	1100	1100	1100	1100	1100	1100	1100	1100
	Siracusa (Kwh / anno)												
90°	706	787	849	891	913	915	913	913	908	885	843	781	699
80°	823	914	986	1040	1070	1090	1090	1090	1070	1030	979	906	817
70°	932	1030	1110	1170	1210	1230	1240	1230	1200	1160	1100	1020	924
60°	1030	1120	1200	1270	1320	1340	1350	1340	1310	1260	1200	1120	1020
50°	1110	1200	1280	1340	1390	1420	1430	1420	1390	1340	1270	1190	1100
40°	1180	1260	1330	1390	1440	1460	1470	1460	1430	1390	1330	1250	1170
30°	1230	1300	1360	1410	1450	1470	1480	1470	1450	1410	1360	1290	1220
20°	1270	1320	1370	1400	1430	1450	1460	1450	1430	1400	1360	1320	1270
10°	1300	1320	1350	1370	1380	1390	1400	1390	1380	1370	1350	1320	1290
0°	1310	1310	1310	1310	1310	1310	1310	1310	1310	1310	1310	1310	1310

Fig. 13: *Power energy production of PV plant in the function of their latitude and "Tilt angle" in some Italian cities*[57].

These conditions restrict the applicability of PV modules in specific locations such as roofs of buildings, farmlands and countryside, canopies or sunshades.

To overcome some of the limitations for large-scale installation of PV technology of first generation, luminescent solar concentrators (LSCs) have been introduced as a promising alternative device.

In its common model, an LSC consists in a thin slab of high refractive index material (glass or polymer), doped with a luminescent optical compound, capable of absorbing solar radiation and concentrating it, through internal reflection mechanisms, at the edges of the slab, downconverting it by fluorescence or phosphorescence. A small area of PV cell, located at the edges of the slab, could absorb the concentrated light and convert it into electricity.

---

[57] https://www.fotovoltaiconorditalia.it/mondo-fotovoltaico.

1.3.1 LSC: historical development

LSC technology was born in the ’70s, when W.H. Weber and J. Lambe[58] described a planar solar collector, utilizing a luminescent medium to concentrate solar energy. As more inventions started observing and simulating nature, Weber and Lambe, working for Ford Scientific Laboratory Group, were inspired by the greenhouse natural process.

Through the total internal reflection process, luminescent material should absorb solar radiation and emit it in a range where its reabsorption would be weak. Neodynium(Nd^{3+})-doped transparent glass appeared an ideal LSC: it showed several strong absorptions in a range of 500-900 nm and high emission of about 1090 nm, well suitable for the absorption of silicon. Its luminescent efficiency was reported to be 50-75%, independent from the incident sunlight. The first organic luminescent material tested was rhodamine-6G (Rh6G), which reported similar results of Nd-doped glass with a Si cell, in a different host matrix (PMMA). The main drawback was the large overlap between absorption and emission spectra of Rh6G, from which a decrease of efficiency was observed. In 1977, B.A. Swart et al.[59], monitoring PMMA slab doped with Rh6G and coumarin 6 (C6), demonstrated the principle of a planar solar concentrator. They also observed a bathochromic effect (which corresponds to a red-shift of the absorption and emission maximum) comparing the polymer slab spectroscopic characteristics with the solution spectroscopic ones.

In 1978, C.F. Rapp and N.L. Baling[60] coined the term “Luminescent Solar Concentrator”, to describe a broad range of luminescent collector. In 1982, A.M. Hermann[61] reported the state of art, the costs and the device features of a modern LSC, in the first review, devoted to it. Some years later, Wittwer reached an efficiency of 4.0%, testing two sheets LSC of 40x40x0.3 cm^3 and connecting one sheet to GaAs and the other to Si cells. The sheets were separated by an air gap. More recently, for the same LSC device, efficiencies of 7.0% and 6.7% were registered for 5x5x0.5 cm^3 of LSC plate, connected *in series* with four solar GaAs and GaInP cells, respectively[62,63].

A LSC device based on a mix of organic dyes, was also realized by Friedman[64] who reported an optical efficiency of the total system of 3.2%. The device was composed by a Si solar cell connected to a thin layer of mixed organic compounds of 14x14x0.3 cm^3. Connecting the same film to a GaAs solar cell, the efficiency increased up to 4.5%.

The research in the LSC field slowed down in the 1980s, due to the energy price drop and the limitations in the availability of new performing luminophores for LSC devices.

The recent increase in energy demand, energy price and the request for alternative energy sources renewed the interest in such technology.

---

[58] W.H. Weber, J. Lambe, *Appl. Optics*, **1976**, *15*, 10, 2299-2300.

[59] B.A. Swartz, T. Cole, A.H. Zewail, *Optics Lett.*, **1977**, *1*, 2, 73-75.

[60] Proc. 13th IEEE Photovoltaic Spec. Conf., p. 690. IEEE, New York (**1978**).

[61] A.M. Hermann, *Solar Energy*, **1982**, *29*, 4, 323-329.

[62] L.H. Slooff, E.E. Bende, A.R. Burgers, T. Budel, M. Pravettoni, R.P. Kenny, E.D. Dunlop, A. Büchtemann, *Phys. status solidi - Rapid Res. Lett.*, **2008**, *2*, 6, 257–259.

[63] J. C. Goldschmidt, M. Peters, A. Bösch, H. Helmers, F. Dimroth, S. W. Glunz, G. Willeke, *Sol. Energy Mater. Sol. Cells*, **2009**, *93*, 2, 176–182.

[64] B. Bollinger, K. Gillingham, *Sol. Energy Res. Inst.*, **1982**, 1987.

1.3.2 Concentrator idea: LSC mechanism

The principle of the mechanism of a typical LSC is illustrated in figure 14.
Solar radiation impacts the surface of LSC; part of the sunlight radiation could be transmitted and part of it could be absorbed by the fluorophore dispersed in the slab. The luminescent specie isotropically emits in a specific wavelength range and, through a series of total internal reflection mechanisms, is guided at the edges of the panel, where a PV cell could absorb it and produce energy[65].

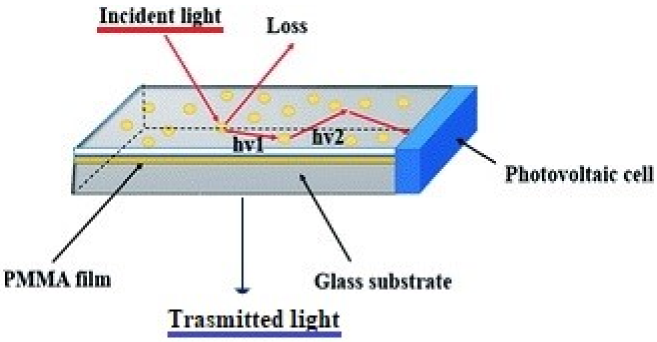

Fig. 14: *LSC general mechanism.*

Total internal reflection is depended on the refractive index of plastic plate, *n*, and controlled by Snell's law. The critical angle $\boldsymbol{\theta_c}$ represents the limited angle for which the emitted light could be totally internal reflected (Fig. 15).

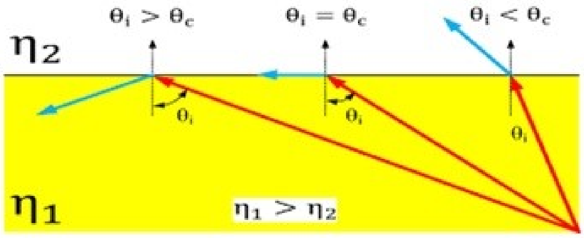

$$\theta_c = \sin^{-1}\left(\frac{1}{\eta}\right)$$

Fig. 15: *Critical angle from Snell's law, in which $\eta_1>\eta_2$ and with $\eta_2=1$ (ari refractive index)*[66].

The choice of the host matrix is fundamental to improve the internal reflection fraction and, consequently, the optical efficiency of the device determining the light entrapping and LSC behavior. For instance a high refractive index could promote the trip of the emitted light to the PV cell, however, can also increase the reflectivity of material, limiting the fraction of light which

---

[65] W. G.J.H.M. van Sark, *Renewable Energy*, **2013**, *49*, 207–210.
[66] M. G. Debije, P. P. C. Verbunt, *Adv. Energy Mater.*, **2012**, *2*, 12.

could cross the surface of the LSC.

Focusing on the academic literature reports about polymeric material used in LSCs, poly(methyl methacrylate) (PMMA) is one of the most common host matrices used.

The Refractive index of PMMA is n=1.5; for this value, the critical angle is 42.2°. Thus, approximately 75% of the all emitted radiation is totally internal reflected[67,68].

1.3.3 Optical efficiency: definition

To determine the optical efficiency some definition are needed. Taking in consideration a typical LSC device as shown in Figure 16, E_1, E_2 and E_3 are the energy of irradiation, the energy that reaches the PV cell, and the energy converted by PV cell respectively; the optical efficiency, η_{opt}, is the efficiency of LSC itself, so without taking in account E_3, the energy converted by the PV cell, η_{opt_e} is obtained by the ratio between the energy contribution of light reaching the solar cell (E_2) and the incident light (E_1) (see Eq.1).

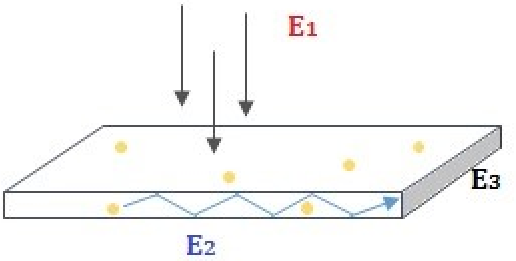

Fig. 16: *Energy contributions for a LSC device.*

In terms of flux of photons, η_{opt_f} is reported as a ratio between the numbers of photons emitted which reaches the PV cell ($Flux_2$) and the number of photons absorbed by the fluorophore ($Flux_1$) (see Eq. 2).

Eq. 1
$$\eta_{opt\_e} = \frac{Energy_2}{Energy_1} 100$$

Eq. 2
$$\eta_{opt\_f} = \frac{Flux_2}{Flux_1} 100$$

Finally, the efficiency of the whole device could be simplified as the ratio between the photocurrent produced by the whole device and the photocurrent produced at the edge of the slab by PV cell, multiplied by a geometric factor (G), which depends on dimensions of LSC and PV cell (Eq. 3).

---

[67] J.S. Batchelder, A.H. Zewail, T. Cole, *Appl. Opt.*, **1981**, *20*, 3733–54.

[68] J.M. Drake, M.L. Lesiecki, J. Sansregret, W.R.L. Thomas, *Appl. Opt.*, **1982**, *21*, 2945–52.

Eq. 3 $$\eta_{opt} = \frac{I_{LSC}}{G \cdot I_{PV}} \quad \text{where} \quad G = \frac{A_{LSC}}{A_{PV}}$$

Commonly, G is about 16.6.
In an ideal LSC device, the optical efficiency would be determined on the trapping efficiency of the waveguide. In a realistic situation, it is influenced by several contributions and it could be described with the followed expression[69]:

Eq. 4 $$\eta_{opt} = (1\text{-}R)\ \eta_{asb}\ \eta_{LQE}\ \eta_{Stokes}\ \eta_{trap}\ \eta_{host}\ (1\text{-}\ \eta_{self})\ \eta_{TIR}$$

where
R = surface reflection coefficient. It is relative to the amount of radiation reflected outside of the panel;
η_{asb} = absorption efficiency. It is the fraction of sunlight absorbed by the fluorophore;
η_{LQE} = quantum efficiency. It is the fraction of emitted radiation of luminophore, which could reach the edges of the panel;
η_{Stokes} = Stokes efficiency. It is the loss of energy caused by auto-absorption and due to the overlap region between absorption and emission spectra;
η_{trap} = efficiency of trapping light. It is the fraction of light lost from the "escape cone", when the critical angle is higher than the limited one, to have total internal refraction;
η_{host} = Matrix efficiency. It is the efficiency contribute to the transmission of light in the host material, depending on the scattering and absorption processes in the matrix;
η_{self} = efficiency of self-absorption by other luminescent specie in the host material (depends on concentration, dispersion in matrix etc.);
η_{TIR} = efficiency of total internal reflection. It is the fraction of radiation, which is reflected inside the thickness of the slab.

Each efficiency contribution is correlated to a series of mechanisms, which can be responsible of loss of power and therefore loss in efficiency (Fig 17).
The mean challenge for LSC technology is that of minimizing the mechanisms of losses of power to maximize the efficiency η_{sys}.

---

[69] W. G.J.H.M. van Sark, *Renewable Energy*, **2013**, *49*, 207–210.

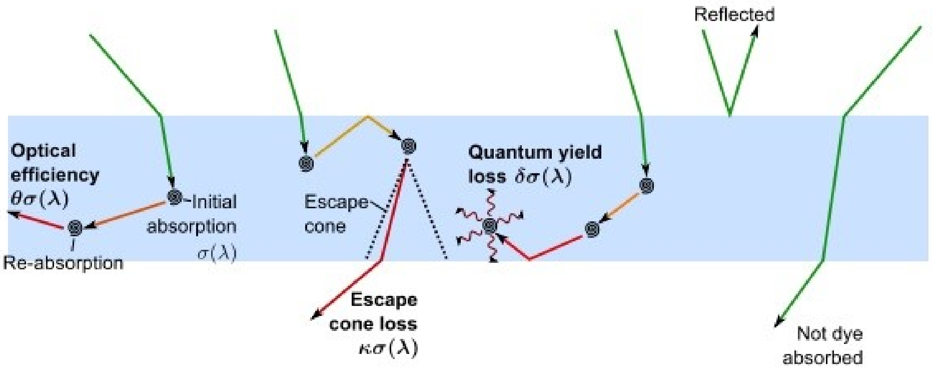

Fig. 17: *Schematic mechanisms of losses of power for a general LSC device*[70].

1.3.3.1 Reflection (R)

A flat surface with a refracting index (*n)* of 1.5 (such as PMMA) reflects 4% of the sunlight radiation[71], which could be considered as a loss. The process is described by Fresnel's law, which is valid only for a homogenous and flat surface *R*, the percentage of reflected light, is defined as a ratio between the reflected intensity (I_r) and the refracted one (I_i).

Another parameter to consider is the polarization of the photons. A photon has a polarized electric field that could be oriented in perpendicular and parallel directions to the surface. The polarization of their electric fields influences the probability of reflection. The Fresnel's law describes that probability, considering both polarization processes.

To reduce the reflection effect, rough surfaces could counter external reflection, thus the downside, rough surfaces are not able to guide photons at the edges and that is not acceptable for the LSC system. On the other hand, a lower refractive index could reduce reflection losses; however, at the same time, reduces also the trapping efficiency.

1.3.3.2 Absorption efficiency (η_{asb})

An LSC requires an active luminescent specie, which could absorb a specific amount of incident light. Different species give a different and peculiar absorption spectrum. The strength of the luminophore absorption depends on its concentration in the host material. The higher is the number of luminescent species in the matrix, the higher will be the probability of a photon to be absorbed. Without absorption, solar radiation is transmitted outside of LSC. This possibility could depend on mismatching of the photon energy with the absorption energy of luminophore, low concentration or short travel length.

According with Lambert-Beer law, absorption is depended on the ratio between the intensity of transmitted light ($\boldsymbol{I_t}$) and incident light ($\boldsymbol{I_0}$) (Fig. 18).

---

[70] C. Tummeltshammer, A. Taylor, A.J. Kenyon, I. Papakonstantinou, *Solar Energy Materials & Solar Cells*, **2016**, *144*, 40–47.

[71] L.A. Rahn, R.E. Palmer, *Appl. Opt.*, **1986**, *25*, 3, 334–6.

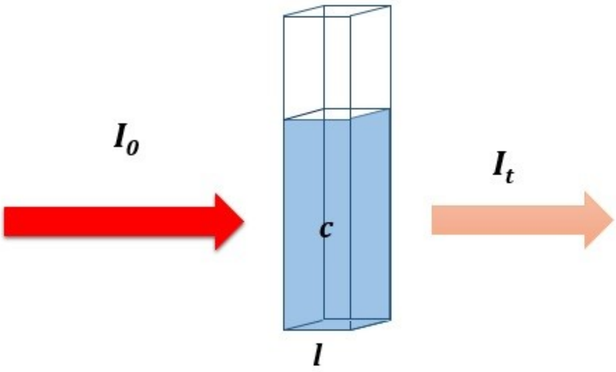

$$A = \log_{10} \frac{I_t}{I_0} = \varepsilon \, l \, c$$

Fig. 18: *Lambert-Beer law.*

Moreover, absorption is strictly dependent on the concentration of photoactive specie (**c**) and the optical path length of light through the solution.

Another important parameter is the extinction molar coefficient that is a wavelength dependent constant. To increase this contribution, a high extinction molar coefficient, capable to cover a high solar spectrum range would be preferred An interesting innovating approach, to increase the absorption range, is that of combining two or more luminophores in the case of multiple LSCs, adding their absorption spectra.

1.3.3.3 Quantum efficiency (η_{LQE})

Not all the absorbed photons could be emitted as useful photons. The complex structure of rotational, vibronic and electronic states of luminophore determines several emission processes, with non and radiative contributions.

Frank-Condon principle explains clearly the emission complexity. Undergoing an electronic transition, the nuclear configuration does not change significantly and the electronic transition to the ground state produces a radiative emission.

The high number of vibronic and rotational states and their higher energy could induce a series of non-radiative processes, which decrease the fluorescence and consequently the quantum efficiency.

The ratio between the number of emitted photons and the absorbed ones, which give fluorescence processes, is called fluorescence quantum efficiency. This parameter depends on the luminophore nature. For a high performing LSC, a high quantum efficiency is necessary.

1.3.3.4 Stokes efficiency (η_{Stokes})

The Stokes shift is the energy separation between the peak closest to the lower energy of the absorption band and the peak nearest to the highest energy at the emission band[72]. Stokes loss depends on the loss in energy between the absorbed and emitted photons, taking in

---

[72] M. G. Debije, P. P. C. Verbunt, *Adv. Energy Mater.*, **2012**, *2*, 12.

consideration only the emitted ones. Such effect is difficult to reduce, however it is not the major loss mechanism as long as the energy of photons is still large enough to generate an electron-hole pair within the PV cell, to overcome this bandgap.

1.3.3.5 Trapping efficiency (η_{Trap}): "Escape cone"

A particle of luminophore emits in all directions; part of such emission could travel through total internal reflection (TIR) into the polymeric slab, with refractive index n_1. The slab is exposed and in contact with another material (as air) with a different refractive index (n_2). From Snell's law, a critical angle ($\boldsymbol{\theta_c}$) determines which trips of emitted light could be reflected internally and supply to the production of electricity of PV cell, at the edges of the slab.
At the interface, if the angle $\boldsymbol{\theta_i}$ is higher than the critical one, $\boldsymbol{\theta_c}$ ($\boldsymbol{\theta_i > \theta_c}$) the photon is totally internally reflected. On the contrary, if the angle $\boldsymbol{\theta_i}$ is equal or lower than $\boldsymbol{\theta_c}$, the emitted light could be reflexed outside the slab, through the so called "*escape cone*" (Fig. 19).

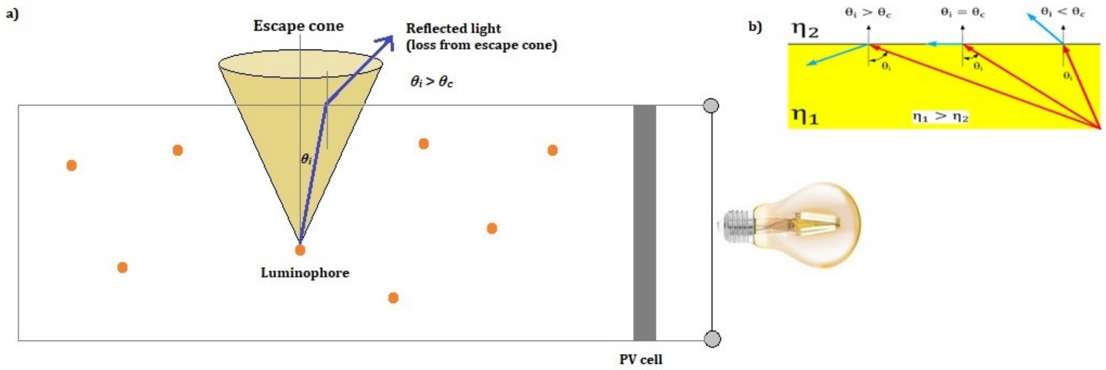

Fig. 19: *a) Escape cone mechanism and b) critical angle between two materials with different refractive index (where $\eta_1 > \eta_2$)*[73].

The escape cone loss for a host material with $n = 1.5$ is about 25%, while the corresponding 75% is approximately reflected.

1.3.3.6 Re-absorption losses ($\eta self$)

A consequence of small Stokes shift (typical for the most common organic LSC fluorophores) is the large overlap region between the absorption and emission spectra. In this area, the possibility to observe re-absorption is high. Re-absorption is the capability of other luminophore particles, dispersed in the polymer slab, to absorb fluorophore-emitted photons during their trip into the waveguide[74].

---

[73] M. G. Debije, P. P. C. Verbunt, *Adv. Energy Mater.*, **2012**, *2*, 12.
[74] R.W. Olson, R.F. Loring, M.D. Fayer, *Appl. Optics,* **1981**, *20*, 2934-40.

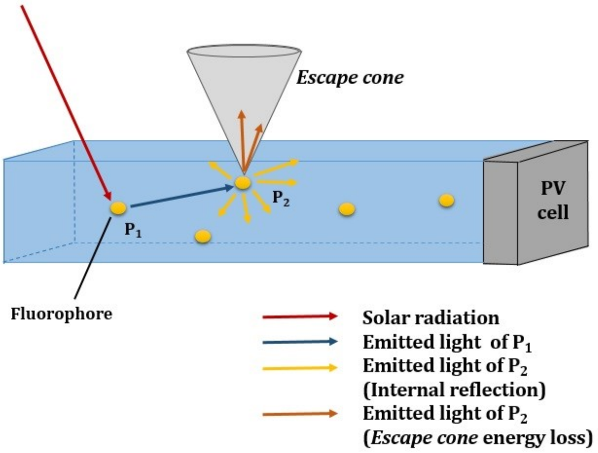

Fig. 20: *Re-absorption mechanism.*

Re-absorption processes are not losses of power themselves, but could become a loss if the other luminophore does not emit (loss of power through non-radiative mechanisms) or losses emitted photons through its escape cone[75] (Fig. 20).

To reduce the re-absorption effect, some techniques are tested from the research community. One of those is based on the use of dopants with a polar and high mobility effect (such as thiosin). The dopant, altering the electronic states of fluorescence and absorption of the fluorophore, might increase the Stokes shift and reduce the overlap region[76].

Another possibility is that of designing a multiple LSC panels, creating a stack number of LSC devices, each of them doped with different and specific luminophores, which absorb in a different range of the solar spectrum[77].

A central drawback of some luminophores is the low effect of re-absorption in the lab-scale, however, the corresponding energy loss through re-absorption in large-scale devices is higher. To avoid it, two techniques could be considered: the introduction of a thin layer doped with luminophore on a surface of the polymeric slab[78](Fig. 21A) or the covering of the polymer surface with thin layer luminophore-doped, physically spaced by stretches of empty waveguide (Fig. 21B)[79]. In both cases, the effect of re-absorption is limited by the lower amount of luminophore, allowing the possibility of obtaining large scale LSC even when using luminophores with high re-absorption effect.

---

[75] a) R. Sóti, É. Farkas, M. Hilbert, Zs. Farkas, I. Ketskeméty, *J. Luminescence*, **1996**, *68*, 105-114; b) K. Geetha, M. Rajesh, V.P.N. Nampoori, C.P.G. Vallabhan, P. Radhakrishnan, J. *Opt. A: Pure Appl. Opt.*, **2004**, *6*, 379; c) L.R. Wilson, B.C. Rowan, N. Robertson, O. Moudam, A.C. Jones, B.S. Richards, *Appl. Optics*, **2010**, *49*, 1651-61.

[76] A.M. Taleb, *Renew. Energ.*, **2002**, *26*, 137-142.

[77] a) M.J. Currie, J.K. Mapel, T.D. Heidel, S. Goffri, M.A. Baldo, *Science*, **2008**, *321*, 226-228; b) M.G. Debije, P.P.C. Verbunt, P.J. Nadkarni, S. Velate, K. Bhaumik, S. Nedumbamana, B.C. Rowan, B.S. Richards, T.L. Hoeks, *Appl. Optics*, **2011**, *50*, 163-169.

[78] a) W.G.J.H.M. van Sark, K.W.J. Barnham, L.H. Slooff, A.J. Chatten, A. Büchtemann, A. Meyer, S.J. McCormack, R. Koole, D.J. Farrell, R. Bose, E.E. Bende, A.R. Burgers, T. Budel, J. Quilitz, M. Kennedy, T. Meyer, C. De Mello Donegá, A. Meijerink, D. Vanmaekelbergh, *Opt. Express* **2008**, *16*, 21773-92; b) A.M. Hermann, *Sol. Energ.*, **1982**, *29*, 323-329; c) R. Reisfeld, M. Eyal, V. Chernyak, R. Zusm, *Sol. Energ. Mater.*, **1988,** *17*, 439-455; d) W. Viehnmann, R.L. Frost, *Nucl. Instr. Meth.*, **1979**, *167*, 3, 405-415; e) T. Dienel, C. BauerIgor, D.D. Brühwiler, *Sol. Energy*, **2010**, *84*, 1366-69; f) R. Reisfeld, *Opt. Mater.*, **2010**, *32*, 850-856.

[79] S. Tsoi, D.J. Broer, C.W.M. Bastiaansen, M.G. Debije, *Opt. Express*, **2010**, *18*, A536-A543.

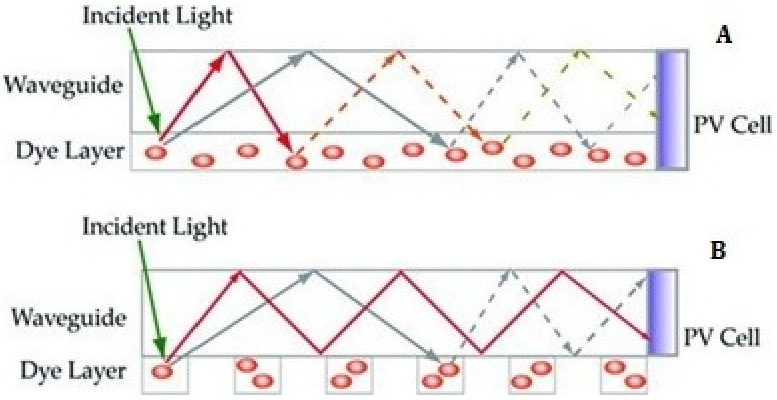

Fig. 21: *Schematic demonstration of the contribution of patterned fluorescent dye waveguide. On the top, mechanism of the standard thin layer luminophore-doped; on the bottom, mechanism of patterned dye layer.*
In both case, the incident light (green arrow) could be absorbed by a luminophore and emit longer wavelengths (red and grey solid arrows). In the best conditions, the emitted light could be re-absorbed by another luminescent particle and re-emitted in long wavelengths, avoiding escape cone losses[80].

1.4 LSC COMPONENTS

As we have already seen, three units compose an LSC device: the PV cell, the polymeric slab and a specific fluorophore inside of the host material.
The PV cell is usually silicon-based, covering one or all the edges of the panel. The thickness is usually around 5 mm.
Even if in literature different designs of LSC have been described such modifications are not the principal variable for the efficiency of the system, while the design and the choice of the host material and luminophore seem to be crucial to improve LSC's performances.

1.4.1 Host material

A compatible LSC matrix requires:

- a good dispersion of the luminescent species in the polymer system. Low compatibility of the luminophore with the matrix causes aggregation, with a high probability of cracks formation and not homogenous polymeric surfaces;
- high transparency, with lower reflection mechanisms of the solar radiation, therefore, a distinct refractive index should be select to the LSC device;
- thermo-resistance as an LSC is subjected to high temperature for a long time exposure;
- high resistance to collisions and shocks as it should work in bad environmental conditions (resistance to moisture, hydrophobicity, etc.);
- low structural defects of the surfaces (to limit reflection and favor trapping light);
- no absorption of the sunlight, especially in the absorption region of luminophore, to avoid loss of efficiency: for instance, the presence of additive or radical initiators, used during the polymerization which persists in the polymeric latter, could absorb sunlight or luminophore's total internal reflected radiation;

---

[80] S. Tsoi, D.J. Broer, C.W.M. Bastiaansen, M.G. Debije, *Opt. Express*, **2010**, *18*, A536-A543.

- ➢ simple polymerization processes, especially for large scale devices;
- ➢ very low cost of starting materials.

According to this list of parameters, poly(methyl methacrylate) (PMMA) seems to be the best host material for this kind of optical device. PMMA, named also as "plexiglass", is transparent, cheap, can be prepared with well known and simple polymerization process under mild conditions (in air atmosphere, heating at 90°C). Homogenous surfaces, large-scale synthesis and high control of physical features (flexibility, resistance, etc.) can be obtained during the polymerization process. PMMA is actually the principal polymeric matrix used for LSCs. However, polycarbonates (PCs), polystyrene (PS) and styrene-acrylonitrile resin (SAN) have also found a place in the LSC industry, for their high thermo-resistance[81] (Fig. 22).

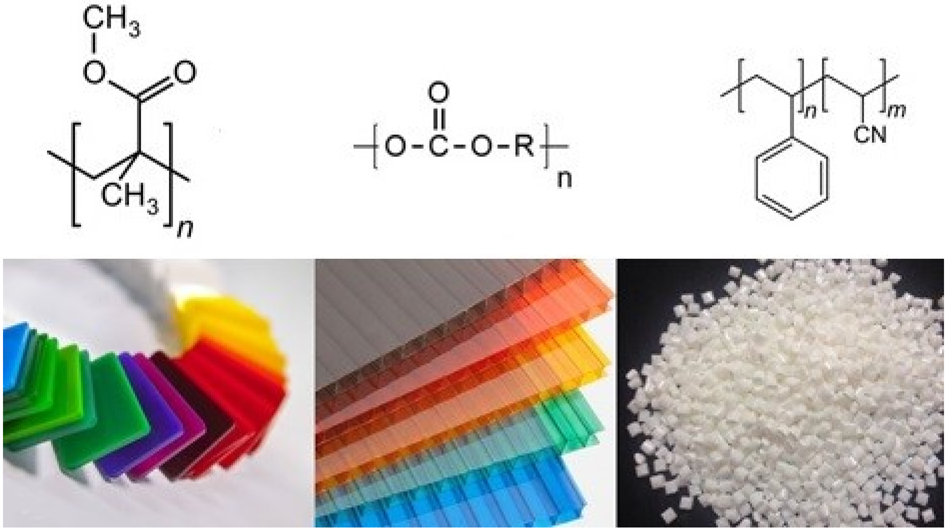

Fig. 22: *Host matrices for LSC: from left to right, PMMA, PC and SAN resin*[82].

These matrices include high optical transparency, sustainability, good dye dispersion and commercial availability. In particular, PCs, tested with different polymeric formulations, show very comparable good results to those obtained with PMMA and offer good optical properties, high impact resistance and high thermal resistance. Otherwise, Compact Disc PC (PCCD), a high thermoplastic with good toughness polymer, exhibits lower critical angle escape and lower transmittance compared with PMMA.

Some other host materials were tested in LSC devices[83]: bio-based polymers, for an eco-friendly approach[84], vacuum-deposited polymer, such as perylene-based thin films obtained through

---

[81] F. Meinardi, F. Bruni, S. Brovelli, *Energy Technol.*, **2017**, *5*, 1037-1044.

[82] Adapted from: a) http://www.arteplastica.it/materiali; b) https://www.indiamart.com/proddetail/polycarbonate-sheet-all-types-of-multiwall-colours; c) https://japanese.alibaba.com.

[83] a) Y. Li, X. Zhang, Y. Zhang, R. Dong, C.K. Luscombe, *Journal of polymer science*, **2019**, *57*, 201-215; b) G. Griffini, *Front. Mater.,* **2019**, *6*, 29, 1– 8.

[84] V. Fattori, M. Melucci, L. Ferrante, M. Zambianchi, I. Manet, W. Oberhauser, G. Giambastiani, M. Frediani, G. Giachi, N. Camaioni, *Energy Environ. Sci.*, **2011**, *4*, 2849– 2853, b) M. Melucci, M. Durso, L. Favaretto, M.L. Capobianco, V. Benfenati, A. Sagnella, G. Ruani, M. Muccini, R. Zamboni, V. Fattori, N. Camaioni, *RSC Adv.*, **2012**, *2*, 8610– 8613; c) F.I. Chowdhury, C. Dick, L. Meng, S.M. Mahpeykar, B. Ahvazi, X. Wang, *RSC Adv.*, **2017**, *7*, 32436-32441

coarse vacuum co-sublimation[85], fluorinated polymers, characterized by high hydrophobicity and long-term durability[86] or inorganic-organic hybrid polymer ureasil-based[87].

1.4.2 Luminophore

The main component of an LSC is the luminophore, whose optical behavior has a major influence on the final efficiency. The choice of luminophore affects many properties, like the light transport efficiency and absorption, the photoluminescent quantum yield, the energy lost due to the heat generation, the re-absorption loss and the number of photons reaching the PV cell.

Therefore, several features need to be considered to maximize the optical performance. Concerning the optical properties, a good luminophores should have:

- broad absorption window;
- high absorption efficiency over the whole spectrum range;
- high fluorescence quantum yield (Φ_f);
- large Stokes shift and consequently limited overlap between absorption and emission spectra; however other properties should also be considered such as high stability (photochemical, thermal, environmental);
- good solubility in the host material for a good dispersion (avoiding aggregation or π-π stacking which could quench fluorescence and decrease fluorescence quantum yield);
- high matching between the emission photons and the working absorption band of PV cell (about 1.14 eV for Silicon);
- low or null toxicity;
- simple preparation processes;
- low costs.

To meet these requirements, a wide variety of compounds have been studied in these last decades. Three main classes of luminophores are defined: Quantum Dots (QDs), late-metal complexes and organic dyes.

QUANTUM DOTs (QDs)

Quantum Dots (QDs) are semiconducting nanocrystals/nanoparticles with dimensions between 10 and 100 nm[88] that were introduced as luminescent species for LSC by Barnham

---

[85] a) G. Maggioni, A. Campagnaro, S. Carturan, A. Quaranta, *Solar Energy Materials & Solar Cells,* **2013**, *108*, 27-37; b) M. Tonezzer, G. Maggioni, A. Campagnaro, S. Carturan, A. Quaranta, M. della Pirriera, D.G. Tauste *Progress in Organic Coatings*, **2014***, 77* (2), 528-536*.*

[86] a) G. Griffini, M. Levi, S. Turri, *Progress in Organic Coatings*, **2014**, *77* (2), 528-536; b) G. Griffini, M. Levi, S. Turri, *Solar Energy Materials & Solar Cells*, **2013**, *118*, 36-42; c) C. Credi, D. Pintossi, C.L. Bianchi, M. Levi, G. Griffini, S. Turri, *Materials & Design,* **2017**, *133*, 143-153.

[87] a) A. Kaniyoor, B. McKenna, S. Comby, R.C. Evans, *Advanced Optical Materials,* **2016**, *4* (3), 444-456; b) R. Rondão, A.R. Frias, S.F.H. Correia, L. Fu, V. De Zea Bermudez, P.S. André, R.A.S. Ferreira, L.D. Carlos *ACS Applied Materials & Interfaces,* **2017**, *9* (14), 12540-46; c) Z. Li, X. Zhao, C. Huang, X. Gong, *Journal of Materials Chemistry A: Materials for Energy and Sustainability*, **2013**, *1* (25), 7339-50; d) A.R. Frias, E. Pecoraro, S.F.H. Correia, L.M.G. Minas, A.R. Bastos, S. García-Revilla, R. Balda, S.J.L. Ribeiro, P.S. André, L.D. Carlos, R.A.S. Ferreira, *Journal of Materials Chemistry A: Materials for Energy and Sustainability*, **2018**, *6* (18), 8712-8723.

[88] M.G. Debije, P.P. C. Verbunt, *Adv. Energy Mater.*, **2012**, *2,* 12–35.

who predicteda concentrator efficiency up to 20%[89].

The production of such species is based on a variety of methods including colloidal or single-molecule precursor growth. Due to their nanodimensions, nanoparticles can hinder the excited electrons in the semiconductor, showing optical and electronical properties similar to atoms. The main advantages of this technique are Large Stokes shift, good photostability. Furthermore being the emission spectra dependent on QDs size it is possible to tune the optical properties by the choice of their dimensions.

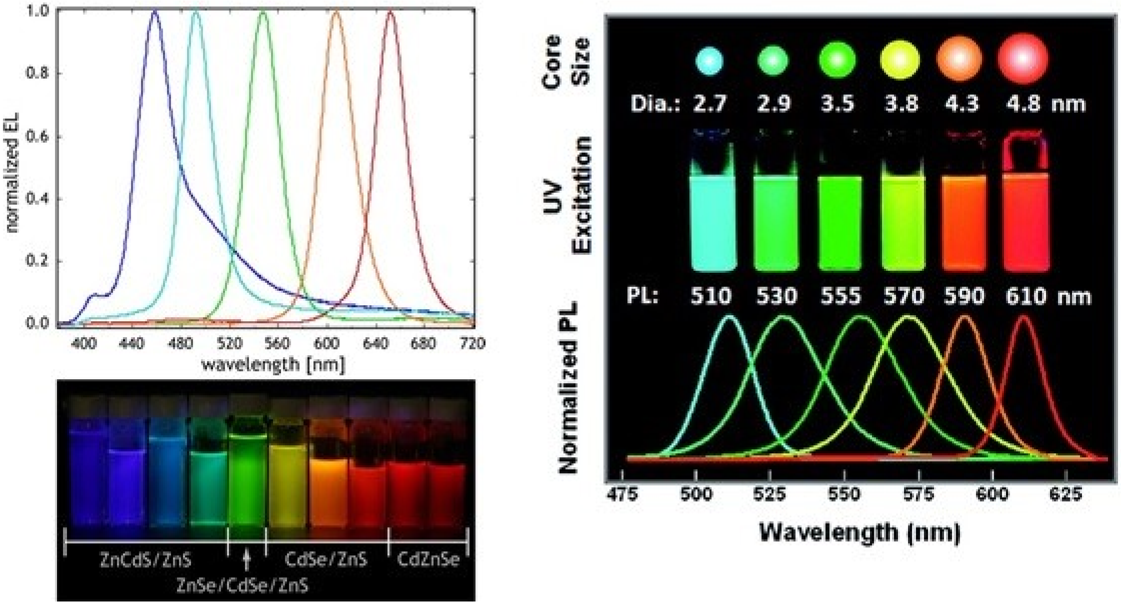

Fig. 23: *LSC quantum dots-based: the effect on absorption and emission spectra of structure (left)*[90] *and dimension (right)*[91]*, which describes the red-shift effect on spectroscopic features of CdSe@ZnS QDs, with the increasing of diameter dimensions.*

QDs can absorb the whole visible spectrum, modulating particle diameter[92] (Fig. 23).

Increasing the dimensions of QD particles, the band gap decreases and consequently the overlap region too, thus the re-absorption loss can be modulated in the function of size: in other words, it is possible to optimize the solar collector performances by the control of re-absorption through the spread of dimensions[93].

QDs have already found some interesting applications in bio labeling, sensing, imaging, drug delivery, nanoelectronics, photonics, light-harvesting and display panel technology. However, there is a mean drawback, which limits their use, which is due to stability issues. In particular, they can be photodegradated in presence of oxygen, or lead to the formation of clusters in the polymer matrix, with blue-shift effect, can lead to polymerization and are toxic both because of their chemical compositions and of their processing conditions (Cd, Hg, Pb, As based QDs e.g.).

---

[89] a) K. Barnham, J.L. Marques, J. Hassard, *Appl. Phys. Lett.*, **2000**, *76*, 1197-99; b) A.J. Chatten, K.W.J. Barnham, B.F. Buxton, N.J. Ekins-Daukes, M.A. Malik, *Sol. Energ. Mater. Sol. C.*, **2003**, *75*, 363-371.

[90] Genesis Nanotechnology, WorldPress.com.

[91] W.R. Algar, K. Susumu, J.B. Delehanty, I.L. Medinzt, *Anal. Chem.*, **2011**, *83,* 8826–8837.

[92] O.I. Mićić, H.M. Cheong, F. Fu, A. Zunger, J.R. Sprague, A. Mascarenhas, A.J. Nozik, *J. Phys. Chem. B* **1997**, *101*, 4904-4912.

[93] J. Bomm, A. Büchtemann, A.J. Chatten, R. Bose, D.J. Farrell, N.L.A. Chan, Y. Xiao, L.H. Slooff, T. Meyer, A. Meyer, W.G.J.H.M. van Sark, R. Koole, *Solar Energy Materials and Solar Cells*, **2011**, *95*, 2087–94.

LATE-METAL COMPLEXES

Rare-earth ions could be another possible solution because of their high photostability and large Stokes shift. Levitt and Weber described in 1977 Nd^{+3}-doped glass as a material for concentrator devices[94]. The main limitation of neodymium LSC was the low efficiency, which is due to its high emission range (in NIR region). To improve it, the first approach was that of doping Nd-based glass with another late metal such as ytterbium ions (Yb^{3+})[95] (Fig. 25).

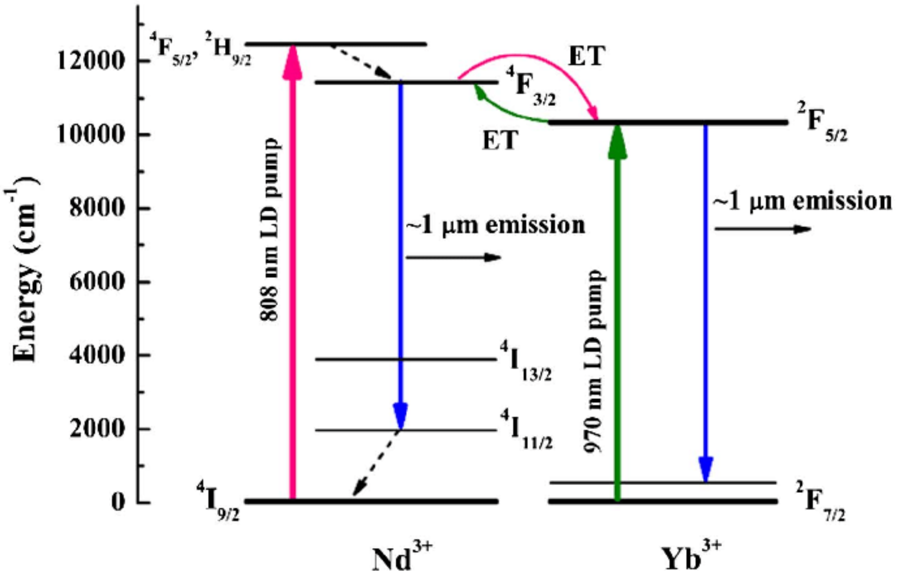

Fig. 24: *Schematic mechanism of photophysical processes, involved for Nd^{3+} codoped with Yb^{3+} ions*[96].

For instance, the emission peak of neodymium is about 1060 nm; in presence of ytterbium, the populated $^4F_{3/2}$ of neodynium transfers its excited electrons on $^2F_{5/2}$ depopulated state of Yb. Yb^{3+} transition is around 970 nm ($^2F_{5/2} \rightarrow {}^2F_{7/2}$), where the response to photons of silicon is still high. Unfortunately there are some limitations mainly due to the low absorption efficiency of neodymium and ytterbium[97] and the dependence of the energy transfer from Nd^{3+} to Yb^{3+} on the type of glass employed: in borate tellurite glasses, the energy transfer is around 90%[98].

Alternatively, Uranyl ions (UO_2^{2+}) could be used as they exhibit an absorption efficiency of five orders of magnitude higher than neodymium codoped with ytterbium LSC. However, the absorption is limited to the blue range of the spectrum (about 430 nm) and the fluorescence is around 550 nm with a moderate fluorescence quantum yield (67%)[99]. For these reasons, uranyl ions can be applied as co-dopant with other rare earth metals.

The limited range of absorption of rare earth metals (430 nm and970 nm), resulting in a loss of the high energy of the visible light, did not improve their applications in LSC.

To shift absorption maximum, organic ligands coordinating to the rare earth ions have been proposed[100].

---

[94] J.A. Levitt, W.H. Weber, *Appl. Optics*, **1977**, *16*, 2684.

[95] R. Reisfeld, Y. Kalisky, *Chem. Phys. Lett.*, **1981**, *80*, 178-183.

[96] F. Riviera-Lopez, P. Babu, C. Basavapoornima, C.K. Jayasankar, V. Lavin, *J. Appl. Phys.*, **2011**, *109*, 123514.

[97] R. Reisfeld, S. Neuman, *Nature*, **1978**, *274*, 144-145.

[98] C. Lurin, C. Parent, G. Le Flemp, P. Hagenmuller, *J. Phys. Chem. Solids,* **1985**, *46*, 1083-92.

[99] N. Neuroth, R. Haspel, *Sol. Energ. Mater.*, **1987**, *16*, 235-242.

[100] a) R. Reisfeld, *J. Less-Common Met.*, **1983**, *93*, 243-251; b) O. Moudam, B.C. Rowan, M. Alamiry, P. Richardson, B.S. Richards, A.C. Jone, N. Robertson, *Chem. Commun.*, **2009**, 6649-51.

Such approach exploits the high localized and shielded 4*f* orbitals of late metals, their high number of possible energy states and the good absorption properties of organic chromophores. It was proposed for the first time by Crosby and Whan:[101] through an *antenna effect,* it is supposed to happen a cascade energy transfer from organic ligand to late metal ion (Fig. 25).

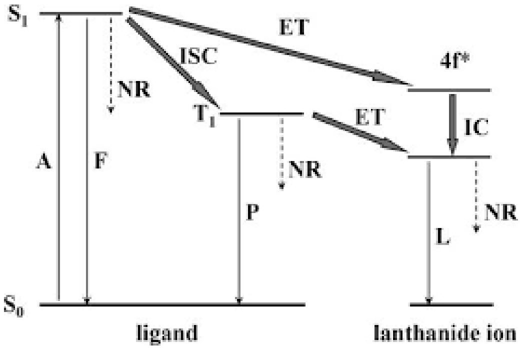

Fig. 25: *Schematic mechanism of photophysical processes involved in the sensitization of lanthanide ion via coordinating organic ligand*[102]*.*

The absorption of solar radiation by organic chromophore promotes a transition from the ground state (S_0) to the lower excited state (S_1). Favored by spin-orbit interaction, which is a heavy atom effect typical of lanthanides, the electron energy is transferred from S_1 to the triplet state, T_1, of ligand, through an intersystem crossing mechanism (ISC) and, in cascade, to the coordinating metal ion, which emits a red-shifted[103] radiation. Therefore compared with the use of free metal ion, it is possible to absorb a broad light range of solar radiation (organic ligand) with a higher molar absorption, and obtain a red-shifted emission (late metal ion) where silicon absorption of PV cell is still high. These kind of sensitizers show high fluorescence quantum yield (around 80-90% for Eu-based dye, e.g.), large Stokes shift (>200 nm), with usually null overlap, and good optical efficiency[104]. The main challenge for using lanthanide complexes is to find the best coordinating organic ligand and the best matching with late metal ions.

ORGANIC DYES

In the last 30 years, organic dyes have been widely investigated for application in LSCs. Their unique optical characteristics (high fluorescence quantum yield, large absorptivity, broad absorption spectra e.g.), the easy tunable optical and chemical properties, the availability through simple and conventional synthetic processes often using tow cost starting materials and the compatibility with different host matrices are only some of the properties matching those of an ideal LSC's luminophore.

Organic dyes are normally π-conjugated organic molecules, which are responsible of the electron transitions from the ground state (S_0) to an excited state at lower energy (S_1), and thus of the light absorption.

The fluorescence process is a π-π* de-excitation from the lower excited state S_1 to the ground

---

[101] G.A. Crosby, R.E. Whan, R.M. Alire, *The Journal of Chemical Physics*, **1961**, *34*, 743.

[102] Y. Cui, Y. Yue, G. Qian, B. Chen, *Chem. Rev.*, **2012**, *112*, 2, 1126–62.

[103] J.C.G. Bünzli, C. Piguet, *Chemical Society Reviews*, **2005**, *34*, 1048–77.

[104] G. Katsagounos, E. Stathatos, N.B. Arabatzis, A.D. Keramidas, P. Lianos, *Luminescence*, **2011**, *131*, 1776-81.

state S_0, a singlet to singlet transition with a short lifetime.

The introduction of an electron donor or acceptor group on the π-structure of an organic dye, generates a polarizable molecule in which the electron mobility could be enhanced, consequently the optical properties can be modulated simply by choosing the right substituent. Such effect is also correlated to the position of substituents, which affects the energy of HOMO and LUMO frontiers orbital. In particular, high planarity and symmetry of the molecule could modify absorption and emission spectra, through bathochromic or hyperchromic effect.

Since the first papers on organic LSCs, a vast library of compounds have been investigated such as: coumarins[105], rylenes[106], in particular perylene imides, bipyridines, dicyano methylenes[107], lactones[108], phtalocyanines[109], phycobilisomes[110], porphyrins[111], pyrromethenes[112], tertiary amine derivates of tetra-cyano-p-quinodimethane[113], thioxanthenes[114], (iso)violanthrones[115] and rhodamines[116].

The most important classes of organic fluorophores will be elaborated on in chapter 2, since they are related to the main topic of this thesis work.

1.5 APPLICATIONS

1.5.1 BIPVs

In the collective imagination, the vision of sustainable cities, in which the growth of population requires an increase of energy demand is often associated with a utopic metropolitan skyline of self-powered glass buildings.

Actually, buildings account for 40% of the energy consumed every year in Europe. In 2015, the

---

[105] a) B. A. Swartz, T. Cole, A.H. Zewail, *Opt. Lett.* **1977**, *1,* 73; b) J. S. Batchelder, A.H. Zewail, T. Cole, *Appl. Optics* **1981**, *20,* 3733-3754; c) A.M. Hermann, *Sol. Energ.* **1982**, *29*, 323-329; d) W. G. J. H. M. van Sark *et al.*, *Opt. Express* **2008**, *16*, 21773-92.

[106] J.S. Batchelder, A.H. Zewail, and T. Cole, *Applied Optics*, **1981**, *20*, 3733–54; b) L.R. Wilson, and B.S. Richards, *Appl. Opt.,* **2009**, *48*, 212–220; c) A.F. Mansour, M.G. El-Shaarawy, S.M. El-Bashir, M.K. El-Mansy, and M. Hammam, *Polymer International*, **2002**, *51*, 393–397; d) M.G. Debije, M.P. Van, P.P.C. Verbunt, M.J. Kastelijn, R.H.L. van der Blom, D.J. Broer, and C.W.M. Bastiaansen, *Appl. Opt.*, **2010**, *49*, 745–751; e) A.F. Mansour, R.M. Ahmed, A.H. Bassyouni, and G.M. Nasr, *International Journal of Polymeric Materials*, **2007**, *56*, 651–662; f) G. Griffi ni, L. Brambilla, M. Levi, M. Del Zoppo, and S. Turri, *Solar Energy Materials and Solar Cells*, **2013**, *111*, 41–48.

[107] M.J. Currie, J.K. Mapel, T.D. Heidel, S. Goffri, and M.A. Baldo, *Science*, **2008**,*321*, 226–228; b) J.M. Drake, M.L. Lesiecki, J. Sansregret, and W.R. Thomas, *Appl. Opt.*, **1982**, *21*, 2945–2952; c) J. Sansregret, J.M. Drake, W.R.L. Thomas, and M.L. Lesiecki, *Appl. Opt*, **1983**, *22*, 573–577.

[108] I. Baumberg, O. Berezin, A. Drabkin, B. Gorelik, L. Kogan, M. Voskobojnik, M. Zaidman, *Polym. Degrad. Stabil.* **2001**, *73*, 403-410.

[109] S.M. Reda, *Sol. Energ*. **2007**, *81,* 755-760.

[110] C.L. Mulder *et al., Adv. Mater*. **2009**, *21*, 3181-85.

[111] a) J. S. Batchelder, A.H. Zewail, T. Cole, *Appl. Optics* **1981**, *20,* 3733-3754; b) S.M. Reda, *Sol. Energ*. **2007**, *81,* 755-760.

[112] I. Baumberg, O. Berezin, A. Drabkin, B. Gorelik, L. Kogan, M. Voskobojnik, M. Zaidman, *Polym. Degrad. Stabil.* **2001**, *73*, 403-410.

[113] Y. Ren, M. Szablenwski, G.H. Cross, *Appl. Optics* **2000**, *39*, 2499-2506.

[114] B.A. Swartz, T. Cole, A.H. Zwail, *Opt. Lett.* **1977**, *1*, 73-75.

[115] G. Seybold, G. Wagenblast, *Dyes Pigm*. **1989**, *11*, 303-317.

[116] B.A. Swartz, T. Cole, A.H. Zwail, *Opt. Lett.* **1977**, *1*, 73-75; b) J. S. Batchelder, A.H. Zewail, T. Cole, *Appl. Optics* **1981**, *20,* 3733-3754; c) R. Reisfeld, R. Zusman, Y. Cohen, and M. Eyal, *Chemical Physics Letters*, **1988**,*147*, 142–147; d) M.A. El-Shahawy, and A.F. Mansour, *Journal of Materials Science: Materials in Electronics*, **1996**, *7*, 171–174.

European Commission indicated ten research and innovation goals that reflected the European priorities in the field of low-fossil fuels exploitation. One of these goals is the development of fully energetically sustainable architecture, called net zero-energy buildings (NZEBs). NZEBs concept assumes that the energy consumption of a building and the renewable energy generated by it is balanced. NZEB concept rapidly becomes an appealing option: individual houses and small buildings have already been supplied by some microgeneration technologies, such as rooftop photovoltaics, micro-turbines, geothermal heat pumps and solar thermal collectors. Dissipations and consumptions are limited through high-performing strategies, applicable to small energetic systems.

Fig. 26: *BIPVs LSC-based, realized in large scale or prototypes: LSCs could be integrated in common buildings such as windows (**D:** Congress palace of Montreal, Canada), penciline (**C:** penciline from Eni) and sound barriers in prototype design (**A**) and in a prospective application on trunk roads (**B**) in Netherlands* [117]*.*

In highly urbanized areas, the NZEB approach is more complex, considering the low surface area available for the installation of photovoltaic panels on the roofs, and the energy needs required of a typical high-density building such as a skyscraper (e.g. 7 m^2 is currently necessary per kW of peak power). Building integrated Photovoltaics (BIPV) can be an important solution to solve this problem.

BIPVs are a series of new photovoltaic technologies focused on the direct integration of photovoltaic systems as integral parts of building (windows, roofs, canopies, etc.). This is related to the common sense that not to affect the aesthetical aspects of landscapes it is

---

[117] Adapted imagines from: https://montreal.eater.com; https://eni.com ; https://electrek.co.

necessary an “invisible” presence.

Some examples developed recently are showed in figure 26.

Following this approach, nowadays the annual installed production capacity of BIPV worldwide is 11 GW. The growth rate in one year has been 30% in Europe, driven by the increasing of renewable energy and green building development, followed by North America, with 27% of annual installations. The total BIPVs market is expected to grow from US$3bilions in 2015 to around US$26 bilions in 2022 (Fig. 27).

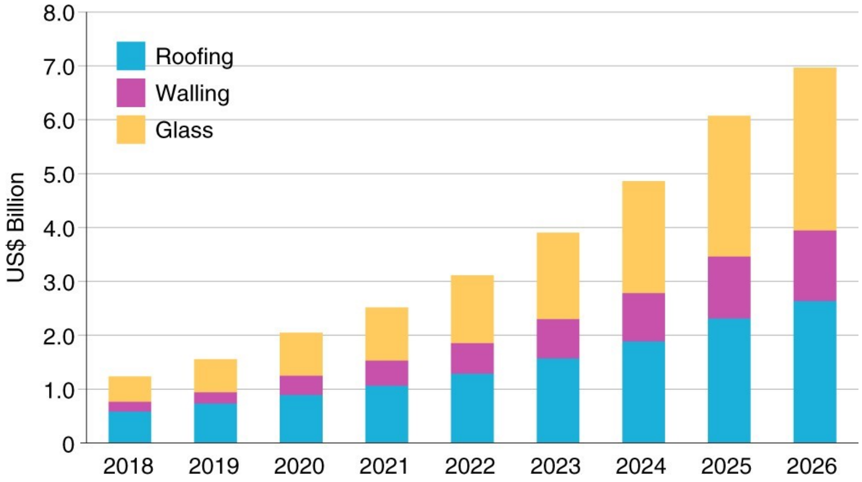

Fig. 27: *Growth of BIPV glazing sector from 2015 with a prediction until 2026*[118].

LSCs technology can satisfy some requirements of BIPVs, following NZEB concept.

Indeed, the first LSC was proposed in 1976, as a cost-effective alternative to the silica-based PV module[119].

LSC panels can work with direct and diffuse light, allow versatile design and fabrication, provide moderate or low costs of materials and installation. Furthermore, their transparency and the possibility to design colorless panels make are particularly attractive for the aesthetical demand of the urban landscape.

Furthermore, in the same conditions, LSCs are less sensitive than PV modules, offering flexibility, no electrical stresses caused by shadowing effects, no specific orienting angle.

Finally, inert doped glass panels reduce overheating, for the capability of absorbing a broad part of solar radiation, maintaining natural lighting for internal illumination.

Considering the BIPVs requirements, LSC chromophores could be divided in two classes: A-type sensitizers, where photoluminescence occurs from the absorption process of the active specie and the absorption and emission spectra are correlated to an overlap region and a defined Stokes shift[120], and B-type sensitizers, where the absorption and emission processes are decoupled (Fig. 28).

A-type emitters include organic molecular compounds and quantum dots (QDs) even if their

---

[118] IEA PVPS Task 15, Subtask E Report IEA-PVPS T15-07, **2019**, February 2019.

[119] W.H. Weber, J. Lambe, *Appl. Opt*. **1976**, *15*, 2299–2300.

[120] F. Meinardi, A. Colombo, K.A. Velizhanin, R. Simonutti, M. Lorenzon, L. Beverina, *Nat. Photonics* **2014**, *8*, 392–399.

Stokes shift is too small to achieve good performances[121]. B-type class consists on late metal complexes, where the decoupling between absorption and emission state comes from the organic ligand and the rare-metal ion, respectively[122]. The mean drawback of B-type emitters is the impossibility to tune the atomic transition of metal.

A comparison between A-type and B-type emitters can explain which parameters need to be considered to use LSC for BIPV. Of course, a proper comparison can be done only by referring to the same spectral coverages.

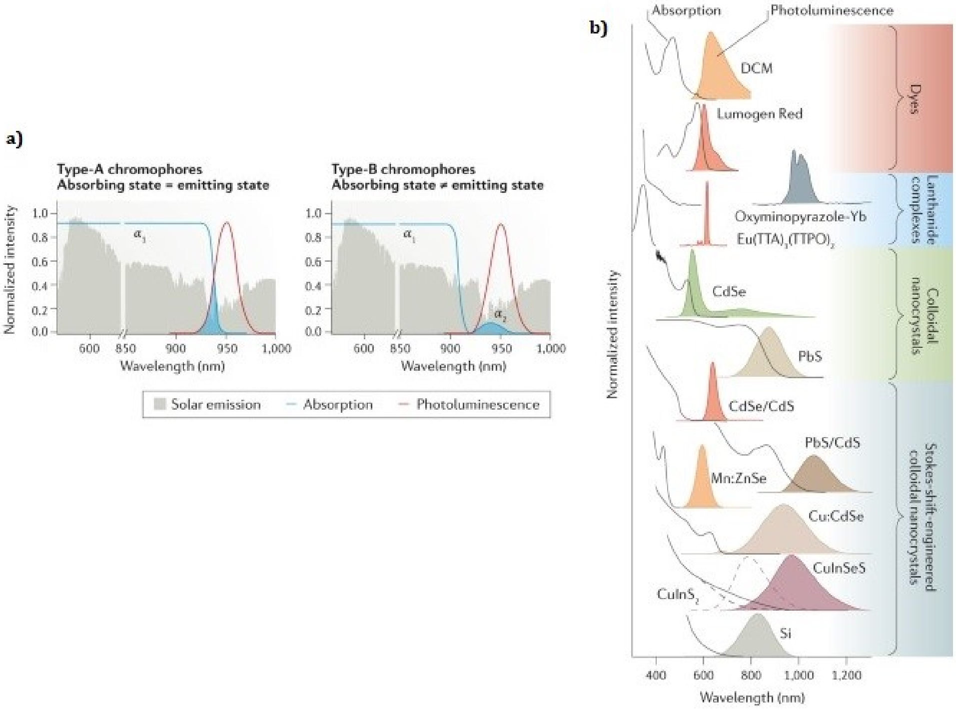

Fig. 28: *Schematic depiction of the optical properties of two types of chromophores suitable for luminescent solar concentrators (LSCs).* ***a)*** *For type-A systems, the optical absorption spectrum (blue) shows a large absorption coefficient, α_1, across the majority of the solar emission spectrum (grey). Photoluminescence (red) occurs from the absorbing state: a minimal overlaps observed, characterized by usually a long-absorption tailing. In type-B chromophores, the absorption and emission processes are decoupled. The light-harvesting state has a large broadband absorption coefficient, α_1, whereas the emitting state has a negligible absorption coefficient, α_2. For type-B chromophores, reabsorption losses are effectively suppressed for $\alpha_1 >> \alpha_2$.* ***b)*** *Optical absorption and emission spectra of the typical chromophores, employed in LSCs*[123]*.*

For instance, **LR 305**[124] and CuInSeS nanocrystal[125] spectra can be compared, using an LSC thickness of 0.5 cm and referring to an identical spectral coverage of 30% of the incident solar

---

[121] Z. Krumer et al., *Sol. Energy Mater. Sol. Cells* **2013**, *111*, 57–65; b) G. V. Shcherbatyuk, R. H. Inman, C. Wang, R. Winston, S.R. Ghosh, *Appl. Phys. Lett*. **2010**, *96*, 191901, c) J. Bomm et al, *Sol. Energy Mater. Sol. Cells* **2011**,*95*, 2087–94.

[122] a) A. Sanguineti, A. Monguzzi, G. Vaccaro, F. Meinardi, E. Ronchi, M. Moret, U. Cosentino, G. Moro, R. Simonutti, M. Mauri, R. Tubino, L. Beverina, *Phys. Chem. Chem. Phys*. **2012**, *14*, 6452–55; b)T.Wang, J. Zhang, W. Ma, Y. Luo, L. Wang, Z. Hu, W. Wu, X. Wang, G. Zou, Q. Zhang, *Sol. Energy* **2011**, *85*, 2571–79.

[123] F. Meinardi, F. Bruni, S. Brovelli, *Nature Reviews Materials*, **2017**, *2,* 17072.

[124] L. Zhu et al., *J. Phys. Chem. A* **2010**, *114*, 3471–82.

[125] F. Meinardi, H. McDaniel, F. Carulli, A. Colombo, K.A. Velizhanin, N.S. Makarov, R. Simonutti, V.I. Klimov, S. Brovelli, *Nat. Nanotechnol*. **2015**, *10*, 878–885.

radiation, an ideal photoluminescence of 100% is considered and the effect of light absorption of host matrix waveguide is neglected. In these conditions, for **LR 305**, 30% of spectral coverage requires a high concentration in the LSC device, with a large overlap region. That means that a strong re-absorption effect is observed for a small-area device (for 2 x 2 cm^2 sample). According to the statistical analysis of light propagation, over 50% of the photons collected at the edges of the device are affected by the re-absorption event. Working on 25x25 cm^2 of the device area, the 64% of the collected photons are re-radiated by re-absorption.

On the contrary, for CuInSeS LSC devices, the overlap is smaller and the re-absorption effect limited. Indeed, in the case of a 2x2 cm^2 sample, the 95% of collected photons are unaffected by re-absorption and also in the case of larger LSCs the re-radiation records for less than 40% of collected photons.

A similar trend is observed for the optical efficiency, η.

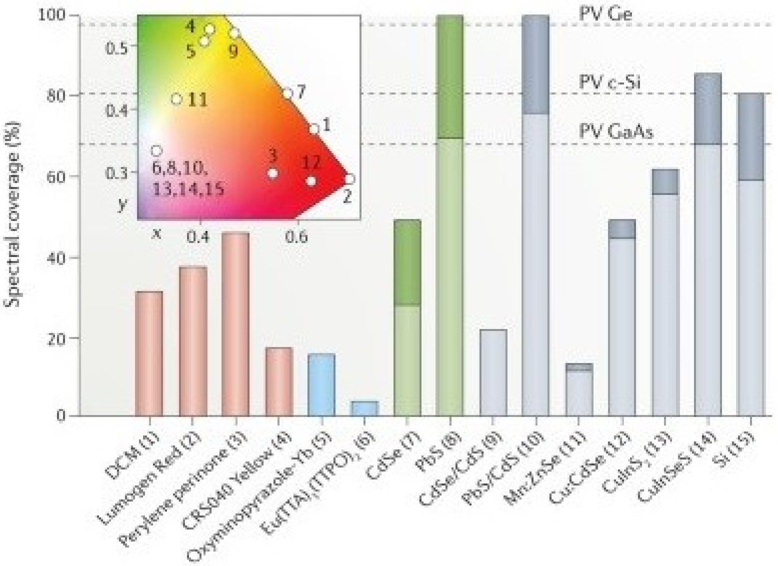

Fig. 29: *Maximum coverage of the principal chromophores, used in LSC devices, calculated in "infinite concentration" limit.*

Using **LR 305**, in the case of a 2x2 cm^2 sample, η =12.4% is recorded, going to a 10x10 cm^2 area, the optical efficiency found is reduced of 1.2%, until the constant value of 10.5%, which remain stable with the increasing of dimensions.

In the case of CuInSeS, the initial optical value is higher than **LR 305** at the same conditions (η ~15%). With a scale-up of LSC dimensions, the optical efficiency decreases constantly. No saturation is observed owing to the residual weak absorption that is resonant with the photoluminescence spectrum[126].

In figure 29, a wide group of A-type and B-type emitters (organic dyes, QDs and rare earth complexes) is reported, tested in different dimensions of LSC panels, for BIPV applications, optimizing all possible parameters with different panel design.[127]

Apart from BIPV, another important application is in the covering of greenhouses. Corrado et

---

[126] F. Meinardi, F. Bruni, S. Brovelli, *Nature Reviews Materials*, **2017**, *2,* 17072.

[127] M. Rafiee, S. Chandra, H. Ahmed, S.J. McCormack, *Optical Materials* **2019**, *91*, 212–227.

al.[128], in California, using again commercial **LR 305**, realized a greenhouse covered by LSC devices. The LSC greenhouse was tested comparing with a correspondent structure, where PV cell, in absence of luminophore doping, was used (control). For this experiment, in both greenhouses, PV cells were placed on the surface of the roof and not at the edges, and the PV efficiency, under solar radiation exposure (Fig. 30) was tested, by monitoring continuously for one year and controlling LSC photostability, resistance and the effect on the plants.

LSC greenhouse showed an improvement of 37% in power production, compared to the control. The 22.3 m^2 greenhouse was to generate 1342 kWh per year. To cover all the energy demand consumed in greenhouse operation, only 1/3 of the greenhouse roof needs to be covered by LSC electricity-generating panels. In presence of **LR 305**, the effect on plants growth is neutral or quite positive.

No degradation effect is observed during the all year, under weather conditions, showing high durability and capacity of exceeding the electricity demand.

Fig. 30: *Greenhouse covered by LSC and the control (on the left, up) and some details of roof. In California, the first LSC greenhouse,* ***LR305****based, was tested controlling efficiency, energy production and plants growth over its for one whole year*[128]*.*

---

[128] C. Corrado *et al.*, *J. RenewableSustainable Energy,* **2016**, *8*, 043502.

CHAPTER 2

AIM OF WORK

2 ORGANIC FLUOROPHORES: STATE OF ART

The potential of organic molecules as photoactive components for application in LSCs has been highlighted since their first use.

As we have already anticipated, an ideal fluorophore needs to fulfil some fundamental requirements[129]:

- good dispersion in the host matrix (polymer, glass, etc.), with high solubility in the matrix;
- high fluorescence quantum yield ($\boldsymbol{\Phi_f}$)
- broad Stokes shift, which allows minimizing phenomena of loss of power (such as re-absorption and self-quenching);
- emission wavelength which matches the PV cell band gap;
- simple structure and scalability of the synthesis;
- low costs of starting materials;
- low toxicity or non toxicity.

The advantage of using organic luminophores is that it is possible to modulate some of these characteristics through molecular design: for instance changing a single functional groups allow the tuning of specific spectroscopic and optical behaviors and maybe to match these properties with the ideal ones.

Thus, for an optimal fluorophore, the optimal emission wavelength should match partial or completely with the absorption wavelengths of the PV cell (for Si-based cell, corresponding to 400-1200 nm, with the maximum absorption range between 700-900 nm), while the absorption spectrum could cover different solar radiation ranges.

For this reason, organic luminophore are divided into three classes, depending on absorption light spectra region: visible light fluorophores, UV and NIR. Of course, an optimal should absorb the broadest solar radiation wavelengths, with the minimum overlap region with its corresponding emission spectrum.

2.1.1 FLUOROPHORES WITH ABSORPTION IN THE VISIBLE LIGHT

Rhodamine and coumarins

Rhodamines and coumarins were the first examples of fluorophore for LSCs used since early '80s. They are a class of organic dyes belonging to the xanthenes family (such as fluorescein and eosin), and are characterized by a high absorption coefficient, good efficiency of fluorescence and good photostability. A flexible synthetic approach allows using of rhodamines in widespread applications such as dye lasers, molecular switches, fluorescent standards or

---

[129] M. G. Debije and P. P. C. Verbunt, *Adv. Energy Mater.* **2012**, *2*, 12–35.

probes and chemosensors for metal ions[130].

The possible variations on their molecular design are reported in a generic molecular structure in figure 29 and are based on different functionalization in three positions[131]:

a) Amino groups on xanthene moiety (R_1 and R_2) ;
b) Para- and meta- positions on carboxyphenyl ring (Z);
c) Carboxy- or carboxylate groups on the carboxyphenyl ring

Commercial and inexpensive available rhodamines are rhodamine B, rhodamine 6G and rhodamine 101 (figure 29).

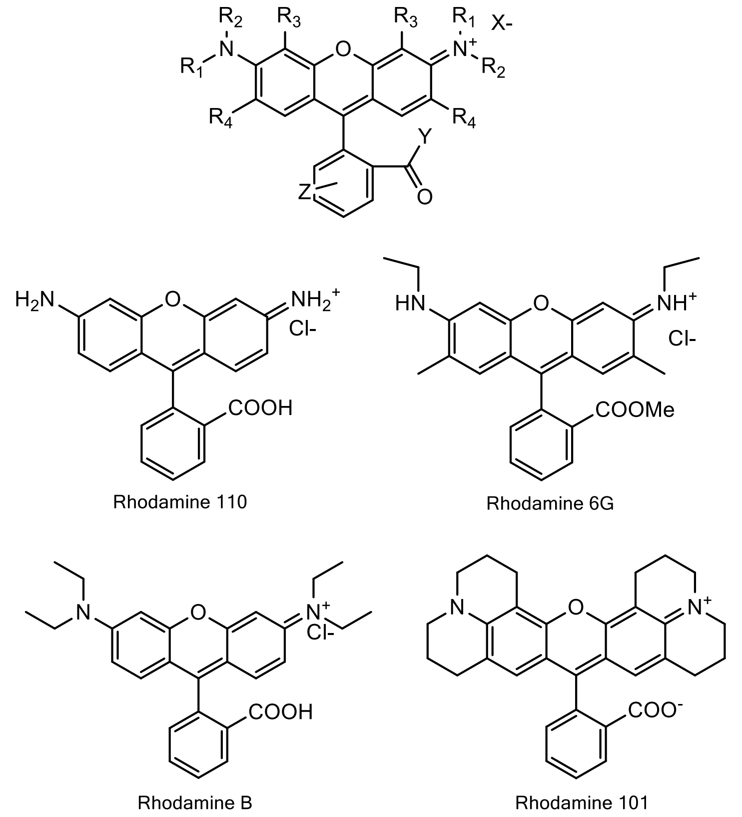

Fig. 29: *Rhodamine general molecular structure and the more representative systems, employed in LSC devices.*

Rhodamines have a planar and quite rigid structure generally responsible of a high fluorescence; however, a peculiar dependence on substituents of xanthene moiety is reported. In particular, the larger is the contribution of substituents on the rigidity and planarity of the molecule, the higher is the fluorescent efficiency. For instance, moving from Rhodamine B to a more rigid Rhodamine 101 the fluorescence quantum yield increases from 50% to 96%.

Mean drawbacks for rhodamines are the large overlap of absorption and emission spectra, and a limited stability in host matrix.

Coumarins (Fig. 30) are a class of luminophores more stable than rhodamines and characterized by a higher Stokes shift, with an emission quantum yield near to unity[132].

---

[130] H. Zheng, X. Q. Zhan, Q. N. Bian, and X. J. Zhang, *Chem. Comm.,* **2013**, *49,* 429–447.
[131] M. Beija, C. A. M. Afonso, and J. M. G. Martinho, *Chem. Soc. Rev.,* **2009,** *38,* 2410–33.
[132] W. G. J. H. M. van Sark *et al., Optics Express*, **2008**, *16,* 21773–92.

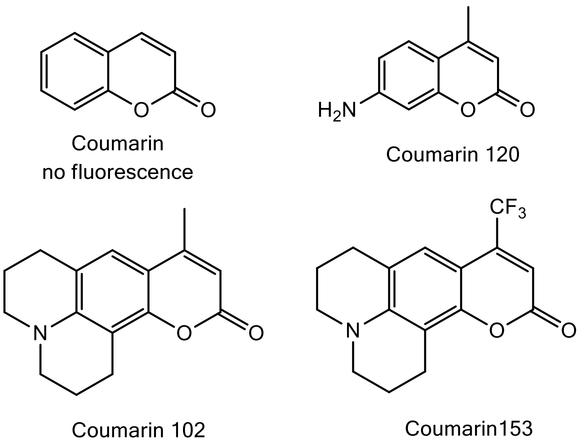

Coumarin
no fluorescence

Coumarin 120

Coumarin 102

Coumarin153

Fig. 30: *Coumarin model and their principal structure employed in LSCs.*

Generally the functionalization of positions 3,4,6 and 7 (in particular, donor substituent on 7-position usually an amino group) can enhance the fluorescence quantum yield, however, these molecules do not possess all the requirements for LSC fluorophores. In particular, their absorption is limited to blue-green part of the visible spectrum and their emission is scarcely adaptable to the PV cell absorption range.

Another important limit is the low stability in the final collector: even if coumarins are more stable than rhodamines, they could be photodegraded under continuous UV irradiation. This is tipically due to disruption of the benzopyrone for [2+2] photocycloaddiction and photoreactions on the substituents (photoxidation).

Rylenes

Since 1913, rylene dyes are known as thermal, chemical, photochemical and photophysical stable compounds. High fluorescence quantum yield, high molar coefficient and tunable absorption range between UV and NIR support their application in concentrators.

The possibility to modulate rylene's features is powered by the core extension on the two directions of the molecular axes (Fig. 31).

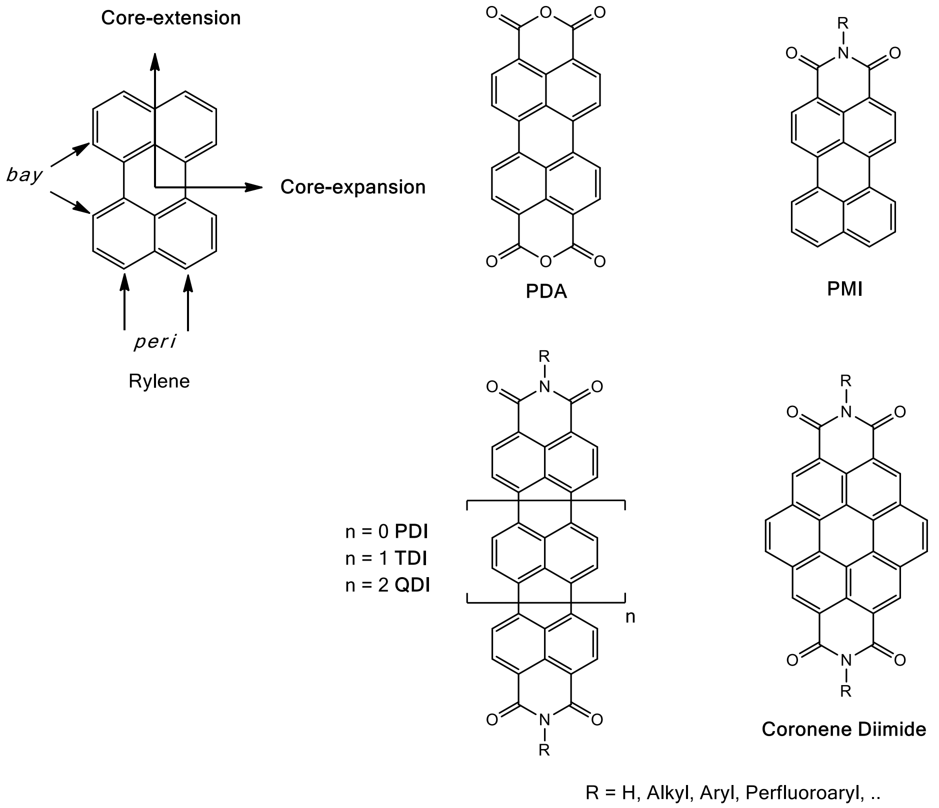

Fig. 31: *Rylene core, with the possible functionalization positions, and the resulted dyes, actually employed.*

The *core-extension* involves *peri* modifications, with elongation of the rylene conjugated system; to the other side, the *bay* positions favor lateral expansion along its short axis (*core-expansion)*. The first modification generates homologs systems, such as terrylene, quaterrylene, pentarylene and hexarylene imides. The alternative expansion promotes benzoannulations, generating coronene imides or dibenzocoronene imides.

These amplifications of the rylene core can be responsible to the mean drawback for rylenes, such as their low solubility. Indeed, functionalization of *peri* and *bay* positions can be exploited to overcome solubility problems, keeping in minda that *bay* functionalization could influence optical proprieties, more than *peri* one.

For instance, 3,4,9,10-perylenetetracarboxylic dianhydride (PDA) (Fig. 31) is a common insoluble precursor of all rylenes. The functionalization of anhydrides (*peri* positions) to imides, with different substitutions, results in a positive effect on PDA solubility. Perylene monoimides (PMIs) and perylene diimides (PDIs) with long alkyl chains as substituents on nitrogen atom show good solubility in the major part of organic solvents.

Furthermore, PDA shows a planar molecular structure that favors face-to-face interaction (π-π stacking) and consequently strong molecular aggregation. Contrarily, the long alkyl chains of PMIs and PDIs induced a perpendicular twisting effect on the aromatic groups, with respect to the perylene core, due to unfavorable steric interactions.

Fortunately, the introduction of long and branched alkyl chains on nitrogen atom introduce no consequences to perylene stability and no evident effect on optical properties.

The new challenge for this organic class of fluorophores is that of being able to further improve their optical features, on order to have a better matching with the absorption range of PV cells, maintaining, at the same time, high solubility and stability.

An extension of the rylene core, introducing some naphthalene moiety (n=0-2), has been shown to induce a bathochromic effect with an increase of fluorescence efficiency proportional to the extension of the perylene system. From molecular orbitals calculations, all the diimides maintain a planar structure, with a consequent large resonance stabilization while N-substituents are located at 90° to the perylene plane (see Fig. 32). The orbital energies show a decreasing of HOMO-LUMO bandgap, due to the increasing of perylene extension[133,134].

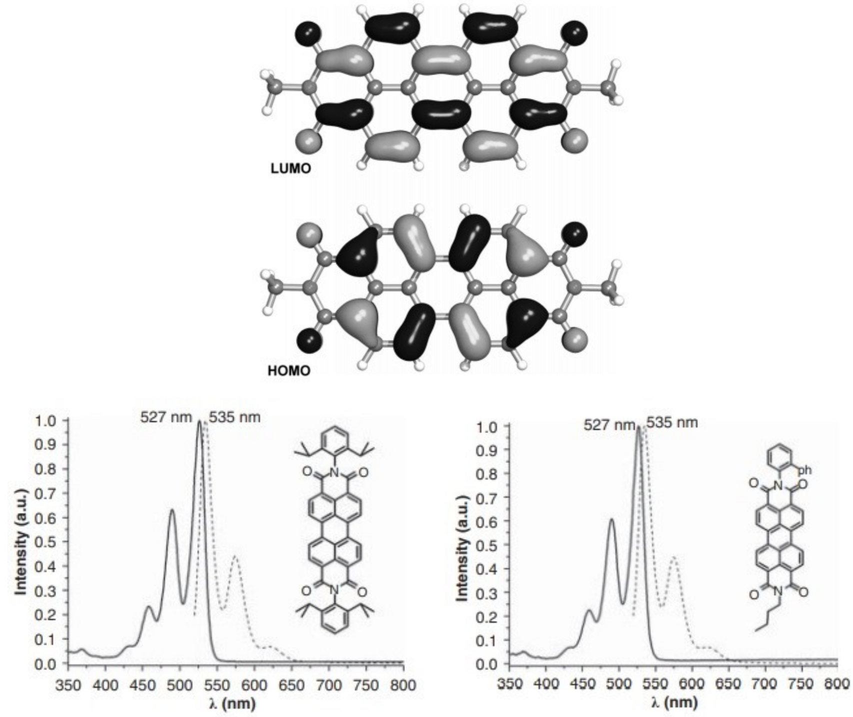

***Fig. 32:** HOMO and LUMO distribution on a peri substituents perylene (left); absorption and emission spectra of symmetrical and asymmetrical peri substituents rylenes(right)*[135]*. Different substituents do not exhibit a specific effect on absorption and emission spectra; the absorption spectrum is perfectly mirrored in emission one and wide vibronic bands are completely distinct.*

Thus, the enhancement of the number of naphthalene moieties in perylene structure should hypothetically generate an ideal organic dye for LSC. However, the extreme extension in *peri* positions promotes planar compounds, losing in solubility and fluorescence efficiency. The loss in efficiency is relative to a peculiar vibronic structure in the transition $S_0 \rightarrow S_1$, allowing coupling between this transition and the vibration mechanisms of the perylene skeleton[136,137]. Nevertheless, the aggregation is enhanced.

To overcome these problems, an alternative approach has been focused extending the *bay*

---

[133] S.K. Lee, Y. Zu, A. Herrmann, Y. Geerts, K. Müllen, A.J. Bard, *J. Am. Chem. Soc.* **1999**, *121*, 3513-20.

[134] C. Huang, S. Barlow, S.R. Marder, *J. Org. Chem*. **2011**, *76*, 2386–2407.

[135] *Solar Energy Nanotechnollogy, Developments in prospective, Organic Fluorophores for Luminescent Solar Concentrators*, **2013**, 317-355 (DOI: 10.1002/9781118845721.ch13).

[136] Z. Chen, U. Baumeister, C. Tschierske, F. Würthner, *Chemistry- - A Eur. J.,* **2007**, *13*, 450–465.

[137] C. Kohl, T. Weil, J. Qu, K. Müllen, *Chemistry*, **2004***, 10*, 5297–5310.

position the molecule . The introduction of four arene substituents, such as phenoxy groups[138], increases the solubility of perylene due to torsion around C-C bond. Furthermore, the extension of the conjugation, along the secondary molecular axis, shows few major advantages compared to unsubstituted PDIs. Modifications on *bay* positions produce an important effect on optical properties in perylene derivatives.

Vibronic structure in absorption and emission spectra decreases, favoring bathochromic shift and larger Stokes shift (for PDIs without bay-substituents is <10 nm), and $S_0 \rightarrow S_2$ UV transition, symmetry forbidden in unsubstituted PDIs. The steric and electronic effect of the substituents changes the position of frontier orbitals, increasing the charge-transfer character of electronic transition. Moreover, the angle torsion in *bay* positions produces an effect of loss of planarity of the perylene core[139].

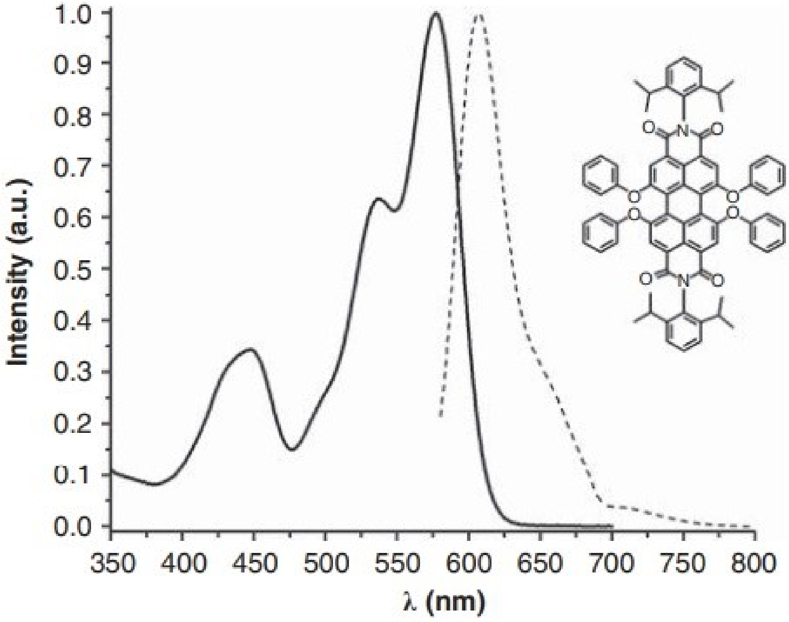

Fig. 32: *Bay-substituents: effect on absorption and emission ranges of typical perylene in PMMA, employed in LSC (Lumogen F Red 305- **LR 305**)*[140].

The most common *bay*-substituted PDIs commercially available are Lumogen F dyes.

Lumogen F dyes are a class of perylene and naphthene derivatives produced by BASF from the '90sa and developed to be employed in organic fluorescent concentrators, due to their ability to absorb and re-emit concentrated light.

In particular, Lumogen F Red 305 (**LR 305**) is widely applied in LSC's. **LR 305** is a perylene diimide (PDI) decorated by two 2,6-diisopropylphenyl groups on the diimide moiety and by two phenoxyl groups on the *bay* position of perylene core. The structure is extremely conjugated and shows two principal transitions, along the two axes of the molecule. Thus, **LR 305** exhibits one intense absorption peak at 578 nm and an emission one at 613 nm in PMMA,

---

[138] H. Quante, P. Schlichtung, U. Rohr, Y. Geerts, K. Müllen, *Macromol. Chem. Phys.*, **1996**, *197*, 4029–44.

[139] J. Hofkens *et al.*, *Chem. Phys. Lett.*, **2001**, *333*, 255–263.

[140] *Solar Energy Nanotechnollogy, Developments in prospective, Organic Fluorophores for Luminescent Solar Concentrators*, **2013**, 317-355 (DOI: 10.1002/9781118845721.ch13).

with a fluorescence quantum yield of 96%. The absorption and emission spectra of **LR 305** are reported in figure 32.

LR 305 is characterized by a moderate solubility, higher than the other rylene derivatives of its class, thanks to the presence of the tetraphenoxy substituents in *bay* sites, and high stability in the polymeric matrix[141]. As demonstrated, its optical performances show a limited change in absorbance (< 7%) and fluorescence (< 10%) after 1.5 years. However, the principal drawback of **LR 305** is a narrow Stoke shift, which is about 30-40 nm. Therefore, the overlap region between absorption and emission spectra is broad, thus, the possibility to observe re-absorption could be high.

High re-absorption could be a limit for the scalability of LSC Lumogen-based. Della Sala and co-workers[142] investigated the impact of re-absorption of **LR 305** in comparison with other organic compounds. The experiment was a typical LSC test, which consisted of the excitation of various parts of the panel, at different distances from the edge. A CCD detector receipted the light signal and quantified the output intensity.

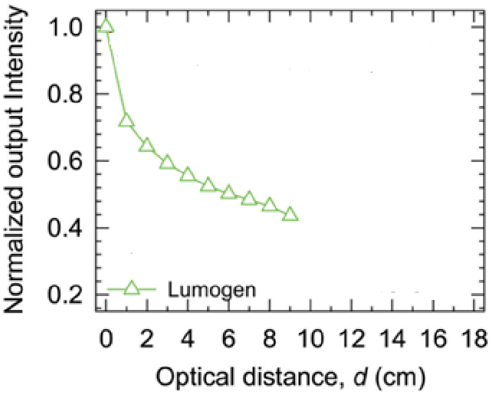

Fig. 33*: Effect of distance on the output intensity trend of Lumogen Red 305, at the edges of typical LSC panel*[143]*.*

The emission intensity decreased of 40% at *d* = 3 cm; while for longer optical distances, output intensity decreased slower (Fig. 33). In these cases, the emission intensity was nearly unaffected by re-absorption, but the detected output luminescence was lower than 50%.

In conclusion, a Lumogen-based LSC is affected by large re-absorption impact, showing a not negligible loss of emission intensity of 50%, for distances longer than 10 cm. The loss of output intensity decreases the emission light that could be absorbed by the PV cell and transformed into photovoltaic energy. Therefore, the scalability of Lumogen-based LSCs is largely influenced by re-absorption processes, with an evident important loss of energy production.

---

[141] G. Seybold, G. Wagenblast, *Dyes and Pigments*, **1989**, *11*, 303–317.

[142] P. Della Sala *et al.*, *Chem. Commun.*, **2019**, *55*, 3160-63.

[143] Adapted from: P. Della Sala *et al.*, *Chem. Commun.*, **2019**, *55*, 3160-63.

2.1.2 FLUOROPHORES WITH ABSORPTION IN UV REGION

This class of fluorophore presents an absorption range between 300 nm to 400 nm. Even if the optical efficiencies of those compounds are far below the LSC full-spectrum luminophores, they result transparent and constitute a hot topic, especially for BIPV applications.

Cycloparaphenylenes (CPPs)

Cycloparaphenylenes (CPPs) are conjugated macrocycles based on a para-linked benzene unit which repeats [*n*] times. CPPs were potential starters for the growth of single-wall carbon nanotubes or the recognition of fullerene, as supramolecular hosts[144].
A very curious feature of CPPs is the independence of absorption range on macrocycle dimensions. They show an absorption centered at 340 nm with a maximum emission in 450-590 nm interval, with an important emission red-shift from *n*=13 to *n*=7. As a result, broad Stokes shifts increase, decreasing the dimensions of macrocycles[145].

Molecular structures and spectroscopic characteristics of **[8]CPP** and **[10]CPP** are reported in figure 35.

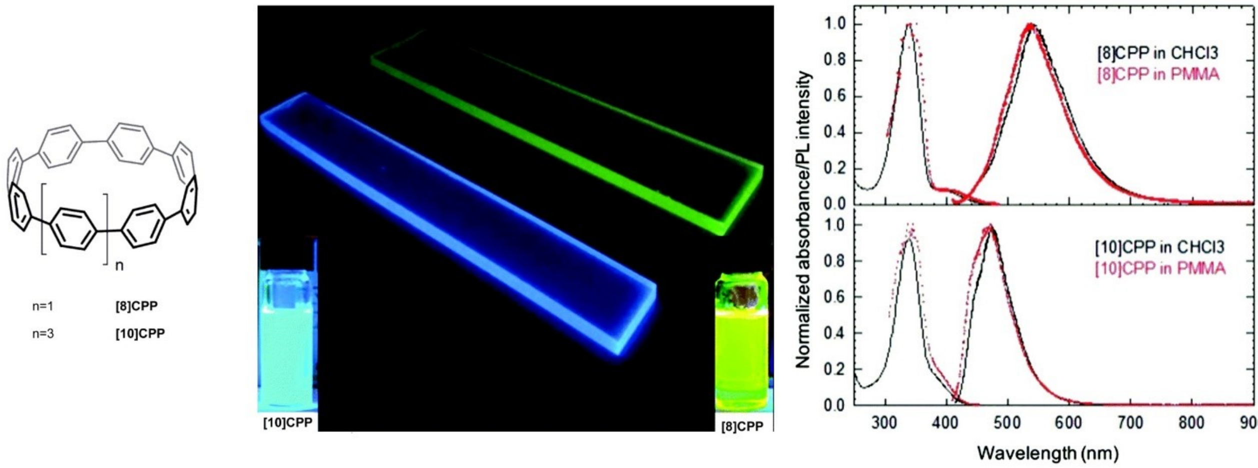

***Fig. 35**: Chemical structure, PMMA films, absorption and emission spectra of **[8]CPP** and **[10]CPP**[145].*

Fluorescence quantum yields are opposite to the Stokes shift trend: Φ_f increases increasing the dimensions of the cycle (from 0.9 for *n*=16 to 0.1 for *n*=8)[146]. Nevertheless, optical efficiency changes significantly with the increasing of dimensions. In particular, there is a discrepancy of a factor of 3, between the 3.8% of **[8]CPP** and 11% of **[10]CPP**. Therefore, **[8]CPP** and **[10]CPP** showed a moderate loss (about 10%) with a stable emission intensity at different amount of fluorophore (300 and 600 ppm). In their cases, the re-absorption was negligible.
A valued advantage of CPPs for BIPV applications is their stable output light intensity in the

---

[144] S.E. Lewis, *Chem. Soc. Rev.*, **2015**, *44*, 2221–2304.
[145] P. Della Sala *et al.*, *Chem. Commun.*, **2019**, *55*, 3160-63.
[146] P. Della Sala, A. Capobianco, T. Caruso, C. Talotta, M. De Rosa, P. Neri, A. Peluso, C. Gaeta, *J. Org. Chem.*, **2018**, *83* (1), 220-227.

function of dimensions of the panel because the phenomenon of re-absorption for these large scale LSCs is limited and negligible, as it is shown in figure 36.

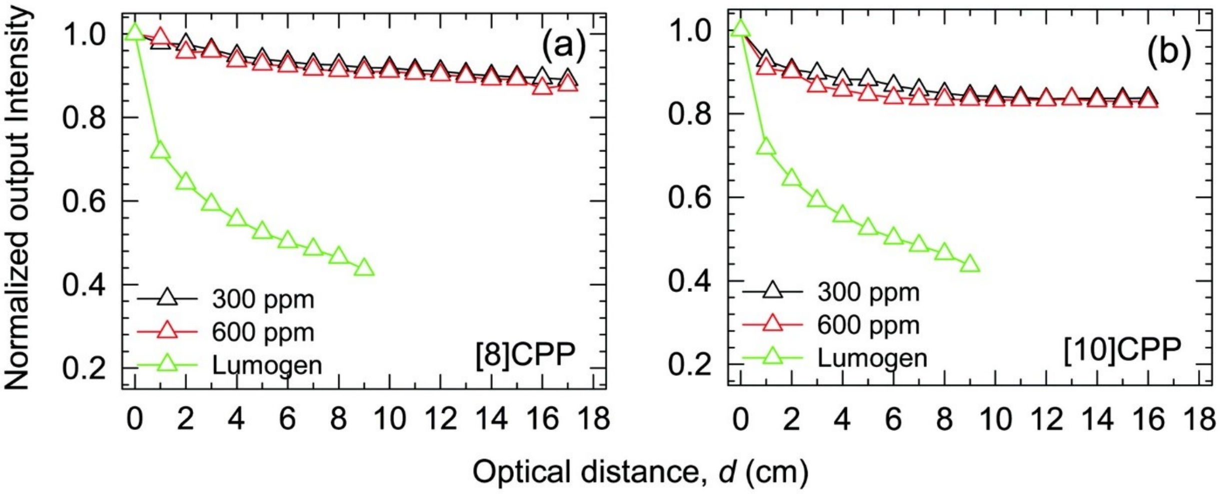

***Fig. 36**: Output light intensity trend of [8]CPP and [10]CPP, comparing to Lumogen Red 305, in function of the distance from the edges of the panel*[147]*.*

p-Phenylenes

Phenylenes are the base of various organic compounds with interesting luminescent and optical properties. In particular, they could be decorated variously on the *para*- and *ortho*-positions with alkyl or aryl substituents. The optical and spectroscopic features could be modulated by playing with the four functional groups. These molecules show two basic absorption transitions, typical of compounds with two molecular axes.

In a recent paper published by Aronica and co-workers[148], phenylenes based on hydroquinone ring showed two maxima of absorption in the UV region (345-403 nm for **1-3**; 334-410 nm for **4-6**), with low Stokes shift and $\mathbf{\Phi_f}$ from 17% to 29%, relative to the increased conjugation of substituents in *ortho*- positions (Fig. 37). Molecules **7** and **8**, which showed an extended π-conjugation due to the introduction of thiophene condensed rings, exhibited a peculiar double absorption spectrum, at 370 nm and 421nm for **7**, at 386 nm and 459 nm for **8**.

---

[147] P. Della Sala *et al.*, *Chem. Commun.*, **2019**, *55*, 3160-63.

[148] a) G. Albano, T. Colli, L. Nucci, R. Charaf, T. Biver, A. Pucci, L.A. Aronica, *Dyes and Pigments*, **2020**, *174*, 108100, 1-8; b) G. Albano, T. Colli, T. Biver, A. Pucci, *Dyes and Pigments*, **2020**, *178*, 108368, 1-11.

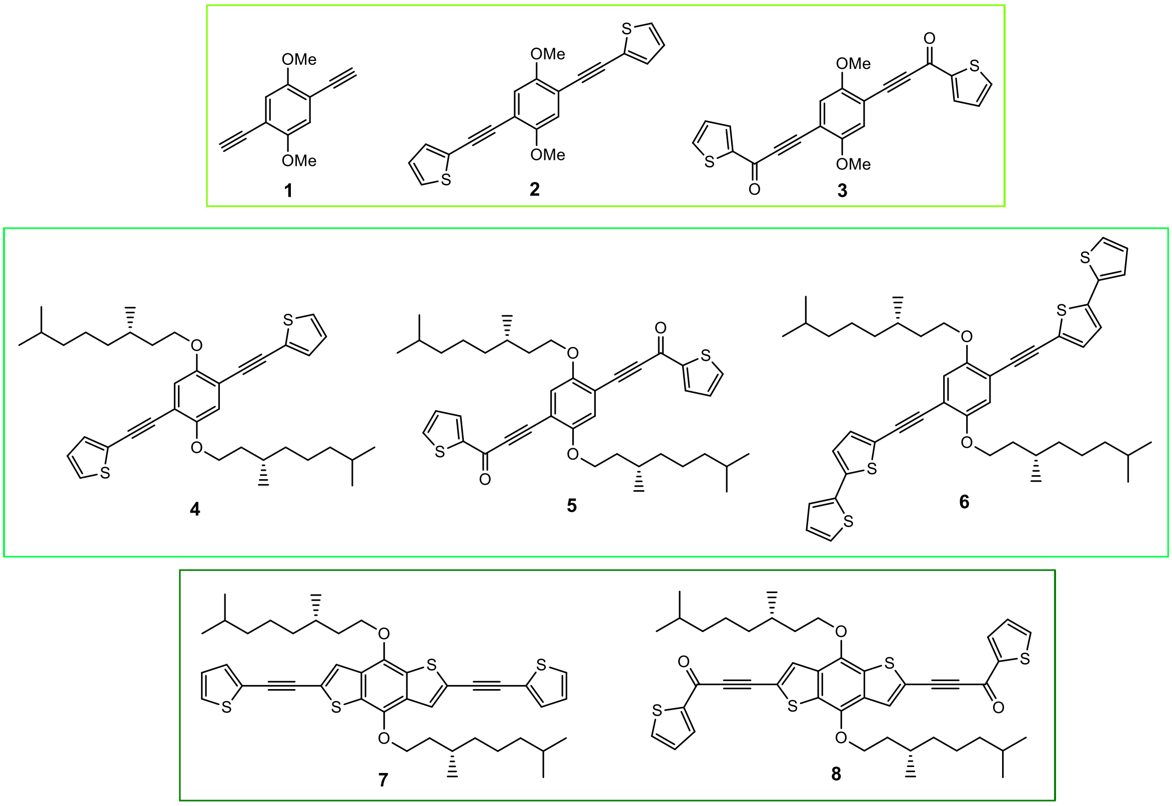

***Fig. 37**: Series of p-phenylenes employed as UV luminophores for LSCs*[25]*.*

Long alkyl chains on the oxygen atoms were introduced to improve the solubility and to reduce the aggregation at the solid state; however, comparing to the corresponding methoxy derivatives, no peculiar shift of absorption and emission maxima was noticed. Instead, the extension of the conjugation on the thiophene moiety in ortho positions produced a bathochromic effect and a rigidity which reduced the probability of de-excitation by non-radiative phenomena. An improvement of the fluorescence quantum yield was observed for derivatives with alkyl chains in comparison with *ortho*-methoxy p-phenylene derivatives (Table 2).

The same effect on spectroscopical and optical characteristics was showed for the benzo[1,2-b:4,5-b']dithiophene (BDT) derivatives **7** and **8**. An electron-rich condensed core such as BDT shifted the two maxima of absorption with a bathochromic effect (370-421 nm and 395-459 nm). However, the $\mathbf{\Phi_f}$ decreased extending the conjugation[149] and didn't exceed the value of 15%.

---

[149] G. Albano, T. Colli, T. Biver, A. Pucci, *Dyes and Pigments*, **2020**, *178*, 108368, 1-11.

Table 2: *Para-ortho-phenylenes spectroscopic and optical features, tested in $CHCl_3$ solution.*

Para-phenylenes	**$\lambda_{max\ abs}$** (nm)	**$\varepsilon_{\lambda max\ asb}$** ($10^4\ M^{-1}\ cm^{-1}$)	**$\lambda_{max\ emis}$** (nm)	**Stokes shift** (nm)	**Φ_f** (%)
1	345	1.0	373	28	12.3
2	377	3.8	409	32	3.3
3	403	1.9	471	68	19.2
4	378	5.7	409	31	21.1
5	334	4.0	472	138	26.0
	410	2.4		62	29.7
6	408	8.5	454	46	29.6
7	370	6.6	485	115	10.6
	421	4.2		64	13.0
8	386	5.5	581	195	10.5
	459	2.4		122	15.3

2.1.3 FLUOROPHORES WITH ABSORPTION NIR REGION

NIR fluorophores are a class of dyes characterized by an absorption range of 650-900 nm, showing usually a high brightness, which is the product of high **ε** and moderate **Φ_f**. The major part of these compounds show a Stokes shift broad enough to avoid light scattering. Therefore, NIR fluorophores are extremely used as biological probes: they are often soluble in water and usually they should not produce aggregated in aqueous solution. They do not interact with biological systems and the absorption and emission ranges are compatible with the absorption of biological tissues and components[150].

As UV fluorophores, the luminescent species of this class are transparent (*TLSC*), but NIR fluorophores show better optical properties, such as high optical efficiency in LCSs devices, for their capacity to absorb in a region of the solar spectrum with a greater fraction of solar photon flux (about 74%)[151].

They find applications as BIPV or in electronic devices on cars and transports. However, their fluorescence quantum yields are lower to 40%[152].

---

[150] a) R. Weissleder, *Nat. Biotechnol.* **2001** , *19* , 316-317; b) V.J. Pansare, S. Hejazi, W.J. Faenza, R.K. Prud'Homme, *Chem. Mater.* **2012,** *24*, 5, 812–827.

[151] Y. Zhao, G.A. Meek, B.G. Levine, R.R. Lunt, *Adv. Optical Mater*., **2014,** *2,* 606-611.

[152] a) G.M. Fischer, M. Isomaki-Krondahl, I. Gottker-Schnetmann, E. Daltrozzo, A. Zumbusch, *Chem.-Eur. J.* **2009**, *15* , 4857-64 ; b) J.C. Ostrowski, K. Susumu, M.R. Robinson, M.J. Therien, G.C. Bazan, *Adv. Mater*. **2003**, *15*, 1296-1300; c) J.O. Escobedo, O. Rusin, S. Lim, R.M. Strongin, *Curr. Opin. Chem. Biol.* **2010**, *14*, 64-70.

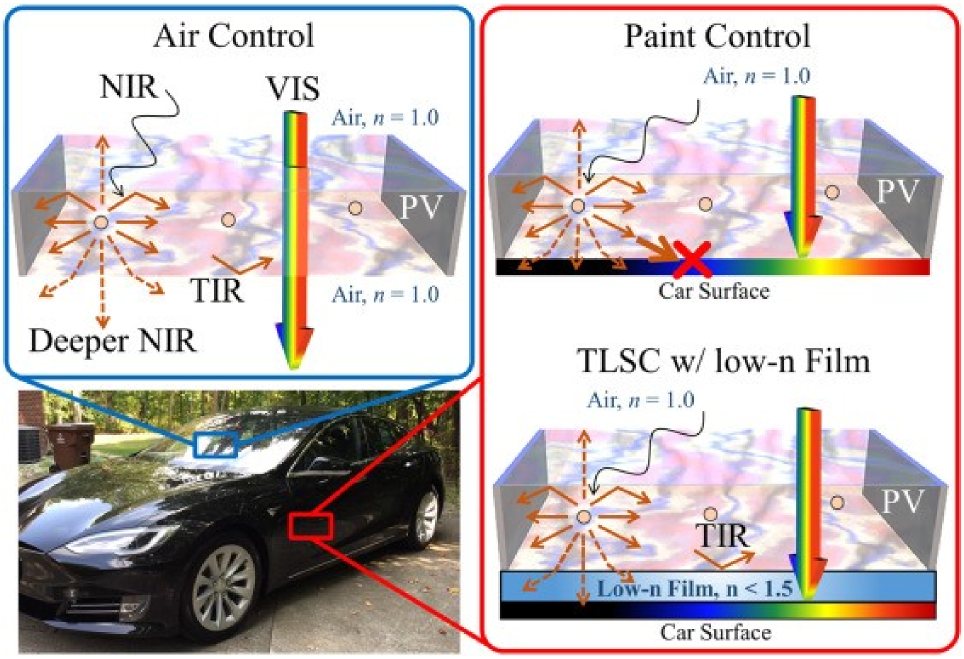

***Fig. 38**: Scheme of NIR TLSC integration onto the window and non-window parts of an automobile[153].*

Carbocyanine dyes

Cyanines are, formally, compounds based on nitrogen atoms, linked by an odd number of methene units[154] and where the two nitrogen atoms are involved in the conjugation. The nitrogen atoms normally take place in a heterocycle moiety, such as indole, benzoxazole or benzothiazole. Carbocyanines are the commonly used chromophores for *in vivo* bioimaging.

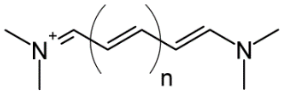

I

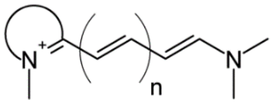

II

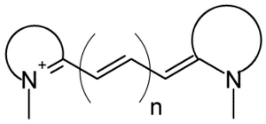

III

***Fig. 39:** Molecular structure of cyanines classes, based on N-substituent (amine or heterocycle) and on the odd number of methene linker[155].*

Cyanines are characterized by long absorption and emission wavelengths (490-740 nm absorption range; 500-770 nm emission range), significant tunability of emission and absorption ranges, depending on the number of methene groups or the extension of aromatic conjugation. They are characterized by high **ε** (around 10^5 M^{-1} cm^{-1}), good solubility in water

---

[153] C. Yang, D. Liu, A. Renny, P.S. Kuttipillai, R.R. Lunt, *Journal of Luminescence*, **2019**, *210*, 239–246.
[154] A. Mishra, R.K. Behera, P.K. Behera, B.K. Mishra, G.B. Behera, *Chem. Rev.*, **2000**, *100*, 1973-2011.
[155] "Discovery of New Synthetic Dyes: Targeted Synthesis or Combinatorial Approach?"- In Demchenko, Alexander P. (ed.). *Advanced Fluorescence Reporters in Chemistry and Biology I*

and, not secondarily, relative simple synthesis. The mean drawback is the small Stokes shift, which decreases with the number of methane units and consequently involves a drastic loss in fluorescence quantum yield, on account of larger non-radiative decays. However, a low-moderate improvement of fluorescence quantum yield is observed with methylene linker elongation (Figure 40 and Table 3)[156].

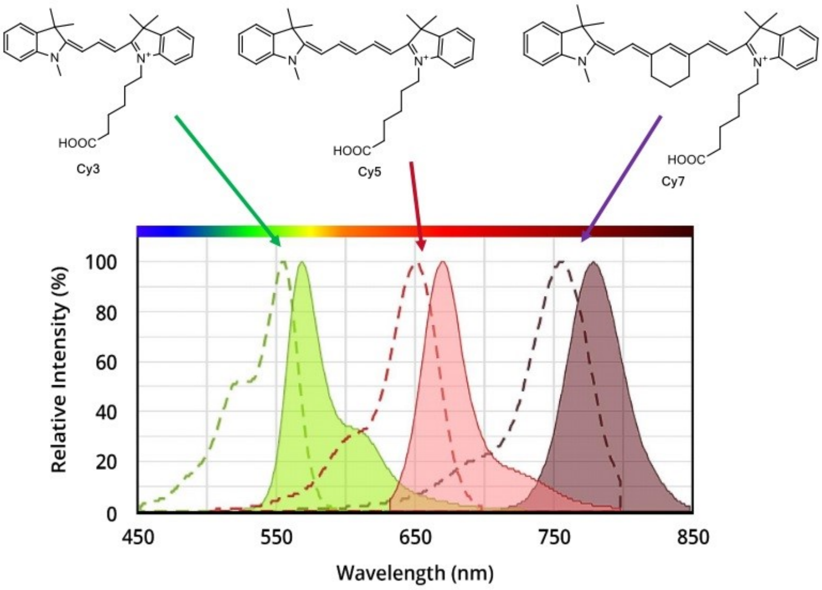

Fig. 40: *Absorption and emission spectra of the principal cyanines (**Cy3, Cy5, Cy7**)*[157].

Table 3: *Spectroscopic and optical properties of some typical employed cyanines.*

Cyanine	$\lambda_{max\ abs}$ (nm)	$\varepsilon_{\lambda max\ asb}$ (10^4 M^{-1} cm^{-1})	$\lambda_{max\ emis}$ (nm)	Stokes shift (nm)	Φ_f (%)
Cy3	550 (512)	15	570 (615)	20 (103)	15
Cy5	650 (625)	25	670	20 (45)	27
Cy7	754	25	767	13	28

Cyanines are used for *TLSC* application, as NIR-selective harvesting chromophores[158]. An interesting cyanine dye was **Cy7**, which showed absorption and emission spectra centred in 760 nm and 787 nm, in DCM solution, and 762 nm and 788 nm, in the polymer matrix (PBMMA). Its **Φ_f** was 24% in DCM solution and 19% in PBMMA. Even if the fluorescence quantum yield in both conditions was not high, **Cy7** found applications on a series of arbitrary surfaces, such as window and no-window parts of an automobile, such as electrical sensors for BAS (Brake Assistant System).

---

[156] a) R.B. Mujumdar, L.A. Ernst, S.R. Mujumdar, C.J. Lewis, *Bioconjugate Chemistry*, **1993**, *4* (2), 105–111; b) M. Levitus, S. Ranjit, *Quarterly Reviews of Biophysics*, **2011**, *44* (1), 123–151.

[157] Adapted from: https://www.aatbio.com/catalog/chemical-reagents-cy-cyanines.

[158] C. Yang, D. Liu, A. Renny, P.S. Kuttipillai, R.R. Lunt, *Journal of Luminescence*, **2019**, *210*, 239-246.

Actually, one of the last work on cyanines for LSC applications reported optical properties of two promising cyanines derivatives in the NIR fluorophores field: 2-[7-(1,3-dihydro-1,3,3-trimethyl-2H-indol-2-ylidene)-1,3,5-heptatrienyl]-1,3,3-trimethyl-3H-indolium iodide (**HITCI**) and 1-(6-(2,5-dioxopyrrolidin-1-yloxy)-6-oxohexyl)-3,3-dimethyl2-((E)-2-((E)-3-((E)-2-(1,3,3-trimethylindolin-2-ylidene)ethylidene)cyclohex-1-enyl)vinyl)-3H-indolium chloride (**CY**)[159] (Fig. 41).

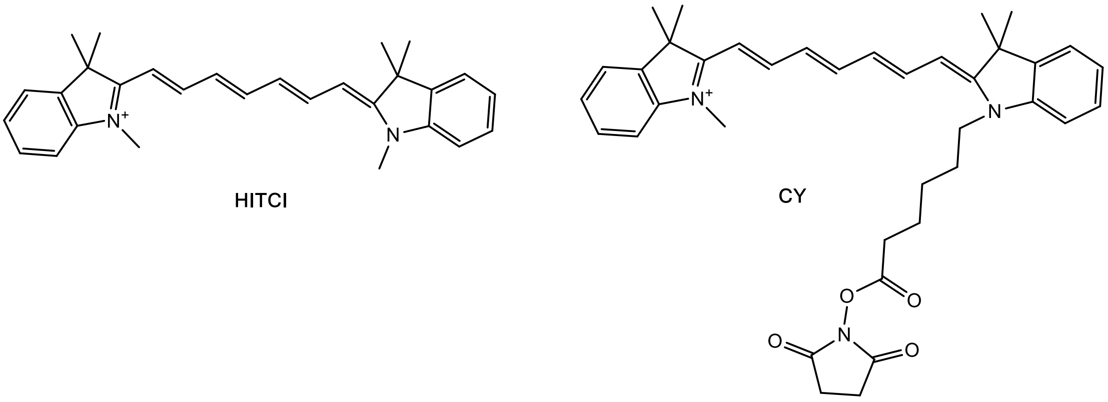

***Fig. 41:** Molecular structure of **HITCI** and **CY**, cyanines derivatives for TLSC[160].*

However, their LSC performances were negatively influenced by the small Stokes shift (20 nm for **HITCI** and 30 nm for **CY**).

CO$_i$8DFIC (O6T-4F)

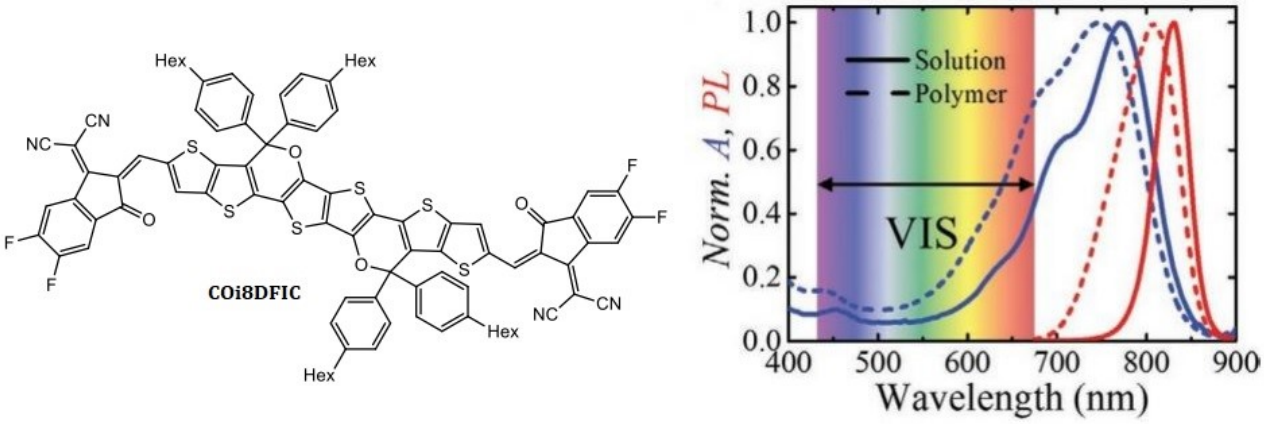

***Fig. 42:** Molecular structure of **CO$_i$8DFIC** and the absorption and emission spectra in different conditions (chlorobenzene solution or polymeric matrix)[161].*

CO$_i$8DFIC has been developed as a non-fullerene organic acceptor for application in photovoltaic devices[161]. It is a highly efficient n-type compound with low-bandgap and strong NIR absorption. Moving from the solution to the polymer matrix, absorption peak shifts from

---

[159] Y. Zhao, G.A. Meek, B.G. Levine, R.R. Lunt, *Adv. Optical Mater*. **2014**, *2*, 606–611.

[160] C. Yang, D. Liu, A. Renny, P.S. Kuttipillai, R.R. Lunt, *Journal of Luminescence*, **2019**, *210*, 239-246.

[161] C. Yang, M. Moemeni, M. Bates, W. Sheng, B. Borhan, R.R. Lunt, *Adv. Optical Mater.*, **2020**, *8*, 1901536.

770 nm to 745 nm and the emission ones from 831nm to 808 nm, showing a hypsochromic effect (Fig. 42). The **Φ_f** remains just the same (from 23% to 25%). Here, the re-absorption processes and non-radiative losses are limited by a high **Φ_f** (comparing with NIR luminescent species for LSCs) at a low bandgap. Actually, **CO_i8DFIC** is the TLSC is the best fluorophore for LSC application due to the good device scalability at the highest visibly transparency.

2.2 AIM OF WORK

This work has been focused on the design of new organic fluorophores for LSC devices.
In particular, we considered visible light molecules, with a specific donor-acceptor-donor (D-A-D) structure. Such molecules always consist of electron rich donor moiety (D) bounded in a conjugated system with an electron-poor acceptor (A). During the excitation process there is a intramolecular charge transfer (ICT) from the donor part of the molecules to the acceptor moiety.
D-A conjugated copolymers have received the attention of several research groups in the last decades, due to their attractive electronic and optoelectronic properties, easily applyed for different applications[162]. A molecule with strong intramolecular charge transfer (ICT) shows low band gap. Improving the ICT effect, compared to the conventional D-A molecules, the introduction of another electron donor group (D-A-D', where D'=D or different donor group) produced a stronger ICT effect and lower band gap and consequently bathochromic shift[163]. These types of chromophores are particularly interesting because their band gap level and other properties (absorption and emission maxima, quantum yield, and solubility) can be tuned through a variety of donor and acceptor substituents.
During this work, three D-A-D molecular structures were designed where benzo[1,2-d:4,5-d']bisthiazole, pyrazine and 1,2,3-benzothiadiazole were selected as electron-poor cores (A). Such choice was due to their different acceptor strength and for the interesting and peculiar spectroscopic and optical features. Moreover, easily synthetic approaches were developed to support their employment in LSC devices.

The first part of this work was focused on benzo[1,2-d:4,5-d']bisthiazole derivatives (**BBT**s). **BBT** core was used to prepare several molecules, in order to evaluate the impact different donor substituents on electronic and optical properties (Fig. 44).
First of all the presence and the position of alkyl chains in the acceptor core was evaluated (**BBT1** and **BBT2**). Due to the best-performing of **BBT1** such core was used to develop three novel D-A-D chromophores (**BBT5-7**). Furthermore, the effect of an acceptor moiety at the edge of the molecules has been evaluated both in symmetrical and asymmetrical structures (**BBT3** and **BBT4**).

---

[162] Y Wang, Q Peng, Z Li, P He, B Li, *J. Mol. Model.* ,**2012**, *18,* 4291–98.
[163] a) G. Qian *et al.*, *Chem. Mater.* **2008**, *20*, 19, 6208–16; b) T. Tao, B. Bin Ma, Y.X. Peng, X.X. Wang, W. Huang, X.Z. You, *J. Org. Chem.* **2013**, *78*, 8669–79.

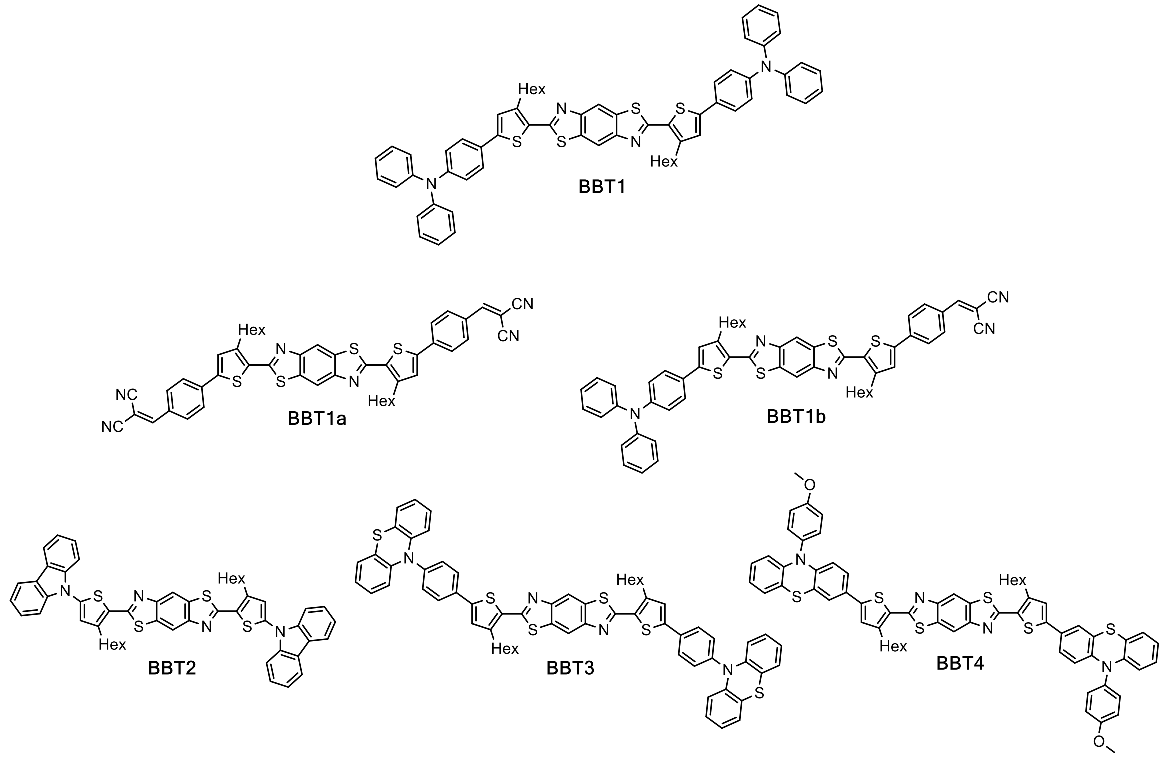

Fig. 44: *Molecular structures of* ***BBT****-based organic fluorophores for LSC applications, developed in this work.*

In the second part of the work, another series of organic LSC compounds was designed, based on a stronger acceptor core such as quinoxaline (**DQ**, Fig. 45). Such core was considered because quinoxaline derivatives show absorption and emission maxima respectively around 450 nm and 550 nm, in solution, with a negligible effect of solvents and moderate fluorescence quantum yield (see Table 4). For their color control, high fluorescence efficiencies, easy preparation and thermal and photochemical stability, **DQ**s are often applied as full-color emitting materials for OLEDs[164]. Furthermore, the ICT promotes a low band gap and consequently, re-absorption and fluorescence quenching impacts are reduced[165]. Thus, **DQ** is a very versatile acceptor moiety, and tuning of the electronic properties can be possible extending the conjugation of the **DQ** core, along the two molecular axes.

---

[164] *J. Org. Chem.*, **2009**, *74,* 3175-78.

[165] X. Lu, S. Fan, J. Wu, X. Jia, Z.S. Wang, G. Zhou, *J. Org. Chem.*, **2014,** *79*, 6480-89.

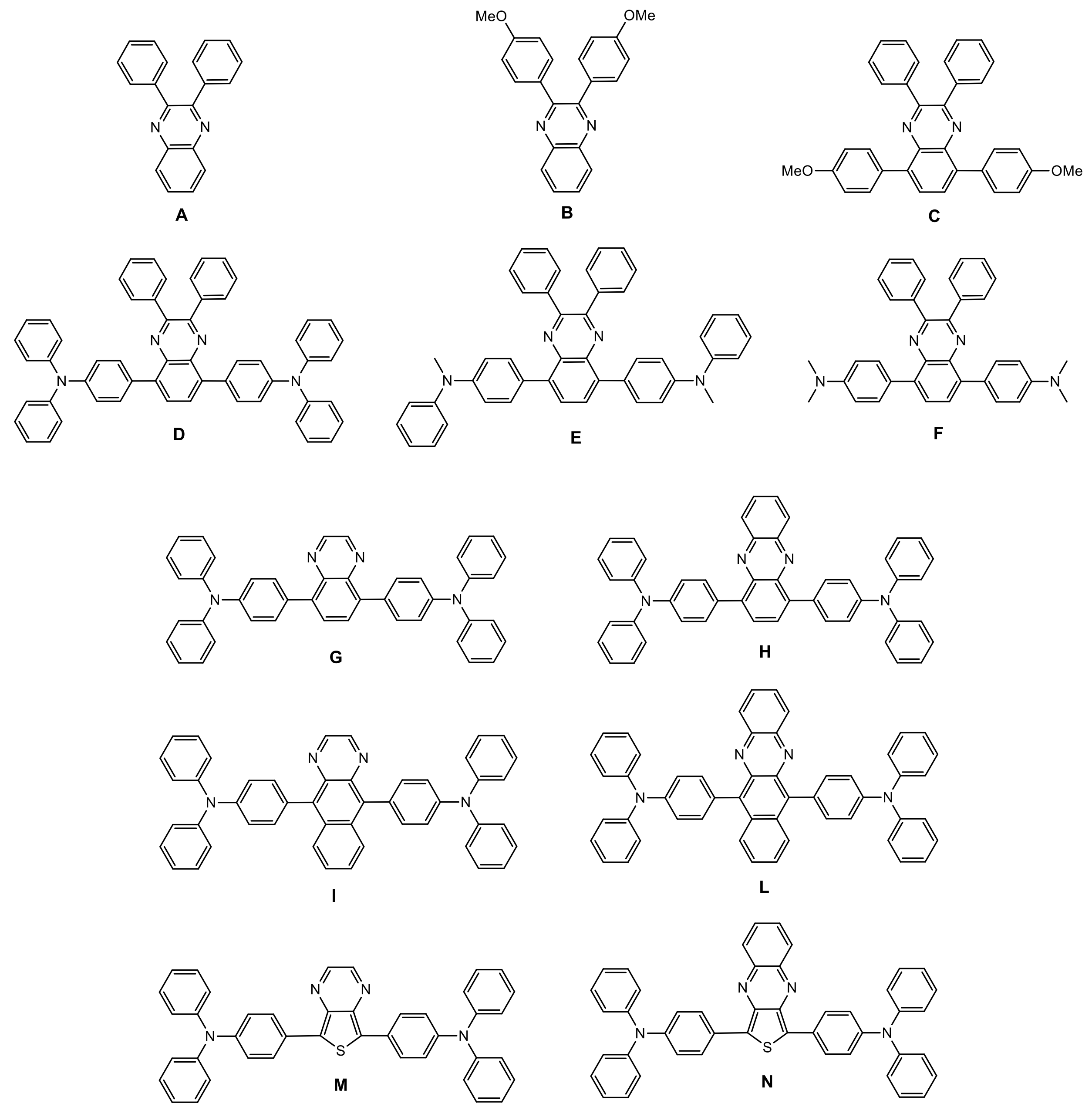

Fig. 45: *Quinoxaline derivatives molecular structures, with different electron-rich donor moiety (****A****-****F****) and electron-poor acceptor moiety (****G****-****N****).*

Table 4: *Optical properties of quinoxaline molecules, in solution, never employed in LSC devices.*

	$\lambda_{max\ abs}$ (nm)	$\lambda_{max\ emis}$ (nm)	Stokes shift (nm)	Φ (%)
A	344	398	54	-[a]
B	368	430	62	18
C	366	502	136	57
D	437	570	133	51
E	476	640	164	1
F	443	597	154	30
G	413	557	144	/[b]
H	493	642	149	/[b]
I	455	590	135	/[b]
L	560	680	120	/[b]
M	544	684	140	/[b]
N	716	-[c]	-	/[b]

a) It was difficult to measure this value due to its low intensity.
b) Not report in the corresponding article.
c) Not detectable with spectrophotometer.

In this part of work, five new chromophores were designed with D-A-D structure, in order to evaluate the effect of donor group and substituents on pyrazine ring effects were evaluated on optical properties (Fig. 46).

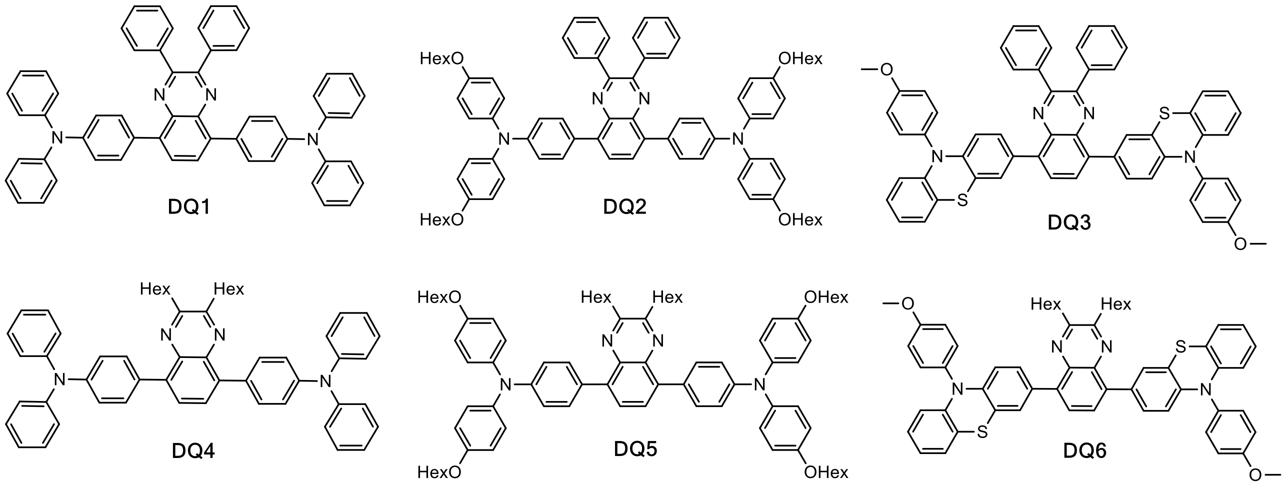

Fig. 46: *Molecular structure of quinoxalines derivatives, developed in this work.*

Finally, the third part of this work was focused on the development of a specific organic molecule, which could be applied as LSC chromophore embedded in large-scale cultivation system for algae.

Algae are a natural resource with a high potential for current commercial products in various diffuse industrial fields, such as biofuels, drugs and food; nevertheless, algae are a tool for carbon dioxide mitigation.

To combine the industrial production of algae and the application of LSC as BIPV, our attention was focused on the design of organic fluorophore, which could be prepared in a very simple and cheap procedure and could be complementary with spectroscopic characteristics of chlorophyll of green algae. In other words, keeping in mind that all algae contain chlorophyll, the natural pigment photosynthetically active, with a peculiar double peaks absorption spectrum of chlorophyll (around 430 nm and 660 nm), we need a perfectly designed complemental absorption range for a LSC fluorophore to be applied for algae production, which should absorb in the spectral window of 460-630 nm.

Thus, compounds **LSCA1** and **LSCA2** were designed and synthetized through an eco-friendly approach (direct arylation coupling). A preliminary spectroscopic characterization, showed suitable optical properties for the desired application (Fig. 47).

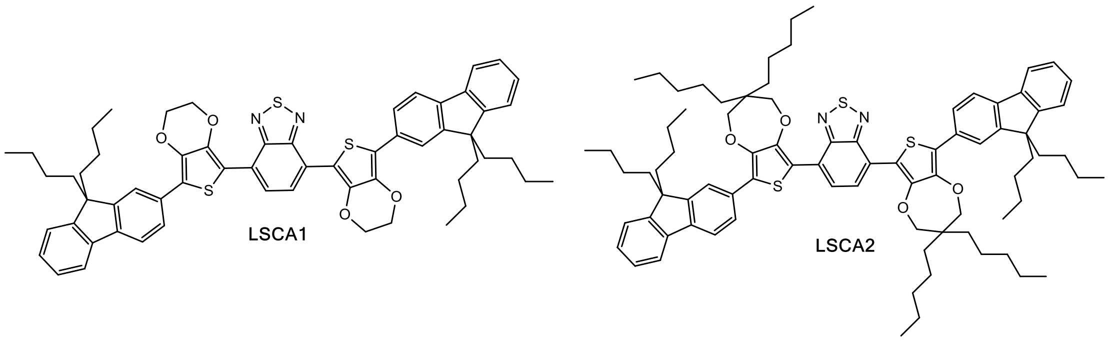

Fig. 47: *Molecular design of* ***LSCA*** *chromophores, for algae production.*

In the last chapter of this work, a new synthetic procedure, based on Green Chemistry approach, was investigated to be applied to prepare some important intermediates. This part of the work was developed during a three months stage at research group of D.J. Ramon from Universidad de Alicant (Alicante) – Spain. The possibility to obtain final products or intermediates with simple and cheap synthetic steps actually is based on the use of volatile organic compounds (VOCs) as solvents. Their low compatibility with new sustainable approach makes VOCs not the first choice of Green Chemistry.

Some known and commonly used cross-coupling organic reactions, such as Suzuki-Miyaura, Sonogashira, Heck and Stille reactions, have already investigated in this eco-friendly synthetic approach, reporting good and moderate results on different substrates. Such reactions are often the main tool to develop new molecules for optoelectronics application.

In particular, arylboronates are very versatile building blocks for organic synthesis, especially used in Suzuki-Miyaura cross coupling reaction. Methods that can synthesize arylboronates are highly demanded and, in this part of the work, Miyaura borylation was tested for the first time in deep eutectic solvent.

Finally, direct arylation coupling has been recently developed as a new synthetic tool, highly appealing froma green chemistry point of view, exhibiting atom economy and considerably reduced *E-factor*, compared to other typical organic cross coupling reactions.

Starting from the synthetic approach involved for **LSCA1** and **LSCA2** (developed in chapter 5), direct arylation was investigated in some common green solvents, to evaluate their compatibility with this novel synthetic strategy.

CHAPTER 3

DESIGN and SYNTHESIS of BENZO[1,2-d:4,5d’]BISTHIAZOLES-BASED LUMINOFHORES

3 BENZO[1,2-D:4,5-D’]BISTHIAZOLES

Benzo[1,2-d:4,5-d’]bisthiazoles (BBTs) are very versatile heterocyclic cores, which could be decorated with several moyieties to extend their conjugation. The synthesis of BBT was reported for the first time in 1903[166]. Subsequent studies showed an incorrect assignment the molecular structure and showed an alternative procedure to obtain BBT compounds[167,168]. Due to their spectroscopic features, BBTs were investigated for nonlinear optics[169] and organic optoelectronics applications[170]. Further investigations reported many applications as fluorescent probes[171], NIR chromophores[172] and liquid crystal precursors[173]. Furthermore, BBTs found a successful employment in solar cells and field-effect transistors, being used as organic photoactive doping in the polymeric matrix[174]. Finally, BBTs were investigated as photosensitizers for DSSC technology, as π-bridge in the widely used D-π-A structure based dyes.[175].

The first BBT derivative for LSC application, in this work, was tested in 2018. In this case, the design of the molecule showed a symmetrical structure, D-A-D, where the donor groups were triphenylamine, bounded through a thiophene bridge to the acceptor BBT core.

3.1 BBT1: THE STARTING POINT

The first D-A-D molecule BBT-based was designed in 2018, **BBT1**. The electron-poor benzo[1,2-d:4,5d’]bisthiazole core was decorated with electron-rich triphenylamine groups, connected *via* thiophene ring as π-bridge. Alkyl chains were placed on the thiophene to increase the solubility of the molecule.

First of all, **BBT1** was analysed through Density Functional Theory (DFT) and time-dependent DFT (TD-DFT) methods, performed in collaboration with Prof. Adalgisa Sinicropi of the University of Siena.

Remarkably, observing BBT’s tridimensional structure of the first excited singlet state, S_1 (Fig. 48), the dihedral angles between the thiophene and triarylammine moieties was 23.7°, due to

---

[166] A. G. Green, A. G. Perkin, *J. Chem. Soc.* **1903**, *83*, 1201-12.

[167] a) A. I. Kiprianov, F. A. Mikhailenko, Chem. Heterocycl. Compd. 1967, 3, 205-209; b) J. K. Landquist, J. Chem. Soc. C 1967, 2212-20; c) G. Grandolini, A. Martani, A. Ricci, N. Cagnoli-Bellavita, Ann. Chim. 1968, 58, 91; d)) S. L. Solar, R. J. Cox, N. J. Clecak, R. Ettinger, J. Org. Chem. 1968, 33, 2132-33.

[168] a) A. I. Kiprianov, F. A. Mikhailenko, I. L. Mushkalo, Chem. Heterocycl. Compd. 1970, 6, 1340; b) J. F. Mike, J. J. Interman, A. Ellern, M. Jeffries-EL, J. Org. Chem. 2010, 75, 495-497.

[169] a) J. A. Osaheni, S. A. Jenekhe,, Chem. Mater. 1992, 4, 1282-90; b) J. A. Osaheni, S. A. Jenekhe, Chem. Mater. 1995, 7, 672-682; c) S.- H. Lee, A. Otomo, T. Nakahama, T. Yamada, T. Kamikado, S. Yokohama, S. Mashiko, J. Mater. Chem. 2002, 12, 2187-88.

[170] a) M. M. Alam, S. A. Jenekhe, Chem. Mater. 2002, 14, 4775-80; b) H. Pang, F. Vilela, P. J. Skabara, J. J. W. McDouall, D. J. Crouch, T. D. Anthopoulos, D. D. C. Bradley, D. M. de Leeuw, P. H. Horton, M. B. Hursthouse, Adv. Mater. 2007, 19, 4438-42; c) I. Osaka, K. Takimiya, R. D. McCullough, Adv. Mater. 2010, 22, 4993-97.

[171] S. Yao, H.-Y. Ahn, X. Wang, J. Fu, E. W. Van Stryland, D. J. Hagan, K. D. Belfield, J. Org. Chem. 2010, 75, 3965-74.

[172] G. M. Fischer, E. Daltrozzo, A. Zumbusch, Angew. Chem. Int. Ed. 2011, 50, 1406-09.

[173] H.-H. G. Tsai, L.-C. Chou, S.-C. Lin, H.-S. Sheu, C. K. Lai, Tetrahedron Lett. 2009, 50, 1906-10.

[174] a) E. Ahmed, F. S. Kim, H. Xin, S. A. Jenekhe, Macromolecules 2009, 42, 8615-18; b) E. Ahmed, S. Subramaniyan, F. S. Kim, H. Xin, S. A. Jenekhe, Macromolecules 2011, 44, 7207-19.

[175] A. Dessì *et al.*, Eur. J. Org. Chem. 2013, 1916–28.

low sterical hindrance of the alkyl chain on thiophene portion of **BBT1**.

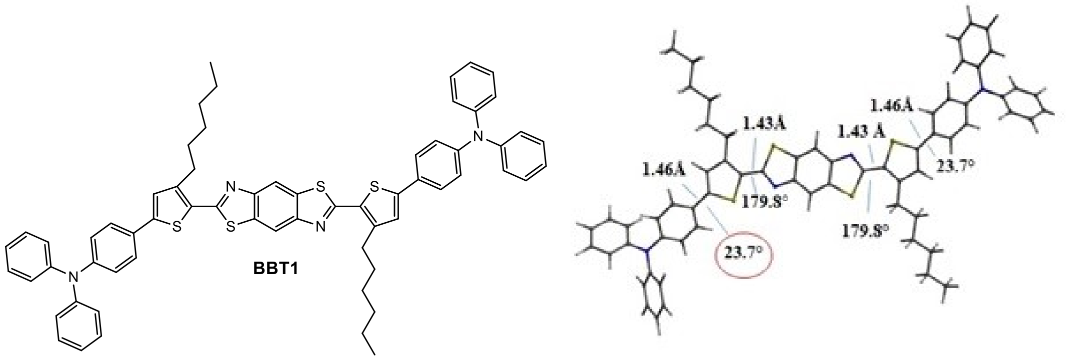

Fig. 48: *Molecular structures and tridimensional structure of the first excited singlet state, S_1, on **BBT1**: dihedral angles and distances of bonds.*

A lower dihedral angle between thiophene ring and triarylamine substituent exhibited a more planar system in the excited state S_1, which could promote higher optical properties, such as bathochromic shift, fluorescence quantum yield and large Stokes shift. Such behaviour is observed in case of **BBT1,** which showed a planar S_1, maintaining a high conjugated structure in the excited state.

Calculated optical properties of **BBT1** were reported in table 5, for its transition $S_0 \rightarrow S_1$ in EtOH and in PMMA. Firstly, no evident difference between solution and PMMA values was observed. **BBT1** exhibited an absorption around 446 nm, which corresponded to 2.77 eV.

The frontier molecular orbitals (FMOs) involved in the lowest energy transition (HOMO→LUMO), were also calculated, showing that the $S_0 \rightarrow S_1$ transition in **BBT1** was characterized by an *intra*molecular charge transfer (ICT).

In general, a charge transfer process is an electronic dislocation from an electron-rich donor moiety to an electron-poor acceptor one, generating a charge separation. Charge transfer from an electron-rich donor moiety to an electron-poor acceptor one located in different molecules is known as *inter*molecular charge transfer. While, if donor and acceptor moieties belong to the same molecule, this phenomenon is called *intra*molecular charge transfer. Such effect generally occurs after a photoexcitation state, due to the absorption of light, at a specific wavelength. The photoexcitation favors an electron transfer from one part of the molecule to another, generating a charge distribution in the excited state, markedly different from the ground state one[176]. Such effect can be improved with the addition of a π-bridge, between donor and acceptor groups, as it happens in our case with the thiophene moiety.

---

[176] R. Misra, S.P. Bhattacharyya, *Intramolecular Charge Transfer : Theory and application,* **2018**, Wiley-VCH Verlag GmbH & Co. KGaA.

Table 5: *TDDFT (MPW1K/6-311+G(2d,p)) absorption maxima ($\lambda_{max\ abs}$ in nm), excitation energies (E_{exc} in eV), oscillator strengths (f) and contributions (%) to the $S_0 \rightarrow S_1$ transition in EtOH and PMMA of compounds **BBT1** .*

Compounds	**Medium**	**$\lambda_{max\ abs}$ (nm)**	**E_{exc} (eV)**	**f**	**Transition H→L (%)**
BBT1	EtOH	446.32	2.77	3.13	78
	PMMA	446.02	2.77	3.16	79

On account with calculation of transition $S_0 \rightarrow S_1$, **BBT1** was analysed with Linear Response – Polirisable Continuum Model (LR-PCM) computed emission maximum, reported in table 6.

Table 6: *TDDFT (MPW1K/6-311+G(2d,p)) emission maxima ($\lambda_{max\ abs}$ in nm), excitation energies (E_{exc} in eV), oscillator strengths (f) and contributions (%) to the $S_1 \rightarrow S_0$ transition in EtOH and PMMA of compounds **BBT1**..*

Compounds	**Medium**	**$\lambda_{max\ em}$ (nm)**	**E_{exc} (eV)**	**f**	**Transition L→H (%)**
BBT1	EtOH	530.44	2.33	3.29	87
	PMMA	526.78	2.35	3.28	87

The calculate emission maximum of **BBT1** was around 530 nm, with comparable values from solution and PMMA values, with a Stokes shift of 0.44 eV.
BBT1 was synthesized following the procedure reported in scheme 1.

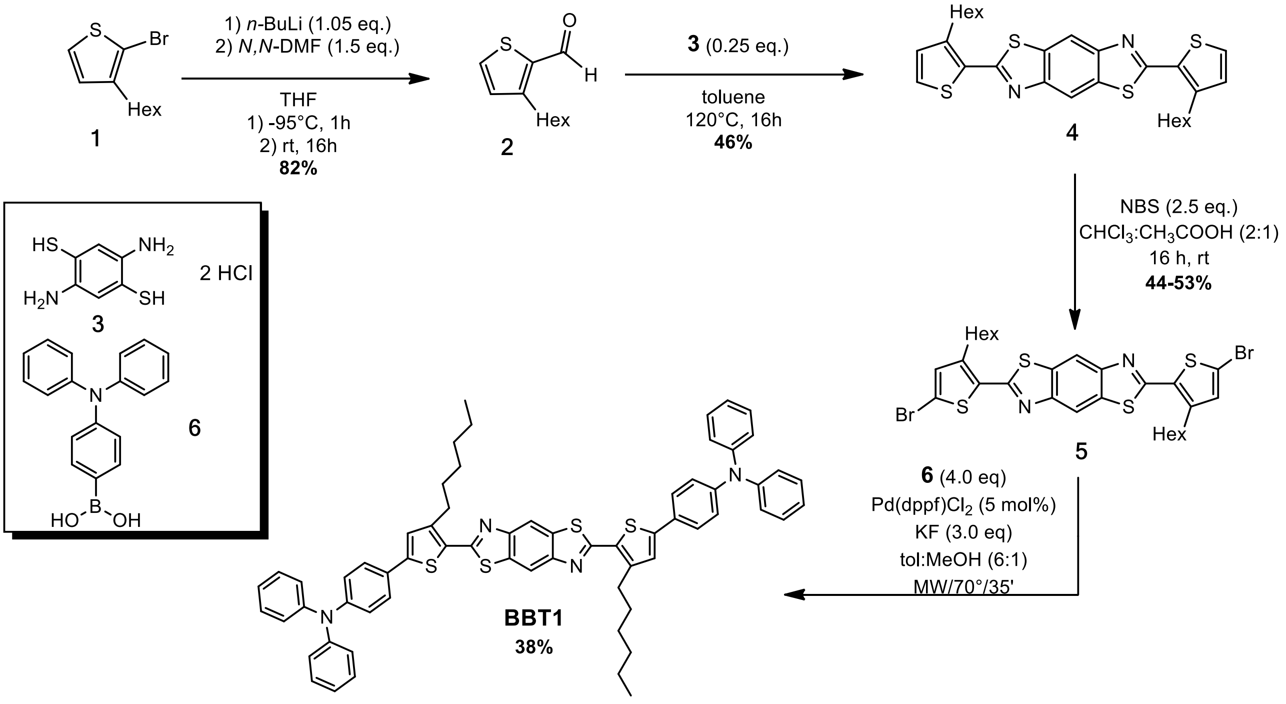

***Scheme 1:** Synthesis of BBT core, employed for **BBT1**.*

Commercially available bromide (**1**) was converted in the corresponding aldehyde (**2**), following a known synthetic procedure[177]. The BBT tricyclic core was obtained by reacting aldehyde **2** with 2,5-diaminobenzene-1,4 dithiol bis-hydrochloride (**3**), in toluene at 120°C for 16h. The choice of anhydrous toluene as solvent, rather than anhydrous *N,N*-DMF as previously reported, allowed a simpler recovery of compound **4** by precipitation in the reaction solvent.

The key dibrominated intermediate (**5**) was then obtained in a moderate yield, through reaction with NBS in a mixture $CHCl_3$:AcOH (2:1) at room temperature, taking care of shielding the reaction from the light. A purification through crystallization was not easy, due to the similar solubility of **4** and **5** in organic solvents. The purification by flash chromatography allowed obtaining dibromide **5** although in moderate yield. Probably, the combination of the low solubility of brominated intermediate and the acid interactions with SiO_2 caused the crystallization of part of the product during the chromatography, hampering its complete recovery.

Finally **BBT1** was obtained through a Suzuki-Miyaura cross coupling reaction, under MW irradiation. Pd(dppf)Cl_2 and KF were employed as catalyst and base, respectively, working in a mixture of toluene and MeOH (6:1), obtaining the final product **BBT1** with moderate yield.

The new compound **BBT1** was spectroscopically characterized.

UV-vis spectra of **BBT1** was recorded in EtOH solution, showing a trend which was in agreement with the DFT calculations, exhibiting absorption and emission maxima at 446 nm and 540 nm (Fig. 49). Moreover, a large Stokes shift was observed, with limited re-absorption impact in solution samples (Table 7).

BBT1 showed broad Stokes shift and high fluorescence quantum yield (68% in EtOH), which

---

[177] E.H. Elandaloussi, P. Frère, P. Richomme, J. Orduna, J. Garin, and J. Roncali, *J. Am. Chem. Soc.* **1997**, *119*, 10774–84.

are very interesting optoelectronic characteristics for LSC application.

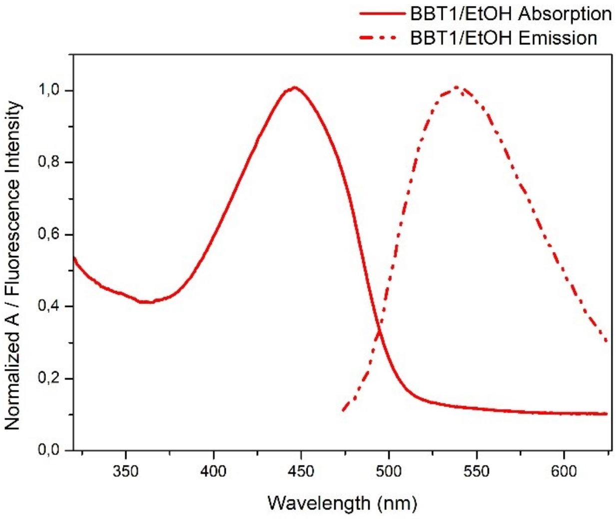

Fig. 49: Normalized absorption and emission spectra in EtOH solution of ***BBT1.***

Table 7: Optical properties in EtOH solution of ***BBT1.***

BBT derivative	$\lambda_{max\ abs}$ (nm)	$\varepsilon_{\lambda max\ asb}$ ($M^{-1}\ cm^{-1}$)	$\lambda_{max\ emis}$ (nm[eV])	Stokes shift (nm)	Φ_f (%)
BBT1	446	14530	540 [0.48]	94	68

BBT1 was then employed in PMMA films and its optical properties and performances were evaluated. Such experiments have been performed in collaboration with Prof. A. Pucci of the University of Pisa.

Polymer films of **BBT1** were designed with different concentration from lower concentration 0.2 wt% to the higher 1.4 wt%; all of them showed high homogeneity, corresponding to a good dispersion and compatibility of **BBT1** in PMMA.-The molecular absorption maximum of **BBT1** was about 450 nm with a broad band at 370-510 nm, comparable with its values in solution. No evident shifting and shape modificationin the absorption spectra, typically attributed to the formation in situ of aggregates, were observed. The enhanced matrix compatibility with **BBT1**, allowed a very low re-absorption effect. Finally, a linear trend between **BBT1** increased content in PMMA films and increased absorbance intensity was observed (Fig. 50**a**).

On the contrary, emission maxima of **BBT1** in PMMA films were affected by red-shifting for high concentrations (i.e. 1.4 wt%), observing in these cases something like a mirrored spectra of the corresponding 1.0 wt% trend (Fig. 50**b**).

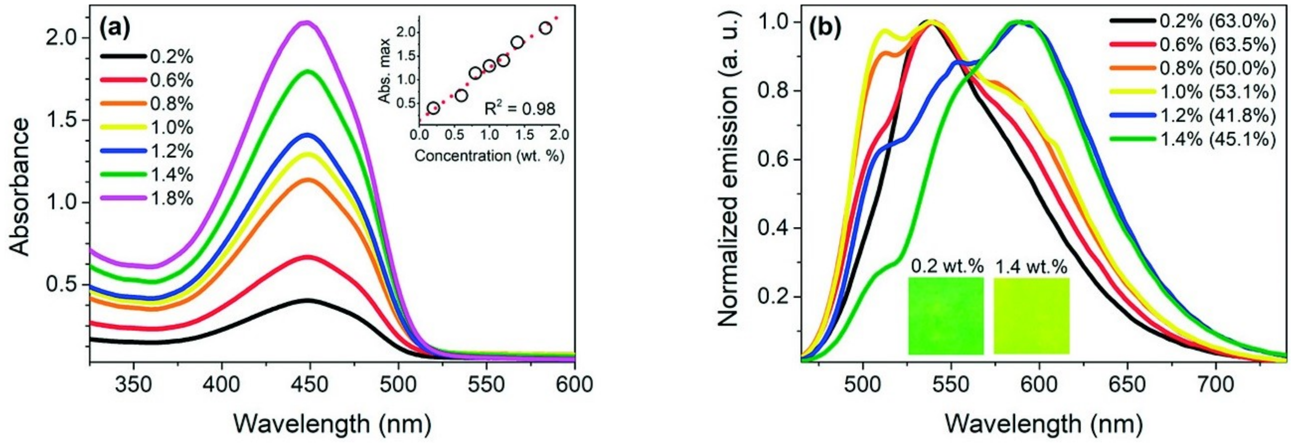

Fig. 50: Absorption(a)/emission(b) spectra of ***BBT1*** *in PMMA films at different concentrations*[178].

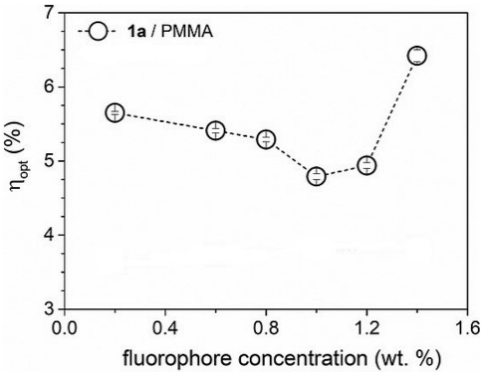

Fig. 51: *Optical efficiency of* ***BBT1*** *in PMMA*[12].

Due to its good properties, **BBT1** performances were evaluated (Fig. 51). The fluorophore showed an optical efficiency of 6.4% at 1.4 wt% concentration, lower than **LR305** (10.1% in PMMA, at 1.4 wt%). However, in contrast with **LR305** behavior, **BBT1** could be employed on a possible large-scale applications. In particular, at low concentration, the fluorescence quantum yield was comparable with the results observed in solution (64% against 68% in solution).while with the increase of concentration fluorescence quantum yield decreased, til 45% at 1.4 wt%. However, optical efficiency at 1.4 wt% was higher than the corresponding value at 0.2 wt%, meaning that power losses at 1.4 wt% of **BBT1** were (such as re-absorption). For higher concentration, a decrease of fluorescence quantum yield was observed, about 45% at1.4 wt% compared with 64% at 0.2 wt%. Moreover, a vibronic band visible as a shoulder in the emission spectrum appeared for concentrations higher than 1.0 wt%. Two effects could explain this phenomenon:

- a fluorescence quenching of the not aggregate form of **BBT1**;
- a red-shift effect on the emission band at around 600 nm due to the formation of emissive aggregates of **BBT1** (eximeres).

Furthermore it showed to be outlined how the red-shift effect is responsible of a color change of PMMA films which turns from green to light yellow, when excited with a long-range UV lamp at 336 nm.

---

[178] C. Papucci et al., *Eur. J. Org. Chem.* **2018**, 2657–66.

From this analysis we can assess that **BBT1** can be successfully be employed in a LSC device. The extended conjugation and D-A-D structure seem to favour good optical properties, especially with limited losses of power and a low re-absorption impact. That means that the employment of **BBT1** on large-scale devices could be more efficient than **LR305**, even if its optical efficiency on lab scale is lower.

It is known that strong donor pendant with more rigid structure exhibits a variation on HOMO energy level and produces different colored derivatives, an aspect which is not negligible for LSC applications. Moreover, more rigid donor moiety can limit energy dissipation, typical of internal conversion through vibrational motions[179]. In these cases, an improvement of fluorescence quantum yield is observed.

For these reasons, as a further step in this study, we decided to prepare a series of BBT1 based chromophores carrying different substituents. The **BBT1** was used as acceptor A, due to the less steric hindrance and better optical properties shown as LSC chromophore.

First two new molecules having a symmetrical A'-A-A' (**BBT1a**) and an unsymmetrical D-A-A' (**BBT1b**) structure (Fig. 52).

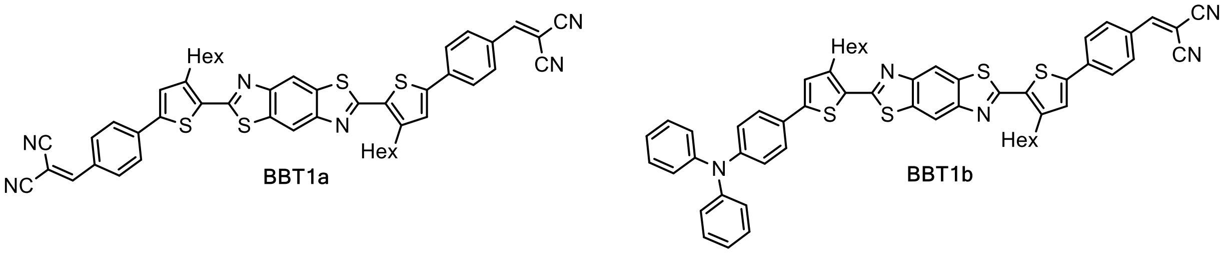

Fig. 52: *Molecular structures of* ***BBT1a*** *and* ***BBT1b****, where is involved the same core of* ***BBT1****.*

Then, another series of new **BBT1**-based D-A-D fluorophores were designed (Fig. 53), providing to evaluate the effect of different groups with different donating character.

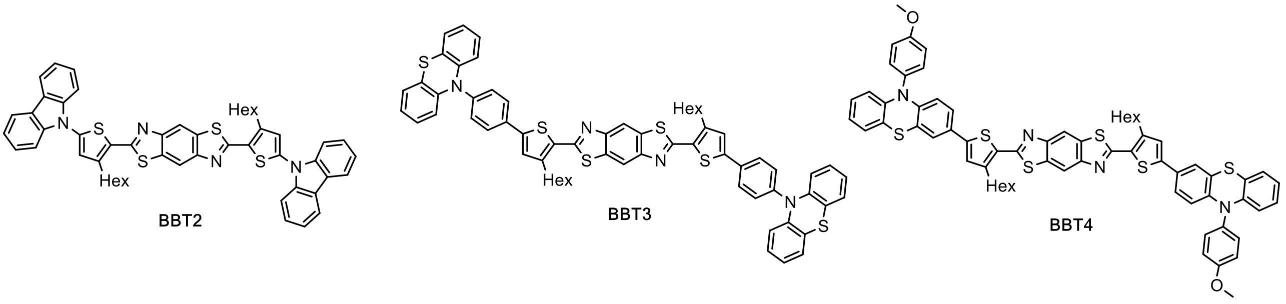

Fig. 53: *Molecular structure of BBT derivatives, with different donor groups.*

In particular, phenothiazine and carbazole groups were selected to study the donor effect on the optoelectronic features.

Thus in the case of compound **BBT2** a carbazole moiety was directly bounded on the external α position of the thiophene. Instead, for **BBT3** and **BBT4**, the core was decorated with phenothiazine groups: in the case of **BBT3**, the phenyl benzothiazine was bounded through the nitrogen atom, using a phenyl group as linker, while for **BBT4**, the phenothiazine moiety is

---

[179] *Encyclopedia of Spectroscopy and Spectrometry*; Elsevier Inc., 2017, 636–653.

directly linked via the C7 atom and has a *para* methoxy-phenyl group as substituent on the nitrogen.

3.2 ALTERNATIVE SYMMETRICAL AND ASYMMETRICAL BBT: BBT1A/1B

BBT1 had shown very interesting optical properties for LSC applications. Its D-A-D structure, studied through DFT calculations, exhibited a strong ICT process, which induced good fluorescence quantum yield and optical efficiency. However, green/yellow emission matched with only a part of silicon absorption range. A bathochromic effect on the emission range would be welcome to better match silicon absorption. As we have seen for NIR-chromophores in chapter 2, the introduction of extended conjugation and the design of stronger acceptor moieties can produce high red-shifted in the absorption spectra, however not high fluorescence quantum yields are observed for this type of molecules.

In the research group were this thesis work has been carried out, D-A-A' structures based on BBT core were designed, synthesized and successfully employed for DSSC application[180]. Such molecules showed very similar spectroscopic properties compared to **BBT1**.

For these reasons, we decided to prepare symmetrical and asymmetrical, **BBT1a** and **BBT1b** and evaluate their spectroscopic characteristics (Scheme 2).

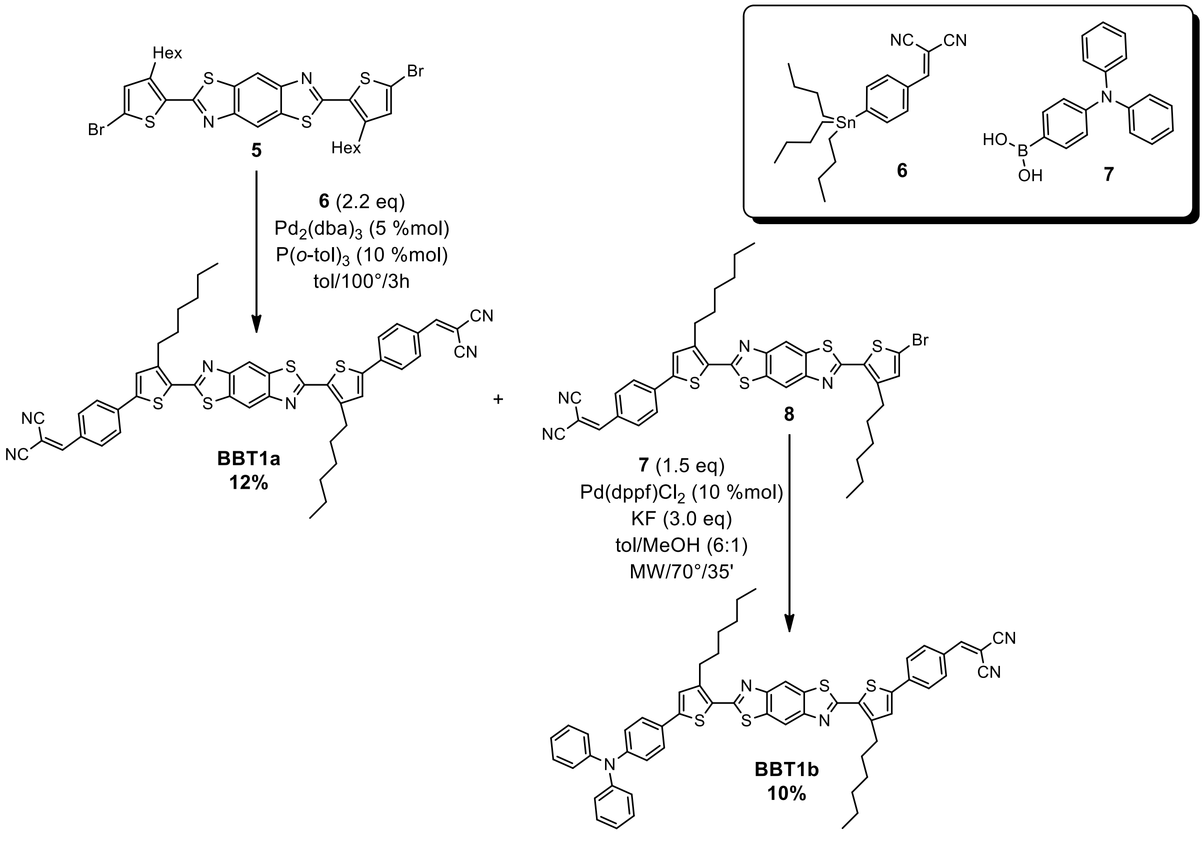

Scheme 2: *Synthetic procedures for* ***BBT1a*** *and* ***BBT1b*** *derivatives.*

---

[180] A. Dessì et al., *Eur. J. Org. Chem.* **2013**, 1916–28.

BBT1a, was prepare starting with the same key intermediate **5,** by reacting with stannyl intermediate **6.**The reaction was carried out in typical Stille conditions using Pd$_2$(dba)$_3$ as Pd source and P(o-tol)$_3$ as ligand, in toluene at 90° for 18 h. **BBT1a** was obtained after purification, albeit with very low yield. A considerable amount of mono-coupling by-product **7** was recovered. Taking advantage of this, we decided to use **7** as starting material to prepare the second luminophore we were interested to obtain. Thus compound **7** was reacted in Suzuki-Miyaura conditions, using the commercially boronic acid **8,** Pd(dppf)Cl$_2$ as catalyst and KF as base. The reaction was carried out in toluene/MeOH, under MW irradiation at 70° for 35'. Unsymmetrical compound **BBT1b** was obtained in low yield after purification.

Despite the synthesis was not efficient, we decided to analyse the spectroscopic properties of the two compounds.

UV-vis spectra of **BBT1a/b** were recorded in EtOH solution, at different concentrations, giving a fluorescence quantum yield of 78% in EtOH[181]. The spectra are reported in figure 54.

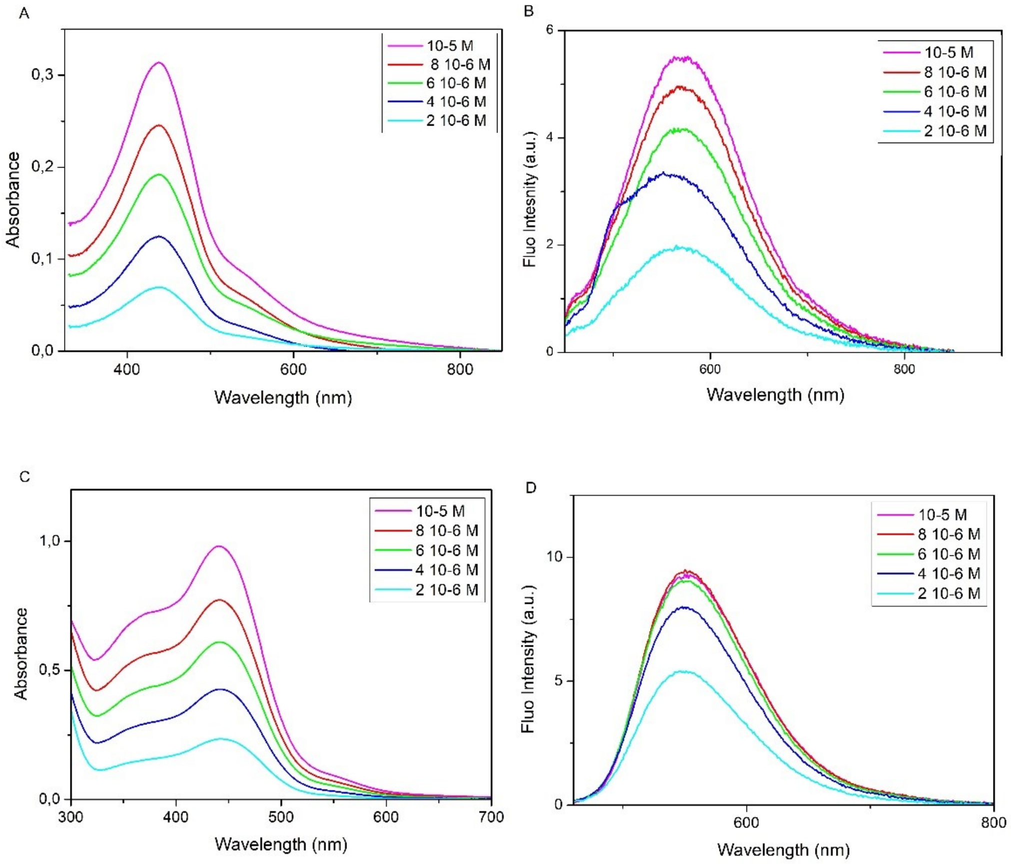

Fig. 54: *Absoprtion (A, C) and emisison (B, D) spectra of BBT1a/1b in EtOH solution, at different concentrations.*

BBT1a/1b showed regular and broad absorption and emission spectra, and intensities increased with concentrations. Thus, processes of loss of energy, such as re-absorption and fluorescence quenching were negligible. Both of them showed high **ε**, in particular **BBT1b** with a value around 10^5 M^{-1} cm^{-1} (see Table 8).

---

[181] *C. R. Chimie*, **2006**, *9*, 1254-59.

***Table 8**: Spectroscopic characteristics of **BBT1a/1b** in solution.*

Compound	λ_{abs}(nm)	ε ($M^{-1} cm^{-1}$)	λ_{em}(nm)	SS (nm)	Φ_f (%)
BBT1a	438	31358	577	139	12
BBT1b	441	102637	550	109	1.7

For both of them, the absorption spectra showed a slight shoulder at longer, for **BBT1a**, and at shorter, for **BBT1b,** wavelengths compared to the principal peak (centered in 438 nm and 441 nm for **BBT1a/1b**, respectively). This peculiar shape was relative to a vibronic band. That means that both chromophores were affected by a rearrangement upon excitation[182], less evident in case of **BBT1** spectra.

Unfortunatly, even if the absorption and emission trend showed interesting preliminary results in solution, the Φ_f were very low (12% for **BBT1a** and 1.7% for **BBT1b**) and for this reason we decided not to optimize the synthetic approach and investigate further the two fluorophores

3.3 EFFECT OF DONOR GROUP (BBT2-4)

As we have already discussed, the emission range of **BBT1,** limited to 500-580 nm, represent a drawback for the application in LSC, due to the low overlap region between **BBT1** emission and silicon absorption spectrum. Definitely, a larger red-shifted effect could improve LSC optical efficiency. As we have already discussed, in order to approach this problem, we designed the three new dyes reported in scheme 53

Once again, preliminary computational studies of S_0 and S_1 states of **BBT2-4** were investigated through Density Functional Theory (DFT) and time-dependent DFT (TD-DFT) methods. The results obtained are reported in figure 55.

All the three dyes **BBT2-4** were characterized by a planar central scaffold where the BBT core and thiophene ring show a dihedral angle <1°. However, a pronounced torsion between the three different donors and thiophene moieties is remarked (24-25° for phenothiazine derivatives, 57° for carbazole moiety).

Calculated geometries of S_1 state suggest that smaller angles are generated by an increase of the planarity of the overall molecules.

Therefore, no significant changes are observed in molecular geometry between the phenothiazine-based BBT (**BBT3** and **BBT4**) and **BBT1**, while **BBT2** shows a high twisted bond of the carbazole, due to its large hindrance.

Calculated optical properties of **BBT2**, **BBT3** and **BBT4** are reported in table 9.

With no substantial difference between solution (toluene) and PMMA values, all fluorophores should have an absorption between 404 and 441 nm, corresponding to 3.06-2.81 eV range. Considering the frontier molecular orbitals involved in the lowest energy transition (HOMO→LUMO for BBT2 and BBT4, HOMO-2→ LUMO for BBT3), a $S_0 \rightarrow S_1$ transition is identified, responsible of ICT from the donor to the acceptor core.

---

[182] *Encyclopedia of Spectroscopy and Spectrometry*, Elsevier Inc., 2017, pp. 636–653.

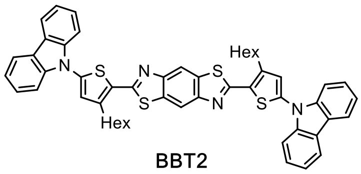

BBT2

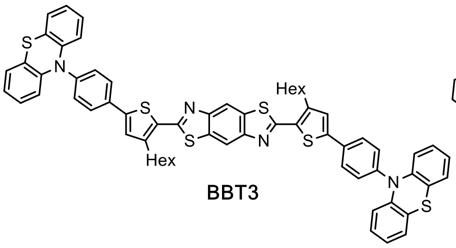

BBT3

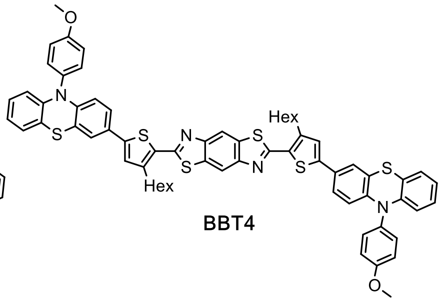

BBT4

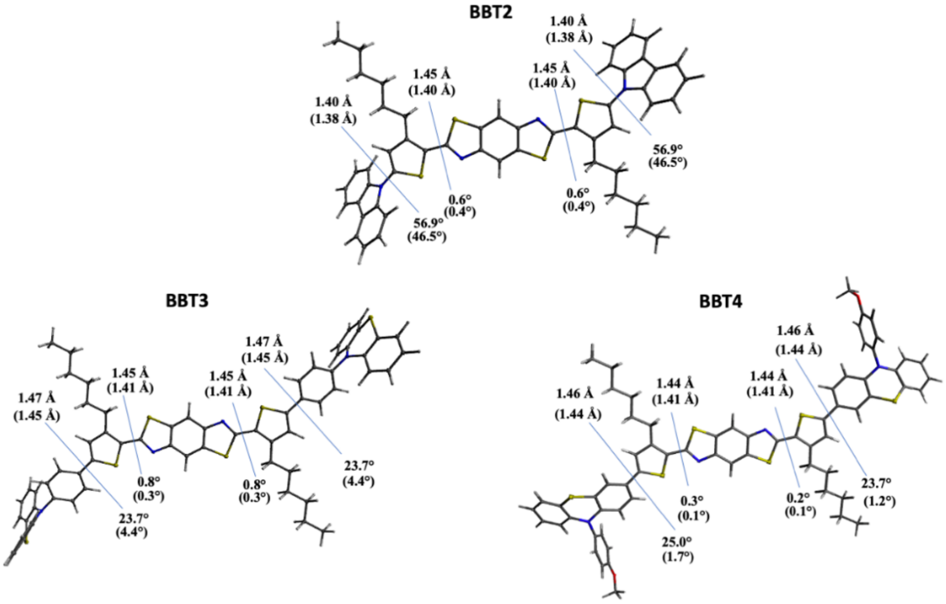

Fig. 55: *Computational optimized geometries of **BBT2, BBT3, BBT4** for S_0 state (degrees) and S_1 state (in brackets).*

Table 9: *TDDFT (MPW1K/6-311+G(2d,p)) absorption maxima (λ_{max} abs in nm), excitation energies (E_{exc} in eV), oscillator strengths (f) and contributions (%) to the $S_0 \rightarrow S_1$ transition in toluene and PMMA of compounds **BBT2**, **BBT3** and **BBT4**.*

BBT	Medium	λ_{max} abs [nm]	E_{exc}	f	Transition (%)
BBT2	toluene	404	3.06	2.20	87 (H→L)
	PMMA	404	3.06	2.20	87 (H→L)
BBT3	toluene	419	2.95	2.78	89 (H-2→L)
	PMMA	419	2.96	2.78	89 (H-2→L)
BBT4	toluene	440	2.81	3.02	79 (H→L)
	PMMA	441	2.81	3.02	78 (H→L)

Analyzing these results compound **BBT2** seems to be the fluorophore with the most pronounced auxochromic shift, with an absorption maximum of 404 nm. Due to the lower donor character of carbazole, compared with phenothiazine ones, and its strong torsion angle of around 56° that reduced molecular planarity and consequently conjugation, **BBT2** is characterized by a significant blue-shift.

On the contrary, **BBT4** presents the higher red-shift effect, thanks to its greater flatness and greater conjugation. However, even if **BBT3** exhibits a phenothiazine pendant and a red-shift compared to **BBT2**, the wavelength difference is only 15 nm. That means that despite the good donor capacity of phenothiazine, the less flatness of the molecule, generated by its direct attachment to the core, limits a strong conjugation, and thus a red-shifted absorption.

A similar analysis can be carried out from Linear Response – Polirisable Continuum Model (LR-PCM) computed emission maxima, reported in table 10.

Table 10: *TDDFT (MPW1K/6-311+G(2d,p)) emission maxima (λ_{max} em in nm), emission energies (E_{em} in eV), oscillator strengths (f) and contributions (%) to the transition $S_1 \rightarrow S_0$ in toluene and PMMA of compounds **BBT2**, **BBT3** and **BBT4**.*

BBT	Medium	λ_{max} em [nm]	E_{exc}	f	Transition(%)
BBT2	toluene	477	2.59	2.40	92 (L→H)
	PMMA	477	2.60	2.40	93 (L→H)
BBT3	toluene	504	2.46	2.82	93 (L→H-2)
	PMMA	504	2.45	2.82	93 (L→H-2)
BBT4	toluene	521	2.38	3.18	88 (L→H)
	PMMA	523	2.37	3.18	88 (L→H)

The calculated emission maxima of BBT derivatives fall around 477-521 nm, with Stokes shifts of 0.47, 0.49 and 0.44 eV for **BBT2**, **BBT3** and **BBT4**, respectively. Such value are comparable with those calculated for PMMA .

From these preliminary studies we can say that all the three compounds look very promising.

3.3.1 SYNTHESIS AND OPTIMIZATION

The synthesis of compounds **BBT2**, **BBT3** and **BBT4** was carried out using the same advanced intermediate **5**. As starting material for simple cross-coupling reactions (such as Suzuki-Miyaura, Stille, etc). For these reasons, we decided to find a flexible and easy synthetic approach to obtain such compound, being crucial for the final overall yield of our desired compounds. The method we applied is described in scheme 3.

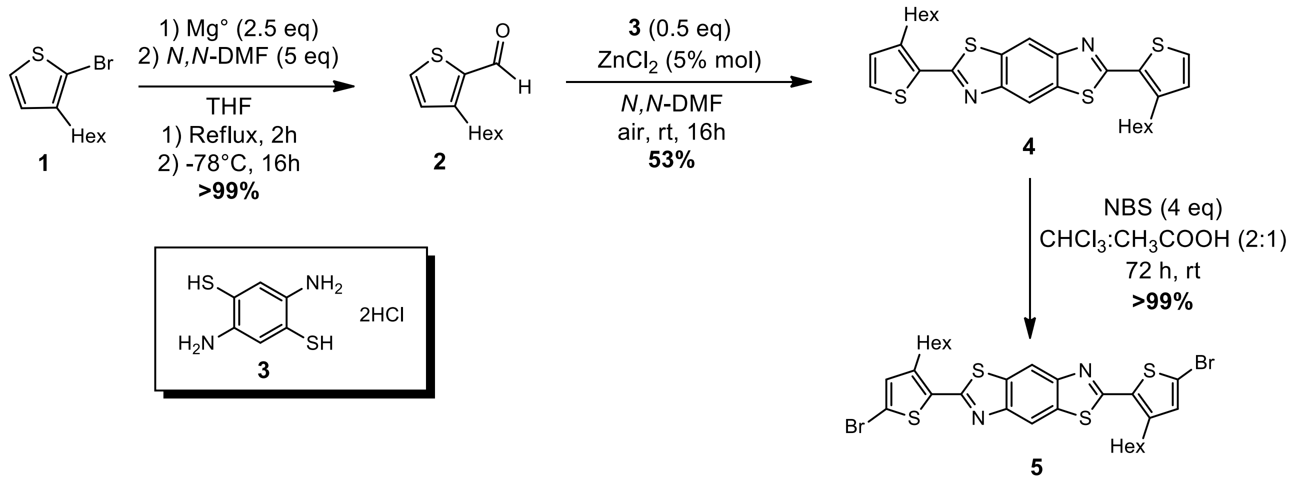

***Scheme 3:** Optimization of synthetic steps of BBT core.*

2-Bromo-thiophene was quantitatively converted in the corresponding aldehyde **2**, by preparing the corresponding Grignard intermediate and which was reacted with *N*,*N*-DMF[183]. Aldehyde **2** was obtained quantitatively and then reacted with the commercial 2,5-diaminobenzene-1,4-dithiol *bis*-hydrochloride to give BBT core **4**. This is the more challenging step, and several conditions were tested. Finally, despite the improvement of yield was not so high, milder conditions (air atmosphere, room temperature) were found and the formation of by-products was limited by the addition of $ZnCl_2$ as Lewis acid, in a catalytic amount. Finally the use of *N,N*-DMF as solvent limited the formation of by-products, thus. Compound **4** was easily obtained by precipitation. Finally, the BBT core **5** was prepared in a quantitative yield, through an electrophilic bromination, using a large excess of NBS. The reaction was left for 72 hours at room temperature and shielded by visible light.

Finally, starting from the key compound **5**, **BBT2**, **BBT3** and **BBT4** were obtained through Pd-catalyzed cross-coupling reactions (Scheme 4).

Cross-coupling reactions are known and reliable reactions, where a catalytic system (based on metals of groups 8-10) promotes the formation of C-C, C-H, C-N, C-O, C-S, C-P or C-M bond through an organometallic reagent in presence of an organic electrophile[184].

BBT2 was obtained in almost quantitative yield, through Buchwald-Hartwig reactions, in presence of carbazole (**9**), using $Pd_2(dba)_3 CHCl_3$ as pre-catalyst, Xantphos as ligand and NaO^tBu as base, heating at 90° for about 24 hours, under inert atmosphere.

Instead, compounds **BBT3** and **BBT4** were synthesized employing a lab-scale microwave (MW) activation protocol, through a typical Suzuki-Miyaura reaction, starting from the corresponding boronic esters (**10** or **11**), using $Pd_2(dba)_3$ $CHCl_3$ and SPhos as catalytic specie and KF as base. In these cases, the lab-scale microwave activation allowed to reduce reaction time from 16-18 hours to 35', working at 70°C, and to limit the formation of by-products, with the consequent simplification of purification by chromatography. In the MW irradiation cross-coupling reactions, a mix of toluene/MeOH (6:1) was used to ensure a proper dissolution of the starting material, which showed a low solubility in the major part of organic solvents.

Both final products were obtained **BBT2**, **BBT3** and **BBT** with satisfactory yields (**BBT3** 43%,

---

[183] W. Zhou *et al.*, *Dye and Pigment.* **2011**, *91* (3), 404–412.

[184] A. Biffis, P. Centomo, A. Del Zotto, and M. Zecca, *Chemical Reviews*. **2018**, doi: 10.1021/acs.chemrev.7b00443.

BBT4 69%) after flash chromatography.

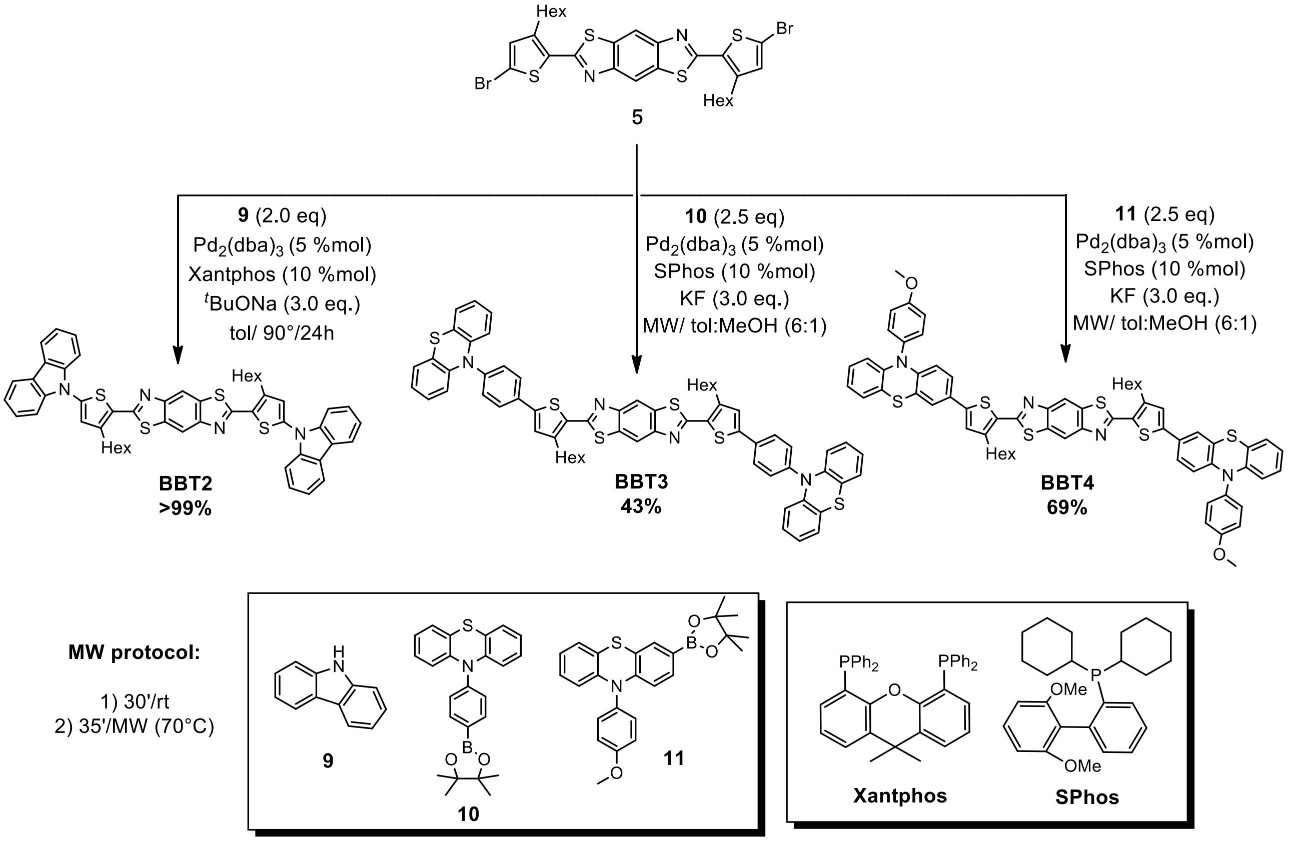

*Scheme 4: Cross-coupling reactions conditions for **BBT2**, **BBT3** and **BBT4**.*

The difference of isolated yields obtained for **BBT3** and **BBT4** could be explained as a lower reactivity of phenothiazine **10** than **11**, in the same reaction conditions. Probably, the donor effect of sulphur in the intermediate **11,** favored the transmetallation of boron with palladium.

3.3.2 SPECTROSCOPICAL AND OPTOELECTRONIC CHARACTERIZATION

The three compounds were spectroscopically characterized in solution (par. 3.3.1) and polymer films (3.3.2). Their excited state behavior was investigated through transient absorption spectroscopy, comparing the effect of solution and polymer matrix (par. 3.3.3).

3.3.2.1 Spectroscopical characterization in solution

UV-Vis and fluorescence emission spectroscopy were recorded in toluene was chosen due to its ability to dissolve efficiently the three organic compounds and for its refractive index of 1.496, which is similar to PMMA one (1.491). The optical properties of **BBT2-4** are reported in table 11.

***Table 11:** Spectroscopic properties of compounds **BBT2**, **BBT3** and **BBT4** in toluene solution.*

Compound	λ_{abs}(nm)	ε (M^{-1} cm^{-1})	λ_{em}(nm[eV])	SS(nm[eV])	Φ_f (%)	E_{0-0} (eV)
BBT2	409	33700	463 [0.13][a]	54 [0.35]	18	2.78
BBT3	420	7800	491 [0.16][a]	71 [0.43]	18	2.67
BBT4	456	18600	527	71 [0.37]	73	2.45

[a] In parenthesis the interval between the two vibronic peaks in the emission spectra (in eV).

The experimental data observed for the absorption maxima of **BBT2-4** were in agreement with the calculated values (see table 9 and 10), with a small differences of 0.1 eV confirming the bathochromic shift of the lowest energy level, from **BBT2** to **BBT4** observed by computational data, which were highly predictive of the experimental values.

BBT2-4 absorption and emission spectra in toluene are reported in figure 56.

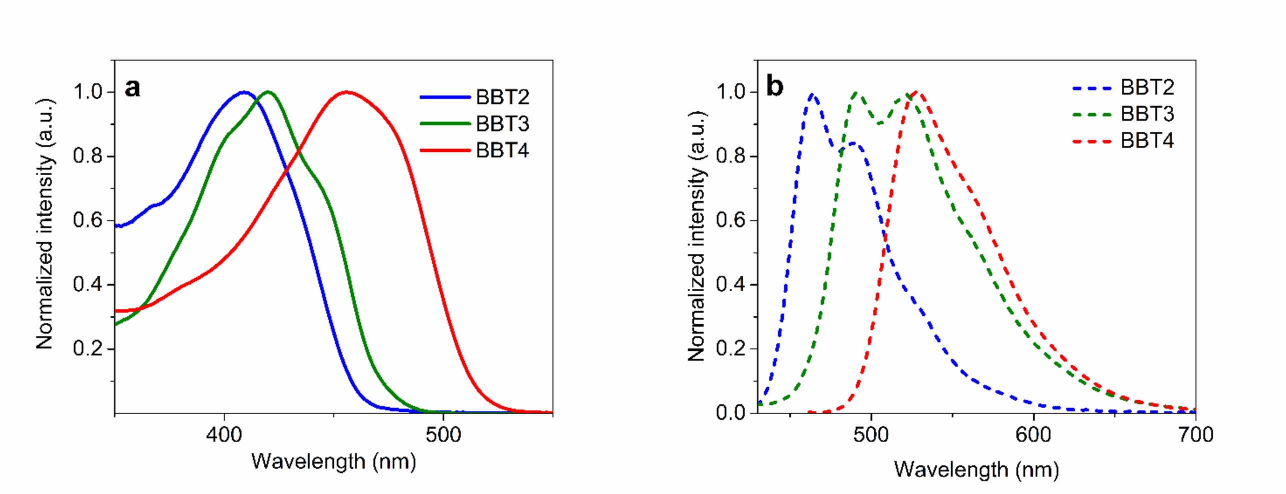

***Fig. 56:** Normalized absorption and emission spectra in toluene of **BBT2-4**.*

Changing the concentration concentrations of the luminophore, absorption and emission trend remained constant for all of BBTs, showing that aggregation phenomena are negligible (Fig. 57). All molecules exhibited strong emissions in a range of 400-650 nm and a large Stokes shift. **BBT2** and **BBT3** showed similar shape and trend of emission spectrum (Fig. 58), where a marked vibronic band remained constant at different concentrations. The presence of vibronic structure demonstrated the occurring of a significant structural rearrangement upon excitation[185]. The consequence of this phenomenon was a decrease in fluorescence quantum yields (0.18 for **BBT2** and **BBT3**).

---

[185] *Encyclopedia of Spectroscopy and Spectrometry*, Elsevier Inc., 2017, pp. 636–653.

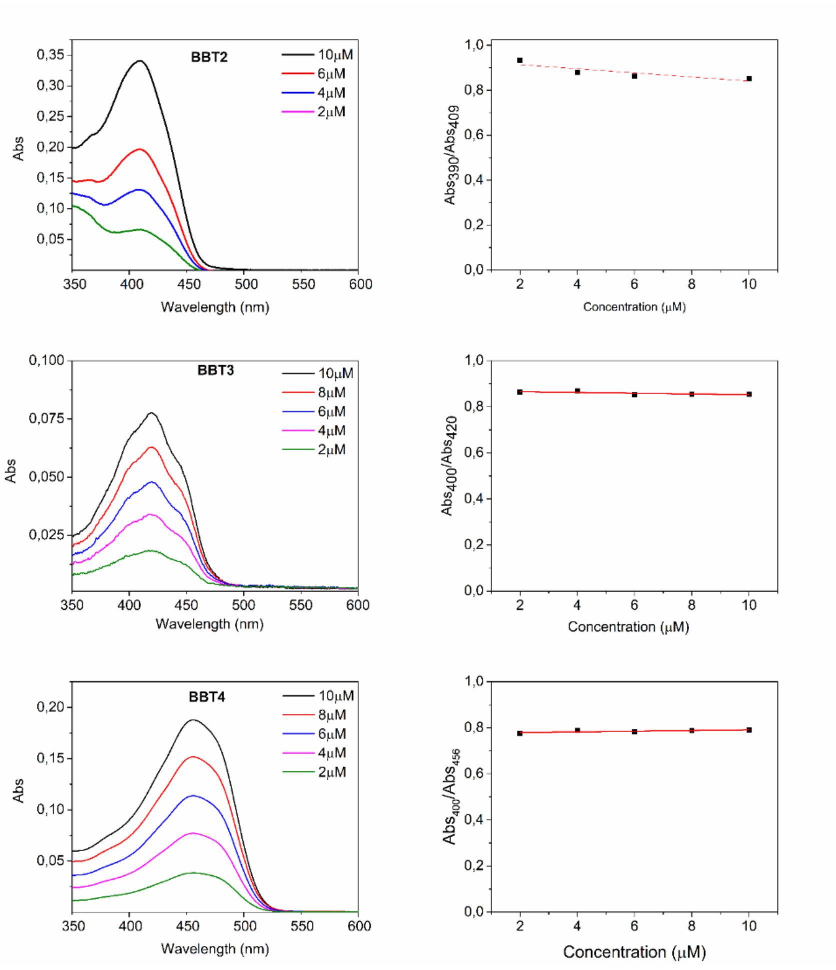

Fig. 57: *Absorption spectra of* ***BBT2-4*** *in function of concentration (on the left) and the ratio between absorbance at two different wavelengths of the absorption band, where one of those is* λ_{abs} *max of absorption.*

The large Stokes shift, the small overlap between absorption and emission spectra and a modest re-absorption impact allowed to consider **BBT2** and **BBT3** as possible chromophore to be engaged for building LSC devices[186].

On the other hand, **BBT4** exhibited a less evident vibronic structure of the emission band, peaked at 527 nm, with a weak shoulder at lower energy, slightly visible at higher concentrations.

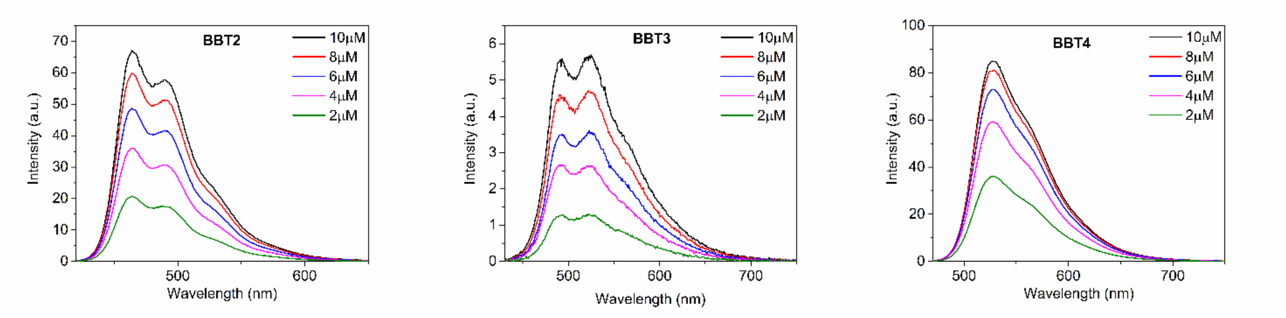

Fig. 58: *Emission spectra of* ***BBT2-4*** *at different concentrations, in toluene, for excitation at 409, 420 and 456 nm respectively.*

---

[186] P. Della Sala *et al.*, *Chem. Commun*, **2019**, *55*, 3160-63.

Remarkably, a large Stokes shift of 71 nm (0.37 eV) was found. The fluorescence quantum yield was 0.78, therefore much higher than **BBT2** and **BBT3**. This increase in fluorescence quantum yield might be due to a greater conjugation between the donor and acceptor groups and to decreased rotational freedom of their connecting bond. The reduced vibrational structure of the emission band and the computed geometry of the excited state confirmed this hypothesis. Thus also **BBT4** can be suitable for the application in LSC.

3.3.2.2 Spectroscopic characterization in PMMA films

Given the promising spectroscopic properties of **BBT2-4** compounds in solution, fluorophore behaviors were analysed in the polymeric matrix. First of all, poly(methyl methacrylate) (PMMA) was chosen, as typical LSC host material, for preliminary studies with the chromophores . Accordingly, compounds were dispersed in PMMA films with a 25μm±5μm of thickness, at different concentrations (from 0.2 to 1.8 wt%).

In all investigated concentrations, **BBT3** and **BBT4** showed homogenous and transparent films (Fig. 54). In contrast, **BBT2** resulted incompatible with PMMA at concentrations higher than 1.4wt%, generating an aggregated system, with clear phase separation. This behaviour was confirmed by optical microscope analysis (Fig. 59). More in detail, the absorbance of **BBT2** in PMMA linearly increased with concentration, til to the value of 1.0 wt%. Beyond this concentration, a drastic reduction was observed, due to the formation of aggregates and phase separation. The formation of aggregates induced red-shift in absorption and, more clearly, in emission spectra and a variation in the spectrum shape (see Fig. 61a-b). Moreover, fluorescence quantum yield decreased with the increasing of concentrations, which was associated to aggregation-caused quenching (ACQ) phenomenon[187].
On the contrary, **BBT3** and **BBT4** resulted compatible with PMMA matrix, showing good dispersion even at high concentrations (1.8 wt%), without evident phase separation at the microscope analysis (Fig. 60).

---

[187] J. Mei, Y. Hong, J.W.Y. Lam, A. Qin, Y. Tang, B.Z. Tang, *Adv. Mater.*, **2014**, *26*, 5429–79.

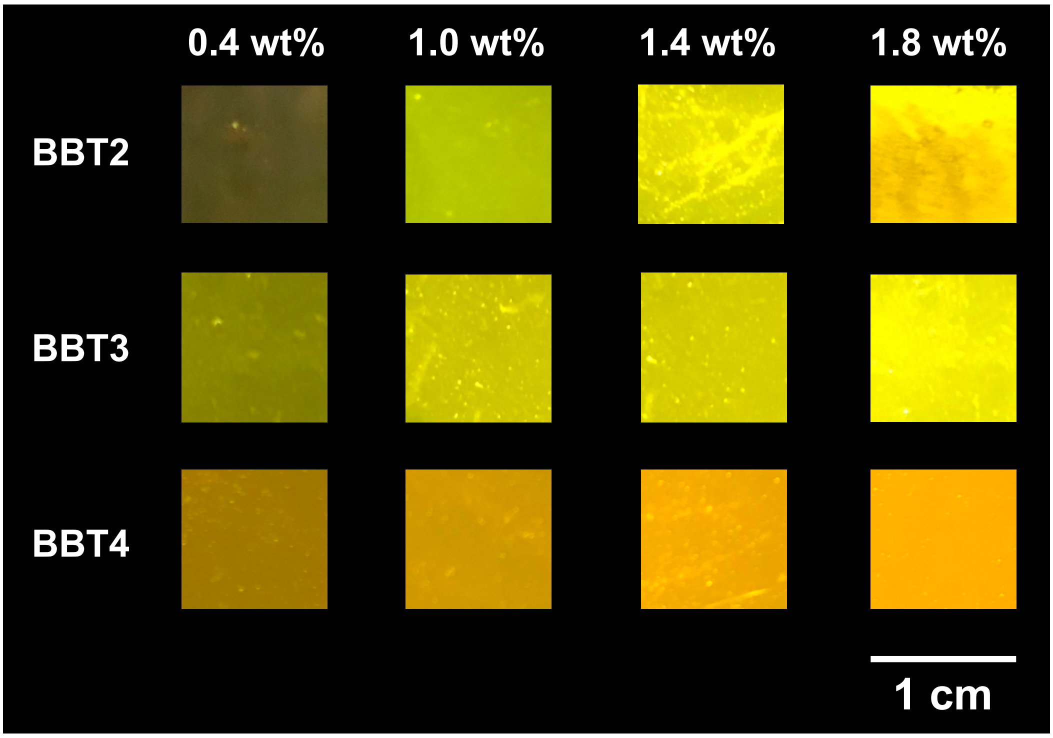

Fig. 59: *PMMA films doped with* ***BBT2-4****, at different concentrations, illuminated by Dark Reader Transilluminator at 450 nm.*

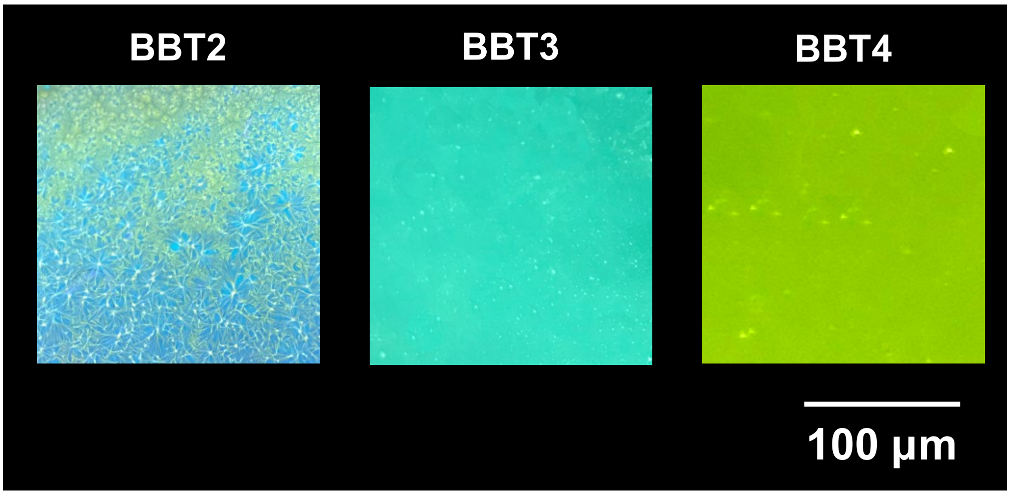

Fig. 60: *PMMA films of* ***BBT2-4****, at 1.8 wt% concentration, under the illumination of a long-range UV lamp, at 366 nm.*

Both dyes showed in PMMA a broad and quite constant absorption and emission behavior, increasing with higher concentrations (see Fig. 61c-f). The vibronic structure, which evident in solution samples, was no longer visible in PMMA, giving a maximum overlap of lowest energy vibronic peak. Due to the impossibility of free rotation of molecule in solid state and the higher polarity of the matrix compared with toluene, charge separation and a consequent strong ICT impact were favored. Thus, bathochromic shift and larger Stokes shift were found for all chromophores.

Finally, for all molecules, Φ_f decreased with increasing concentrations due to consistent overlap between absorption and emission spectra, favoring self-absorption phenomena. In particular, Φ_f of **BBT2** in PMMA was around 13% at the common concentration employed in LSC device (1.4 wt%), and was thus considered too low for practical applications.

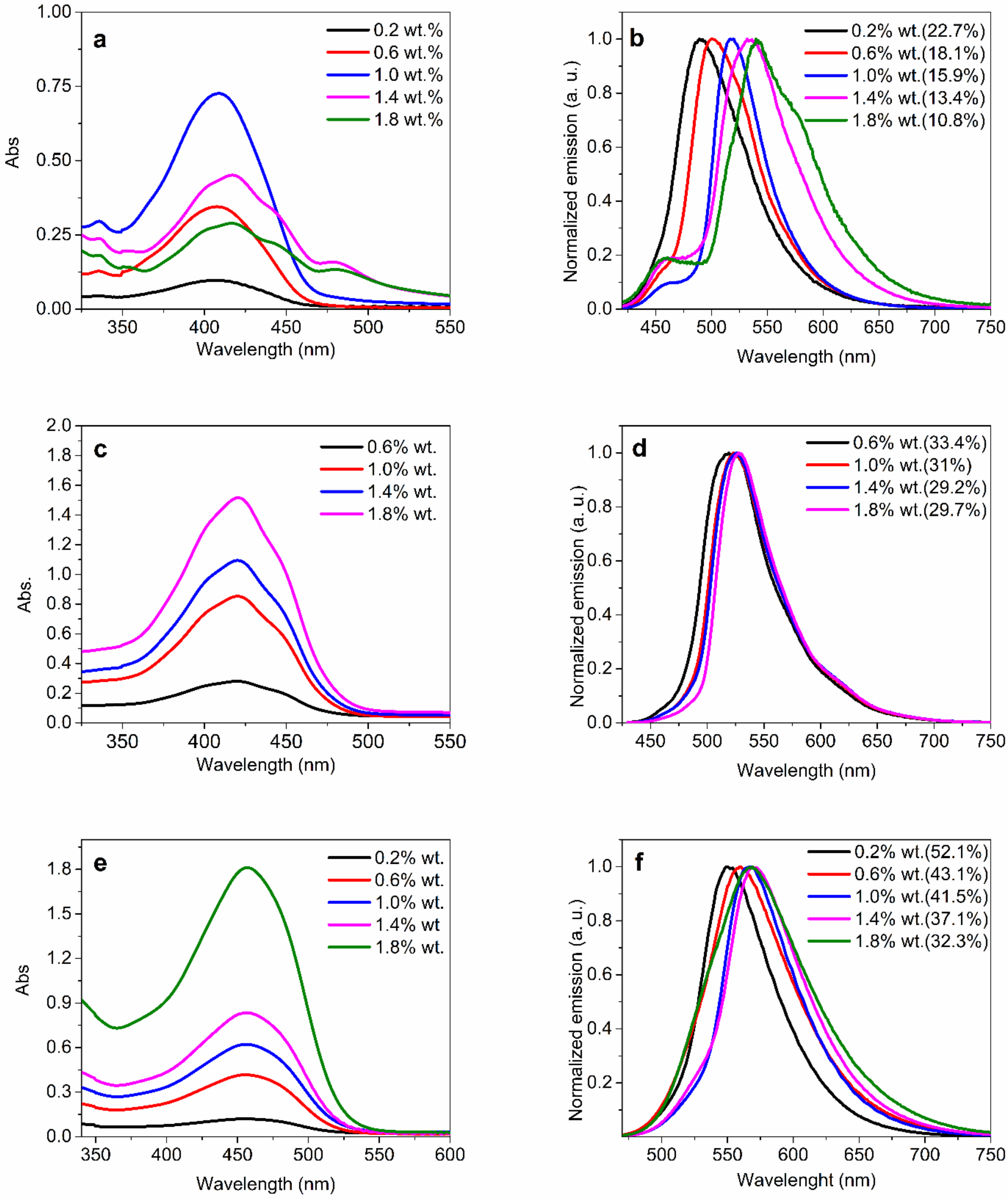

Fig. 61: ***BBT2****/PMMA films absorption (a) and emission (b) spectra at different concentrations (excitation at 409 nm);* ***BBT3****/PMMA films absorption (c) and emission (d) spectra at different concentrations (excitation at 424 nm);* ***BBT4****/PMMA films absorption (e) and emission (f) spectra at different concentrations (excitation at 456 nm).* Φ_f *are reported in parenthesis.*

3.3.2.3 Transient absorption spectroscopy

To investigate the behavior of the excited state and investigate the dynamics of relaxation mechanisms after light absorption, femtosecond transient absorption spectra have been recorded.

These experiments have been carried out in collaboration with Dr. Mariangela Di Donato, from LENS. Transient absorption spectroscopy is a technique, based on the excitation of excited

molecules: the possible induced spectroscopic processes describe the dynamic behavior of a molecule, through the studying of non- and radiative processes, excited-state energy migration, ISC or electron/photon transfer process. That is possible through the irradiation of the sample with a low-intensity pump-probe technique: the sample is excited with a laser at a specific wavelength and for a time τ the excited state is irradiated with a white light pump. The contribution on absorption is calculated as a difference between the absorption spectrum of the excited sample and the absorption spectrum of the sample in the ground state (**ΔA**).
By changing delay τ between the white light pump and the probe, registering at each delay time ΔA contribution, a ΔA profile could be obtained in the function of τ and λ.

In general, ΔA is composed of a series of contributions:

- Ground-state bleach: under the first excitation of the pump pulse, some photons have been already promoted to the lowest excited state of the molecules (S_1). The remaining photons on the ground state for the excited sample are less than the non-excited sample; the same absorption is lower. Consequently, a negative contribution in ΔA spectrum is observed in the absorption range of the molecule, non-excited.
- Stimulated emission: in the approximation of a two-level system, the coefficient of absorption of transition $S_0 \rightarrow S_1$ (A_{12}) and the corresponding coefficient of transition $S_1 \rightarrow S_0$ (A_{21}) are equal. Thus, a stimulated emission from an excited state to the ground one could occur when the pump pulse could be absorbed by excited photons. That it is possible for optically allowed transitions. The resulting trend on ΔA spectrum is a negative band around the fluorescence emission range of the molecule, with an overlapped profile. The mechanism requires a pump-probe photon which could induce emission in an excited photon to the ground state. The photon released by stimulated emission follows the same direction as the probe photons and, consequently, is detected within the probe. Usually, this process could contribute to a small Stokes shift which could spectrally overlap with the ground-state bleach.
- Excited-state absorption (ESA): in this process, excited photons, placed in the excited state, after the pump beam absorption, could be excited again by the delayed pump-probe. Photons could be excited from the populated excited state to a higher excited state that might exist in certain wavelength regions. The absorption of white light pump-probe at these wavelengths could occur and be a positive contribution of ΔA spectrum, in those wavelengths regions where the absorption at higher excited states are allowed.

Keeping in mind this real-time spectroscopic technique, **BBT2-4** were investigated in solution and PMMA matrix. The samples were excited at 400 nm, wavelength edge of absorption of BBT core, and their transient spectra recorded in the 0.1 ps -1.5 ns time interval. The results were analyzed by simultaneously fitting all the kinetic traces with a combination of exponential functions (global analysis), and using a kinetic scheme based on a sequential decay. Besides kinetic constants, the global analysis also retrieved the correspondent spectral components, indicated as Evolution Associated Difference Spectra (EADS).

Since **BBT3** and **BBT4** showed comparable spectroscopic behavior, only **BBT2** and **BBT4** were analyzed by transient absorption spectroscopy, with the correspondent Evolution Associated

Difference Spectra (EADS) obtained from global analysis.

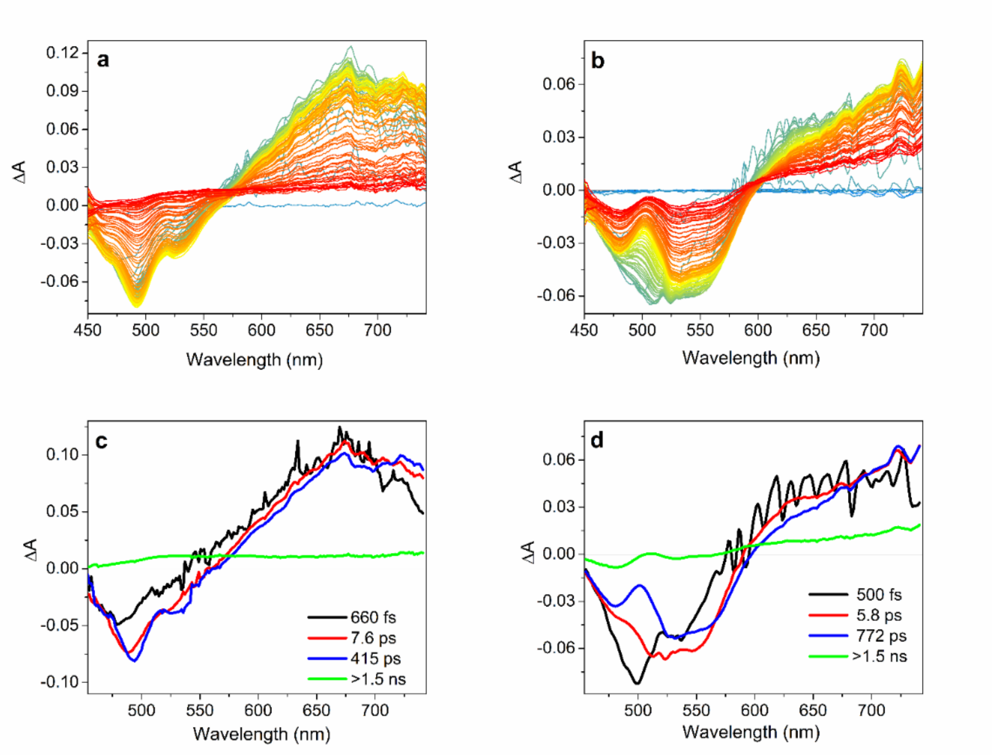

Fig. 62: Transient absorption spectra recorded for a) ***BBT2*** *and b)* ***BBT4*** *in toluene with excitation at 400 nm. Panels c) and d) reports the corresponding Evolution Associated Difference Spectra and lifetimes obtained from Global Analysis of the transient data.*

The transient spectrum of **BBT2** exhibited a negative band around 500 nm, in a wavelength range of **BBT2** fluorescence. The negative contribution to ΔA was associated with a stimulated emission process; on the other hand, a broad absorption band with a positive ΔA impact from 570 nm to >750 nm was assigned to ESA (Fig. 62a-b).

BBT4 transient profile was qualitatively comparable. However, a red-shift effect was observed compared to **BBT2**, with a negative double peaks contribution to ΔA. The band at about 500 nm could be assigned to a ground-state bleach, more visible than for **BBT2**, which showed an absorption center in 409 nm, closer to the excitation wavelength (400 nm).

Analysis, reported in figure 62c and 62d, allowed to register the spectral changes, associated with the excited state decay, in time-scale.

The colored lines expressed the ΔA trend in a time scale between femtoseconds and nanoseconds (<1.5 ns). The black line represented the transient spectrum of the Franck-Condon state, reached immediately after excitation. For timeframe <1ps, an evolution is observed, probably associable to a fast electronic relaxation of the molecules.

For **BBT2** the relaxation was observed in the first 660 fs, with increased intensity and red-shift of the stimulated emission contribution. In the following timescale (for 7.6 ps) the stimulated emission signal become more structured, particularly evident with its double peak structure centered at 495 nm and 535 nm. This drastic evolution could be associated with molecular relaxation that occurred in the excited state, under solvent rearrangement effect. Moreover, planarization of the molecule due to the rotation of donor groups was involved in this evolution, supporting from the computed geometrical changes from ground to an excited state. **BBT2** intensity signal mostly decayed on 415 ps timescale showing a small residual component, whose lifetime is longer than the pump-probe delay of 1.5 ns.

For both compounds, the ESA band evolved constantly with no particular variations, suggesting a constant electronic distribution on the excited state in the analyzed time interval of measurement. Therefore, no dark states (no absorption or emission photons state) were involved in the relaxation of systems towards the ground state.

Excitation at 400 nm brought the molecules in their S_1 state, which was a charge-transfer state because of their D-A-D structure, and a large Stokes shift observed from which they decayed directly to the ground state.

Comparing the kinetic behaviors of **BBT2** and **BBT4** on the ESA band at 665 nm, **BBT2** decayed faster than **BBT4** (Fig. 63). Moreover, **BBT4** showed a minor residual on the long timescale. This result was in agreement with the lower fluorescence quantum yield of **BBT2** in comparison with **BBT4**.

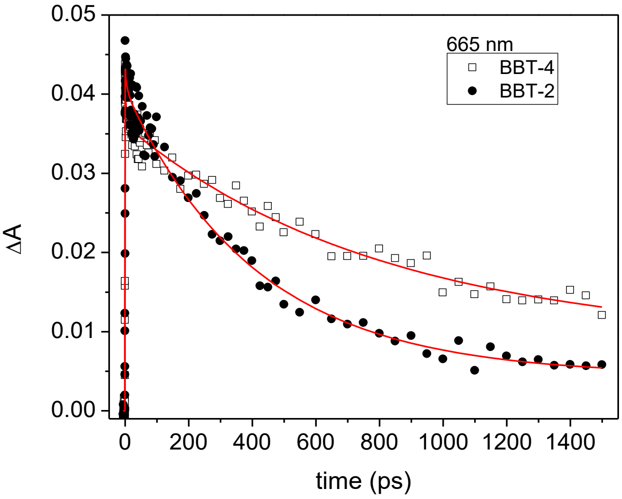

Fig. 63: *Kinetic traces comparison between **BBT2** (full circles) and **BBT4** (empty squares) behaviors, at 665 nm (ESA band), in toluene. Continous lines describe the fit obtained from Global analysis.*

For a comprehensive assessment of excited state characterization, transient spectra were also registered for PMMA samples.

Choosing 1.0 wt% dispersion **BBT2-4** in PMMA as samples, for all dyes, the evolution of transient spectra were qualitatively similar to those recorded in solution (see Fig. 64a-c).

A negative bleaching/stimulated emission band and a broad ESA band were observed in all cases. Therefore, for all dyes, the negative signal appeared less structured and presented a less extended band shape evolution in time, compared to solution ones.

This could readily explain through the limit of rotational and vibrational freedoms and structural relaxation of molecules induced by the interactions in the polymer matrix.

Comparing the kinetic traces at 665 nm for **BBT4** in solution and PMMA at 1.0 wt% concentration (Fig. 64d), the signal recovery was faster in the matrix than in solution and the residual signal on the long timescale had lower intensity. That means that **BBT4** showed an increased radiationless relaxation in PMMA compared to the solution. Thus, it agreed with the high decrease of fluorescence quantum yield in PMMA compared to solution one (73% in solution against 41.5% at 1.0 wt% concentration in PMMA).

These results could be in agreement with the possibility for **BBT4** to reveal a more twisted molecular geometry in PMMA, stabilizing charge separation.

A lower energy band gap between the excited and the ground states could explain a decrease of the excited state lifetime and a decrease of $\mathbf{\Phi}_f$.

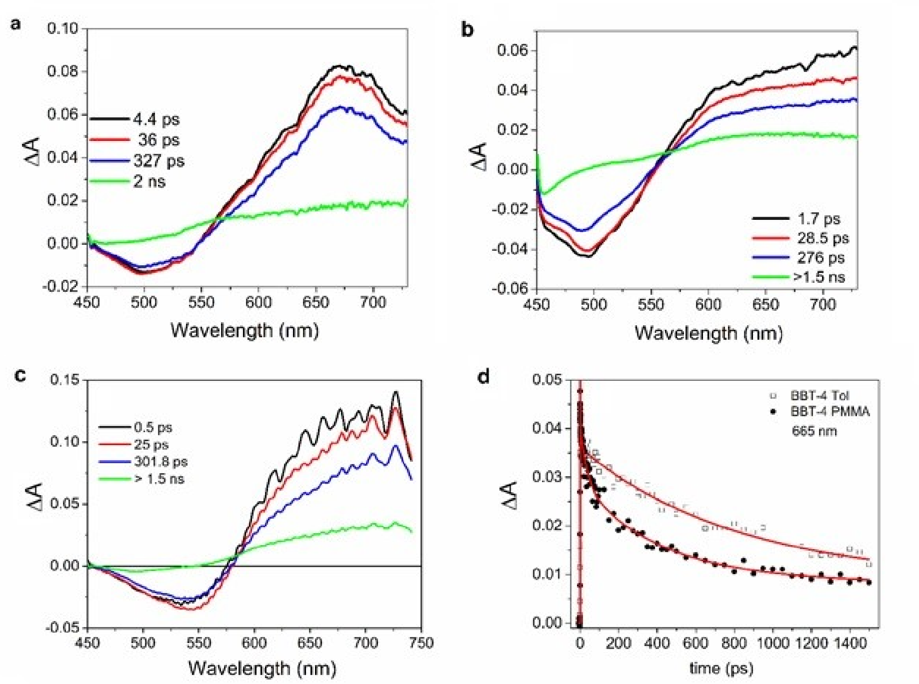

Fig. 64: Evolution Associated Difference Spectra of ***BBT2****/PMMA (a),* ***BBT3****/PMMA (b) and* ***BBT4****/PMMA (c) at 1.0 wt%, upon excitation at 400 nm, at different timescales; d) Kinetic traces comparison between* ***BBT4****/solution and* ***BBT4****/PMMA at 665 nm (ESA band) with the corresponding fit (red lines).*

3.3.2.4 Spectroscopic characterization in other polymer matrices (PCMA/PBzMA)

The three fluorescent compounds showed poor solubility in the major part of organic solvents and the best compatibility with aromatic no polar solvent (toluene). In a quite polar polymer matrix, such as PMMA, the two of the three compounds showed good compatibility, while **BBT2** exhibited a high capacity of aggregating, generating cracks and no homogenous polymer films.

Considering the behaviors of all dyes in no polar medium, we decided to investigate two new alternative polymeric matrices, poly(cyclohexyl methacrylate) (PCMA) and poly(benzyl methacrylate) (PBzMA), in order to evaluate the effect on the optical features of the derived films,. The two matrices were chosen thanks to the less polar lateral substituent (i.e., benzyl and cyclohexyl), compared to the traditional polar methyl ester group in PMMA. Notably, PBzMA and PCMA are 100% amorphous matrices, transparent and commercially available, suitable for LSC applications.

Compounds **BBT2** and **BBT3** showed poor compatibility with both of them, showing marked segregation and macroscopic aggregates.

On the contrary, **BBT4** was well dispersible within both matrices, even at a high concentration (1.8 wt%). This is clearly shown by microscopy images in PBzMA and PCMA (Fig. 65).

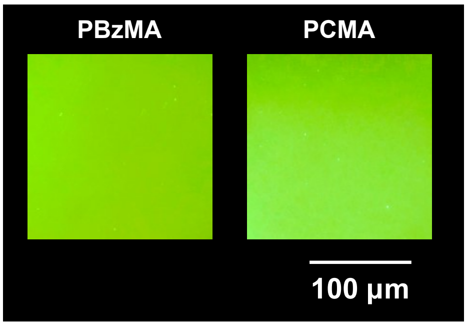

Fig. 65: *Optical microscopy images of* ***BBT4*** *in PBzMA (left) and PCMA (right) films, at concentration 1.8 wt%, under the illumination with a long-range UV lamp at 366 nm.*

Thus, BBT4 was examined in the two matrices at different concentrations. For the three concentrations examined (1.0, 1.4, 1.8 wt%), the absorption maximum was constant compared to the value obtained with fluorophores in PMMA (around 450-460 nm). The emission peak changed shape with the increase of concentration (Fig. 66b-d). Thus, the shoulder appeared at short emission wavelengths could be a consequence of possible intermolecular interactions among fluorophore molecules, favored in these no polar matrices. The different interactions between **BBT4** molecules and no polar matrices could favor the formation of small-size emissive aggregates (such as excimers), however they seemed not adversely affect phase dispersion in the matrix. Moreover, the effect on spectroscopic features, such as Stokes shift in PBzMA and PCMA, with a value of 0.50 eV, was negligible and comparable with PMMA ones.

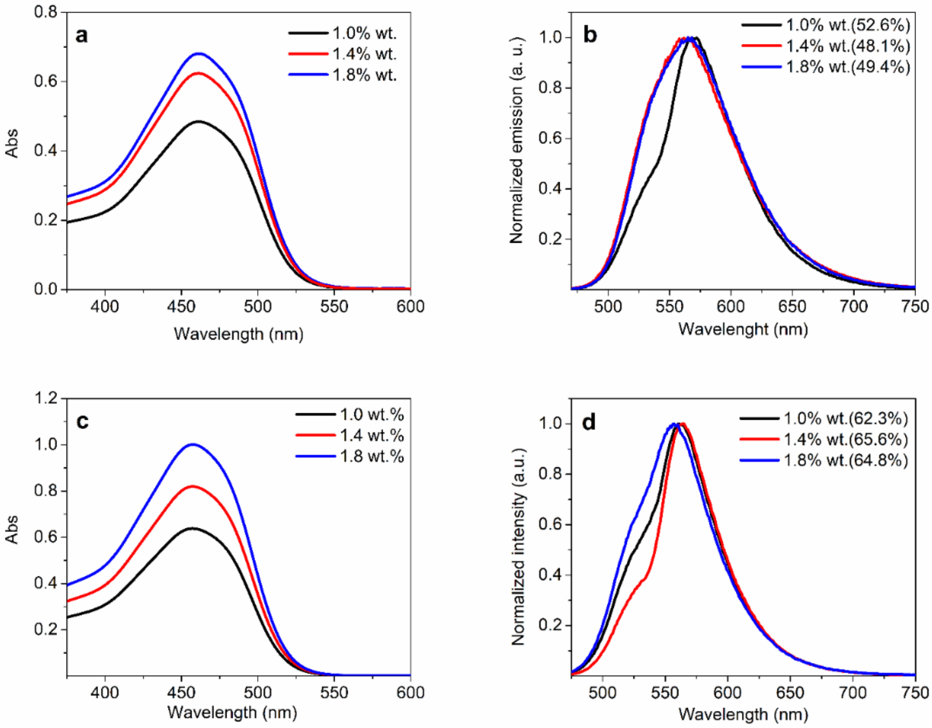

Fig. 66: *(a) UV/Vis absorption spectra of* ***BBT4****/PBzMA films as a function of fluorophore concentration (wt.%);(b) fluorescence spectra of the same* ***BBT4****/PBzMA films with excitation wavelength of 456 nm (absolute quantum yields are reported in parentheses); (c) UV/Vis absorption spectra of* ***BBT4****/PCMA films as a function of fluorophore concentration (wt.%); (d) fluorescence spectra of the same* ***BBT4****/PCMA films with excitation wavelength of 456 nm (absolute quantum yields are reported in parentheses).*

Finally, the fluorescence quantum yield in polymer matrix raised to 52.6% in PBzMA (1.0 wt%) and 62.3% for PCMA (1.0 wt%), compared to 41.5% in PMMA. Worth noting, in PCMA, **BBT4** showed an increase of fluorescence quantum yield with the concentration. The greater hydrophobicity of PBzMA and PCMA matrices, compared to PMMA, could induce, for their high compatibility with the fluorophore, a smaller stabilization of the charge separation state of **BBT4** in its excited state, probably reducing the loss of energy for non-radiative contribution processes[188].

3.3.2.5 Optical efficiencies

Optical efficiency η_{opt} is the power generated by the PV cell when LSC device is exposed to direct sunlight. On lab scale, this value is measured by exposing LSC device to the lighting of the Air Mass (AM) 1.5 solar simulator and is measured as the ratio between the power produced by the simulator (P_{SC}) and the power registered at the edges of the LSC device (P_{LSC}). As known, a geometric factor G takes into account the ratio between the area of the film, exposed to the light source, and the collecting area of the PV cell place at its edge.

In our studies, G factor was 16.6.

The results obtained for BBTs compounds were compared to that obtained for reference **LR305**, measured in the same experimental conditions.

The results obtained for **BBT2-4** and **LR305** are reported in table 12.

***Table 12**: Optical efficiency (η_{opt}) obtained for the fluorophore/polymer BBTs series in comparison with LR305.*

Compound	Matrix	Conc (wt%)	η_{opt} (%)
BBT2	PMMA	1.0	5.8±0.5
BBT3	PMMA	1.0	6.5±0.5
BBT4	PMMA	1.4	7.5±0.5
BBT4	PBzMA	1.0	8.5±0.5
BBT4	PCMA	1.4	9.0±0.5
LR305	PMMA	1.4	10.1±0.5
LR305	PCMA	1.0	9.1±0.5

Despite of low fluorescence quantum yield and low compatibility with polymer matrix, **BBT2-4** showed good values of optical efficiency, which suggested low energy losses (Fig. 67).

---

[188] T.M. Clarke, K.C. Gordon, W.M. Kwok, D.L. Phillips, D.L. Officer, *Phys. Chem. A*, **2006**, *110*, 7696–7702.

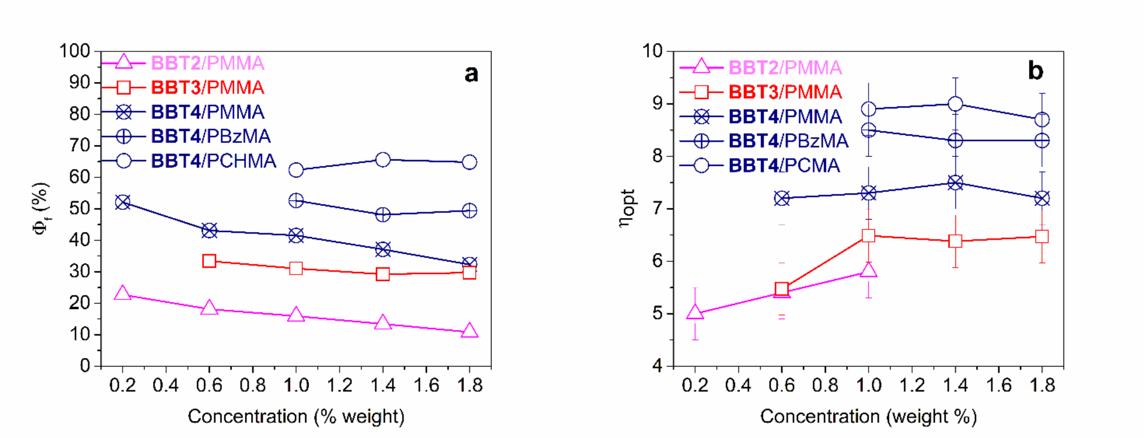

Fig. 67: *(a) Fluorescence quantum yield (Φ_f) and (b) Optical efficiency (η_{opt}) of **BBT2-4** in polymer matrices, in function of concentration (wt%).*

More in detail **BBT2** showed an optical efficiency of around 5-6%, even if its Φ_f was lower than 20%. The large Stokes shifts and Φ_f > 30% found at 1.0 wt% of **BBT3** and **BBT4** resulted in increased optical efficiency in PMMA up to about 6% and 7%, respectively. The difference between **BBT3** and **BBT4** could be ascribed to the evident bathochromic shift of about 50 nm of absorption and emission maxima of **BBT4**.

In the case of **BBT4**, the red-shifted absorption range matched better with the maximum intensity of the solar spectrum and the corresponding shifted maximum of emission was towards the best operation window of the silicon-based cell. Therefore, the good matching with PV cell absorption increased the efficiency of the light-current process, which in turn boost LSC overall performance.

Remarkably, the changing of polymer matrices favored a considerable increase of Φ_f for **BBT4**, aligned with the increase of concentration. Consequently, greater improvement of η_{opt} was observed for this compound in both non-polar matrices (PBzMA 8.5% at 1.0 wt%; 9.0% at 1.4 wt%).

Probably, for this kind of fluorophore, a matrix with less polarity favored a better dispersion in the polymer lattice and increased the relaxation mechanisms of the excited state through radiative channels.

Compared to **LR305**, in PMMA at the same conditions and for the same geometry of polymer films (on lab scale) **BBT4** showed lower value; however, the large overlap, typical of **LR305**, between absorption and emission spectra induced high loss of power for self-absorption processes. Therefore, **LR305** could find limited applications for large-scale LSC devices, where the possibility of self-absorption can be high and the consequent decrease of **LR305** performances not negligible.

More remarkably in the case of PCMA matrix, **BBT4** reached performances very close to those measured for the reference **LR305** in the same conditions. Moreover, while BBT4 in PCMA showed an increase of performances, **LR305** did not show any beneficial effect from PCMA matrix, in the range of concentration investigated.

In summary, in this part of the work, we prepared three new BBT-based molecules with a straightforward synthesis, optimizing the preparation of the common intermediate **5**, which was carried out in three steps starting from commercially available material. The overall yield was 52% without the need of chromatographic purification. The final fluorophores were prepared from intermediate **5** by Buchwald-Hartwig (**BBT2**) or Suzuki-Miyaura (**BBT3-4**) reactions in good yields. The simplicity of preparation and the cost-effectiveness of fluorophores is essential for their subsequent use in LSC technology. All the three molecules showed an intense emission spectrum between 460-550 nm, overlapping the light-absorption spectrum of a Si-based photovoltaic cell, down-converting the blue part of the solar spectrum where the efficiency of Si-cells is usually very low. Furthermore, in all cases, Stokes shifts were large enough to minimize the self-absorption effects.

Computational analysis showed that the main transition involves a charge separation process that causes a planarization of the molecule in the excited state. **BBT2** and **BBT3** behave very similarly and exhibit a rather low fluorescence quantum yield, which is ascribable to non-radiative relaxation phenomena, while $\mathbf{\Phi_f}$ values up to 73% were recorded for **BBT4** in toluene solution. In more polar environments, such as in PMMA, the charge-separated excited state geometry is more twisted, causing a lowering of the quantum yield compared to non-polar environments, such as in toluene. This was confirmed by the results of the TAS studies, showing that in PMMA the excited state absorption of **BBT4** decayed more rapidly than in toluene and was characterized by a lower residual intensity. In the case of **BBT4**, this phenomenon could be mitigated by dispersion in less polar matrices such as PBzMA and PCMA, as highlighted by an increase in $\mathbf{\Phi_f}$. In agreement with theoretical predictions, ultrafast time resolved spectroscopy results confirmed the charge transfer nature of the low-lying excited state, showing that no dark states are involved in the excited state relaxation process. Furthermore, the pump-probe spectra suggested that preventing large excited state conformational relaxation, as it happens in the polymeric matrix, results in increased fluorescence quantum yields and improved LSC performances.

Although $\mathbf{\Phi_f}$ values for compound **BBT2** and **BBT3** were rather low (approx. 16% and 31% respectively), good optical efficiencies were measured for **BBT2**/PMMA and **BBT3**/PMMA devices (5.8% and 6.5% respectively) possibly due to beneficial effects conferred by the large Stokes shift. More interesting was the performance of **BBT4**, which gave LSCs with optical efficiencies of 7.5 % in PMMA, which were increased to 8.5% and 9.0% in the less polar matrices of PBzMA and PCMA, respectively, in agreement with the indications of the computational and TAS investigation. The latter value is very similar to that found for **LR305** in the same matrix (9.1%) and only 1.2% minor if compared to the best data obtained by **LR305** in PMMA. Nevertheless, the large Stokes shifts and the consequent low self-absorption of **BBT4** compared to **LR305** suggest that using BBT-series fluorophores better optical efficiencies could be obtained on large surface area LSC.

3.4 EXPERIMENTAL PROCEDURE: CHAPTER 3

3-hexylthiophene-2-carbaldehyde

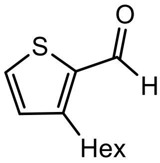

2

In a Schlenk tube, under inert atmosphere of N_2, 2-bromo-3-hexylthiophene **1** (1.5 g, 6.10 mmol, 1.0 eq) was dissolved in dry THF (12 mL). Mg° (370 mg, 15.20 mmol, 2.5 eq), pre-activated in a solution of HCl 1 M under vigorous stirring, and 1,2-dibromoethane (1 drop) were then added. The mixture was stirred on reflux for 2 h. After two hours, the mixture was cooled to room temperature and then to -78°C. *N*,*N*-DMF (2.36 mL, 30.5 mmol, 5.0 eq) was added dropwise to the solution. The mixture was maintaining at room temperature for 16h. Then a satured solution of NH_4Cl (10 mL) was added under vigorous stirring. The mixture was extracted with dietyl ether (15 mLx2). The organic phase was washed with H_2O (12 mL) and brine (12 mL) and dried on Na_2SO_4. The solvent was removed under reduced pressure, recovering the product **2** as colourless oil(1.1 g, 5.55 mmol, 91%,).

^{1}H NMR (200 MHz, $CDCl_3$): δ = 10.03 (s, 1 H), 7.63 (d, J = 5.4 Hz, 1 H), 7.00 (d, J = 5.2 Hz, 1 H), 2.95 (t, J = 7.4 Hz, 2 H), 1.55–1.74 (m, 2 H), 1.21– 1.40 (m, 6 H), 0.80–0.95 (m, 3 H) ppm.

Spectroscopic data are in agreement with those reported in literature (*Eur. J. Org. 2018 2657-2666*).

2,6-bis(3-hexylthiophen-2-yl)benzo[1,2-d:4,5-d']bis(thiazole)

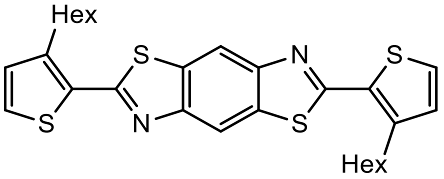

4

In a Schlenk tube, **2** (1.1 g, 5.55 mmol, 2.5 eq) was dissolved in *N,*N-DMF (32 mL). 2,5-diamino-1,4-benzenedithiol dihydrochloride **3** (544 mg, 2.22 mmol, 1.0 eq) and $ZnCl_2$ (15 mg, 0.11 mmol, 0.05 eq) were added to the solution. The mixture was stirred in air at rt for 16 h obtaining the precipitation of a yellow solid. The supernatant was removed and the solid was washed twice with EtOAc (15 mLx2). The product was centrifuged, using a mix of PE:EtOAc (50:1), obtaining the final product **4** as a yellowish solid (617 mg, 1.17 mmol, 53%).

^{1}H NMR (200 MHz, $CDCl_3$): δ = 8.49 (s, 2 H), 7.42 (d, J = 2.9 Hz, 2 H), 7.02 (d, J = 3.0 Hz, 2 H), 3.07 (t, J = 4.0 Hz, 4 H), 1.70–1.79 (m, 4 H), 1.21–1.43 (m, 12 H), 0.80–0.95 (m, 6 H) ppm.

^{13}C NMR (50 MHz, $CDCl_3$): δ = 161.5, 150.6, 144.9, 134.4, 131.4, 130.9, 128.4, 114.5, 31.6, 30.2, 30.1, 29.3, 22.6, 14.1 ppm.

ESI-MS: m/z = 525.3 $[M + H]^+$.

2,6-bis(5-bromo-3-hexylthiophen-2-yl)benzo[1,2-d:4,5-d']bis(thiazole)

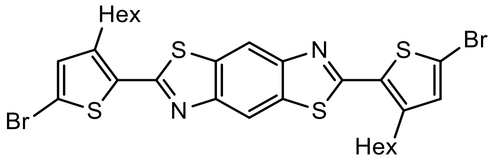

5

In a round-bottom flask, **4** (930 mg, 1.77 mmol, 1.0 eq) was dissolved in a solution of $CHCl_3$:CH_3COOH (2:1) (40 mL). The mixture was shielded from light and cooled at 0°C and NBS (1.3 g, 7.09 mmol, 4.0 eq) was added. The mixture was stirred at room temperature for 72 h. Then to the mixture was added $CHCl_3$ (60mL) the organic phase was washed with H_2O (20 mL), brine (20 mL) and finally dried on anhydrous Na_2SO_4. The solvent was removed under vacuum obtaining the product **5** as a yellow solid (1.2 g, 1.76 mmol, 98%).

^1H NMR (400 MHz, $CDCl_3$ + 10 % v/v TFA-d): δ = 8.81 (s, 2 H), 7.28 (s, 2 H), 3.00 (t, J = 7.9 Hz, 4 H), 1.75–1.85 (m, 4 H), 1.44–1.54 (m, 4 H), 1.30–1.39 (m, 8 H), 0.91 (t, J = 6.9 Hz, 6 H) ppm.

^{13}C NMR (100 MHz, $CDCl_3$ + 10 % v/v TFA-d): δ = 165.8, 155.6, 140.1, 135.7, 131.7, 127.4, 124.7, 112.6, 31.4, 31.2, 29.4, 29.1, 22.4, 13.8 ppm.

ESI-MS: m/z = 685.3, 683.2, 681.2 (1:2:1) $[M + H]^+$.

4-(tributylstannyl)benzaldehyde

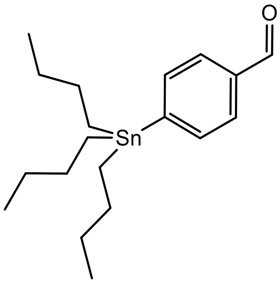

6a

In a schlenk tube, under nitrogen atmosphere, 4-bromobenzaldehyde (100 mg, 0.54 mmol,1.0 eq) was dissolved in anhydrous THF (3 mL) and N,O-dimethyl hydrossilamine (33 mg, 0.54 mmol, 1.0 eq) was added at room temperature. The mixture was stirred for 30 minutes, then cooled at -78°C and *n*-BuLi (369 µL, 0.59 mmol, 1.1 eq) was added dropwise in a 1 h. Then, tributyltin chloride (161 µL, 0.59 mmol, 1.1 eq) was added dropwise for 1 h, at -78°C. After 30 minutes the cooling bath was removed and the mixture was stirred for additional 18h. Then a saturated solution of NH_4Cl was added at the mixture and the organic solvent was evapoured under vacuum. The mixture was extracted with DCM (5 mLx2) and the organic phase was washed with H_2O (10 mLx2) and brine (10 mL). The organic phase was dried with anhydrous Na_2SO_4 and the organic solvents were removed under vacuum. A pale yellow oil corresponding to the stannyl intermediate **6a** was obtained and used directly, without further purification (200.6 mg, 0.51 mmol, 94%)

^{1}H NMR (400 MHz, $CDCl_3$): δ = 10.00 (s, 1 H), 7.78 - 7.83 (m, *J*=7.8 Hz, 2 H), 7.60 - 7.72 (m, *J*=7.8 Hz, 2 H), 1.49 - 1.60 (m, 6 H), 1.34 (sxt, *J*=7.4 Hz, 6 H), 1.01 - 1.20 (m, 6 H), 0.89 (t, *J*=7.4 Hz, 9 H) ppm.

^{13}C NMR (100.0 MHz, $CDCl_3$): δ = 192.9, 152.6, 136.9, 136.9, 135.8, 128.4, 29.0, 27.3, 13.7, 9.7 ppm.

GC-MS: r.t. = 24.90 min, M/z = 398 (100).

2-(4-(tributylstannyl)benzylidene)malononitrile

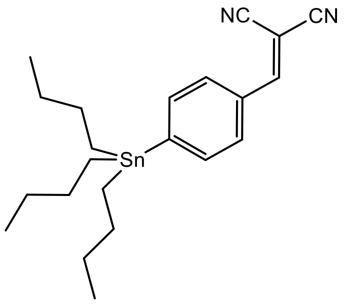

6

In a schlenk tube, under nitrogen atmosphere, **6a** (200.6 mg, 0.51 mmol, 1.0 eq) was dissolved in anhydrous AcCN (5 mL), on molecular sieves. Piperdine (1 drop) and malonitrile (40.4 mg, 0.61 mmol, 1.2 eq) were added at the mixture and stirred for 10 minutes at room temperature. After that, water (10 mL) was added at the mixture and the solution was extracted with EtAOc (10 mLx2). The organic phase was washed with H_2O (10 mLx2) and dried with anhydrous Na_2SO_4. The solvents were removed under vacuum obtaining the crude product, **6**, that was used directly, without further purification (122 mg, 0.29 mmol, 54%).

^{1}H NMR (200 MHz, $CDCl_3$): δ = 7.79 - 7.87 (m, 2 H), 7.77 (s, 1 H), 7.64 - 7.72 (m, 2 H), 1.42 - 1.66 (m, 6 H), 1.28 - 1.41 (m, 6 H), 1.06 - 1.19 (m, 6 H), 0.85 - 0.95 (m, 9 H) ppm.

^{13}C NMR (50.5 MHz, $CDCl_3$): δ = 160.3, 154.5, 137.5, 130.3, 129.1, 113.9, 82.0, 29.0, 27.2, 13.6, 9.8 ppm.

GC-MS: r.t. = 29.36 min, M/z = 388 (100).

2,2'-(((5,5'-(benzo[1,2-d:4,5-d']bis(thiazole)-2,6-diyl)bis(4-hexylthiophene-5,2-diyl))bis(4,1-phenylene))bis(methanylylidene))dimalononitrile

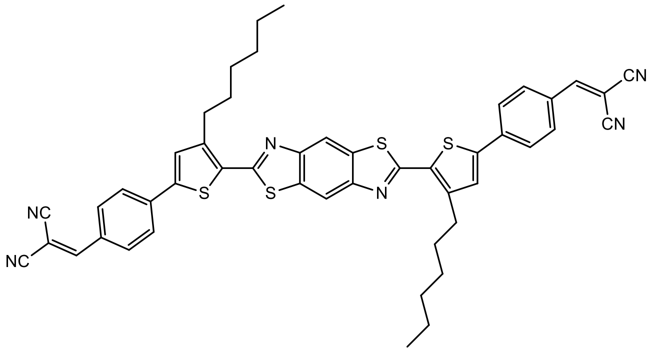

BBT1a

In a schlenk tube, under nitrogen atmosphere, **5** (85.4 mg, 0.13 mmol, 1.0 eq) $Pd_2(dba)_3$ (5.9 mg, 0.06 mmol, 0.05 eq), P(*o*-tol)$_3$ (3.9 mg, 0.013 mmol, 0.1 eq) and stannyl intermediate **6** (122.0 mg, 0.29 mmol, 2.2 eq) were suspended in toluene (5 mL) and heated at 100°C for 3 h. The mixture was then cooled at room temperature and water (10 mL) was added. The mixture was extracted with EtOAc (10 mLx2) and the organic phase was washed with H_2O (10 mLx2) and dried on anhydrous Na_2SO_4. The solvents were removed under vacuum and the crude was purified with flash chromatography (SiO_2, petroleum ether / DCM 2:1), obtaining the product **BBT1a** as an orange solid (12.8 mg, 0.015 mmol, 12%).

^1H NMR (200 MHz, $CDCl_3$): δ = 8.50 (s, 2H), 8.05 (s, 2H), 7.77 (s, 2H), 7.91 (d, J = 10.1 Hz, 4H), 7.55 (d, J = 11.6 Hz, 4H), 3.14-3.10 (m, 4H), 1.55-1.48 (m, 4H), 1.46–1.36 (m, 2H), 1.29-1.25 (m, 8H), 0.89 (t, *J* = 8.1 Hz, 6H) ppm.

ESI-MS: m/z = 829.6 $[M+H]^+$.

2-(4-(5-(6-(5-(4-(diphenylamino)phenyl)-3-hexylthiophen-2-yl)benzo[1,2-d:4,5-d']bis(thiazole)-2-yl)-4-hexylthiophen-2-yl)benzylidene)malononitrile

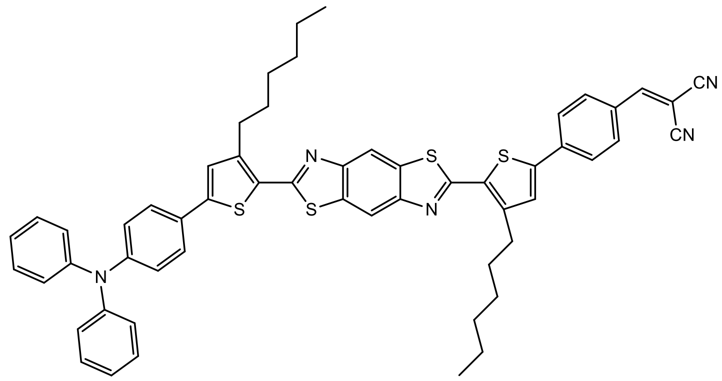

BBT1b

In a MW tube, under nitrogen atmosphere, 2-(4-(5-(6-(5-bromo-3-hexylthiophen-2-yl)benzo[1,2-d:4,5-d']bis(thiazole)-2-yl)-4-hexylthiophen-2-yl)benzylidene)malononitrile (30.4 mg, 0.03 mmol, 1.0 eq), Pd(dppf)Cl_2 (2.2 mg, 0.003 mmol, 0.1 eq), KF (5.2 mg, 0.09 mmol, 3.0 eq) and 4-(diphenylamino)phenylboronic acid (13.0 mg, 0.06 mmol, 2.0 eq) were suspended in degassed mixture of toluene (3 mL) and MeOH (0.5 mL).. The solution was heated at 70°C for 35', through MW irradiation. The mixture was then cooled at room temperature and water (5 mL) was added. The mixture was extracted with DCM (5 mLx2) and the organic phase was washed with water (10 mLx2) and brine (10 mL) and dried on anhydrous Na_2SO_4. The solvents were removed under vacuum and the crude was purified with flash chromatography (SiO_2, petroleum ether /DCM/tol 4:2:1), obtaining the final product as a yellow solid (3.4 mg, 0.37 μmol, 10%).

^{1}H NMR (200 MHz, $CDCl_3$): δ = 8.50 (s, 2H), 7.95 (s, 1H) 7.80 (s, 1H), 7.71 (s, 1H), 7.65-7.60 (m, H), 7.45-7.38 (m, H), 7.21-7.15 (m, H), 7.05-7.00 (m, H), 3.15-3.08 (m, 2H), 2.35-2.25 (m, 2H), 1.50–1.32 (m, 4H), 1.20-1.15 (m, 8H), 0.90 (t, *J* = 8.1 Hz, 6H) ppm.

ESI-MS: m/z = 920.6 $[M+H]^+$.

10-(4-bromophenyl)-10H-phenothiazine

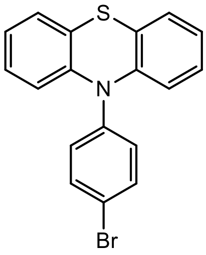

10a

In a Schlenk tube under inert atmosphere of N_2, $Pd_2(dba)_3$ (52 mg, 0.05 mmol, 0.05 eq) and Xantphos (58 mg, 0.1 mmol, 0.1 eq) was solubilized under stirring for 20' in dry toluene (10mL). Phenothiazine (200 mg, 1.0 mmol, 1.0 eq), 1-bromo-4-iodio benzene (311 mg, 1.1 mmol, 1.1 eq) and NaO^tBu (288 mg, 3.0 mmol, 3.0 eq) were added and the mixture was heated at 90°C for 1h. The mixture was filtrated on celite and the residue washed with EtOAc (20mL). The organic phase was washed with water (10 mL) and brine (10 mL) and then dried on anhydrous Na_2SO_4. The solvent was removed under vacuum obtaining the product **10a** as a white solid (350 mg, 0.99 mmol, 98.8%).

^{1}H NMR (200 MHz, $CDCl_3$): δ = 7.72 (d, J= 8.2 Hz, 2H), 7.25 (d, J= 8.4 Hz, 2H), 7.08 (dd, J= 7.0, 2.0 Hz, 2H), 6.75-6.90 (m, 4H), 6.24 (dd, J= 7.2, 1.8 Hz, 2H) ppm.

Spectroscopic data are in agreement with those reported in literature (*J. Mater. Chem. B*, 2019, 7, 2454-2462).

10-(4-(4,4,5,5-tetramethyl-1,3,2-dioxaborolan-2-yl)phenyl)-10H-phenothiazine

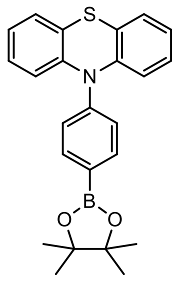

10

In a Schlenk tube under inert atmosphere of N_2, **10a** (350 mg, 0.99 mmol, 1.0 eq) was dissolved in dry THF (8 mL). Then bis-(pinacolato)diboron (501 mg, 1.97 mmol, 2.0 eq), Pd(dppf)Cl_2 (81 mg, 0.01 mmol, 0.1 eq) and AcOK (291 mg, 2.96 mmol, 3.0 eq) were added to the solution. The mixture was stirred at room temperature for 24h. The solvent was removed under vacuum and the crude product dissolved in EtOAc (20 mL) and was washed with water (10 mL) and brine (10 mL). Then the organic phase was dried on anhydrous Na_2SO_4 and the solvents evaporated under reduced pressure. The crude product was purified by flash column chromatography (SiO_2, petroleum ether / DCM 3:1) obtaining the product **10** as a white solid (234 mg, 0.58 mmol, yield 59%).

^{1}H NMR (200 MHz, $CDCl_3$): δ = 7.63 (d, J= 8.0 Hz, 2H), 7.28 (d, J= 8.2 Hz, 2H), 7.08 (dd, J= 7.0, 2.0 Hz, 2H), 6.75-6.90 (m, 4H), 6.24 (dd, J= 7.2, 1.8 Hz, 2H), 1.65 (s, 12) ppm.

Spectroscopic data are in agreement with those reported in the literature (*J. Am. Chem. Soc.* 2018, 140, 15, 5290–5299).

2,6-bis(5-(9H-carbazol-9-yl)-3-hexylthiophen-2-yl)benzo[1,2-d:4,5-d']bis(thiazole): BBT2

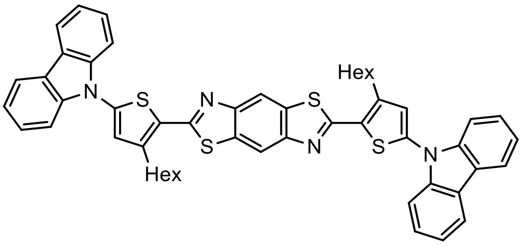

BBT2

In a Schlenk tube under inert atmosphere of N_2, $Pd_2(dba)_3$ (10.5 mg, 0.011 mmol, 5% mol) and Xantphos (13.3 mg, 0.023 mmol, 10% mol) was dissolved in dry toluene (3 mL) at rt under stirring for 20’. In a second schlenk tube under nitrogen, ammine **9** (96.1 mg, 0.57 mmol, 2.5 eq) and KF (40.1 mg, 0.69 mmol, 3.0 eq) were dissolved in MeOH (0.5 mL). The solution of MeOH were added in the first Schlenk and finally the compound **5** (158.6 mg, 0.23 mmol, 1.0 eq) was added. The mixture was heating at 90°C for 24 hours. The mixture was cooled at room temperature and the solvent removed by filtration. The residue was washed with XXX obtaining the product **BBT2** as a pale yellow solid (150 mg, 0.18 mmol, >99%).

^{1}H NMR (400 MHz, THF-d_8): δ = 8.62 (s, 2H), 8.16 (d, *J* = 8.0 Hz, 4H), 7.71 (d, *J* = 8.2 Hz, 4H), 7.47 (dt, J_1 = 7.0, J_2 = 1.2, 4H), 7.36 (s, 2H), 7.34-7.29 (m, 4H), 3.28-3.22 (m, 4H), 1.96-1.87 (m, 4H), 1.65-1.56 (m, 4H), 1.50-1.35 (m, 8H), 0.95 (t, *J* = 7.0, 6H) ppm.

^{13}C NMR (100 MHz, THF-d_8): δ = 152.1, 145.5, 142.3, 142.2, 135.8, 129.9, 128.6, 127.4, 125.1, 122.1, 121.2, 115.9, 115.8, 111.3, 32.8, 31.5, 31.3, 30.8, 23.7, 14.6 ppm.

ESI-MS: m/z = 855.27 $[M+H]^+$.

2,6-bis(5-(4-(10H-phenothiazin-10-yl)phenyl)-3-hexylthiophen-2-yl)benzo[1,2-d:4,5-d']bis(thiazole): BBT3

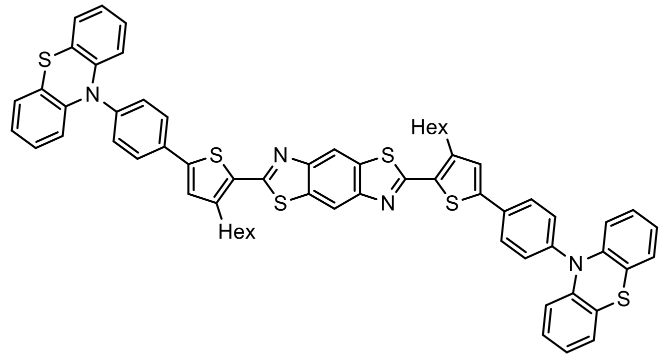

BBT3

In a microwave tube, $Pd_2(dba)_3$ (10.5 mg, 0.011 mmol, 5% mol) and SPhos (9.4 mg, 0.023 mmol, 10% mol) was dissolved in dry toluene (3mL) at rt under stirring for 20' in dry toluene (3 mL). In a second schlenk tube, the boronic ester **10** (234 mg, 0.58 mmol, 2.5 eq) and KF (40.1 mg, 0.69 mmol, 3.0 eq) were dissolved in MeOH (0.5 mL). The solution of MeOH were added in the microwave tube and compound **5** (158.6 mg, 0.23 mmol, 1.0 eq) was also added. The mixture was stirring for 30' at room temperature and then heated at the MW at 70°C, for 35'. The mixture was cooled at room temperature and the solvent was removed under vacuum. The crude product was purified by flash column chromatography (SiO_2, petroleum ether / DCM / tol 6:2:1) obtaining **BBT3 as** a pale orange solid, (33.4 mg, 0.031 mmol, 43%).

^{1}H NMR (400 MHz, THF-d_8): δ = 8.58 (s, 2H), 8.14 (d, *J*=7.8Hz, 4H), 7.97 (d, *J*=7.8Hz, 4H), 7.64 (s, 2H), 7.56 (d, , *J*=8.6Hz, 4H), 7.46-7.40 (m, 4H), 7.23 (t, , *J*=7.4Hz, 4H), 6.83 (d, , *J*=8.6Hz, 4H), 3.21-3.18 (m, 4H), 1.60-1.30 (m, 16H), 0.94 (t, *J* = 8.0 Hz, 6H) ppm.

^{13}C NMR (100 MHz, THF-d_8): δ = 152.2, 147.2, 146.1, 145.1, 140.7, 139.9, 135.7, 133.1, 132.8, 132.5, 129.8, 129.3, 127.9, 125.4, 123.8, 122.9, 118.1, 115.8, 32.9, 31.4, 31.3, 30.5, 23.7, 14.6 ppm.

ESI-MS: m/z = 1070.27 $[M\cdot]^+$.

2,6-bis(3-hexyl-5-(10-(4-methoxyphenyl)-10H-phenothiazin-3-yl)thiophen-2-yl)benzo[1,2-d:4,5-d']bis(thiazole): BBT4

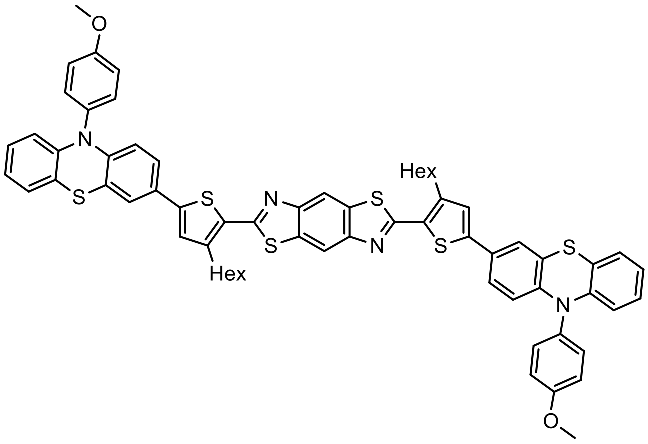

BBT4

In a microwave tube, $Pd_2(dba)_3$ (13.2 mg, 0.014 mmol, 5% mol) and SPhos (11.9 mg, 0.029 mmol, 10% mol) was dissolved in dry toluene (3 mL) at rt under stirring for 20' in dry toluene (3 mL). In a second schlenk tube, the boronic ester **11** (312.6 mg, 0.72 mmol, 2.5 eq) and KF (50.5 mg, 0.87 mmol, 3.0 eq) were dissolved in MeOH (0.5 mL). The solution of MeOH were added in the microwave tube and compound **5** (200 mg, 0.29 mmol 1.0 eq) was also added. The mixture was stirring for 30' at room temperature and then heated at the MW at 70°C, for 35'. The mixture was cooled at room temperature and the solvent was removed under vacuum. The crude product was purified by flash column chromatography (SiO_2, petroleum ether / DCM 3:1) obtaining **BBT4 as** an orange solid, (226 mg, 0.2 mol, 69%).

^{1}H NMR (400 MHz, THF-d_8): δ = 8.49 (s, 2H), 7.37 (d, J=2.1 Hz, 2H), 7.34 (d, J = 8.8 Hz, 4H), 7.29 (s, 2H), 7.21 (d, J_1 = 8.8 Hz, 4H), 6.98 (dd, J_1 = 7.2 Hz, J_2 = 2.0 Hz, 2H), 6.85-6.77 (m, 4H), 6.21 (d, J_1 = 8.2, 2H), 6.18 (dd, J_1 = 7.2 Hz, J_2 = 2.0, 2H), 3.89 (s, 6H), 3.12-3.08 (m, 4H), 1.56-1.51 (m, 4H), 1.42–1.36 (m, 4H), 1.28-1.27 (m, 8H), 0.89 (t, J = 8.1 Hz, 6H) ppm.

^{13}C NMR (100 MHz, THF-d_8): δ = 161.5, 160.9, 152.2, 147.1, 145.8, 145.1, 135.5, 134.0, 133.1, 128.9, 127.9, 127.4, 127.1, 125.3, 124.3, 123.5, 120.1, 117.1, 116.9, 116.8, 56.0, 32.8, 32.7, 31.3, 30.6, 23.7, 14.6 ppm
(some quaternary carbon signal missed due to low solubility).

ESI-MS: m/z = 1131.30 [M+H]$^+$.

CHAPTER 4

DESIGN and SYNTHESIS of QUINOXALINE-BASED LUMINOPHORES

4 QUINOXALINE DERIVATIVES

Quinoxalines are very strong acceptor moieties, employed in several organic optoelectronic devices. Organic light emitting diodes (OLEDs)[189], photovoltaic cells[190], field-emitting transistors (FETs)[191], non-linear optics[192] and fluorescent chemosensors[193] are some of the principal optical devices in which quinoxaline derivatives were employed. For these devices, molecules with low band gap between HOMO and LUMO levels are ideal photoactive specie.

Considering D-A-D' structures properties, pyrazine-fused unit has been already considered as a strong acceptor building blocks, in fact the possibility of tuning LUMO energy, the color control and the typical high fluorescence quantum yield highlight quinoxaline electron-deficient unit an ideal acceptor moiety for LSC organic compounds[194].

Moreover, the quinoxaline core allows simple synthetic procedure and easy functionalization and is characterized by photochemical and thermal stability.

Starting from all these considerations, we decided to design a new class of D-A-D molecules based on the quinoxaline core.

Two different acceptor moieties bearing alkyl and arene groups on the pyrazine ring were considered, and the central core was elongated using three different tryarilamine donor groups (Fig 68). The aim was investigating the tunability of the electronic and optical properties of the final compounds and their possible applications in LSC devices.

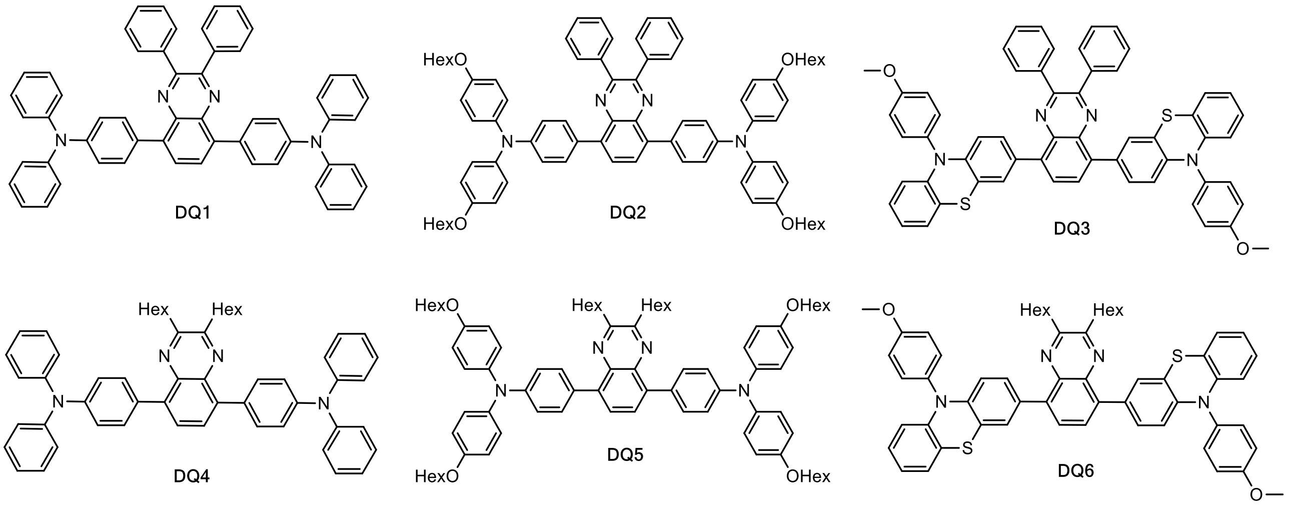

Fig. 68: Molecular structures of pyrazine derivatives, designed for LSC application.

---

[189] a) C.W. Tang, S.A. Vanslyke, *Appl. Phys. Lett.* **1987**, *51*, 913; b) C.D. Müller *et al.*, *Nature* **2003**, *421*, 829-833; c) F.-M. Xie, H.-Z. Li, G.-L. Dai, Y.-Q. Li, T. Cheng, M. Xie, J.-X. Tang, X. Zhao, *ACS Appl. Mater. Interfaces* **2019**, *11*, 26144–51.

[190] a) C W. Tang, *Appl. Phys. Lett.* **1986**, *48*, 183; b) D. Wöhrle, D. Meissner, *Adv. Mater.* **1991**, *3*, 129.

[191] a) A. Tsumura, H. Koezuka, T. Ando, *Appl. Phys. Lett.* **1986**, *49*, 1210; b) Z. Bao, A.J. Lovinger, J. Brown, *J. Am. Chem. Soc.* **1998**, *120*, 1, 207–208; c) Y. Zhou *et al.*, *J. Am. Chem. Soc.* **2007**, *129*, 41, 12386-87.

[192] D.J. Williams, *Angew. Chem., Int. Ed. Engl.* **1984**, *23*, 690.

[193] a) R. Martínez-Máñez, F. Sancenón, *Chem. Rev.* **2003**, *103*, 11, 4419–76; b) S.W. Thomas, G.D. Joly, T.M. Swager, *Chem. Rev.* **2007**, *107*, 4, 1339–86.

[194] a) H.J. Son *et al.*, *J. Org. Chem.* **2009**, *74*, 3175–78; b) X. Lu, S. Fan, J. Wu, X. Jia, Z.S. Wang, G. Zhou, *J. Org. Chem.* **2014**, *79*, 6480–89.

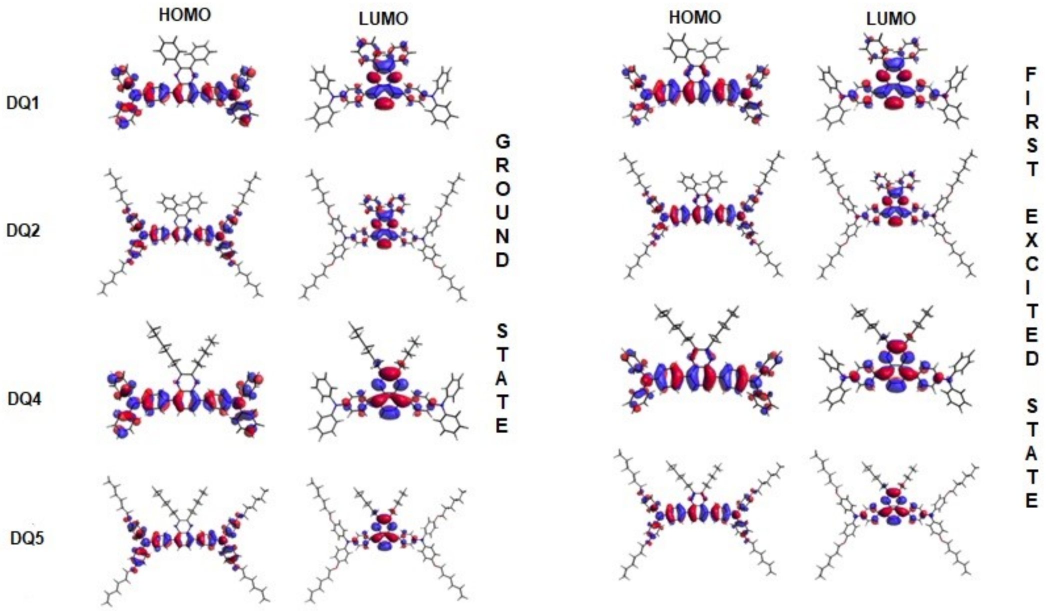

Fig. 70: *Calculated HOMO and LUMO levels at S_0 e S_1 of* ***DQ1, DQ2, DQ4*** *and* ***DQ5****, calculated for toluene solutions.*

Frontiers Molecular Orbitals electron density distributions of S_0 and S_1, calculated in toluene, showed, as expected, a delocalization of HOMO on triarilammine donor moiety and of LUMO on the quinoxalline moiety. Moreover, in the case of **DQ1** and **DQ2**, LUMO was partially delocalized on phenyl groups (Fig. 70).

Table 13: *TD-MPW1K/6-311+G(2d,p) absorption maxima (λ_{max} abs in nm), excitation energies (E_{exc} in eV), oscillator strengths (f) and contributions (%) to the $S_0 \rightarrow S_1$ transition in toluene in PMMA of compounds* ***DQ1, DQ2, DQ4*** *and* ***DQ5****.*

DQ	Medium	λ_{max} abs [nm]	E_{exc}	f	Transition (%)
DQ1	toluene	409	3.02	0.66	90 (H→L)
	PMMA	409	3.03	0.66	89 (H→L)
DQ2	toluene	434	2.85	0.66	90 (H→L)
	PMMA	434	2.86	0.66	90 (H→L)
DQ4	toluene	386	3.21	0.94	89 (H→L)
	PMMA	386	3.21	0.94	89 (H→L)
DQ5	toluene	406	3.06	0.94	89 (H→L)
	PMMA	405	3.06	0.95	89 (H→L)

Absorption maxima and excitation energies were also calculated both in toluene and PMMA and are reported in table 13 and 14. Calculations predicted that, in general, a stronger donor group induced a bathochromic shift both in absorption and in emission maxima, showing a red-shift of 20-30 nm, in molecules with the same core (**DQ1<DQ2** and **DQ4<DQ5**). Moreover, the effect

of phenyl groups, which extended π-conjugation more than hexyl chains on the acceptor core, favoured bathochromic shift of absorption and emission maxima, with a red-shift of around 20-30 nm for **DQ1/DQ2** and **DQ4/DQ5** couples.

Table 14: *TD-MPW1K/6-311+G(2d,p) emission maxima (λ_{max} emis in nm), excitation energies (E_{exc} in eV), oscillator strengths (f) and contributions (%) to the $S_0 \rightarrow S_1$ transition in toluene and in PMMA of compounds* ***DQ1, DQ2, DQ4*** *and* ***DQ5****.*

DQ	Medium	λ_{max} emis [nm]	E_{exc}	f	Transition (%)
DQ1	toluene	537	2.31	0.83	96 (L→H)
	PMMA	539	2.30	0.84	96 (L→H)
DQ2	toluene	561	2.21	0.83	95 (L→H)
	PMMA	562	2.21	0.84	95 (L→H)
DQ4	toluene	514	2.41	1.07	96 (L→H)
	PMMA	515	2.41	1.08	96 (L→H)
DQ5	toluene	532	2.33	1.08	95 (L→H)
	PMMA	533	2.33	1.09	95 (L→H)

4.1 SYNTHETIC APPROACH

The new class of fluorophores were synthesized following different synthetic approaches. Considering the two acceptor cores, a common strategy was investigated, that is shown in scheme 5.

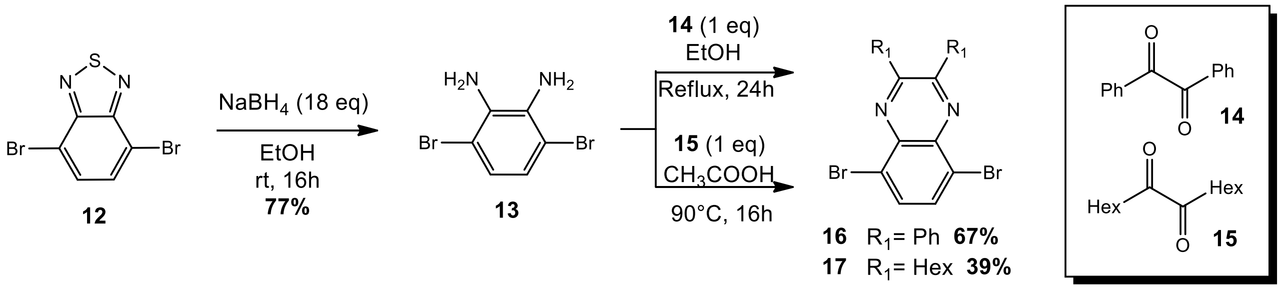

Scheme 5: *Synthetic procedure of acceptor quinoxaline cores.*

The diamine **13** was obtained through the reduction of commercially available 4,7-dibromo-2,1,3-benzothiadiazole (**12**) using a large excess of $NaBH_4$ in EtOH. After 16 hours at room temperature, diamine **13** was obtained with a good yield. Due to the low stability to the air, compound **13** was used immediately for the subsequent step, without needing purification. The low stability of this particular diamine is well known, due to the equilibrium with redox forms

(Scheme 6)[195].

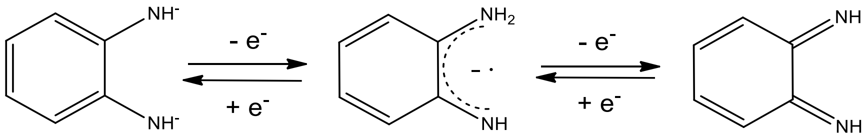

1a **1b** **1c**

Scheme 6: *Redox forms of o-phenylenediamine.*

Cyclization of intermediate **13** in presence of diketones **14** or **15** gave the desired compounds, **16** and **17** respectively, which were obtained in 67% and 39%, without purification. While diketone **14** was commercially available, compound **15** needed to be synthesized starting from 1-bromohexane, through the formation of corresponding Grignard intermediate and reaction with the oxalyl chloride.

To prepare the final-quinoxalines a Suzuki-Miyaura cross-coupling reactions, using the suitable corresponding boronic acid or ester was performed (Scheme 7)[196].

Optimal reaction conditions needed to be adapted to single cases.

Initially we investigated a MW irradiation procedure. Such approach gave already positive results in the synthesis of BBT chromophores allowing to short reaction time (approx. 35 min) and to limit formation of side-products.

Thus, the same conditions already employed for BBTs were applied to prepare compound **DQ3**, by reacting boronic ester **20** in standard Suzuki-Miyaura condition[197], using Pd(dppf)Cl_2 as catalyst, KF as base and a mixture of toluene and MeOH as reaction medium. Compound **DQ3** was obtained with 46% yield after purification.

The same reaction approach was used to prepare compounds **DQ2** and **DQ4**. Unfortunately, the applied condition resulted not of general efficiency, as **DQ2** was obtained only in a 21% yield, by reaction with a small excess of boronic ester **19**; on the other hand, when dibromide **17** was reacted with commercial boronic acid **18**, a better yield was observed, leading to compound **DQ4** in 55% yield.

---

[195] a) T.-A. Koizumi, H. Hayashi, S. Shiozaki, T. Yamamoto, *Inorg. Chim. Acta*, **2014**, *421*, 427–432; b) H.L. Chan *et al.*, *Inorganic Chemistry*, **2002**, *41*, 12, 3161-71; c) J. Iqbal, B. Bhatia, N.K. Nayyar, *Chemical Reviews*, **1994**, *94*, 2, 519-564; d) F.N. Rein, R.C. Rocha, H.E. Toma, *Electrochem. Comm*., **2002**, *4*, 5, 436-441; e) B. Milliken, L. Borer, J. Russell, M. Bilich, M.M. Olmstead, *Inorg. Chim. Acta* **2003**, *348*, 212-216; f) A.L.R. Silva *et al.*, *Inorg. Chem. Comm*., **2005**, *8*, 1154-58.

[196] L.F. Warren, *Inorganic Chemistry*, **1977**, *16*, 11, 2814-19.

[197] a) A. Migliorini, C. Oliviero, T. Gasperi, M.A. Loreto, *Molecules* **2012**, *17*, 4508-21; b) A. Hooper, A. Zambon, C.J. Springer, *Org. Biomol. Chem*. **2016**, *14*, 3, 963–969; c) D. Blakemore, Ch 1:Suzuki–Miyaura Coupling , in *Synthetic Methods in Drug Discovery: Volume 1*, **2015**, pp. 1-69 DOI: 10.1039/9781782622086-00001.

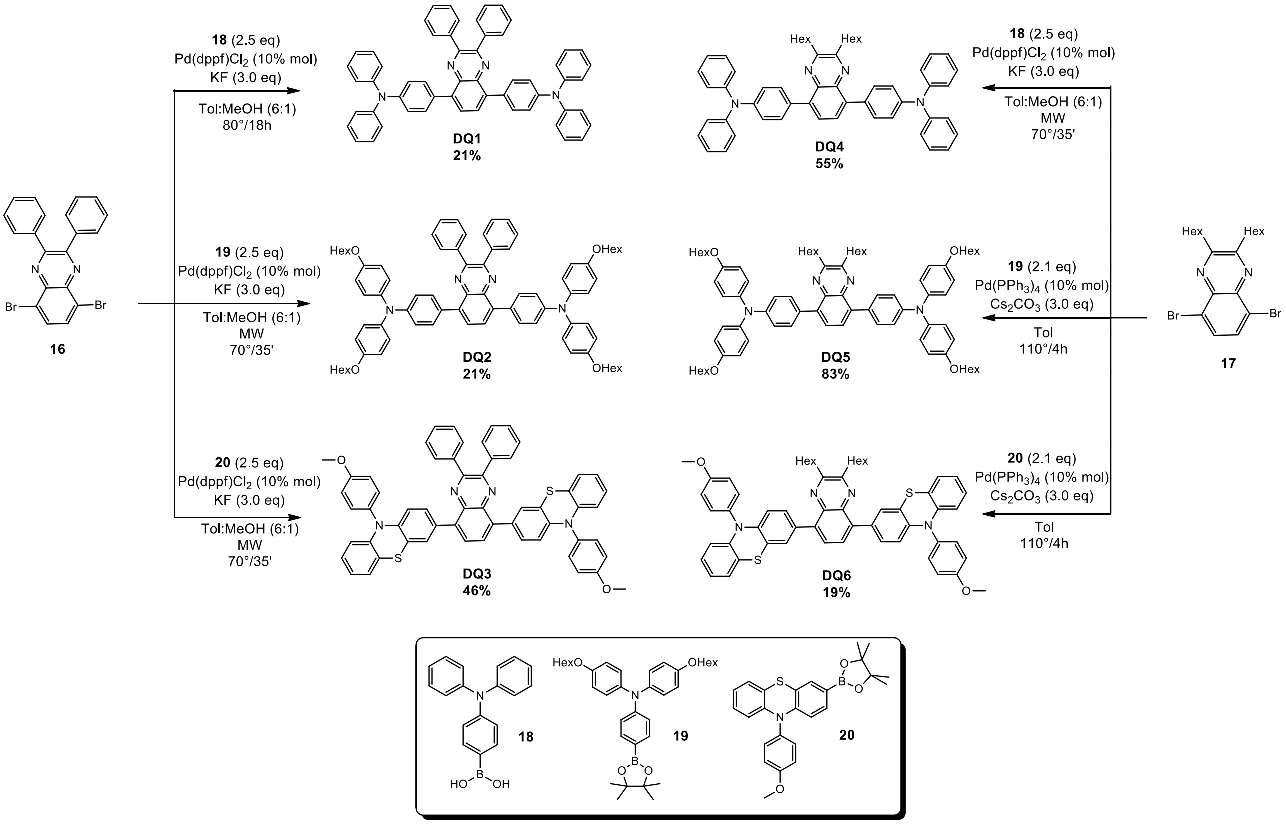

Scheme 7: *Cross-coupling conditions for the synthesis of final products* ***DQ1-6****.*

Aiming to obtain better yields a thermal procedure was employed for the other DQs.

Indeed the synthesis of compound **DQ1** was already reported by Kang C using thermal heating at 110°C for 48h, $Pd(PPh_3)_4$ as catalyst and Cs_2CO_3. In order to find milder conditions we tried to use a different catalyst such as $(Pd(dppf)Cl_2$, KF as base and and tol:MeOH as solvent reaction. In these reaction conditions, reduced reaction time, from 48 hours to 18 hours, and a lower temperature could be used, however some by products were formed leading to **DQ1** only in 21% yield after purification.

Finally compounds **DQ5** and **DQ6** were prepared following the conditions reported by Kang such as $Pd(dppf)Cl_2$, and KF as base. Thus, quinoxaline core **17** was reacted with the corresponding boronic ester and acid (**18** and **19**) using $Pd(PPh_3)_4$ and Cs_2CO_3 were as catalyst and base respectively, and a mixture of tol:MeOH, as solvent. Both reactions were carried out heating at 110° for 4 hours. In this way compound **DQ5** was obtained with a high yield and with few by-products, on the contrary compound **DQ6** was isolated only in a very low yield probably due to decomposition during the purification procedure. Despite several effort were made trying to prepare a reasonable amount of compound **DQ6**, they were all unsuccessful.

4.2 SPECTROSCOPIC CHARACTERIZATION

Five of quinoxaline derivatives were characterized spectroscopically in solution (par. 4.3.1) and polymer matrices (4.3.2). Their excited state behaviour was investigated through transient absorption spectroscopy, comparing the impact of different medium (par. 4.3.3).
Due to the difficulties encountered in the synthesis, which did not allow us to recover a suitable amount of compound needed for the spectroscopic analysis in polymer matrices, **DQ6** has not been taken in consideration for this study.

4.2.1 Spectroscopic characterization in solution

All the new molecules prepared were characterized through UV-Vis and fluorescence emission spectroscopy.
Toluene was chosen as solvent for its capability of solubilizing efficiently all samples at different concentrations. Compound **BBT4** and **BBT3** were used as standard compounds for the calculation of fluorescence quantum yield.

Table 15: *Optical properties of DQ 1-5 in toluene: absorption maximum wavelength (nm), molar extinction coefficient, emission maximum wavelength (nm), Stokes shift, expressed in nm and eV, and fluorescence quantum yield.*

Compound	λ_{abs}(nm)	ε (M^{-1} cm^{-1})	λ_{em}(nm)	SS(nm[eV])	Φ_f (%)
DQ1	433	30929	538	105 [0.56]	64[a]
DQ2	457	32685	567	110 [0.53]	34[a]
DQ3	452	11629	601	149 [0.68]	46[b]
DQ4	398	12000	515	117 [0.71]	44[b]
DQ5	416	20480	529	112 [0.62]	70[c]

[a] Fluorescence quantum yield, using BBT4 as the standard compound.

[b] Fluorescence quantum yield, using the integrated sphere in spectroscopic measurement.

[c] Fluorescence quantum yield, using BBT3 as the standard compound.

The spectroscopic properties were summarized in table 15, which were in agreement with the calculated ones. The corresponding DQs absorption and emission spectra at different concentrations were described in figure 71.

All the fluorophores of the quinoxalines series showed a wide range of absorption wavelengths, from 400 nm to 460 nm. Such absorption spectra presented broad peaks, maintaining a constant shape of spectra a different concentration (see the linear fit of each DQ in figure 72). Thus, no aggregation phenomena were observed. All molecules exhibited high molar extinction coefficient, demonstrating their strong and high capacity of harvesting of light.

DQs showed also a broad emission spectrum in a range of 515-600 nm and large Stokes shifts. In addition, no vibronic band were observed.

More in detail**, DQ2** showed the lower fluorescence quantum yield. Thus, **DQ2** presented results in decreasing fluorescence quantum yield in the liquid phase more than in the solid one. Indeed, molecular conformation in the solid state was more constrained in more compatible solid phase, while, in solution, the presence of alkyl chains improved solubility and their molecular DOFs.

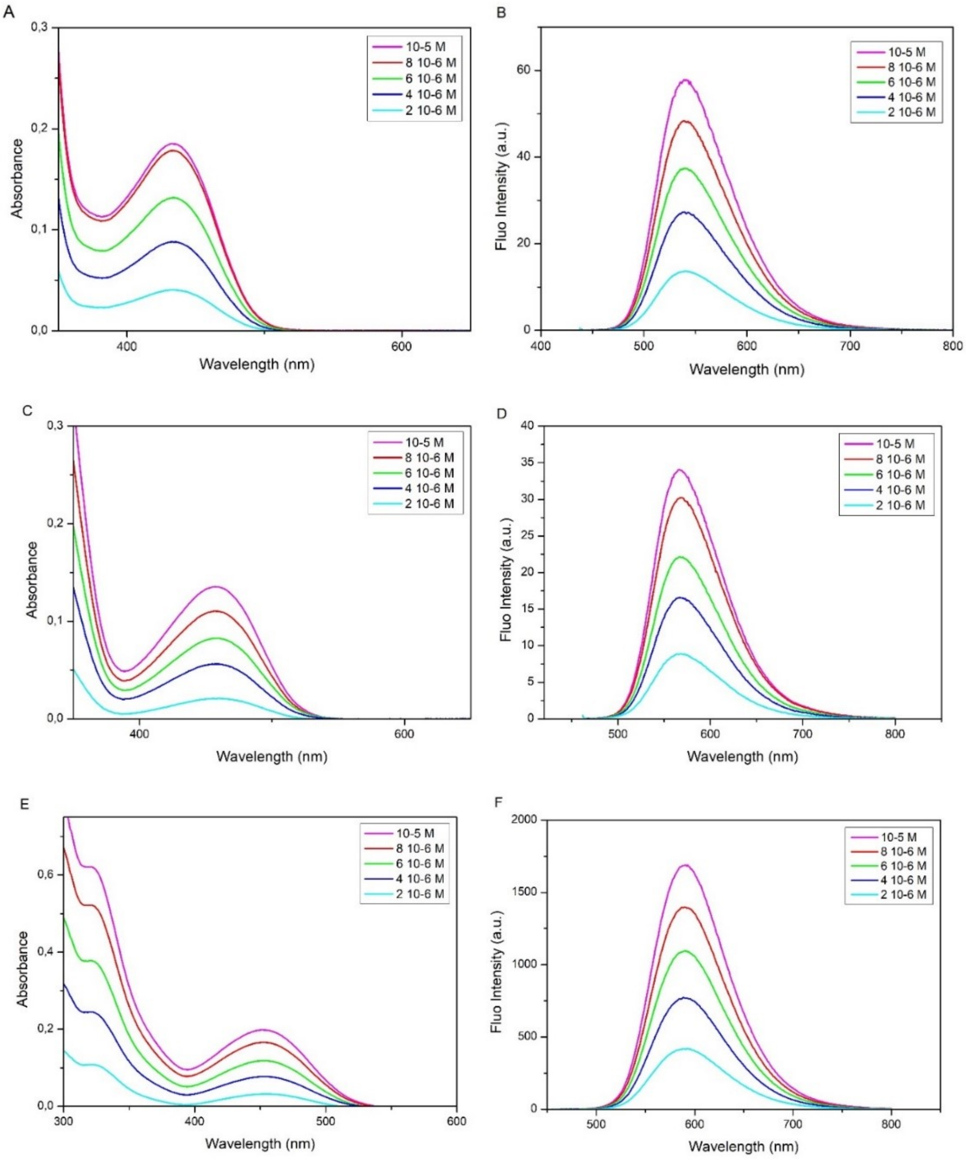

*Fig. 71: Absorption (A) and emission (B) spectra of **DQ1** (excitation at 433 nm); absorption (C) and emission (D) spectra of **DQ2** (excitation at 457 nm) and absorption (E) and emission (F) spectra of **DQ3** (excitation at 452 nm) in toluene, at different concentrations.*

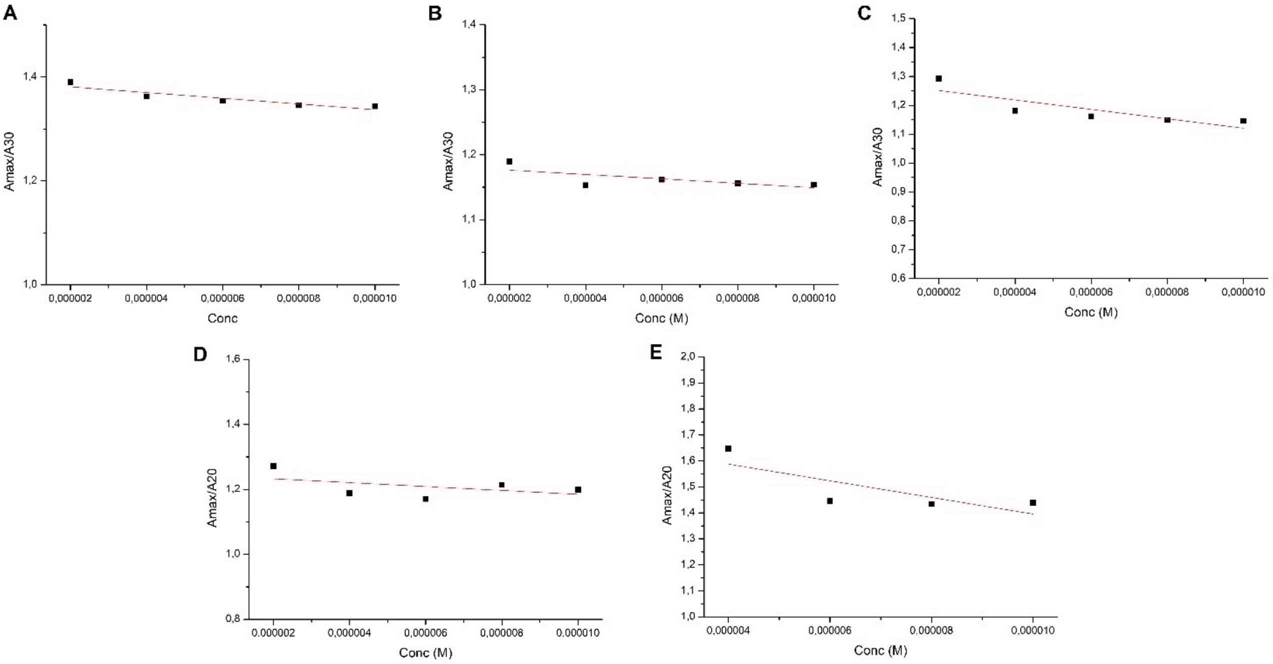

Fig. 72: *Linear fit between the ratio of absorbance at two different wavelenghts of the absorption band, where one of those is λ_{abs} max of absorption, and concentration.*

Comparing the donor effect, for the same acceptor core, red-shift was observed for both absorption and emission spectra, with the increasing of donating property.

For instance, in the series **DQ1-3** characterized by the same 2,3-diphenylquinoxaline core (Fig. 72), a small overlap region and a large Stokes shift were found, which might suppress self-absorption phenomena. **DQ1** was the more blue-shifted quinoxaline of this series, showing absorption and emission peaks at 433 and 538 nm, respectively. However, the limited rotation of triphenylamine around C-C bond with quinoxaline ring possibly favored a partial co-planarity between donor and acceptor moieties[198]. **DQ1** HOMO level was delocalized principally on donor group and partially on the acceptor moiety, favoring a high molar extinction coefficient. Moreover, its high fluorescence intensity in toluene involved fluorescence quantum yield, which resulted to be the highest of **DQ1-3** group. That means that energy loss through non-radiative processes was lower for **DQ1** than **DQ2** and **DQ3**, in solution samples.

DQ2 and **DQ3** showed larger Stoke shifts and higher bathochromic effect for the absorption and emission spectra. However, their fluorescence quantum yields were lower than **DQ1**. In particular, **DQ2** showed the lowest Φ_f, around 34% in solution.

For **DQ3**, a stronger ICT effect at the excited state was confirmed by red shifted emission range, where the charge transfer was redistributed and delocalized. However, this rearrangement caused a decrease of fluorescence quantum yield[199] (46%).

Focusing on **DQ4-5**, similarly to **DQ1-3**, a bathochromic effect was observed from **DQ4** to **DQ5**, due to the presence of more electron-rich groups. Long-wavelengths emission ranges (around 500 nm) and very large Stoke shifts characterized both of them (Fig. 73).

---

[198] V.A. Chiykowski, B. Lam, C. Du, C.P. Berlinguette, *Chem. Commun.,* **2017**, *53*, 2367-70.

[199] D.B.G. Williams, M. Lawton, *J. Org. Chem.* **2010**, *75*, 24.

While **DQ5** showed the highest **Φ_f** value (70%) of all DQs.

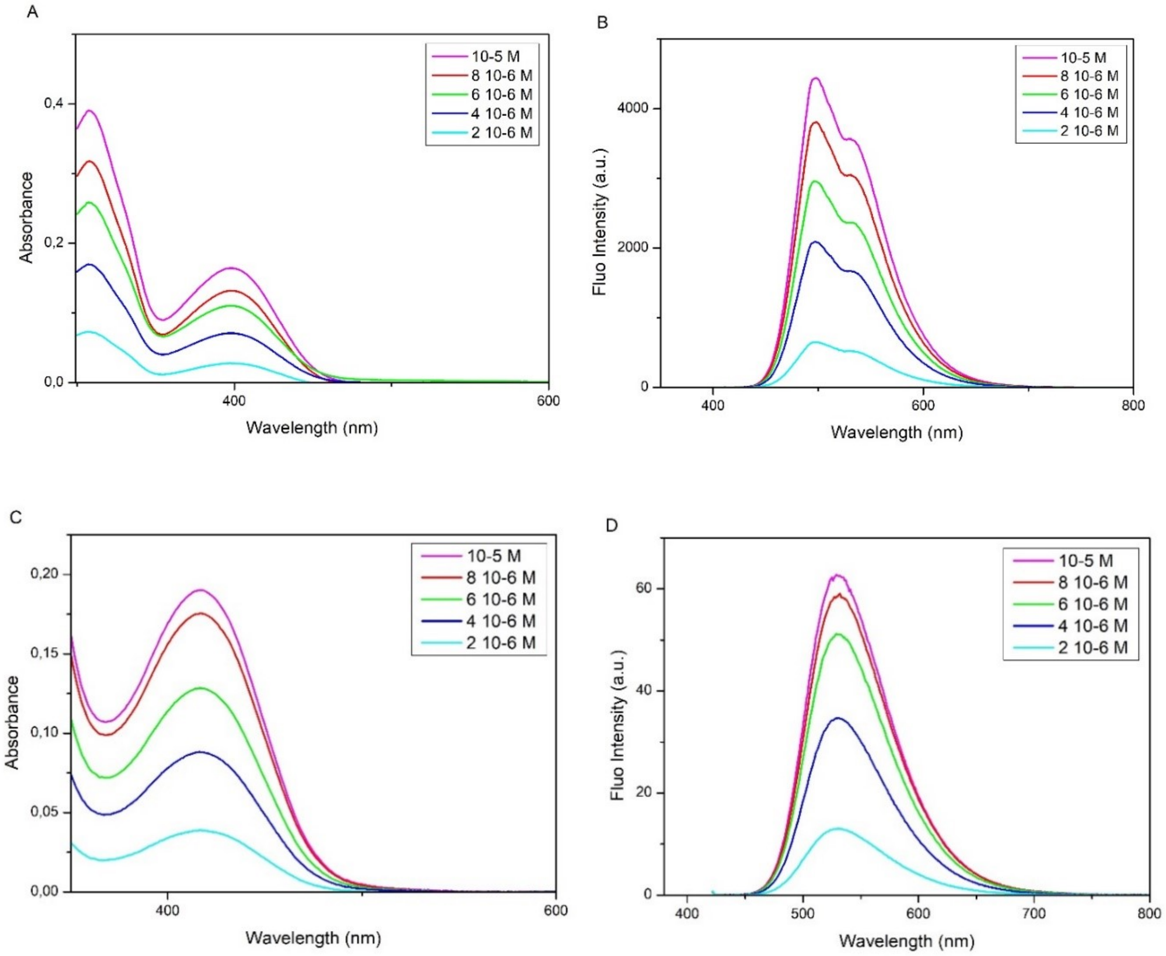

Fig. 73: *Absorption (A) and emission (B) spectra of* ***DQ4*** *(excitation at 398 nm) and absorption (C) and emission (D) spectra of* ***DQ5*** *(excitation at 416 nm) in toluene, at different concentrations.*

On the other hand, comparing molecules with different acceptor core and common donor moiety (**DQ1** vs **DQ4**, **DQ2** vs **DQ5**), phenyl substituents exhibited a bathochromic effect compared with the hexyl ones. The ICT mechanism was stronger for arenes than the alkyl substituents, due to their great extended conjugation and high sp^2 character. Moreover, LUMO level of **DQ4-5** was lower than the **DQ1-3** ones, due to their lower delocalized electrons density (see computational studies, par 4.1.1).

Comparing fluorescence quantum yields for molecules which presented the same donor group (**DQ1** and **DQ4**, **DQ2** and **DQ5**), considering the absence of particular steric hindrance, and the similar diedhrical angles between donor and acceptor moieties for all DQs (around 43°), these different behaviors can be explained through a comparison among the excited states.

4.2.2 Spectroscopic analysis in polymer matrix

After the preliminary study of optical properties in solution, DQs were characterized in polymer matrices. Organic luminophores were dispersed in PMMA and PCMA films with a 25μm±5μm of thickness, at different concentrations.

DQ1-3/PMMA films absorption (A) and emission (B) spectra at different concentration are shown in Fig 74. As it is possible to see all the molecules showed a comparable behaviour which was independent from the polymeric matrix.

In particular, all DQs exhibited broad absorption peak, whose intensity increased with concentration following a linearity trend, according to Lambert-Beer law, without evident differences in spectrum shape. Thus, no aggregates were formed at higher concentrations and good dispersion was observed, without evident phase separation at microscope analysis. More in detail, **DQ1**/PMMA and **DQ2**/PMMA absorption spectra presented two intense peaks (313 and 430 nm for **DQ1**; 325 and 454 nm for **DQ2**). **DQ3**/PMMA showed a broad absorption peak at 446 nm.

Concerning fluorescence spectra, they presented in all cases a regular shape with slight or marked red-shift of fluorescence peak and a decrease of fluorescence intensity for high concentrations. This behaviour was correlated to re-absorption phenomena, which produced a consequent quenching of fluorescence.

Moreover, with the increase of concentration, the emission maxima wavelength moved to high frequency of about 20 nm for **DQ1** and **DQ2**, while a more evident shift was observed for **DQ3** (around 40 nm) (Fig. 74). This behaviour was due to the typical structural reorganization of phenothiazine derivatives at the excited state, which showed less conformational freedom in solid state than in solution.

On the contrary, fluorescence quantum yield behaved differently depending of the molecular structure of the fluorophore.

For **DQ1**/PMMA, **Φ_f** increased with concentration, from 90% to 97%, showing higher values than those recorded in solution. The quenching effect was observed only for a concentration higher than 1.8 wt%, where **Φ_f** decreased marginally. That means, the energy loss, through non-radiative mechanisms, observed in solution were less evident or negligible in solid state, where the excited state was probably more stable, with limited structural rearrangements.

DQ2/PMMA and **DQ3**/PMMA showed values of **Φ_f** comparable with those found in solution: in the case of **DQ2** the value was around 35%, stable for all concentrations. That means the alkyl character of **DQ2** and its structural reorganization in a low compatible matrix, such as PMMA, allowed less stable excited state, which was affected by energy losses through non-radiative mechanisms. Thus, fluorescence quantum yield not increased at high concentration, remained constant and low.

Instead, **DQ3** showed 57% of **Φ_f a**t low concentration (0.2 wt%), higher than in solution, which gradually decreased with increasing of concentration. The increase of **Φ_f** in **DQ3**/PMMA sample supported again lower free rotational degrees in polymer matrix compared with those of solution samples. Thus, the structural rearrangement of **DQ3** was limited in solid phase, favouring a moderate increase of **Φ_f.** This behaviour, although more evident for **DQ3** samples affected all the three DQs chromophores.

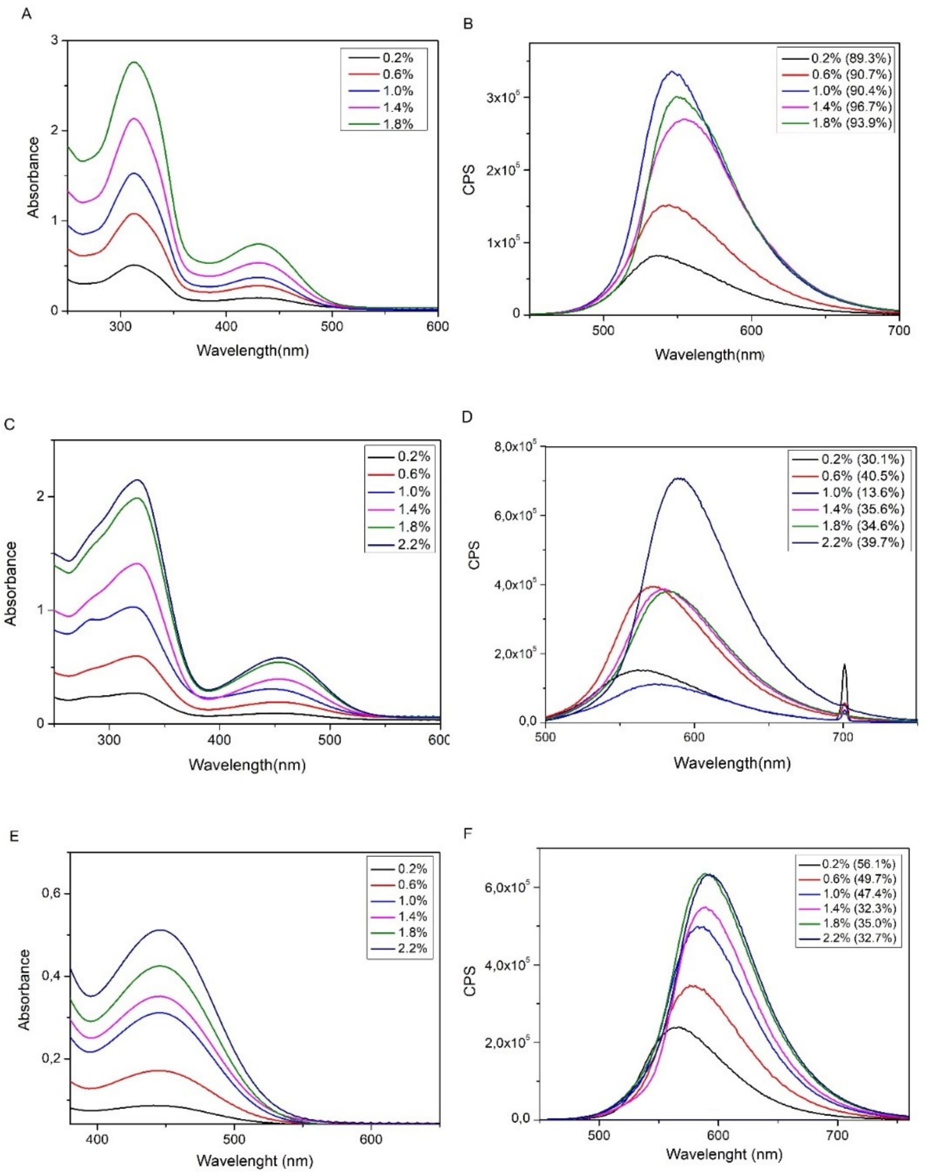

Fig. 74: *DQ1/PMMA films absorption (A) and emission (B) spectra at different concentration (excitation at 430 nm); DQ2/PMMA films absorption (C) and emission (D) spectra at different concentration (excitation at 454 nm); DQ3/PMMA films absorption (E) and emission (F) spectra at different concentration (excitation at 456 nm).*

DQ1-3 were also dissolved in PCMA films. PCMA films absorption (A) and emission (B) spectra at different concentration are shown in Fig 75.

The spectra recorded in this case are comparable with the corresponding spectra in PMMA. Again, the absorption maxima increased with concentration, showing a slightly blue-shift of the absorption maximum in the case of **DQ3**/PCMA compared to **DQ3**/PMMA (around 10 nm). The same was found for the emission spectra that presented a red-shift for high concentrations.

Large Stokes shifts were exhibited by all molecules, similarly to those observed in PMMA.

Quenching of fluorescence were observed, more evident in the case of **DQ1** and **DQ2**, increasing with concentration; while **DQ3** showed a moderate decrease in fluorescence intensity only from concentration in the range of 1.8% to 2.2%.

A different behaviour for fluorescence quantum yields was observed in this matrix.

In particular, the lipophilic character of PCMA compared to PMMA improved the **Φ_f** of **DQ2** and **DQ3**.

DQ3/PCMA showed a **Φf** around 70% at 1.4% and 1.8% concentration, higher to that observed (57%) in PMMA sample at lower concentration (0.6 wt%). Therefore, **DQ3** in PCMA films showed a high **Φf** at higher concentrations, that is very attractive for LSC applications; this can be due to a stabilization of **DQ3** excited state in PCMA better than in PMMA.

Moreover, **DQ2**, which registered low values in PMMA, in PCMA exhibited a drastically increase in **Φf**, till 87%. However, high **Φf** values were observed, till 1.8 wt% (around 70%).

Similarly to BBTs behavior, observed PCMA films, due to the effect of stabilization of the charge separation state, in a less polar matrix such as PCMA, molecular distortion was less evident. This is more evident for molecules with stronger donor moiety (**DQ2** and **DQ3**). Thus, their **Φf** in PCMA were higher than in solution and PMMA samples.

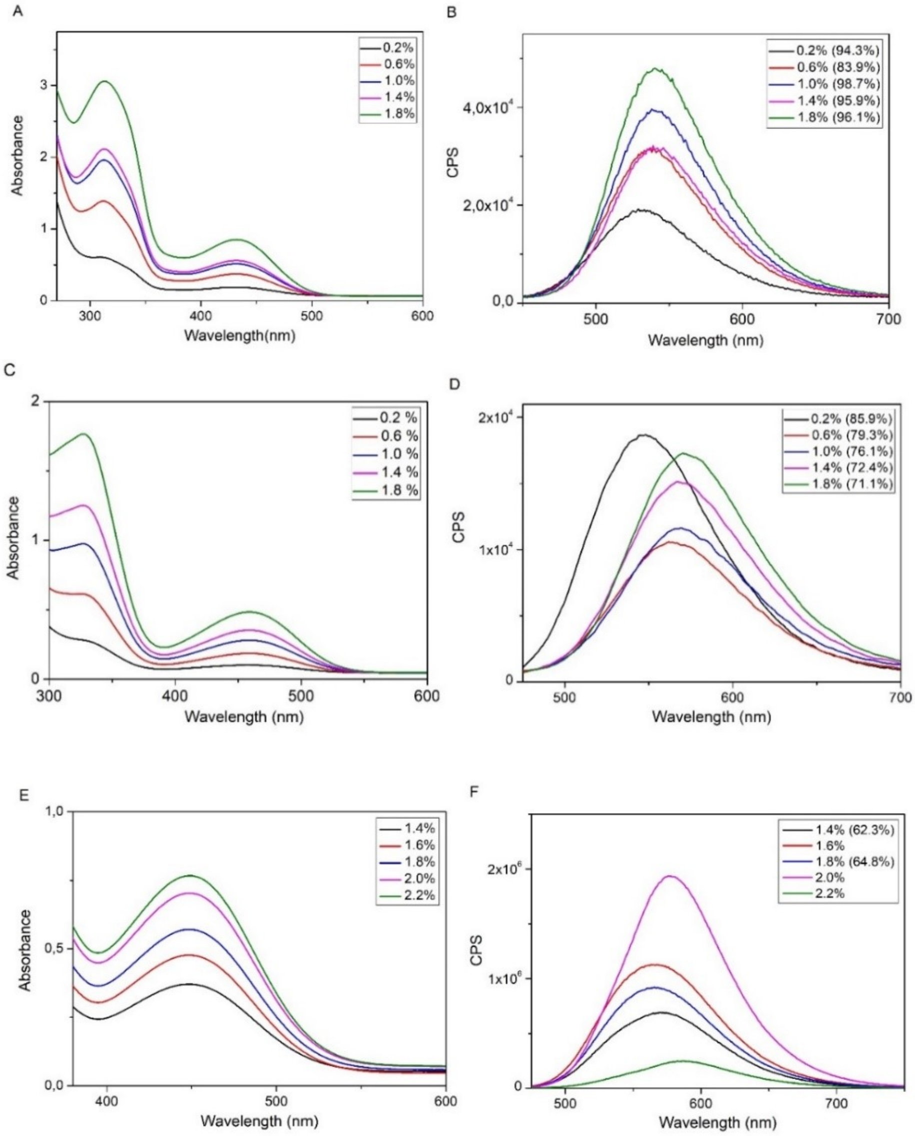

***Fig. 75: DQ1**/PCMA films absorption (A) and emission (B) spectra at different concentration (excitation at 430 nm); **DQ2**/PCMA films absorption (C) and emission (D) spectra at different concentration (excitation at 459 nm); **DQ3**/PCMA films absorption (E) and emission (F) spectra at different concentration (excitation at 447 nm).*

On the other hand, **DQ1**/PCMA **Φf** remained stable and high for all concentrations, similarly to PMMA samples.

However, the films obtained for **DQ1**/PCMA were not stable: several surface defects or cracks were observed after a few hours from the preparation of the film. In some cases (0.6% and 1.4%) the effect was more evident than in others (0.6% and 1.4%). In general, we can affirm that **DQ1** was not compatible with PCMA polymeric matrix. This could be related to the structure of **DQ1** as the absence of alkyl moieties might be responsible of lower compatibility and dispersion in a more lipophilic matrix, as PCMA. This effect was confirmed by optical efficiency analysis (see par. 4.3.3).

The same analysis was performed also on **DQ4** and **DQ5** fluorophores, which were dispersed both in PMMA and PCMA. Absorption (A) and emission (B) spectra at different concentration in PMMA films are reported in Fig 76. The two compounds showed similar absorption spectra with a two-peaks shape. **DQ4**/PMMA presented an absorption range between 250 nm to 480 nm. The lower wavelength absorption, observed at around 300 nm was due to the absorption of Edmund glass, used for PMMA casting, which added to **DQ4** peak. The absorbance improved linearly with concentration, according to Lambert-Beer law, and the absorption peak was not affected by shape variation (Fig. 76 A –C).

DQ4/PMMA emission spectra exhibited an emission peak around 500 nm, which endured a red-shift of 25 nm at the highest concentration tested. The Stokes shift increased from 102 nm to 129 nm. Moreover, the fluorescence intensity improved with concentration, til 1.4%, before starting to decrease at 1.8% (Fig. 76 B-D).

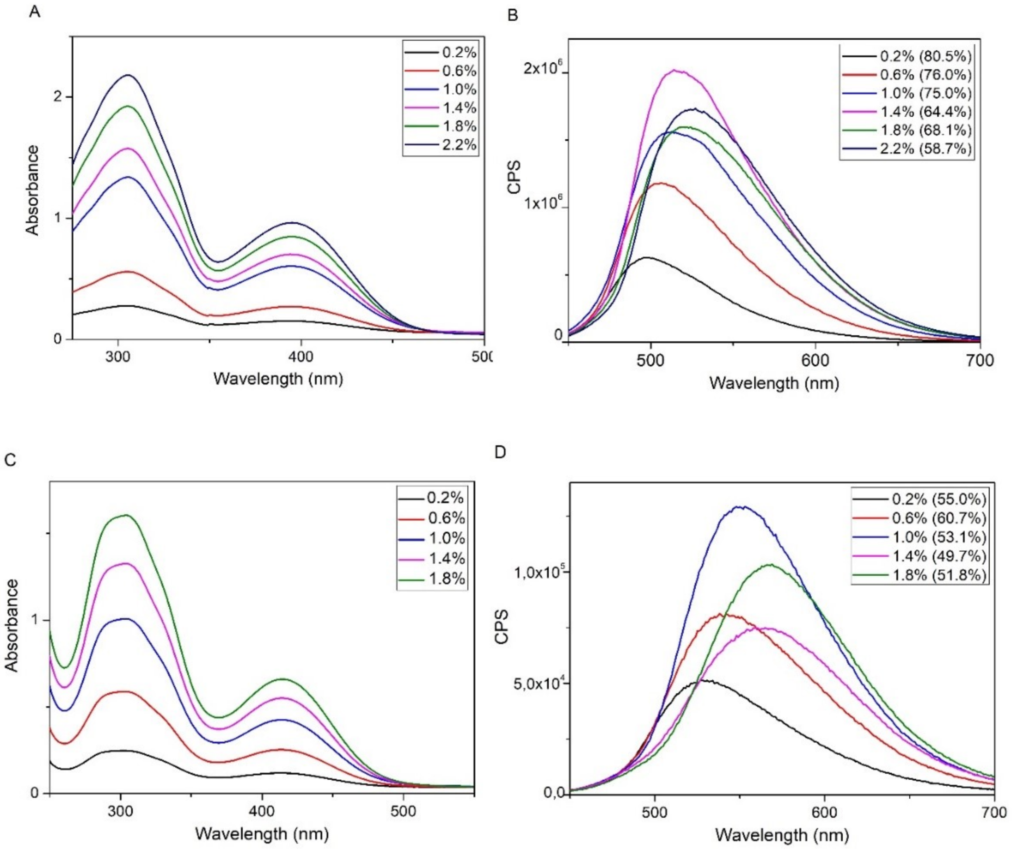

Fig. 76: DQ4*/PMMA films absorption (A) and emission (B) spectra at different concentration (excitation at 400 nm);* ***DQ5****/PMMA films absorption (C) and emission (D) spectra at different concentration (excitation at 415 nm).*

A similar trend was observed for **DQ5**/PMMA spectra at different concentrations, presenting an absorption peak at 414 nm and a fluorescence one which moved from 527 nm for 0.2% to

569 nm for 1.8%. The Stokes shift shifted from 113 to 155 nm. Quenching effect was observed for concentration higher than 1.0%, with an improved red-shift of emission maximum. However, quenching impact was more evident for **DQ4**/PMMA than **DQ5**/PMMA.

Considering the quantum yield, **DQ5**/PMMA showed moderate constant values, between 50-61%, recording the lower (50%) at 1.4% concentration. On the contrary **DQ4**/PMMA reported high Φ_f values, that varied with concentration, starting from 80-75% at lower concentration (from 0.2% to 0.6%). Increasing the concentration to 1.4%, Φ_f started to decrease gradually, till to 60% at 2.2%, due to the significant quenching effect.

Absorption (A) and emission (B) spectra of **DQ4** and **DQ5** at different concentration of PCMA films are reported in Fig 77. Both compounds exhibited a slight absorption range, around 350-480 nm. The intensity of absorption showed good linearity with concentration, with good dispersion of chromophores in the polymer matrix. As already observed for PMMA samples, **DQ4**/PCMA and **DQ5**/PCMA absorption wavelengths were not shifted with the increase of concentration, presenting a peak at 397 nm for **DQ4**/PCMA and at 419 nm for **DQ5**/PCMA (Fig. 77 A-C). Both of fluorophores showed constant Stokes shift around 93-96 nm for **DQ4** and 96-102 nm for **DQ5**, with a fluorescence maximum stable and peaked around 490 nm for **DQ4**/PCMA and at 519 nm for **DQ5**/PCMA. The red-shift effect was negligible (Fig. 77 B-D).

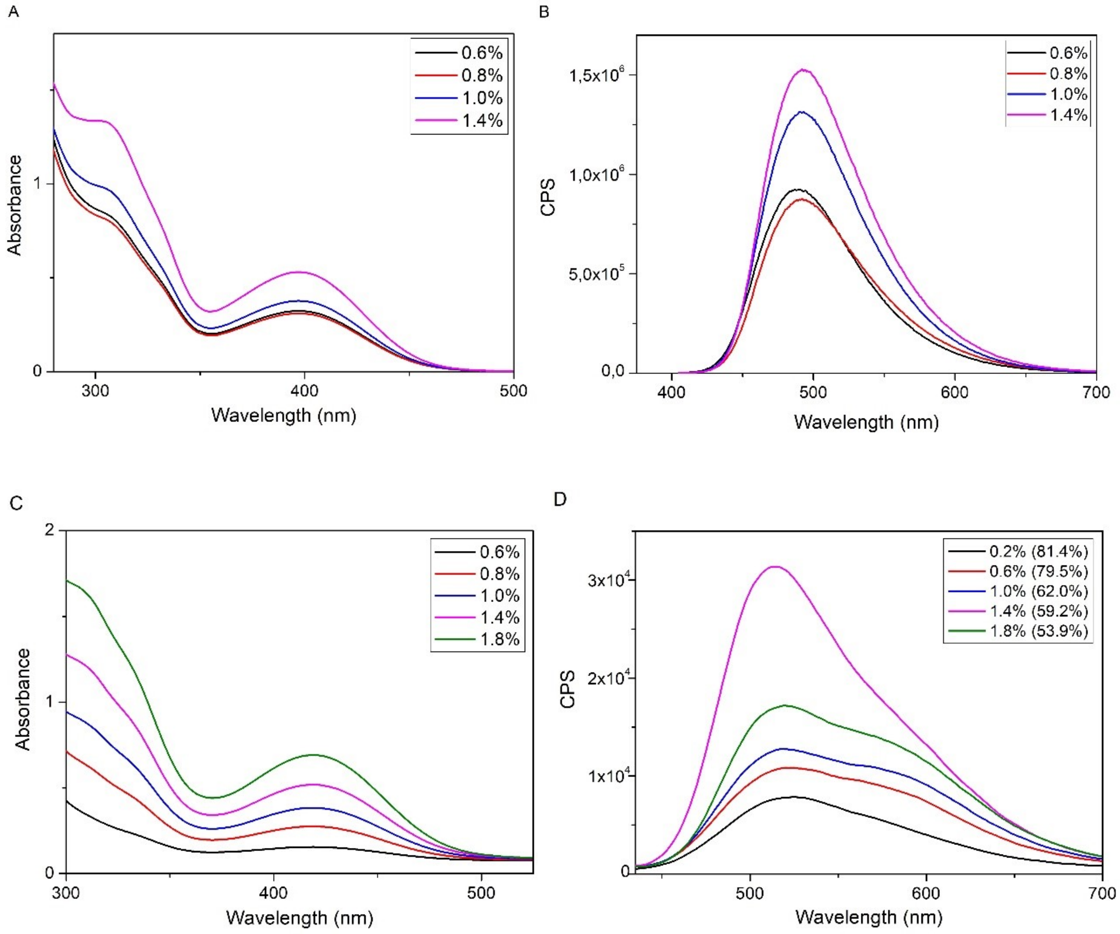

***Fig. 77: DQ4**/PCMA films absorption (A) and emission (B) spectra at different concentration (excitation at 400 nm); **DQ5**/PCMA films absorption (C) and emission (D) spectra at different concentration (excitation at 419 nm).*

In both cases, an increase of fluorescence quantum yields was registered going from PMMA to PCMA. In the case of **DQ4**, **Φ_f** was 90% in PCMA against 80% in PMMA. Furthermore, the quantum yield remained constant in PCMA even for high concentration such as those employed in LSC devices (1.4-1.8%), on the contrary with what observed in the case of PMMA samples, which decreased gradually, reaching 60% at the 1.8%.
In that case, compound **DQ5** exhibited comparable values of **Φ_f** in PCMA and PMMA films for high concentrations (around 50-60% at 1.4-1.8%) were observed. A general increase in **Φ_f** was registered in the case of PCMA matrix.

4.2.3 Optical efficiencies

To evaluate DQs performances in LSC devices, PMMA and PCMA films of DQs samples were tested under solar simulator irradiation, at different concentrations. Data are reported in table 6 and 7.

For the series **DQ1-3**, all optical efficiencies improved with concentration, in both matrices. In sporadic cases (see red data, Table 13), higher concentrations induced a decrease of optical efficiency due to quenching phenomena that reduced the quantum yield of fluorescence, and to self-absorption phenomena.
In particular, **DQ1** showed high values of optical efficiency in both materials, with high and stable **Φ_f**, for all concentrations. This means that **DQ1** has good compatibility with the matrix as the best value of 11.0% in optical efficiency was registered at 1.4% in PMMA. Increasing the concentration, auto absorption phenomena take place with the consequent decrease in performance.
As reported before (par. 4.3.2), **DQ1**/PCMA films were unstable and affected by defects, after few hours from solvent casting. Thus, the optical efficiency of **DQ1**/PCMA was registered after a few hours and checked after a day from the formation of cracks, using the same conditions. The variations observed are reported in table 6 and the trend of loss in efficiency of **DQ1** in PCMA is also reported in figure 70. Remarkably, despite the low compatibility with PCMA material, optical efficiency remained high.
DQ2 showed opposite different behaviour. The performances of **DQ2**/PCMA films were higher than **DQ2**/PMMA, showing appreciable **Φ_f** values. The best result for **DQ2**/PCMA was 10.5 at 1.0%, comparable with **DQ1**/PMMA efficiencies. In these case the increase of efficiency can be attributed to the increase of fluorescence quantum yield, due to the less polarity of PCMA in comparison with PMMA: the less polar environment reduces the stabilization of the ICT excited state, resulting in a reduction in the structural rearrangement of the excited state and decreasing the energy dissipation through non-radiative phenomena,
Remarkably, **DQ2**/PMMA exhibited good optical efficiencies, considering the low **Φ_f** in comparison with **DQ1** in the same condition (≤40%). That means that **DQ2** in PMMA was not affected by significant energy loss for self-absorption. Furthermore, **DQ2**/PCMA at 1.0% and 1.4% have the same optical efficiency: thus, **DQ2** can give a high efficiency even if employed with lower concentrations (1.0% instead of 1.4%), working at the common conditions of the LSC device.

Table 16: *Optical efficiency of* ***DQ1-3*** *in PMMA and PCMA films at different concentrations; in parenthesis, fluorescence quantum yield at different concentrations.*

	η_{opt} (%) [Φ (%)]					
Conc	**DQ1**		**DQ2**		**DQ3**	
(wt%)	*PMMA*	*PCMA*	*PMMA*	*PCMA*	*PMMA*	*PCMA*
0.2	8.4 [89.3]	7.3±0.4[a] [94.3]	6.8 [30.1]	8.4 [85.9]	5.5 ±0.5 [56.1]	-
0.6	8.5 [90.7]	8.8±0.2[a] [83.9]	7.3 [40.5]	9.1 [79.3]	6.6±0.5 [49.7]	-
1.0	**10.1** [90.4]	9.6±0.9[a] [98.7]	7.6 [13.6[b]]	**10.5** [76.1]	7.0±0.5 [47.4]	8.2±0.5 [-]
1.4	**11.0** [96.7]	8.3±0.9[a] [95.9]	7.9 [35.4]	**10.3** [72.4]	7.5±0.5 [32.3]	8.8±0.5 [62.3]
1.8	9.6 [93.9]	9.5±1.0[a] [96.1]	8.1 [39.7]	10.1 [71.1]	7.9±0.5 [35.0]	9.8±0.5 [64.8]
2.2	-	-	-	-	7.8±0.5 [32.7]	8.6±0.5 [54.0]

[a] Variation on optical efficiency depending on the formation of cracks in polymer films; the measurements were conducted after few hours and after one day, from the formation of cracks, at the same conditions.

[b] Damaged film.

In both polymeric matrices compound **DQ3** showed a behaviour similar to **DQ2**, with comparable values of $\boldsymbol{\Phi_f}$ (around 40% for PMMA samples, 60% for PCMA ones at LSC performances concentration). However, the $\boldsymbol{\Phi_f}$ values decreased with the increase of concentration in both polymers, more evident for PMMA samples. Probably, low compatibility of **DQ3** in both polymer matrices induced the formation of aggregates in the solid phase.

Therefore, Φ_f decreased with concentration. Similarly to **DQ2, DQ3** was affected by lower Φ_f values in PMMA than in PCMA. However, the optical efficiencies of **DQ3**/PMMA films showed interesting values, comparable with optical efficiencies of **DQ2**/PMMA. Thus, **DQ3** in PMMA was affected by less energy loss for self-absorption, similarly to **DQ2** behaviour.

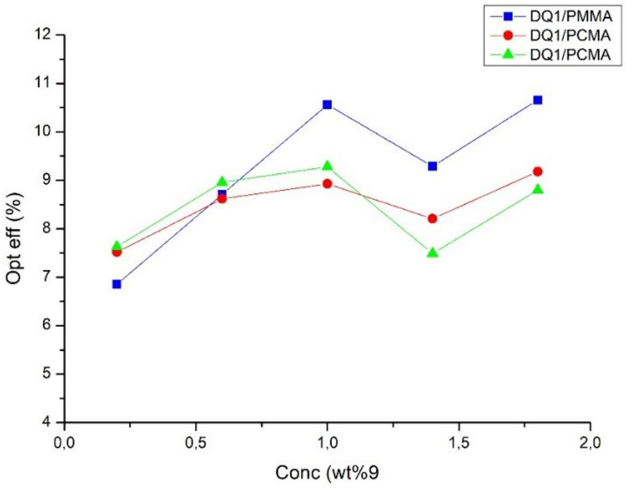

Fig. 78: *Comparison between **DQ1**/PMMA (blue) and **DQ1**/PCMA (red and green) optical efficiency; fluctuations of **DQ1**/PCMA after few hours (red) and after a day (green) from the solvent casting.*

It is evident that the performance of fluorophores in host matrices are influenced by the molecular structure. For instance, **DQ1** recorded higher optical performances in PMMA than PCMA, showing high and stable Φ_f, in both materials, for all concentrations. With the formation of cracks in the polymer matrix, **DQ1**/PCMA performances showed a rapid decay after some hours, after films preparation, making incompatible this chromophore with a less polar matrix such as PCMA (Fig. 78). On the other hand, **DQ2** reported the best performances in PCMA, with an opposite behaviour to **DQ1**.

Clearly, PCMA was more compatible with chromophore having hydrophobic groups, such as the hexyloxy chains of **DQ2,** which are present on the donor moiety. This effect can be also responsible for the high value of optical efficiency, even if Φ_f of **DQ2** were lower than **DQ1** Φ_f.

The introduction of a more donating group such as phenothiazine did not produce an evident effect on the performances of the device. **DQ3** showed better performances in PCMA than PMMA with higher Φ_f.

In table 17, **DQ4** and **DQ5** performances were reported in both matrices. In particular, **DQ4** showed similar behaviours in both matrices. For lower concentrations, optical efficiency was around 7.0%. For **DQ4**/PMMA samples, optical efficiency slightly increased, to 8.5% at higher concentration (1.8 wt%). The same behaviour was observed for **DQ4**/PCMA samples, with a higher improvement of optical efficiency, getting 9.3% (1.4 wt%).

DQ5 showed in PMMA opposite trend to PCMA: optical efficiency in PMMA films increased with concentration, maintaining a constant Φ_f between 50% and 60%. On the contrary, PCMA samples showed better performances with higher Φ_f at lower concentration. In this case, with the increase of concentration, optical efficiency and Φ_f decreased gradually. Thus, **DQ4** and **DQ5** exhibited similar performances, in PMMA; while in PCMA **DQ4** samples showed an opposite behaviour with respect to **DQ5**. High concentrations favoured best performances for **DQ4**; while, **DQ5** was better performing at low concentrations. Again, such behaviour can be explained considering the structures of these compounds.

***Table 17:** Optical efficiency of **DQ4-5** in PMMA and PCMA films at different concentrations; in parenthesis, fluorescence quantum yield at different concentrations.*

	η_{opt} (%) [Φ (%)]			
Conc	**DQ4**		**DQ5**	
(wt%)	*PMMA*	*PCMA*	*PMMA*	*PCMA*
0.2	5.5±0.5 [80.5]	-	6.8 [55.0]	**8.5** [81.4]
0.6	7.0±0.5 [76.0]	7.0±0.5	6.9 [60.7]	**8.7** [79.5]
1.0	7.6±0.5 [75.0]	**9.5±0.5** [64.9]	7.3 [53.1]	8.2 [62.0]
1.4	7.7±0.5 [64.4]	**9.3±0.5** [84.5]	8.0 [49.7]	7.6 [59.2]
1.8	8.5±0.5 [68.1]	8.9±0.5 [87.0]	8.7 [51.8]	7.6 [53.9]
2.2	**7.8±0.5** [58.7]	-	-	-

The presence of alkyl chains on quinoxaline core stabilized both fluorophores, in PCMA matrix, where a good dispersion and homogeneity in all films was observed. However, the significant quenching effect of **DQ5** in PCMA films at high concentrations could affect **DQ5** performances. This can be explained with the formation of **DQ5** aggregates, which reduced fluorescence quantum yield from 81% at lower concentration (0.2 wt%) to 54% at higher concentration (1.8

wt%). However, the good results obtained for the 0.2% and the 0.6% **DQ5**/PCMA films could in any case interesting for application LSC device with a low fluorophore loading. Compound **DQ4** presented in PCMA the best efficiency at the typical concentration employed for LSC device (9.3% at 1.4%).

In conclusion, all the five fluorophores we have synthesized showed interesting values of efficiency and can be very promising for LSC application, providing optimization of the performances with the more suitable matrix. A more polar matrix like PMMA favoured the most conjugated compound (**DQ1**), that reached best value of 11,0% of all series at 1.4% concentration. Otherwise, the less polar matrix PCMA allowed to obtain better performances with **DQ2**, where the added effect of conjugated structure and alkyl chains on the donor part of the molecule determined high compatibility between chromophore and PCMA, and a remarkable efficiency higher than 10.5%.

***Table 18:** Comparison of optical efficiencies (η_{opt}) of DQ chromophores and commercial standard **LR305** at the same conditions, in both matrices.*

Compound	**Matrix**					
	PMMA			PCMA		
	η_{opt} (%)	**C**	**Conc (wt%)**	**η_{opt} (%)**	**C**	**Conc (wt%)**
DQ1	**11.0**	1.83	1.4	9.6	1.59	1.0
DQ2	7.9	1.31	1.4	**10.5**	1.74	1.0
DQ3	7.5	1.24	1.4	8.8	1.46	1.4
DQ4	7.7	1.28	1.4	9.5	1.58	1.0
DQ5	8.0	1.33	1.4	8.2	1.36	1.0
LR305	10.1	1.68	1.4	9.1	1.51	1.0

Optical efficiencies of the new luminophores were also compared to that of the standard reference **LR305**, using the same experimental conditions, and working at 1.0 wt% and 1.4 wt% concentrations, which are the more attractive for application in a LSC device (Table 18).

In table 18 performances of DQs and **LR305** in different matrices, at same concentrations, were reported. Moreover, the factor *C* was introduced, calculated as the ratio between the maximum power measured for the cell over the LSC edge (P_{LSC}) and that of the bare cell when perpendicular to the light source (P_{SC}) without correction with geometrical factor. Factor *C* is very important parameter which evaluates a realistic application of a LSC fluorophore and must be higher than 1.

Remarkably, compared to **LR305, DQ1** in PMMA presented higher efficiency (11.0%), when compared with **LR305** (10.1%), at the same conditions and using the same geometry of polymer films (on lab scale). All the other compounds showed values around 7-8%, which were lower than the reference, but still good. In fact it should be taken into account that the large overlap, typical of **LR305**, between absorption and emission spectra induced high loss of power for self-absorption processes, thus **LR305** applications on large-scale found several limitations. From this point of view, our fluorophores might be quite interesting as they exhibited large Stoke shift with lower overlap region, which avoided self-absorption.

In the case of PCMA matrix, all the new compounds showed an efficiency comparable or even higher than that found for **LR305**, in the same conditions. In particular, **DQ2** reported the highest value of 10.5%.

Considering the concentration factor C, it is higher than 1 for all the dyes. To our knowledge[200], there are few examples in the literature where small area devices (25cm^2 or less) have a C factor greater than 1, and only two greater than 1.86 which is the value we measure for
DQ1/ PMMA[201].

Taking into account all these consideration, we can conclude that all the compounds of the series can be very promising for large-scale applications, especially in case of **DQ**1/PMMA and **DQ2**/PCMA, which are better performing than the reference **LR305**, both in terms of efficiency and C factor**.**

4.2.4 Transient absorption spectroscopy

Finally also for DQs series, the behaviour of excited state and the dynamics of relaxation mechanisms after light absorption were investigated through femtosecond transient absorption spectroscopy.

DQs were analysed on the basis of acceptor cores, comparing **DQ1, DQ2** and **DQ3** and, on the other hand, **DQ4** and **DQ5**.

The sample were excited at 400 nm; the transient absorption spectra were recorded in time interval 0 ps-1.5 ns and consequently analysed with a global fit based on a sequential decay scheme. Transient absorption spectra and Evolution Associated Difference Spectra (EADS) obtained from global analysis were showed in figure 80.

---

[200] J. Roncali, *Adv. Energy Mater.* **2020**, *10*, 2001907.

[201] a) F. Mateen, M. Ali, S. Y. Lee, S. H. Jeong, M. J. Ko, S.-K. Hong, *Sol. Energy* **2019**, *190*, 488; b) J. Bomm, A. Büchtemann, A. J. Chatten, R. Bose, D. J. Farrell, N. L. A. Chan, Y. Xiao, L. H. Slooff, T. Meyer, A. Meyer, W. G. J. H. M. van Sark, R. Koole, *Sol. Energy Mater. Sol. Cells* **2011**, *95*, 2087.

DQ1 and **DQ2** spectra were similar. A negative band at 440 nm, assigned as the ground state bleaching band was observed. However, a broad positive excited state absorption (ESA) band was registered, covering almost all the probed spectral interval. The deep intensity of ESA band, centred at 532 nm, evolved red-shifting in time, especially evident for **DQ1**. It corresponded to an overlapping contribution of the negative stimulated emission (SE) band. In the case of **DQ2**, the broad positive ESA band was extended from 450 nm to 750 nm, with the overlapping SE band shifted in time from 542 nm to 562 nm.

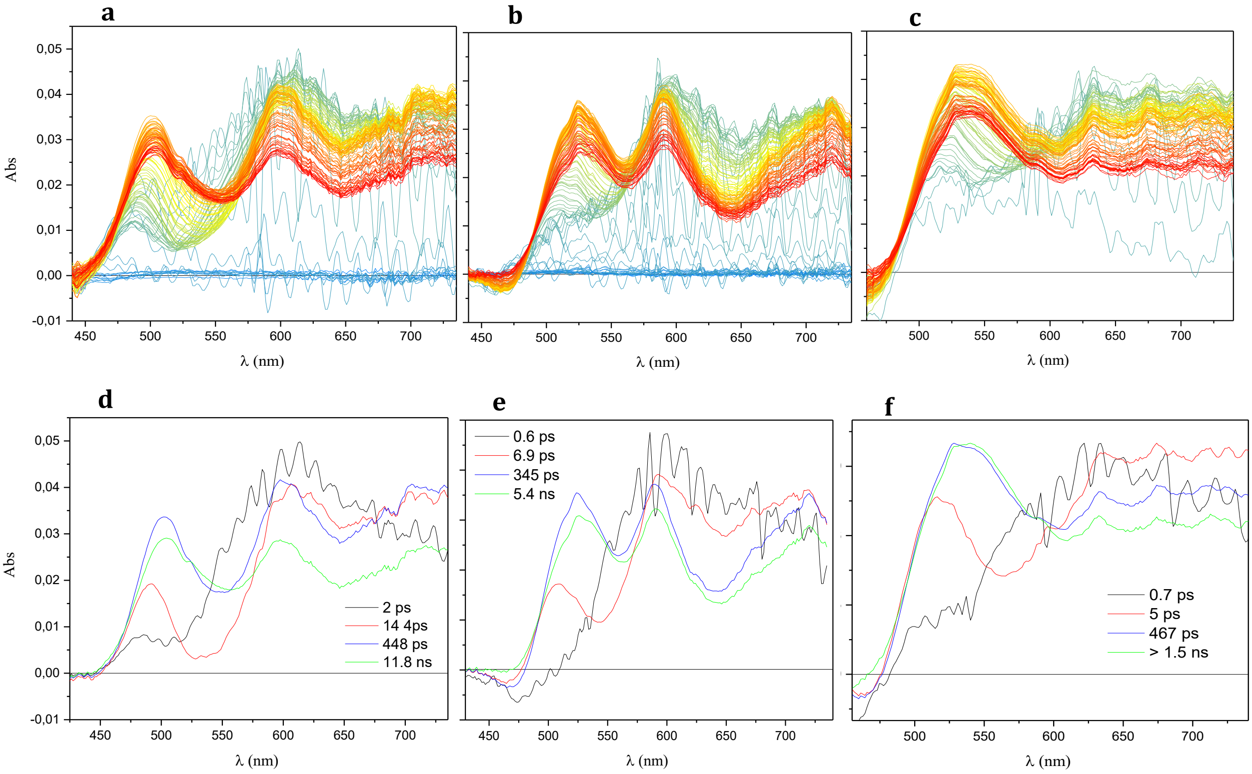

*Fig. 80: Transient absorption spectra (**a**, **b**, **c**) and Evolution Associated Difference Spectra, EADS (**d**, **e**, **f**) of **DQ1-3** in toluene solutions.*

Analysing EADS development, both samples presented a first component (black line), relative to the broad positive band peaked at 600 nm, which lived about 2 ps for **DQ1** and 600 fs for **DQ2**. The following evolution (red line) showed a double peaks ESA band. The increase of positive signal in a region of 450-500 nm and the superposition between the broad positive absorption band with SE one, peaked at 530 nm for **DQ1** and 550 nm for **DQ2**, explained the evolution of ESA band shape. This spectrum was assigned to a fast electronic relaxation, as evidenced by the large red shift of SE signal.

The state reached on fast timescale was probably a charge transfer state, typical for D-A-D molecules. The structure of the excited state absorption band was similar to the absorption spectrum measured for the quinoxaline radical anion[202] with the peak centred at 720 nm. This absorption range could be due to the localization of positive charge on the triphenylamine donor, whose radical cation absorbs at 700 nm[203]. After 14.4 ps for **DQ1** and 6.9 ps for **DQ2**, the

---

[202] K. Lušpai *et al.*, *J Solid State Electrochem*, **2014**, *19*, 113–122.

[203] K.Y. Chiu, T.X. Su, J.H. Li, T.H. Lin, G.S. Liou, S.H. Cheng, *Journal of Electroanalytical Chemistry*, **2005**, *575*, 95–101.

EADS evolved following the blue development (Fig. 80 **d** and **e**). The shape of spectrum remained unaffected, but the SE signal partially recovered and red shifted of 30 nm, reflecting a dynamic Stokes shift, due to the solvent induced excited state relaxation. At this timescale, the band at 600 nm narrowed and slightly blue-shifted for the effect of vibrational relaxations in the excited state. This was particularly evident in **DQ2** spectrum. Finally, even if the signal decreased, the ESA band lived beyond the time interval of investigation (1.5 ns).

Selected kinetics traces obtained from the global analysis were reported in figure 81.

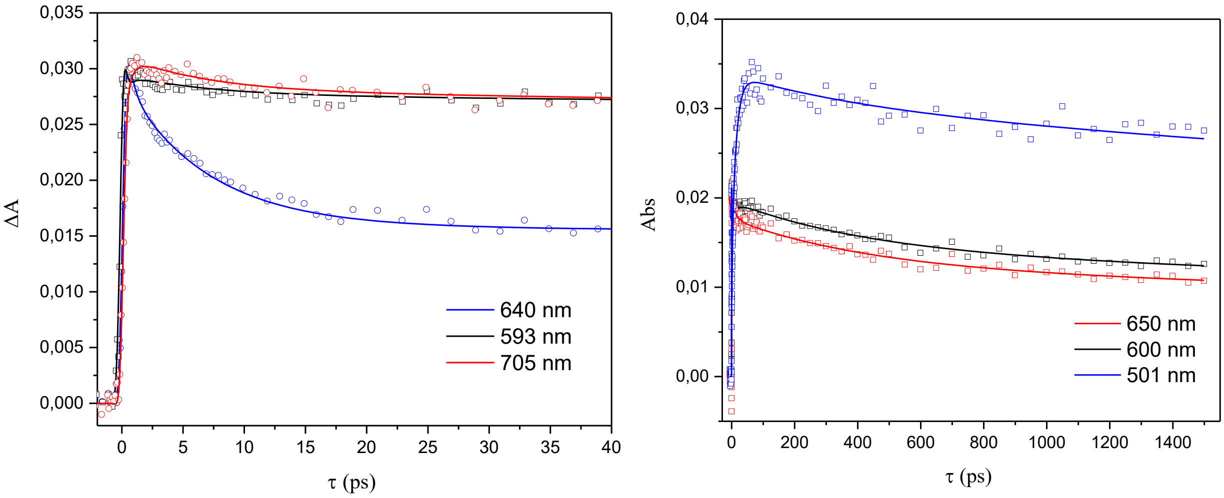

Fig. 81: *Comparison between kinetic traces at 640 nm (blue line), at 593 (black line) and 705 nm (red line) for* ***DQ2*** *(on the left) and comparison of kinetics traces at 650 nm (red line), at 600 nm (black line) and at 501 nm (blue line) for* ***DQ1*** *(on the right).*

Comparing the kinetic traces of **DQ1** and **DQ2**, investigated around ESA band, no evident dramatical decay was observed for both of DQs at different wavelengths of ESA band (Fig. 81). For **DQ3**, the transient absorption spectrum was a bit different, reflecting the different donating effect of phenothiazine group (Fig. 80 **c** and **f**). The ESA band was initially broad and covered the full investigated spectral interval, evolving rapidly in about 700 fs, due to its faster electronic relaxation. In the following evolution time (red line), a positive signal at 450-500 nm was observed. Due to the superposition between ESA band and SE one, a deep peaked at 570 nm was formed. During the following timescale, SE partially recovered and red shifted of about 50 nm, reflecting a dynamic Stokes shift. The peaked 560 band reflected the localization of positive charge on the phenothiazine ring, superimposed to the signals of the quinoxaline anion. The transient signal slightly decayed on the following 467 ps timescale (blue line) and the ESA component lived longer than the timescale investigated (green line).

In agreement with transient absorption solution data, PMMA transient absorption spectra were registered of **DQ1-3**. PMMA films at 1.0 wt% were analysed. Very similar shape was recorded for the three molecules in PMMA films.

An intense and broad positive excited state absorption band covered the major part of the spectrum. The decreased signal in the blue part of spectrum was correlated to the overlapping contribution of the negative SE and bleaching signals. The dynamic Stokes shift was barely observed in matrix, where vibrational and structural relaxations were enhanced compared to solution. Looking at EADS (Fig. 82, d,e,f), spectral shape showed a minimal evolution in time.

The intensity of the signal decayed bi-exponentially in all DQs samples; however, the excited state lived longer than the timescale analysis.

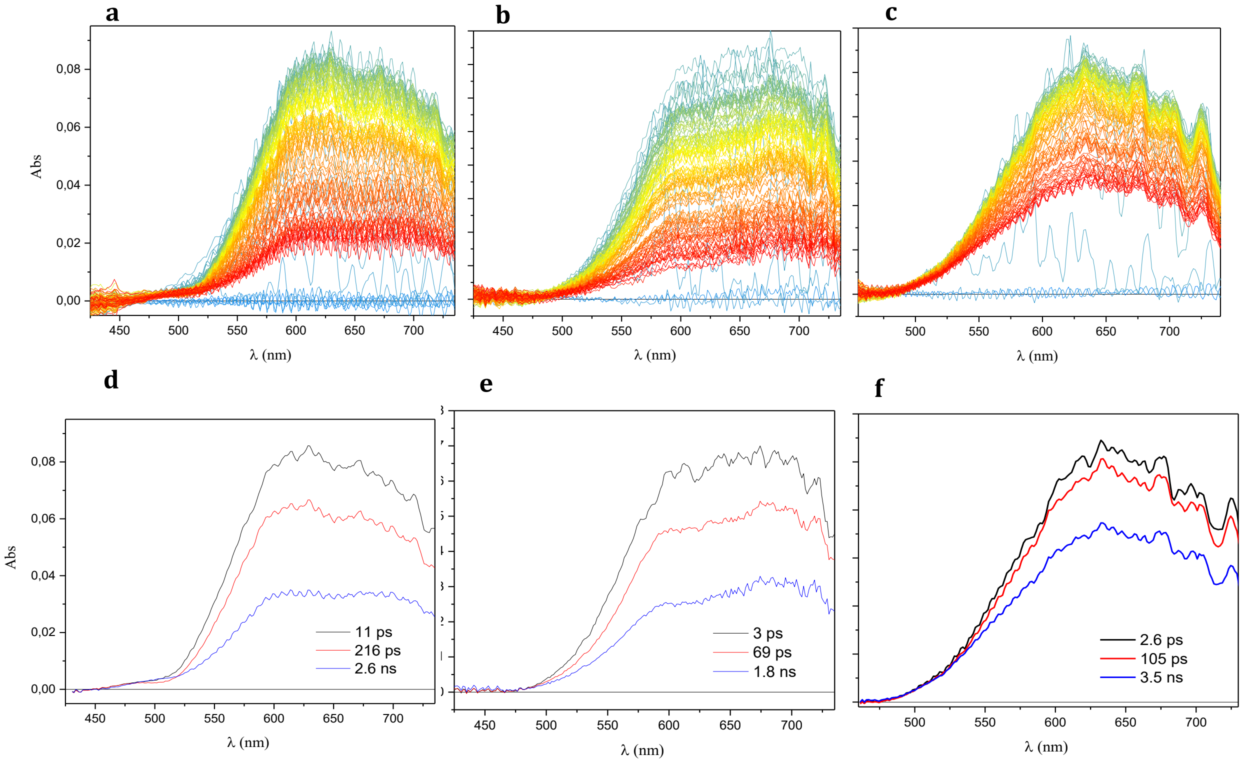

***Fig. 82:** Transient absorption spectra (**a**, **b**, **c**) and Evolution Associated Difference Spectra, EADS (**d**, **e**, **f**) of **DQ1-3** in PMMA films.*

Transient absorption spectra and EADS analysis of **DQ4** and **DQ5** are reported in figure 83. For both samples, transient spectra presented a negative band, assigned as the SE signal, and a broad positive ESA band (Fig 83 c and d). The initial component evolved into the following within 700 fs. The intensity of SE increased and a red-shift of SE band beyond 500 nm was observed.

The ESA band decreased in the blue part of spectrum. An evident band peaked at 600 nm was registered. All these contributions had already observed for **DQ1/DQ2**, due to the overlapping contribution and red-shift of SE band; the peak at 600 nm was most probably relative to the partial localization of a positive charge on the triphenylamine groups. The excited state relaxation took place in the followed 7.8 ps timescale. The signal intensity decreased on a 338 ps and, as already noticed for the corresponding DQ samples, the final spectral signal lived longer than the investigation time.

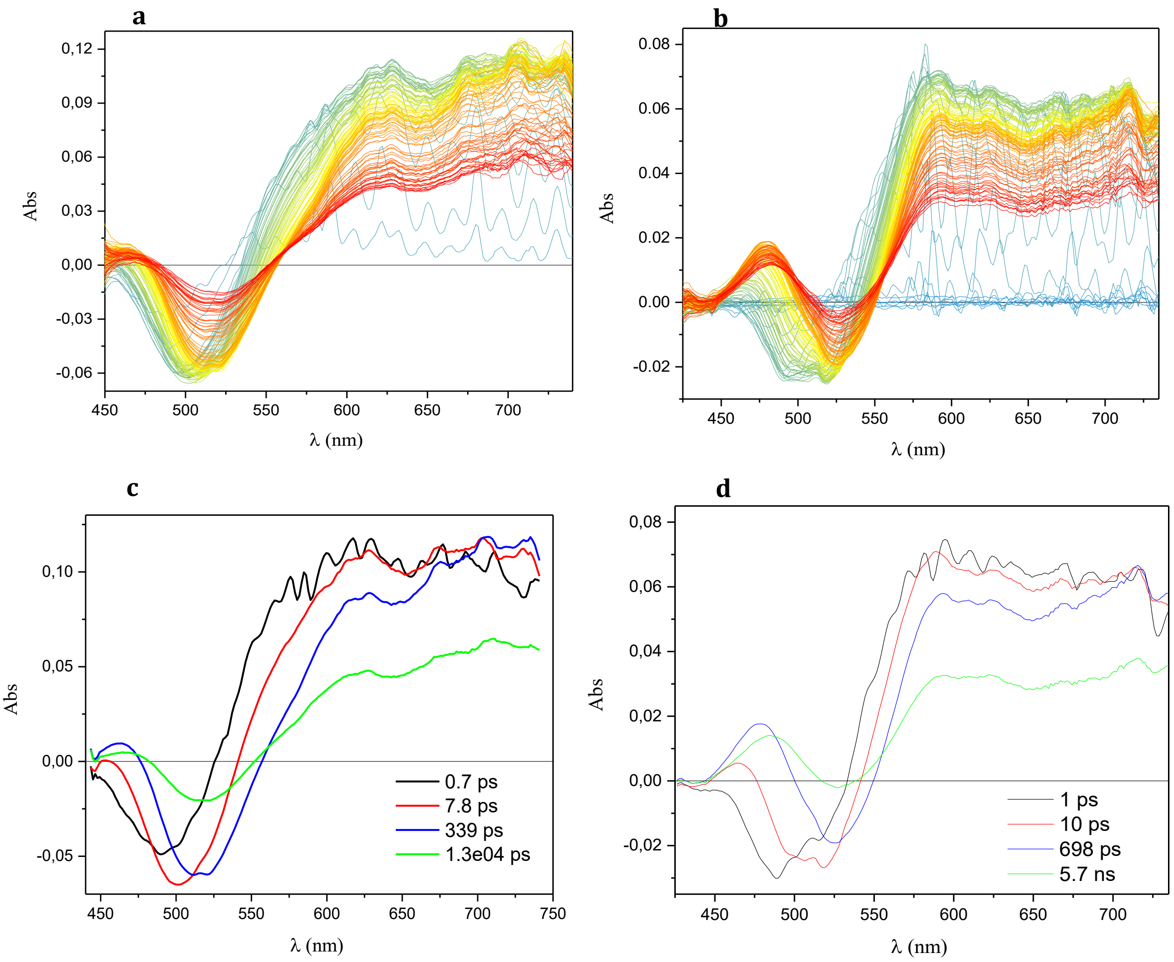

Fig. 83: *Transient absorption spectra (**a**, **b**) and Evolution Associated Difference Spectra, EADS (**c**, **d**) of **DQ4** and **DQ5** in solution.*

Uniformly, the transient spectra in PMMA films of **DQ4** and **DQ5** were recorded at concentration of 1.0 wt%. negative band centred at 550 nm and a broad positive band between 550 and 750 nm, respectively assigned to SE signal and ESA band, characterized **DQ4-5** absorption spectra. According to **DQ1-3** analysis, the dynamic Stokes shift of the stimulated emission band is highly reduced for samples dispersed in polymer medium (Fig. 84).

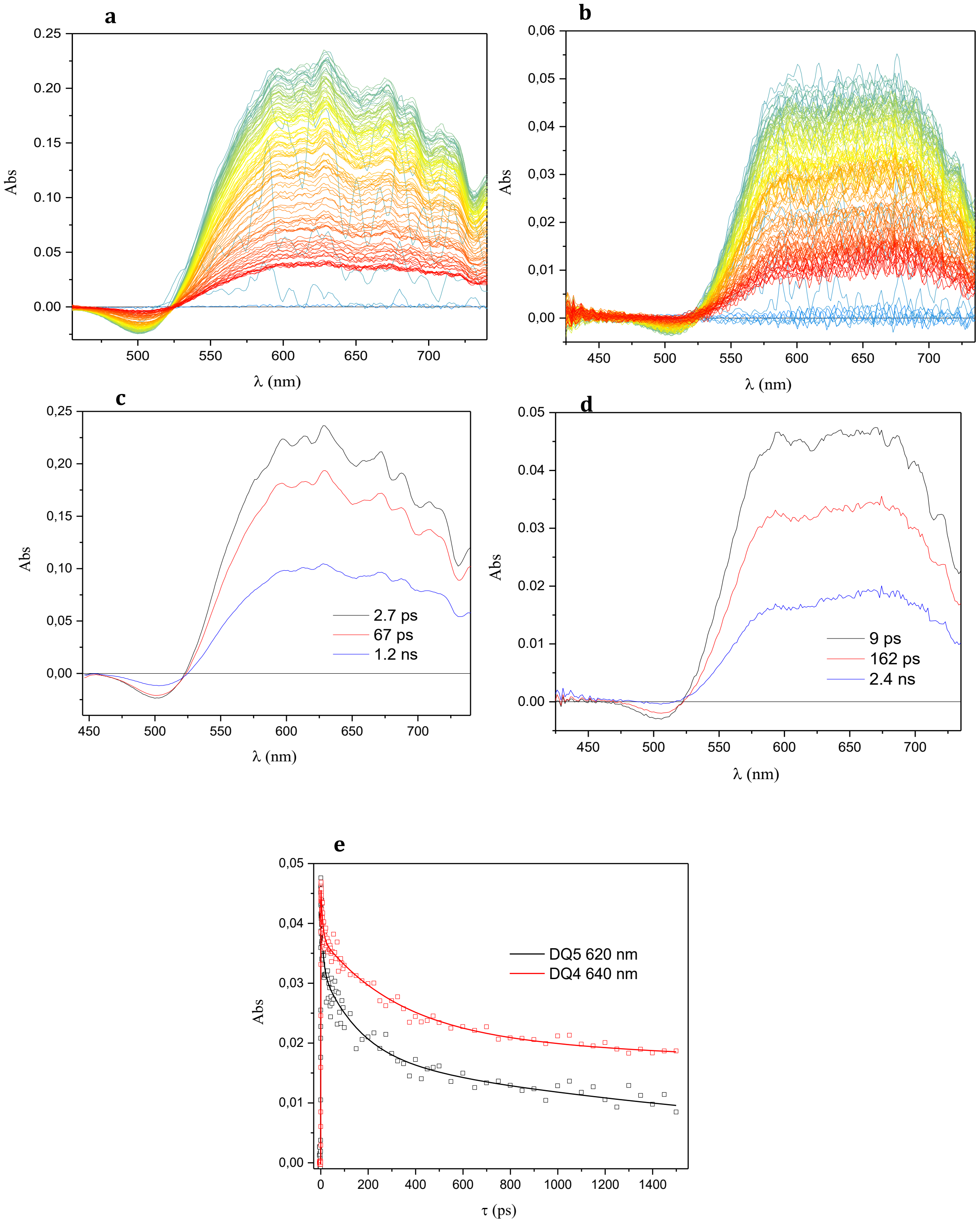

***Fig. 84:** Transient absorption spectra (**a**, **b**) and Evolution Associated Difference Spectra, EADS (**c**, **d**) of **DQ4** and **DQ5** in PMMA films; (**e**) comparison between kinetic traces at 640 nm for **DQ4** (red line) and the kinetic traces at 620 nm for **DQ5** (black line).*

Further transient absorption analysis was made on **DQ5**/PCMA film at 1.0 wt%, to evaluate the impact of different polymer matrix on the excited state for this type of compound.
The sample was excited at 400 nm; transient absorption spectrum and Evolution Associated Difference Spectra (EADS), obtained from global analysis, were recorded (Fig. 85): apparently,

DQ5/PCMA behaviour was an intermediate among solution (toluene) and PMMA trend.

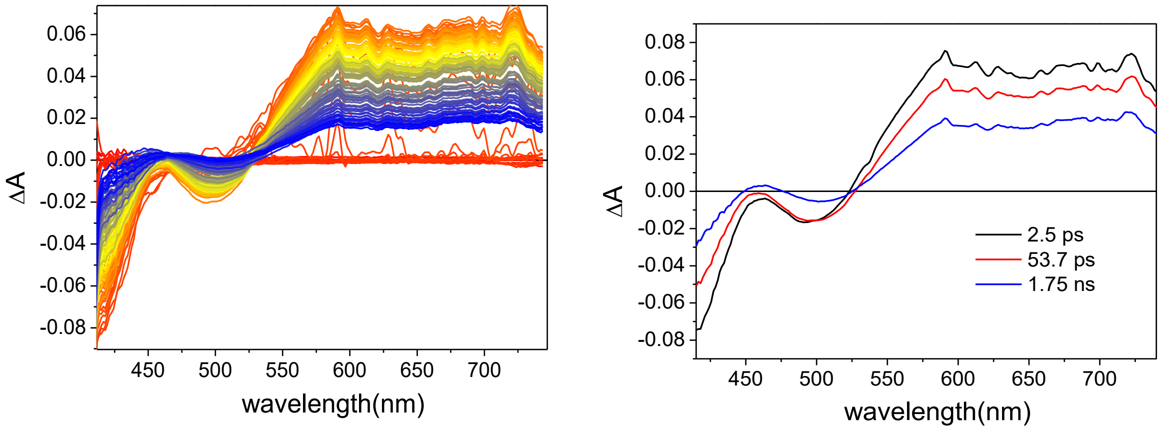

Fig. 85: *Transient absorption spectra (left) and EADS obtained from global analysis (right) for* ***DQ5*** *dispersed in PCMA (excitation at 400 nm).*

Absorption spectra showed two negative bands, peaked respectively at 420 nm and 500 nm. The first one was assigned to the ground state bleaching (GSB), the second one on the stimulated emission (SE).

Furthermore, a broad and flat excited state absorption (ESA) band was noticed in a range of 550-750 nm. The shape of transient spectra was comparable and more similar to that registered in toluene. However, the dynamic Stoke shift of the emission band, observed for PCMA film, was similar to PMMA evolution in the timescale of analysis. It appeared to be quite limited, due to the high conformational constrain imposed by PCMA matrix.

The same rate of excited state decay was an intermediate development among solution and PMMA ones, as shown in figure 78 from the comparison among the kinetic traces in different media (Fig. 86).

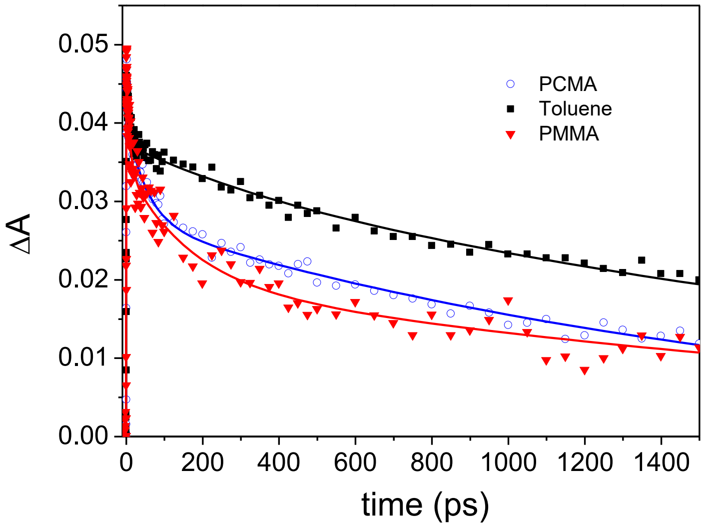

Fig. 86*: Comparison of the kinetic trace at 640 nm measured for* ***DQ5*** *in toluene (black full squares); PCMA (blue empty circles); PMMA (red full triangles).*

4.3 EXPERIMENTAL PROCEDURE: CHAPTER 4

3,6-dibromobenzene-1,2-diamine

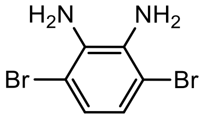

13

To a suspension of 4,7-dibromo-2,1,3-benzothiadiazole (**12**) (500 mg, 1.7 mmol, 1.0 eq) in EtOH (85 mL) at 0°C, under atmosphere of N_2, $NaBH_4$ (1.16 g, 30.6 mmol, 18.0 eq) was added in four parts to the solution. The mixture was stirred at 0°C for 10' and then to room temperature for 16h. Then the mixture was cooled at 0°C, the excess of $NaBH_4$ neutralized with H_2O (15 mL). The mixture was concentrated under reduced pressure to eliminated EtOH and then extracted with Et_2O (2x20 mL). The organic phase was washed with brine (30 mL) and dried on anhydrous Na_2SO_4. The solvents were removed at reduced pressure and the crude product purified by washing with EtOH, to eliminate the insoluble **1**. The organic solution was filtrated and concentrated under vacuum, obtaining the product **2** as white solid (348 mg, 1.32 mmol, 77%).

^{1}H NMR (400 MHz, $CDCl_3$): δ = 6.39 (s, 2H), 4.26 (s, 4H) ppm.

Spectroscopic data are in agreement with those reported in the literature (*Org. Lett.*, **2016**, 18, 7, 1562–65).

5,8-dibromo-2,3-diphenylquinoxaline

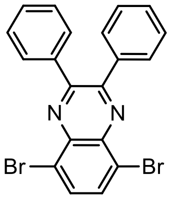

16

To a solution of **13** (721 mg, 2.7 mmol, 1.0 eq) in EtOH (15 mL), 1,2-di(phenyl)etan-1,2-dione **14** (567 mg, 2.7 mmol, 1.0 eq) was added to the solution, under inert atmosphere. The mixture was heated to reflux for 24h. The precipitated obtained was recovered by filtration washed and dried at the vacuum pump, obtaining the product as a pale yellow solid (761 mg, 1.74 mmol, 67%).

^{1}H NMR (400 MHz, $CDCl_3$) δ = 7.91 (s, 2H); 7.65-7.67; (m, 4H); 7.34-7.43 (m, 6 H) ppm.

Spectroscopic data are in agreement with those reported in literature (*Macromolecules* 2013, 46, 18, 7158–7165).

5,8-dibromo-2,3-dihexylquinoxaline

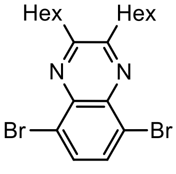

17

To a solution of 1,2-di(hexyl)etan-1,2-dione **15** (230 mg, 1.01 mmol, 1.0 eq) in acetic acid (5 mL), under inert atmosphere, **13** (269 mg, 1.01 mmol, 1.0 eq) was added and the mixture was heated to 90°C for 16h. The mixture was cooled to room temperature and the mixture was extracted with EtOAc (5x2 mL). The organic phase was washed with H_2O (10x2 mL) and dried on anhydrous Na_2SO_4. The solvents were evapoured under vacuum. The crude product was purified by flash chromatography (SiO_2, petroleum ether / DCM 3:1), obtaining the product **17** as a pale white solid (180 mg, 0.39 mmol, 39%).

^{1}H NMR (400 MHz, $CDCl_3$): δ = 7.81 (s, 2H); 3.07 (t, J= 9.4 Hz, 4H), 1.80-2.00 (m, 4H); 1.35-1.50 (m, 12 H); 0.89-0.91 (m, 6H) ppm.

^{13}C NMR (100 MHz, $CDCl_3$): δ = 158.4, 139.4, 132.1, 123.5, 34.9, 31.9, 29.3, 27.9, 22.8, 14.3 ppm.

ESI-MS: m/z = 458.05 456.32, 454.06 (1:2:1) $[M+H]^+$.

General procedure for Suzuki-Miyaura coupling (A):

In a microwave tube Pd(dppf)Cl_2 (10% mol) was added to a solution of toluene (3 mL) of dibromoquinoxaline derivative (1.0 eq). In a schlenk, boronic ester/acid (2.5 eq) and KF (3.0 eq) were dissolved in MeOH (0.5 mL). The solution of MeOH were added in the MW tube. The mixture was stirring for 30' at room temperature and then heated at the MW at 70°C, for 35'. The mixture was cooled at room temperature and the solvent was evapoured.

4,4'-(2,3-diphenylquinoxaline-5,8-diyl)bis(N,N-diphenylaniline): DQ1

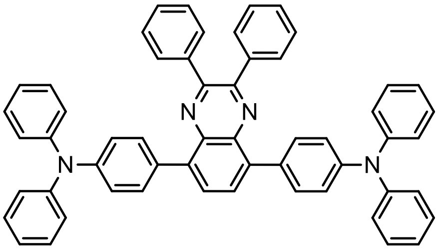

DQ1

The compound **16** (167 mg, 0.22 mmol, 1.0 eq) was solubilized in tol:MeOH (6:1); Pd(dppf)Cl_2 (16.1 mg, 0.022 mmol, 10% mol), boronic ester/acid **18** (156.1 mg, 0.54 mmol, 2.5 eq) and KF (38.3 mg, 0.66 mmol, 3.0 eq) were added and the mixture was heated at 80° for 18 h.

The crude product was purified by flash column chromatography (SiO_2, petroleum ether/DCM 3:1) obtaining the product **DQ1** as an orange solid (35 mg, 0.045 mmol, 21%).

^{1}H NMR (400 MHz, $CDCl_3$): δ = 7.89 (s, 2H), 7.80 (d, J= 8.4 Hz, 4H), 7.63 (d, J= 7.6 Hz, 4H), 7.27-7.38 (m, 14H), 7.20-7.27 (m, 12H), 7.07 (dd, J= 7.6, 6.4 Hz, 4H) ppm.

^{13}C NMR (100 MHz, $CDCl_3$): δ = 151.0, 147.7, 147.3, 139.1, 138.6, 138.4, 132.1, 131.7, 130.1, 129.4, 129.3, 128.8, 128.2, 124.7, 123.0, 122.7 ppm.

ESI-MS: m/z = 769.4 $[M+H]^+$.

4,4'-(2,3-diphenylquinoxaline-5,8-diyl)bis(N,N-bis(4-(hexyloxy)phenyl)aniline): DQ2

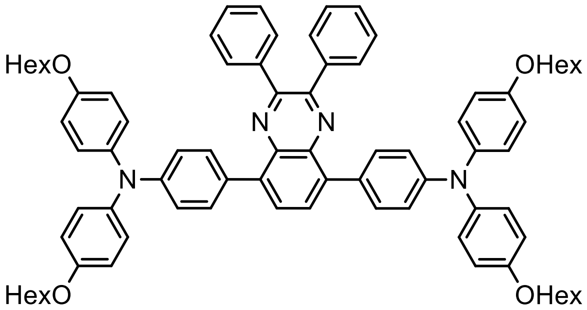

DQ2

DQ2 was prepared starting from **16** (86 mg, 0.11 mmol,1.0 eq), Pd(dppf)Cl_2 (8.0 mg, 0.011 mmol, 10% mol), boronic ester/acid **19** (157 mg, 0.27 mmol, 2.5 eq) and KF (19 mg, 0.33 mmol, 3.0 eq) using general procedure A. The crude product was purified by flash column chromatography (SiO_2, petroleum ether/DCM 5:1 → 3:1) obtaining **DQ2** as an orange solid (28 mg, 0.024 mmol, 21%).

^{1}H NMR (400 MHz, $CDCl_3$): δ = 7.86 (s, 2H), 7.69 (d, J = 9.0 Hz, 4H), 7.58 (d, J = 7.4 Hz, 4H), 7.37-7.29 (m, 6H), 7.15 (d, J = 9.0 Hz, 8H), 7.04 (d, J = 11.9 Hz, 4H), 6.88 (d, J = 9.1 Hz, 8H), 3.96 (t, J = 6.4 Hz, 8H), 1.83-1.74 (m, 8H), 1.52-1.44 (m, 8H), 1.40-1.33 (m, 16H), 0.93 (t, J = 6.6 Hz, 12H) ppm.

^{13}C NMR (100 MHz, $CDCl_3$): δ = 155.8, 151.1, 148.4, 140.4, 139.2, 138.3, 131.3, 129.9, 129.8, 129.15, 128.6, 128.1, 127.0, 118.9, 115.2, 68.3, 31.6, 29.3, 25.7, 22.6, 13.8 ppm.

ESI-MS: m/z = 1168.6 $[M\cdot]^+$.

3,3'-(2,3-diphenylquinoxaline-5,8-diyl)bis(10-(4-methoxyphenyl)-10H-phenothiazine): DQ3

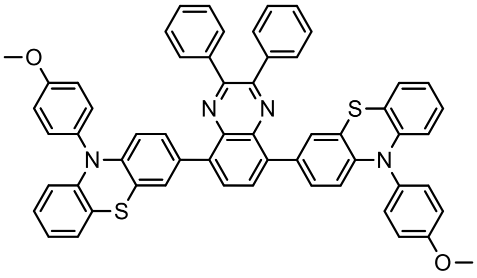

DQ3

DQ3 was prepared starting from **16** (174 mg, 0.23 mmol, 1.0 eq), Pd(dppf)Cl_2 (16.8 mg, 0.023 mmol, 10% mol), boronic ester/acid **20** (248 mg, 0.57 mmol, 2.5 eq) and KF (40 mg, 0.69 mmol, 3.0 eq) using general procedure A. The crude product was purified by flash column chromatography (SiO_2, petroleum ether / DCM 4:1 → 2:1) obtaining **DQ3** as a yellow solid (93 mg, 0.10 mmol, 46%).

^{1}H NMR (400 MHz, $CDCl_3$): δ = 7.74 (s, 2H), 7.59 (dd, J= 6.0, 3.6 Hz, 6H), 7.36 (d, J=6.0 Hz, 4H), 7.33-7.29 (m, 8H), 7.15 (dd, J= 7.6, 3.2 Hz, 4H), 7.03 (dd, J= 5.6, 1.6 Hz, 2H), 6.82 (ddd, J= 9.2, 4.0, 1.2 Hz, 4H), 6.30 (d, J= 8.8 Hz, 2H), 6.19 (dd, J= 4.0, 2.0 Hz, 2H), 3.92 (s, 6H) ppm.

^{13}C NMR (100 MHz, $CDCl_3$): δ = 159.2, 151.1, 144.4, 144.0, 138.3, 137.5, 133.2, 132.3, 132.2, 130.1, 129.1, 128.8, 128.7, 128.2, 126.8, 126.6, 122.3, 119.5, 118.9, 115.9, 115.6, 115.2, 55.5 ppm.

ESI-MS: m/z = 889.3 $[M+H]^+$.

4,4'-(2,3-dihexylquinoxaline-5,8-diyl)bis(N,N-diphenylaniline): DQ4

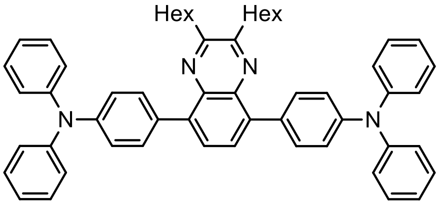

DQ4

DQ4 was prepared starting from **17** (66 mg, 0.14 mmol, 1.0 eq), Pd(dppf)Cl_2 (10.2 mg, 0.014 mmol, 10% mol), boronic ester/acid **18** (101 mg, 0.35 mmol, 2.5 eq) and KF (24.4 mg, 0.42 mmol, 3.0 eq) using general procedure A. The crude product was purified by flash column chromatography (SiO_2, petroleum ether / DCM 4:1 → 2:1 → EtOAc) obtaining **DQ4** as a yellow solid (67 mg, 0.08 mmol, 55%).

^{1}H NMR (400 MHz, $CDCl_3$): δ = 7.77 (s, 2H), 7.72 (d, J= 8.4 Hz, 4H), 7.29 (dd, J= 15.9, 8.0 Hz, 8H), 7.24-7.15 (m, 12H), 7.04 (m, 4H), 2.97 (t, J= 7.6 Hz, 4H), 1.91-1.81 (m, 4H), 1.46-1.37 (m, 4H), 1.36-1.21 (m, 6H), 0.86 (t, J= 6.0 Hz, 6H) ppm.

^{13}C NMR (100 MHz, $CDCl_3$): δ = 155.1, 148.0, 147.1, 138.8, 138.3, 132.9, 131.8, 129.4, 128.5, 124.7, 123.0, 34.9, 32.0, 29.3, 27.3, 22.8, 14.2 ppm.

ESI-MS: m/z = 785.4 $[M + H]^+$.

4,4'-(2,3-dihexylquinoxaline-5,8-diyl)bis(N,N-bis(4-(hexyloxy)phenyl)aniline): DQ5

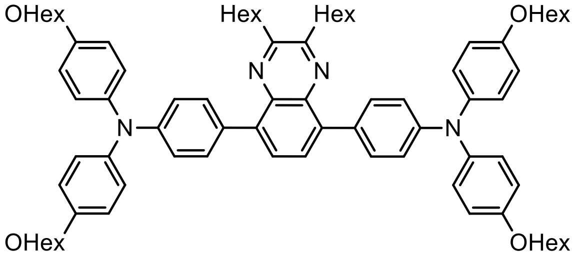

DQ5

In a schlenk, under inert atmosphere of N_2, dibromoquinoxaline derivative **17** (50 mg, 0.11 mmol, 1.0 eq) and $Pd(PPh_3)_4$ (12.8 mg, 0.011 mmol, 10% mol) were dissolved in toluene (4 mL). In another schlenk, boronic ester/acid **19** (132 mg, 0.23 mmol, 2.1 eq) and Cs_2CO_3 (116 mg, 0.33 mmol, 3.0 eq) were dissolved in MeOH. The solution in MeOH was added to the solution in toluene. The mixture was stirred and heated to 110°C for 4 h. Then water was added to the mixture and the solution was extracted with EtOAc (4 mL x 3). The organic phase was washed with water (10 mL x 2) and brine (10 mL) and then dried on anhydrous Na_2SO_4. The solvent was removed under reduced pressure. The crude product was purified by flash column chromatography (SiO_2, petroleum ether / DCM 3:1 → 1:1) obtaining **DQ5** as an orange solid (108 mg, 0.091 mmol, 83%).

^1H NMR (400 MHz, $CDCl_3$): δ = 7.72 (s, 2H), 7.65 (d, J= 8.4 Hz, 4H), 7.13 (d, J= 9.2 Hz, 8H), 7.03 (d, J= 8.4 Hz, 4H), 6.84 (d, J= 9.0 Hz, 8H), 3.94 (t, J= 1.2 Hz, 8H), 2.96 (t, J= 1.2 Hz, 4H), 1.74-1.90 (m, 14H), 1.51-1.43 (m, 10H), 1.37-1.33 (m, 21H), 0.95-0.89 (m, 14H), 0.88-0.82 (m, 7H) ppm.

^{13}C NMR (100 MHz, $CDCl_3$): δ = 155.4, 154.7, 147.9, 140.8, 138.7, 138.0, 131.4, 130.6, 128.1, 126.7, 119.6, 115.2, 68.2, 34.7, 31.8, 31.6, 29.3, 29.2, 27.3, 25.8, 22.6, 14.1, 14.0 ppm.

ESI-MS: m/z = 1185.9 $[M + H]^+$.

CHAPTER 5

DESIGN OF A LUMINOPHORE for LSC: “A GREEN APPLICATION”

5 A GREEN WORLD: THE CHALLENGE OF ALGAE

The goal of reducing energy dependence on fossil resources and consequently slowing down the production of CO_2 can only be achieved if all the other renewable resources available to us will be used.

The increasing CO_2 emissions and the importance to store or mitigate them have promoted research groups to look for methods for capture CO_2 and mitigate emissions. Looking at nature, plants are natural reactors for CO_2 mitigation. Their photosynthetic process is powered by carbon dioxide, naturally photocatalyzed by sunlight.

A peculiar vegetable class widely investigated in last years are microalgae. Microalgae are eukaryotic unicellular organisms, with dimensions 1 μm-10 μm of diameter, belonging to the class of aquatic plants.

Microalgae have been used for many environmental applications, especially for CO_2 mitigation, wastewater treatments and biofuels production[204].

Moreover, microalgae are exploited for bioremediation, an important, suitable, low-priced and efficient alternative process for contaminants removal, which is based on the exploitation of microorganisms to remove and to metabolize toxic, mutagenic and carcinogenic substances to non-toxic compounds[205]. Due to their photosynthetic ability to quickly grow in reaction site, the exploitation of organic/inorganic carbon substrate and the mild working conditions Together with their capacity to proliferate in wastewater and to exploit several compounds, such as pesticides, hydrocarbons, cyanides, as nitrogen and phosphorous sources, microalgae play a crucial role in environment remediations. Finally, wide biotechnological applications of microalgae allow producing valuable substances for feed, food, pharmaceutical and nutraceutical factories[206].

Looking at world numbers, global seaweed agriculture production occupies around 20% of total world marine agriculture production by weight. In 2013, the annual value was of US $ 6.7 billions, with Asia as the most manufacturer. In 2017, the seaweed agriculture production demand rose in America and Europe too, with 54000 tons of microalgae[207].

In the microalgae scenario, light availability is one of the most important factor for the growth: like all the vegetable in the world, they need the energy input of the Sun for their photosynthetic process. To allow such process, only a part of solar radiation is necessary, which is in the range between 400 and 700 nm and it is known as photosynthetically active radiation (PAR). This is due to the absorption of chlorophyll pigment, which is the photoactive species in all plants and is characterized by double absorption peaks, centred at 430 nm and 660 nm (Fig. 87).

To improve algae growth photobioreactors can be used. Our idea was finding suitable conditions to power photobioreactors, using LSC devices In this way, two different sustainable

---

[204] a) Y. Chisti, *Biotechnol. Adv.*, **2007**, *25*, 294-306; b) F.G.A. Fernández, C.V. Gonzáles-López, J.M. Fernández Sevilla, E.M. Grima, *Appl. Microbiol. Biotechnol.*, **2012**, *96*, 577-586.

[205] A.M. Hammed, S.K. Prajapati, S. Simsek, H. Simsek, *Algae* **2016**, *31*(3), 189-204.

[206] a) P. Spolaore, C. Joannis-Cassan, E. Duran, A. Isambert, *J. Biosci. Bioeng.*, **2006**, *101*, 87-96; b) D. Han, Y. Li, Q. Hu, *Algae* **2013**, *28*(2), 131-147.

[207] J.K. Kim, C. Yarish, E.K. Hwang, M. Park, Y. Kim, *Algae* **2017**, *32*(1), 1-13.

technologies can be used to mitigate CO_2 emission using renewable energy.

To exploit the possibility of applying LSC device on microalgae photobioreactor, the first requirement is an absorption range of the fluorophore, which must leave out the absorption wavelengths of chlorophyll. To achieve this goal it is important to design suitable, LSC fluorophore with an absorption range between 460 nm and 630 nm.

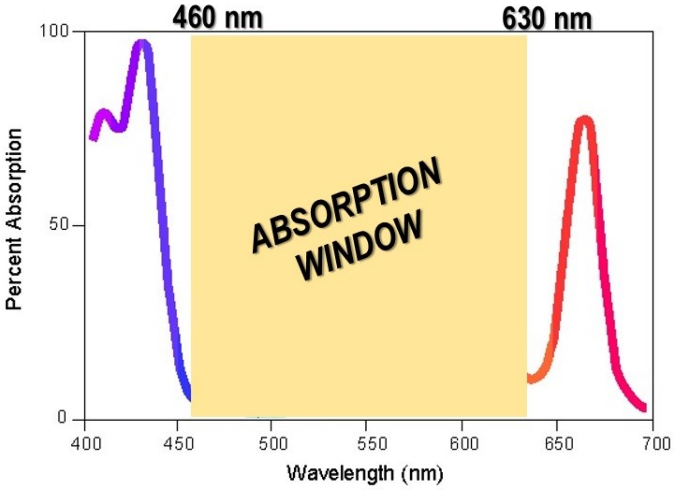

Fig. 87: *Absorption wavelengths of Chlorophyll and the absorption window exploitable for LSC fluorophore*[208].

At the same time, the fluorophore should answer to the other typical requirements, needed for application in LSC devices, such as high emission range, high fluorescence quantum yield, low interaction with polymer matrix, low or moderate costs and simple synthesis.

5.1 LSC FOR ALGAE (LSCA): Π-D-A-D-Π MOLECULES

To match all these issues we focused our attention on π-D-A-D-π structure. We have seen in previous chapters that D-A-D molecules might favour a strong ICT process, increasing fluorescence transition and the corresponding fluorescence quantum yield.
However, not all donor and acceptor moieties could exhibit bathochromic absorption, in order to cover the absorption window required for this kind of application (460-630 nm).
Hence, we were interested to evaluate if the introduction of π conjugated pendants could generate a redshift to long wavelengths on the absorption and emission spectra, allowing a better matching with chlorophyll spectroscopic properties.
In order to plan a simple and easy synthesis, we decided to design a symmetrical molecule.
We were attracted by a peculiar π-D-A-D-π structure which was reported by Yang and co-workers[209] in 2017, for tumor imaging applications. The fluorescent probe FEB-2000 (Fig. 88) showed benzo-2,1,3-thiadiazole (BTD), 3,4-ethoxylene dioxythiophene (EDOT) and fluorene as acceptor, donor and π moieties respectively.

---

[208] Credit: University of Winsconsin-Madison (adapted image)

[209] D. Yang *et al.*, *Chem. Sci.*, **2017**, *8*, 6322–26.

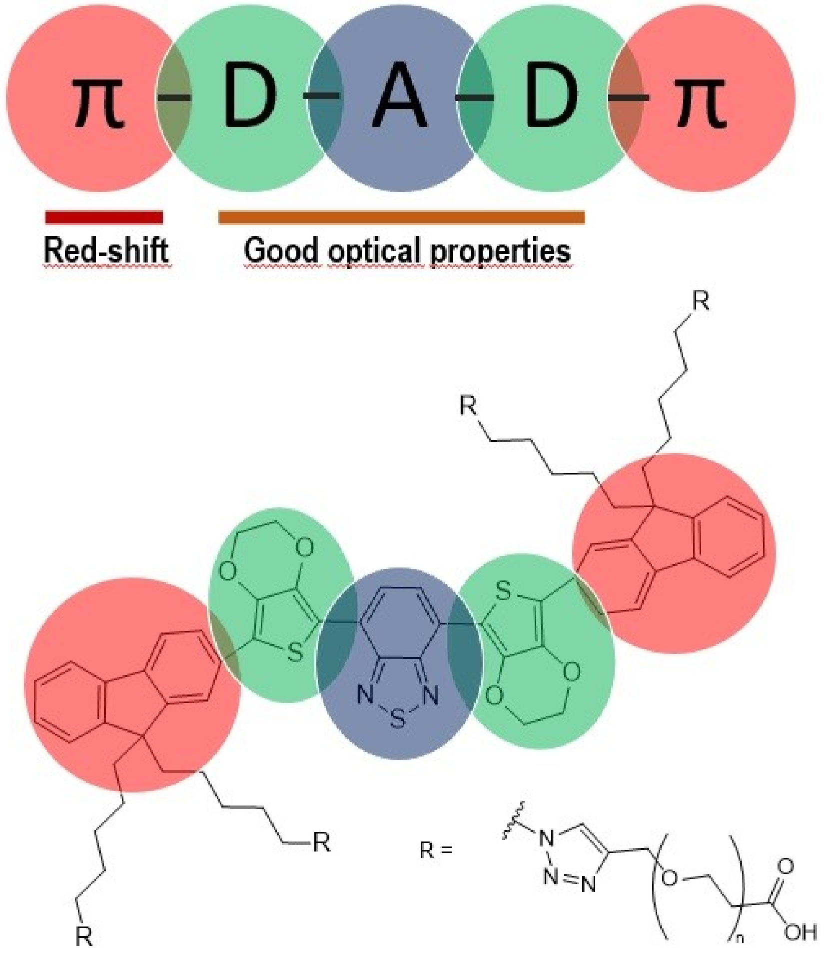

Fig. 88: *π-D-A-D-π organic derivatives (FEB 2000) for tumour imaging.*

Benzothiadiazole (BTD) is a strong electron-poor core, widely applied for fluorescent probes[210]. That exhibits high fluorescence quantum yields. 3,4-Ethylenedioxythiophene (EDOT) and fluorene are commercially available low-priced starting materials; moreover, fluorene could be easily functionalized on position 9, due to weakly acid hydrogens on C9[211] (pK_a= 22.6 in DMSO). The corresponding carbanion is a stable aromatic system, prepared in presence of a strong organic base (such as sodium tert-butoxide, NaOtBu)[212] and able to react in presence of a weak electrophile (such as alkyl halides).

Thus the EDOT-BTD-EDOT, as D-A-D structure, could be an interesting starting point which was supported by its optoelectronic characteristics: low band gap between HOMO and LUMO levels and long wavelengths absorption and emission maxima[213].

---

[210] a) B.A.D. Neto, P.H.P.R. Carvalho, J.R. Correa, *Acc. Chem. Res.* **2015**, 48, 6, 1560–69; b) H. He *et al.*, **Org. Biomol. Chem.**, **2020**,**18**, 6357-63; c) F.F.D. Oliveira *et al.*, *Bioorg. Med. Chem. Lett.*, **2010,** *20*, 6001–07; d) F. Chen, J. Zhang, W. Qu, X. Zhong, H. Liu, J. Ren, H. He, X. Zhang, S. Wang, *Sensors and Actuators B: Chemical*, **2018**, *266*, 528-5333.

[211] a) F.G. Bordwell, *Acc. Chem. Res.*, **1988**, *21* (12), 456–463, b) J.T. Fan, X.H. Fan, C.Y. Gao, Z. Wang, L.M. Yang, *RSC Adv.*, **2019**, *9*, 35913–16.

[212] G.W.H. Scherf, R.K. Brown, *Can. J.Chem.* **1960**, *38*, 69.

[213] J.M. Raimundo, P. Blanchard, H. Brisset, S. Akoudad, J. Roncali, *Chem. Commun.*, **2000**, 939–940.

The optical and electronic properties of different EDOT-BTD-EDOT molecule were compared in figure 89 and reported in table 19.

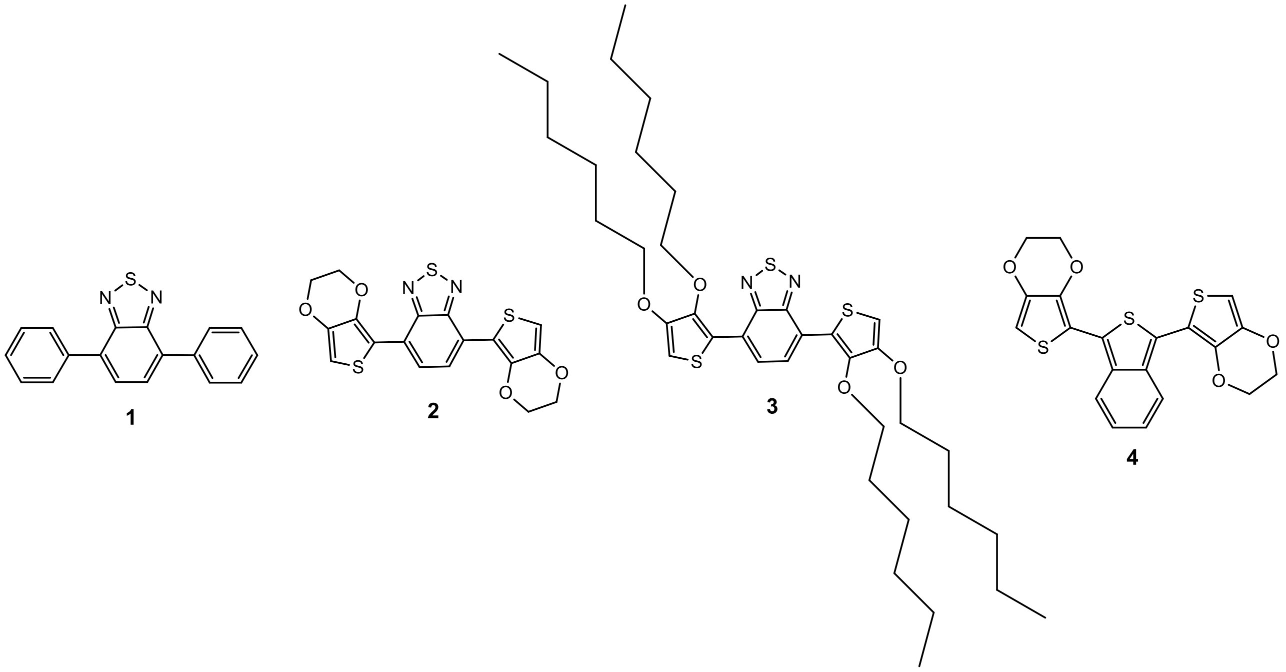

Fig. 89: *Molecular designs of D-A-D structure.*

Thiophene-based derivatives (**2** and **3**) exhibited a smaller energy band gap (ΔE) compared to compound **1**, due to thiophene lower resonance energy and to the electron releasing effect of alkoxy groups on the thiophene ring[214]. Withdrawing substituents increased the HOMO level or reduced the LUMO one. Moreover, the low decrease in ΔE for **2** to **3** and its slight reduction of relative anodic peak potential (E_{pa}) reflected the stronger electron-donating effect of the ethylenedioxy bridge compared to dialkoxy chains[215] (Table 19).

Table 19: *CV[a] and optical[b] data for compounds **1-3**, respectively anodic peak potential (E_{pa}), reduction peak potential (E_{pr}), absorption and emission wavelengths (λ_{abs} and λ_{em}), energy band gap (ΔE) and fluorescence quantum yields (Φ_f).*

Entry	E_{pa} (V)	E_{pr} (V)	λ_{abs} (nm)	λ_{em} (nm)	ΔE (eV)	Φ_f (%)
1	1.82	-1.36	380	490	2.87	0.8
2	0.92	-1.40	481	630	2.19	0.75
3	1.06	-1.28	456	542	2.29	0.73
4	0.56	-1.80	450	613	2.33	0.92

[a] *In 0.1 M NBu4PF6–MeCN, ref. SCE, 100 mV s21.* [b] *In CH_2Cl_2*.

---

[214] J. Roncali, *Chem. Rev.* **1997**, *97*, 173–205.

[215] S. Akoudad, P. Frère, N. Mercier, J. Roncali, *J. Org. Chem*., **1999**, *64*, 4267-72.

On the other side, the positive potential shift of 0.40 V and 0.36 V for E_{pa} and E_{pr}, respectively, observed in molecule **2** compared with **4**, confirmed the stronger acceptor capacity of BTD. Thus, BTD electron-deficient core and EDOT electron-donating moiety seem to favour high electron affinity, high fluorescence quantum yield in solution, long-wavelength emission spectrum, large Stokes shift and low energy band gap between HOMO and LUMO levels.
However, EDOT-BTD-EDOT core was a non-planar configuration: the hindrance of six-component cycle in 3,4 position of EDOT moiety and the electronic repulsion between thiazole ring and EDOT reduced molecular flatness and avoided *inter* and *intra* molecular interactions.
Finally, the presence of fluorine in *FEB 2000*, decorated with some alkyl chains, is important to avoid fluorescence quenching and to increase molecular solubility.
FEB 2000 showed an absorption peak at 550 nm, an emission one at 670-675 nm in toluene, with a high fluorescence quantum yield (85%).

5.2 π-D-A-D-π LSC DYES: DESIGN AND SYNTHESIS

Due to the very interesting preliminary optical values of *FEB 2000,* we designed and synthesized a new and simpler analogous in order to evaluate its possible application in LSC devices.

Our target molecules are shown figure 89. Donating-effect of withdrawing moiety was evaluated and 9-dibutyl-fluorene was chosen as π group. **LSCA1** differing from *FEB 2000* compound for simple butyl groups on fluorine moiety; while **LSCA2** differing for the presence of 3,4-(2,2'-dipentylpropylene)dioxythiophene (Prodot) donor group.

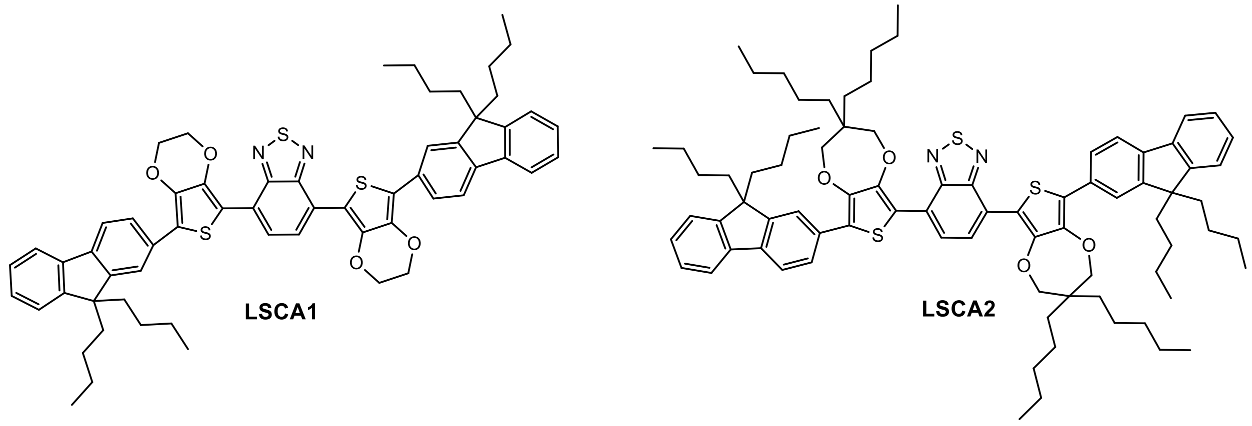

Fig. 89: *Design of chromophores LSCA1 and LSCA2.*

Typically, the synthetic approach was based on cross-coupling reactions (Scheme 8). The previously reported synthesis of *FEB-2000* followed a convergent approach. Intermediate **3** was prepared through Stille cross-coupling reaction between 2-bromo-9*H*-fluorene **1** and tributyl(2,3-dihydrothieno[3,4-b][1,4] dioxin-5-yl)stannane (**2**). $Pd(PPh_3)_4$ was chosen as the catalytic specie, working in toluene at reflux for 6 h. The following alkylation on C9 of fluorene was carried out through an electrophilic substitution in presence of *t*-BuOK, as base, which gave compound **4** in good yield. The final product was synthesized by symmetrical Stille cross-coupling reaction on dibromide (**5**) using the stannyl intermediate obtained by lithiation of **4** and reaction with tributhyl stannil chloride**.** The reaction was performed one-pot, in presence of Pd(PPh3)2Cl2 as the catalyst.

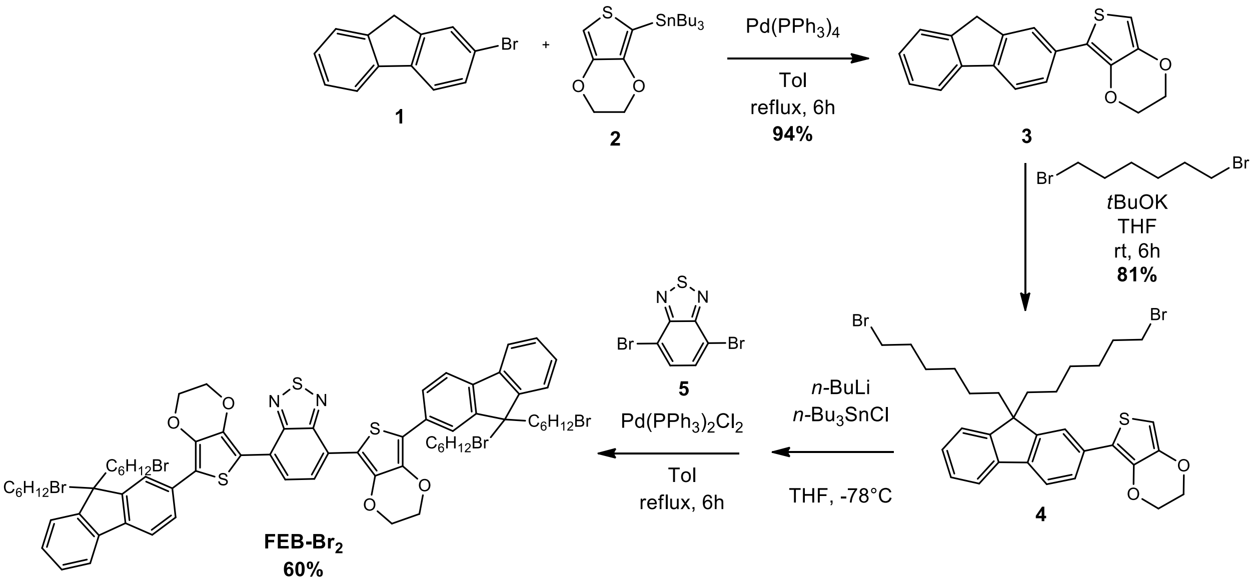

Scheme 8: *Synthesis of FEB 2000 precursor.*

This approach is based on five synthetic steps, where two of them need the preparation of stannyl intermediates to perform a Stille cross coupling reaction.

In order to find more efficient conditions, we decided to investigate the possibility to modify this approach using a direct C-H arylation process [216].

Direct C-H arylation had become a viable alternative method to the conventional cross-coupling approach. The emerging synthetic view is based on the formation of C-C bond through a cleavage of a non-preactivated C-H *sp*^{2}-bond in presence of a C-X reagent, usually catalysed by a Pd complex.

A general catalytic cycle of direct arylation is shown in figure 91[217].

---

[216] a) H. Bohra, M. Wang, *J. Mater. Chem. A*, **2017**, *5*, 11550–71; b) N.S. Gobalasingham, B.C. Thompson, *Progress in Polymer Science*, **2018**, *83*, 135–201.

[217] H. Bohra, M. Wang, *J. Mater. Chem. A*, **2017**, *5*, 11550–71.

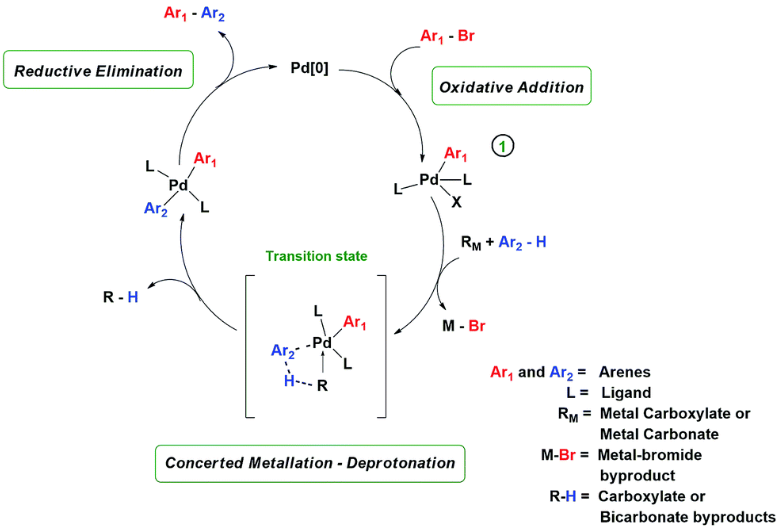

Fig. 91: *Catalytic cycle of a generic direct C-H arylation*[14].

The cycle begins with the oxidative addition of the aryl halide to the catalytic Pd(0) complex, in presence of ligand (L), with the formation of the corresponding aryl-halo Pd complex. According to the catalytic system, a carboxylate or a carbonate ion coordinates with aryl-halo complex, promoting the deprotonation of Ar_2-H and simultaneously the formation of Ar_2-Pd bond. The TS evolves through a lower energy state, with the elimination of the corresponding carboxylic acid. The followed reductive elimination favors the formation of C-C bond and regenerates the Pd(0) source. The evolution of TS depends on the catalytic conditions, the electronic properties of substrates, the ligand and the solvent, which involved in the reaction[218].

Direct C-H arylation is easy and economically efficient, avoiding intermediates production and purifications, toxic or dangerous reactants and with an ecologically green effect (high atom economy and E-factor).

Its applications on pharmaceutical, semiconductors and high performance π-conjugated materials have recently received a lot of attention[219].

In order to exploit direct C-H arylation cross coupling reaction to prepare **LSCA1** and **LSCA2** we considered the following retrosynthetic scheme (Scheme 9).

---

[218] a) D. Alberico, M.E. Scott, M. Lautens, *Chem. Rev.*, **2007**, *107*, 174–238; b) K. Ueda, S. Yanagisawa, J. Yamaguchi, K. Itami, *Angew. Chem., Int. Ed.*, **2010**, *49*, 8946–49; c) C. Colletto, S. Islam, F. Juliá-Hernández, I. Larrosa, *J. Am. Chem. Soc.*, **2016**, *138*, 1677–83.

[219] a) A. Facchetti, L. Vaccaro, A. Marrocchi, *Angew. Chem., Int. Ed.*, **2012**, *51*, 3520–23; b) K. Okamoto, J. Zhang, J.B. Housekeeper, S.R. Marder, C.K. Luscombe, *Macromolecules*, **2013**, *46*, 8059–78; c) S. Kowalski, S. Allard, K. Zilberberg, T. Riedl, U. Scherf, *Prog. Polym. Sci.*, **2013**, *38*, 1805–14; d) S.L. Suraru, J.A. Lee, C.K. Luscombe, *ACS Macro Lett.*, **2016**, *5*, 724–729.

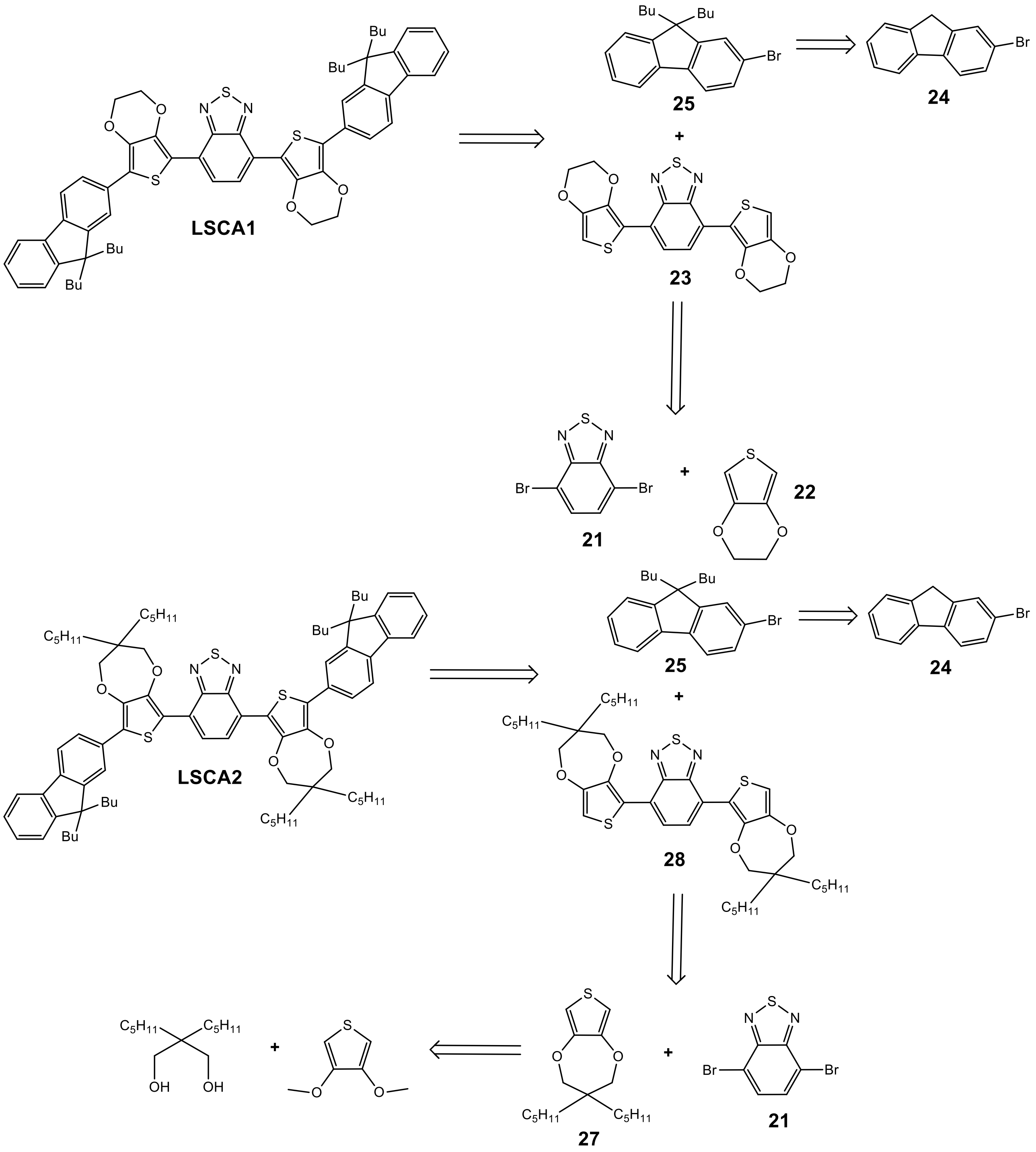

Scheme 9: *Retrosynthetic approaches for* ***LSCA1*** ***(6)*** *and* ***LSCA2*** ***(9)****.*

The synthetic approach for **LSCA1** is reported in scheme 10.

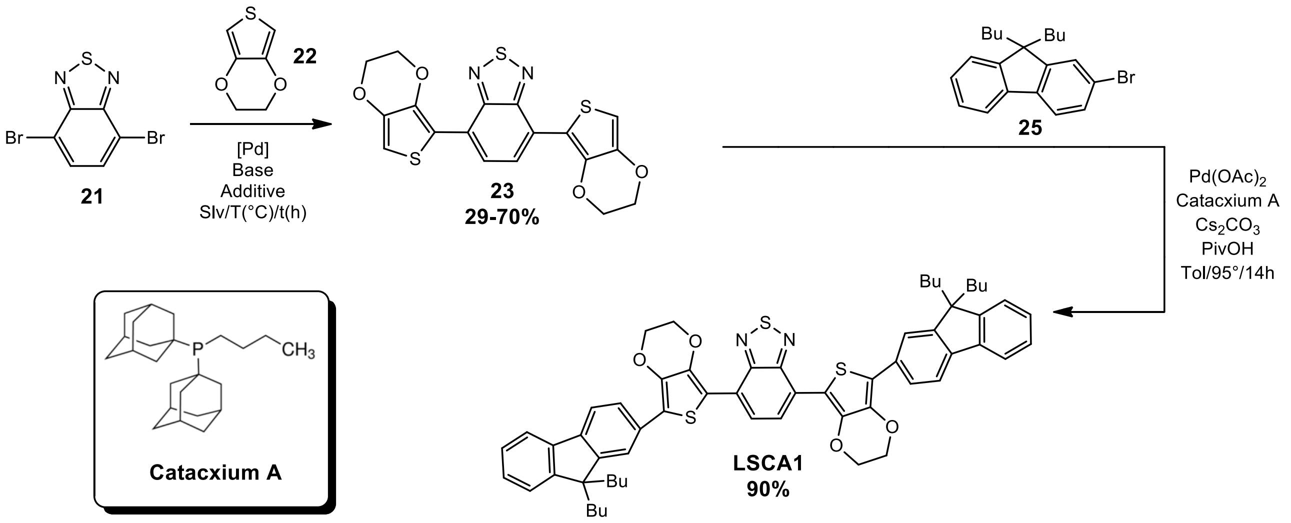

Scheme 10: *Synthetic procedure of **LSCA1**, based on direct C-H arylation approach.*

The commercial available 4,7-dibromo-benzo-2,1,3-thiadiazole BTD (**21**) and 3,4-ethoxylene dioxythiophene EDOT (**22**) were reacted in presence of $Pd(OAc)_2$ as Pd source. Catacxium A was chosen as ligand as it is widely employed in direct C-H arylation. K_2CO_3 and AcOH were used as base and additive; the reaction was carried out in toluene, heating at 90°C for about 24 hours. The product **23** was obtained with low yield (29%) (Entry 1 in Table 20). Unfortunately, in these conditions, the reaction was not clean and a series of polymeric side-products were obtained. **23** shows a low solubility in the most common organic solvents, thus hampering purification through chromatography.

Table 20: *Synthetic conditions of direct C-H arylation between BTD and EDOT.*

Entry	EDOT (eq)	[Pd] (%mol)	L (%mol)	Base (eq)	Additive (%mol)	Slv/T/t	Yield (%)
1	2.2	$Pd(OAc)_2$ (5)	Cat A (10)	K_2CO_3 (1.5)	AcOH (30)	Tol/95/24	29
2	2.2	$Pd(OAc)_2$ (5)	PCy_3 (10)	Cs_2CO_3 (1.5)	AcOH (30)	Tol/95/5	30
3	5.0	$Pd(OAc)_2$ (5)	Cat A (10)	Cs_2CO_3 (1.5)	PivOH (30)	Tol/95/24	56
4	5.0	$Pd(OAc)_2$ (8)	-	K_2CO_3 (1.5)	PivOH (12)	*N,N*-DMF 140/3	70

Trying to improve the yield of the reaction, some modification were considered.

Using $Pd_2(dba)_3$ as Pd source instead of $Pd(OAc)_2$, less trace of product were observed. A large amount of side products, probably oligomers and polymers obtained from EDOT-BTD derivatives, were found. Moreover, the mono-substituted compound (EDOT-BTD) was observed during all reaction time and a good part of it was isolated at the end.

To increase the yield of **23**, limiting the polymeric side-products, a large excess of EDOT was used[220], in absence of ligand[221], trying to limit the formation of polymeric products and improving the probability for EDOT to take part in the second direct C-H arylation.

N,N-DMF was chosen as solvent, allowing to increase temperature from 95° to 140°C, as the thermal activation. The use of polar solvent such as *N,N*-DMF usually favors the formation of cross-coupling

---

[220] P. Giannopoulos *et al.*, *Dyes and Pigments* **2018**, *148*, 167-179.

[221] N.S. Gobalasingham, B.C. Thompson, *Progress in Polymer Science*, **2018**, *83*, 135–201.

compounds. In presence of Pd(OAc)$_2$, K$_2$CO$_3$ and PivOH as catalyst, base and additive, respectively, compound **23** was finally obtained with a very good yield (70%, Entry 4 in Table 20). The final product **LSCA1** was obtained through direct C-H arylation between the intermediate **23** and 2-bromo-9-dibutyl-fluorene (**25**).

Compound **25** was prepared, with quantitative yield (>99%), starting from the commercial 2-bromofluorene through a double electrophile substitution on 9 position, in presence of *t*-BuONa as base and 1-iodobutane as electrophile, working from 0°C to room temperature for 16 hours. Finally **LSCA1** was obtained using Pd(OAc)$_2$ and Cataxium A as catalytic system, with Cs$_2$CO$_3$ and PivOH as base and additive, with a very good yield (90%). The final compound was easily purified by flash chromatography, thanks to its high solubility, increased from the intermediate **23** for the presence of alkyl chains on fluorine moiety, that avoided π–π staking of the molecule.

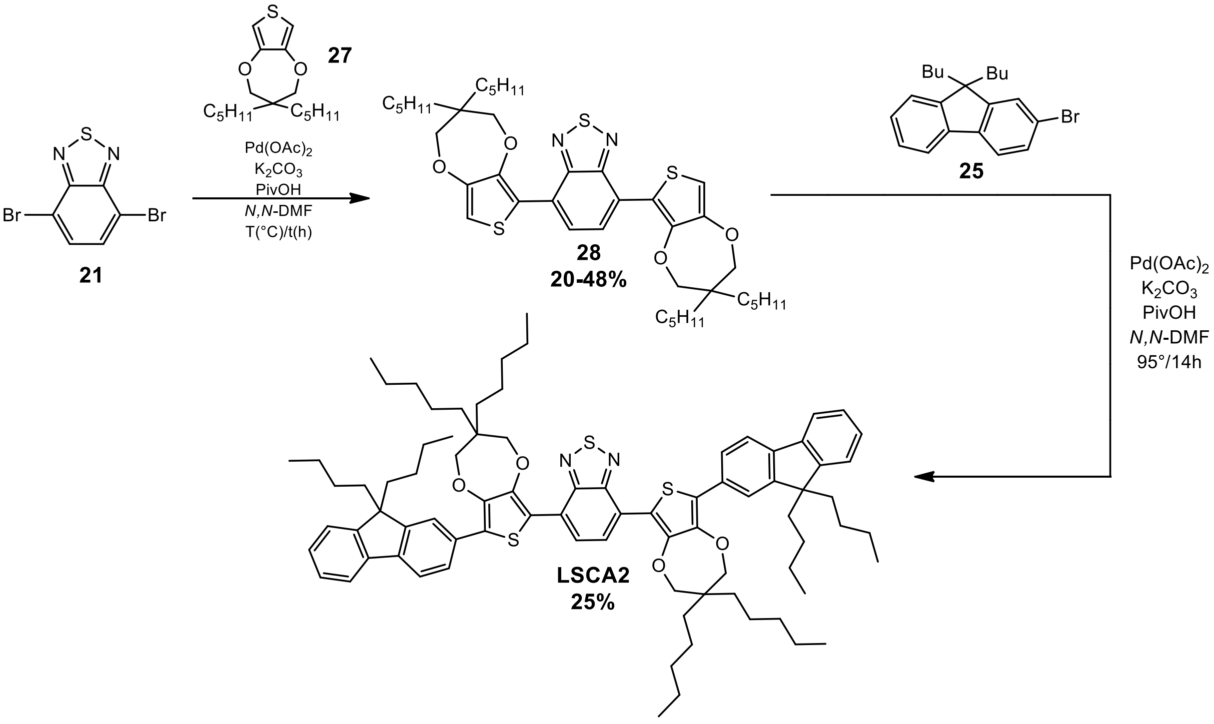

*Scheme 11: Synthetic procedure of **LSCA2**, following direct C-H arylation approach.*

Using an identical approach, **LSCA2** was synthesised .The same commercially available core, BTD (**21**) was reacted with **27**. After 20 minutes of reaction at 100°C, all the starting material was consumed giving a mixture of compounds **28** (48%) and polymeric side-products. Trying to perform the reaction at lower temperature reduced conversion and decreased the yield of product **28** (20%, at 50°C after 20 minutes). The intermediate **28** was then reacted with 2-bromo-9-dibutyl-fluorene (**25**), using the same conditions optimized for the synthesis of **28** (Scheme 11). The final product **LSCA2** was obtained, albeit with a low yield (25%).

5.3 SPECTROSCOPIC CHARACTERIZATION IN SOLUTION

The new two molecules were analysed through UV-Vis and fluorescence emission spectroscopy. Two solvents, DCM and toluene, were selected for measurements. Both of them were able to solubilize efficiently **LSCA1** and **LSCA2**, thanks to the high number of alkyl chains presented on these molecules. The optical properties are reported in table 21.

Table 21: *Optical properties of LSCA1 and LSCA2 in both DCM and toluene.*

Compound	Slv	λ_{abs}(nm)	ε (10^4 M^{-1} cm^{-1})	λ_{em}(nm[eV])	SS(eV)
LSCA1	DCM	550 [385][a]	49681 [71795][a]	670	0.40 [1.37][a]
	Tol	550 [387][a]	48074 [64867][a]	650	0.35 [1.30][a]
LSCA2	DCM	528 [371][a]	31082 [50671][a]	662	0.47 [1.47][a]
	Tol	531 [374][a]	31694 [46752][a]	638	0.39 [1.37][a]

[a] In parenthesis, values of λ_{abs}, ε, SS relative to a second absorption peak at short wavelength.

Compound **LSCA1** exhibited two broad absorption range, an absorption peak at short wavelength (385 nm) corresponding to π–π* transition, and another band between 400 and 600 nm, corresponding to intramolecular charge transfer (ICT)[222].

The spectra showed similar shape in both solvents (Fig 92, A and D).

In the range between 410 and 480 nm, where chlorophyll exhibits one of its peculiar absorption peaks, the fluorophore showed a depression, where the absorption was relatively low. The absorption increased with concentration, independently of the choice of solvent with a comparable trend in both solvents. For both absorption maxima, **LSCA1** exhibited very high **ε**, which corresponded to a higher capacity of light harvesting of solar radiation.

The emission spectra were registered in both solvents, after excitation at 385 nm and at 550 nm. Excited at different absorption wavelengths, the emission spectra showed only one peak at 670 nm for DCM solutions and at 650 nm in toluene one. Comparing the two emission spectra, the maximum in DCM was red-shifted of 20 nm, compared to toluene. However, toluene solutions showed a narrow emission range with higher intensity than DCM samples, with a higher contribution from absorption at 385 nm. Thus, the overlap region between absorption and emission spectra and consequent self-absorption processes were reduced.

Moreover, the large Stokes shifts and the limited overlap regions between absorption and emission spectra were common characteristics of the π-conjugated compound, attributed to a stronger ICT effect visible in both solvents. The presence of alkyl chains and the extremely twisted molecular geometry in the solution allowed high solubility and favored radiative mechanisms in the excited state. Furthermore, a regular shape of emission spectra demonstrated the absence of aggregation in solution; no vibronic states were observed.

---

[222] R. Martín *et al.*, *J. Mater. Chem. C*, **2019**,*7*, 9996-10007.

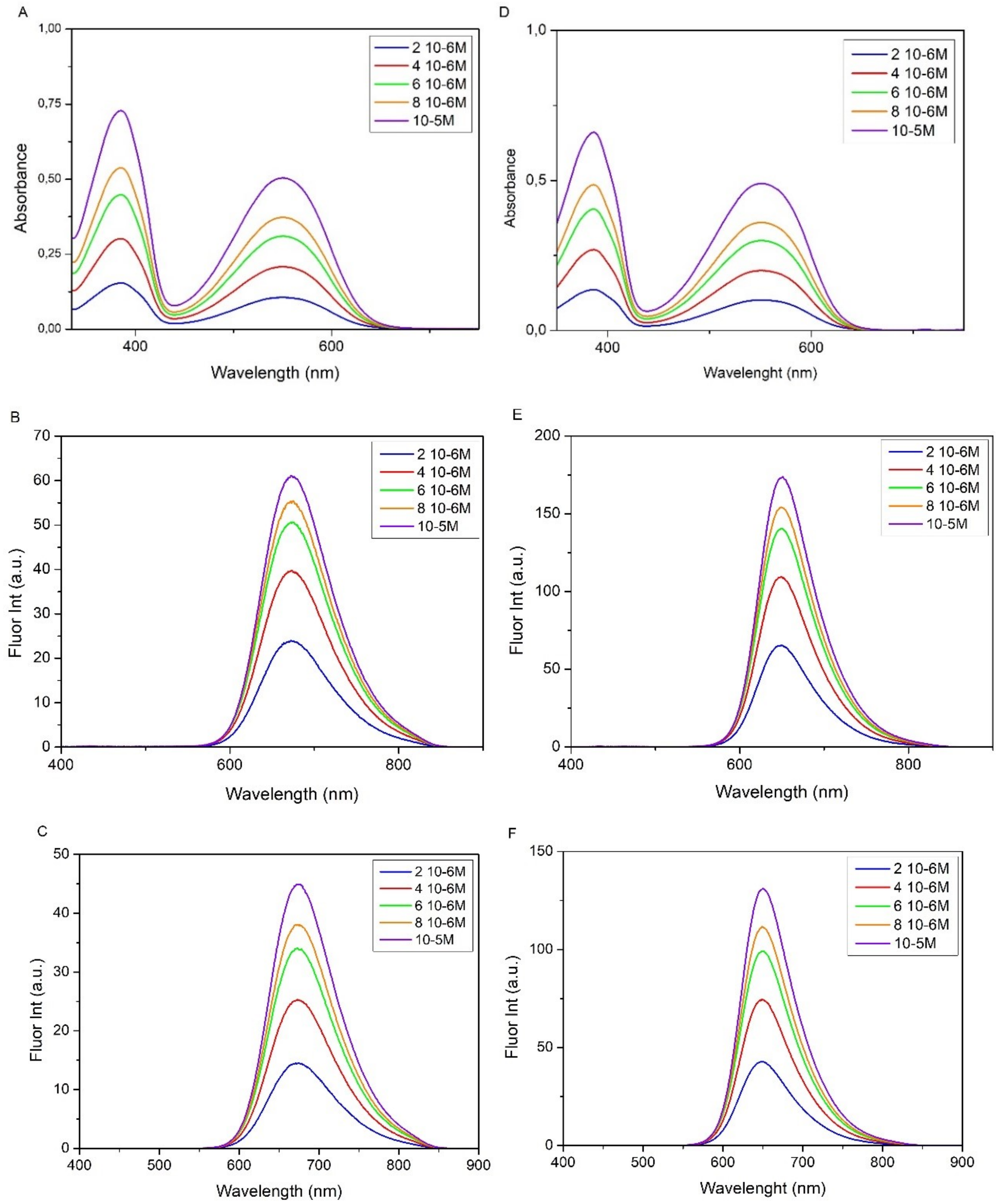

Fig. 92: *Absorption spectra in DCM (A) and in toluene (D), the corresponding emission spectra in DCM (B) and toluene (E) with excitation at 385 nm and the corresponding emission spectra in DCM (C) and toluene (F) with excitation at 550 nm of* ***LSCA1*** *at different concentration.*

Similarly, **LSCA2** presented good optical properties, comparable with **LSCA1** ones (Fig. 93).
The absorption range was described by two different peaks, around 370 and 530 nm. In addition, in this case, an evident depression in the absorption spectra was again observed, in a range similar to **LSCA1** case, with a barely perceptible blue-shift. Moreover, **LSCA2** showed good **ε**, which allowed to harvest and capture a higher amount of sunlight, even if they were lower than the corresponding **LSCA1** coefficients.

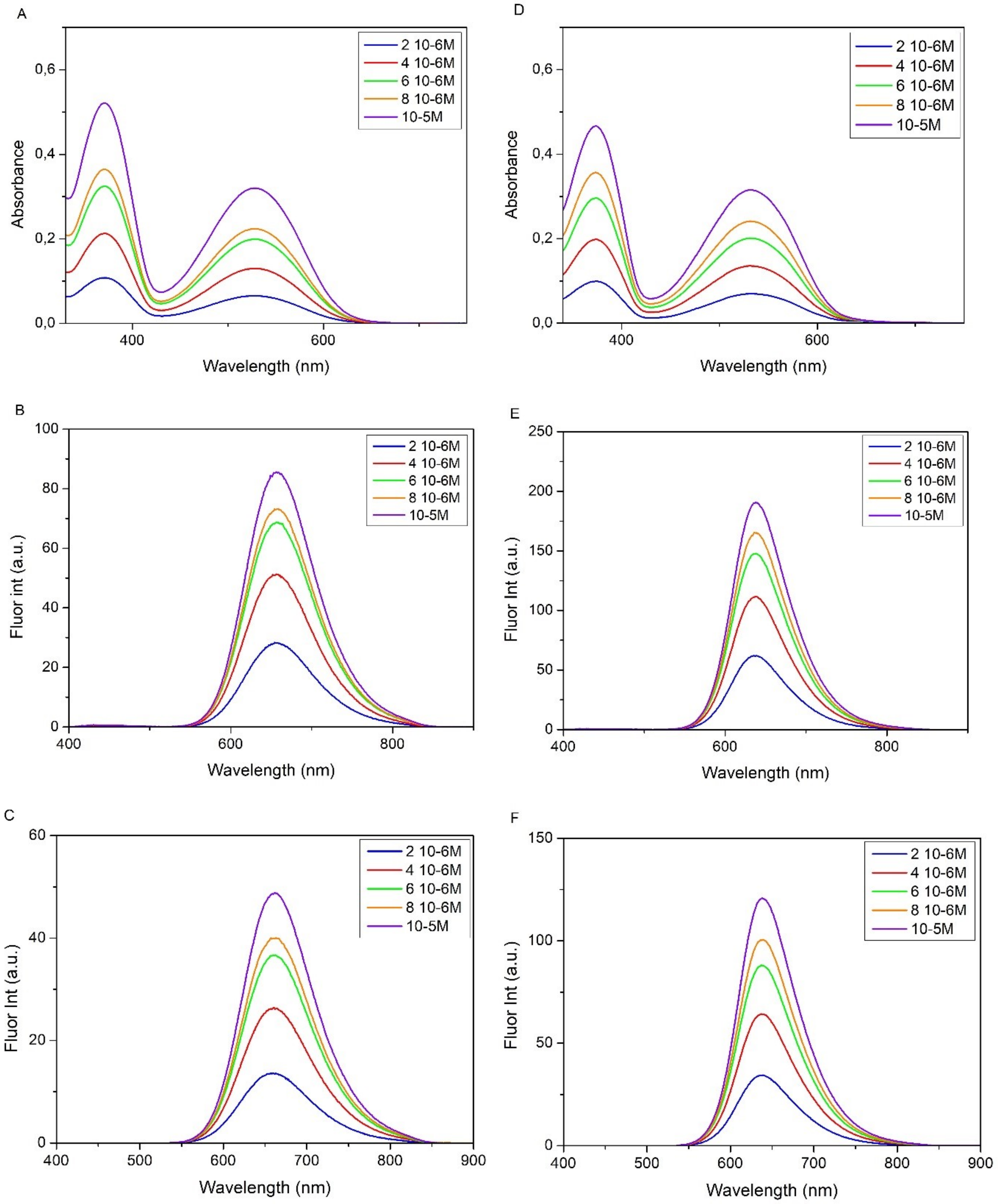

*Fig. 93: Absorption spectra in DCM (A) and toluene (D), and the corresponding emission spectra in DCM at 371 nm (B) and at 528 nm (C) excitations, and in toluene at 374 nm (E) and at 531 nm (F) excitation of **LSCA2** at different concentration.*

LSCA2 was excited at 371 and 528 nm in DCM solution, while toluene samples were excited at 374 and 531 nm. The emission spectra were characterized by one peaks centred to 662 and 638 nm, in DCM and toluene respectively. Likewise **LSCA1**, toluene solutions exhibited a blue-shift of 24 nm at different concentrations, with more intensive fluorescence emission.

Also in this case, large Stokes shift, around 100-130 nm, and limited overlap between absorption and emission spectra were observed. No bathochromic effects and no shoulders in emission spectra were

noticed; thus, like of **LSCA1**, **LSCA2** was not affected to self-absorption losses, fluorescence quenching and formation of emissive aggregates.
Moreover, fluorescence intensity was higher for toluene samples than DCM ones, with similar behavior of **LSCA1** solutions.

Thus, both **LSCA1** and **LSCA2** showed optical properties in solution compatible with the requirements for this peculiar LSC application.
LSCA1 manifested a slight bathochromic shift of absorption and emission spectra and higher absorption coefficient ε than **LSCA2**, due to a stronger ICT impact and the higher donating capacity of EDOT compared to PRODOT. Qualitatively, the stronger effect as donating group of EDOT compared to PRODOT was visible through the color change of their solutions, from light purple in the case of **LSCA2** to an intense violet for **LSCA1**.
The good solubility in solution, for both chromophores, suggested a simple procedure to disperse these chromophores in typical polymerization conditions, employed for LSC device production, and probably with a better dispersion in non-polar matrices.
Furthermore the limited self-absorption processes, might offer an important advantage on large-scale LSC applications.
Further investigation to measure fluorescence quantum yields and preparation of polymeric are needed to asses the possibility to use this kind of structures for the desired application.

5.4 EXPERIMENTAL PROCEDURE: CHAPTER 5

2-bromo-9,9-dibutyl-9H-fluorene

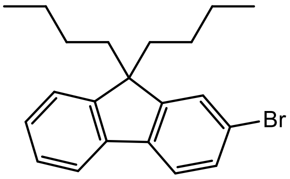

25

In a bottom flask, under nitrogen atmosphere, 2-bromofluorene **24** (300 mg, 1.22 mmol, 1.0 eq) was dissolved in anhydrous THF (10 mL) and cooled at 0°C, shielding from light. NaO^{t}Bu (360 mg, 3.67 mmol, 3.0 eq) was added to the mixture and reacted for 30 minutes at rt. After that, 1-iodobutane (417 µL, 3.67 mmol, 3.0 eq) was added to the solutions and the mixture stirred at rt for 20 h. Then NH_4Cl sat (10 mL) was added to the mixture and THF was removed under vacuum. The aqueous phase was extracted with EtOAc (10 mLx2) and the organic phase washed with water (15 mL) and brine (15 mL) and then dried on anhydrous Na_2SO_4. The organic solvents were removed under vacuum obtaining the final product **25** as a pale yellow oil with quantitative yield (436 mg, 1.20 mmol, >99%).

H^1NMR (200 MHz,$CDCl_3$): δ = 7.75-7.70 (m, 1H), 7.62 (d, J = 8.2 Hz, 1H), 7.51 (d, J = 7.1 Hz, 2H), 7.33 (s, 3H), 12.05-1.89 (m, 4H), 1.10-1.04 (m, 4H), 0.80-0.75 (t, J =7.8 Hz, 6H), 0.60-0.50 (m, 4H) ppm.

Spectroscopic data are in agreement with those reported in literature (*J. Mater. Chem. C*, 2015, 3, 3730-3744).

C-H direct arylation cross-coupling reaction $Pd(OAc)_2$ catalyzed:

4,7-bis(2,3-dihydrothieno[3,4-b][1,4]dioxin-5-yl)benzo[c][1,2,5]thiadiazole

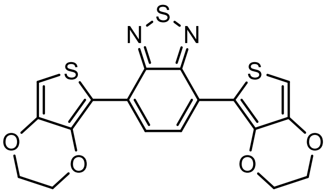

23

In a schlenk tube, under N_2 atmosphere, 4,7-dibromobenzo-1,2,5-thiadiazole, **21**, (40 mg, 0.14 mmol, 1.0 eq), EDOT, **22**, (722 µL, 0.68 mmol, 5.0 eq), $Pd(OAc)_2$ (2.5 mg, 0.012 mmol, 0.08 eq), PivOH (1.7 mg, 0.017 mmol, 0.12 eq) and K_2CO_3 (29.0 mg, 0,21 mmol, 1.5 eq) were added and solubilized in anhydrous *N,N*-DMF ([S]=0.14M). The mixture was stirred at 140°C for 3 h, then cooled at room temperature, filtrated on celite and washed with EtOAc (10mL). The organic phase was washed with water (5 mLx2) and brine (5 mLx1) and dried with anhydrous sodium sulfate. The solvet was removed under vacuum and the crude was purified by column chromatography (PE:DCM = 1:1), obtaining the product **3** as a bordeaux solid (40.8 mg, 0.1 mmol, 70%).

^{1}H NMR (400 MHz, $CDCl_3$): δ = 8.50 (s, 2H), 6.91 (s, 2H), 4.58-4.54 (m, 4H), 2.36-2.32 (m, 4H) ppm.

Spectroscopic data are in agreement with those reported in literature (*Dyes and Pigments*, 2018, 148, 167 – 179).

4,7-bis(7-(9,9-dibutyl-9H-fluoren-2-yl)-2,3-dihydrothieno[3,4-b][1,4]dioxin-5-yl)benzo[c][1,2,5]thiadiazole: LSCA1

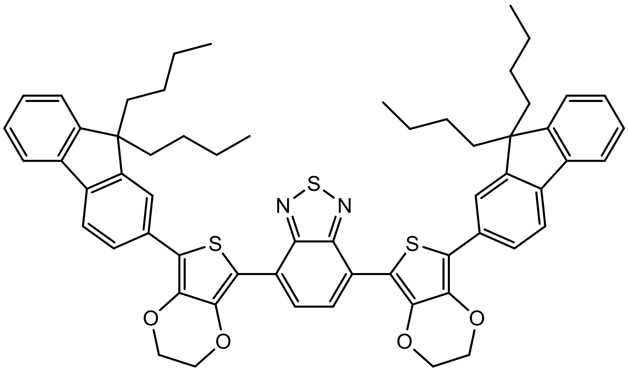

LSCA1

In a schlenk tube, under nitrogen atmosphere **23** (122.4 mg, 0.3 mmol, 1.0 eq), 2-bromo-9-dibutyl-fluorene **25** (231.0 mg, 0.61 mmol, 2.2 eq), $Pd(OAc)_2$ (3.3 mg, 0.015 mmol, 0.05 eq), Cataxium A (10.74 mg, 0,03 mmol, 0.1 eq), PivOH (0.9 mg, 0.09 mmol, 0.3 eq) and Cs_2CO_3 (146.7 mg, 0.45 mmol, 1.5 eq) were solubilized in anhydrous toluene ([S]=0.08M). The mixture was heated at 95°C for 18h, then cooled at room temperature, filtrated on celite and washed with EtOAc (30 mL). The organic phase was washed with water (10 mLx2) and brine (10 mL) and the collected organic phase was dried with anhydrous sodium sulfate. The solvent was removed under vacuum and the crude was purified by column chromatography (PE:DCM = 3:1), obtaining **LSCA1** as a violet solid (261.7 mg, 0.27 mmol, 90%).

^{1}H NMR (400 MHz, $CDCl_3$): δ = 8.53 (s, 2H), 7.91 (dd, J = 6.4, 1.6 Hz, 2H), 7.83 (s, 2H), 7.76-7.71 (m, 4H), 7.40-7.36 (m, 2H), 7.36-7.29 (m, 4H), 4.49 (dd, J = 14.3, 4.8 Hz, 8H), 2.05 (quint, J= 5.8 Hz, 8H), 1.15-1.06 (m, 8H), 0.69 (t, 7.6 Hz, 14 H), 0.65-0.56 (m, 6H) ppm.

^{13}C NMR (100 MHz, $CDCl_3$): δ = 152.3, 151.2, 150.9, 141.3, 140.8, 140.0, 138.3, 131.9, 127.0, 126.8, 126.4, 125.1, 123.3, 122.9, 120.4, 119.7, 119.5, 111.5, 65.0, 64.6, 55.1, 40.2, 26.1, 23.1, 13.7 ppm.

ESI-MS: m/z = 968.13 $[M\cdot]^+$.

4,7-bis(3,3-dipentyl-3,4-dihydro-2H-thieno[3,4-b][1,4]dioxepin-6-yl)benzo[c][1,2,5]thiadiazole

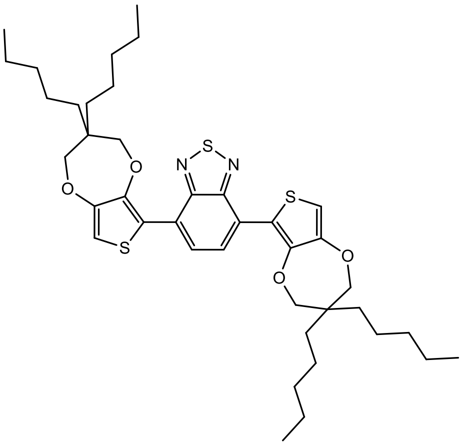

27

In a schlenk tube, under N_2 atmosphere, 4,7-dibromobenzo-1,2,5-thiadiazole, **21**, (40 mg, 0.14 mmol, 1.0 eq), PRODOT, **26**, (207.5 mg, 0.70 mmol, 5.0 eq), $Pd(OAc)_2$ (2.5 mg, 0.012 mmol, 0.08 eq), PivOH (1.7 mg, 0.017 mmol, 0.12 eq) and K_2CO_3 (29.0 mg, 0.21 mmol, 1.5 eq) were solubilized in anhydrous *N,N*-DMF ([S]=0.14M). The mixture was heated from 70°C to 100°C in 20'. The mixture was cooled at room temperature, filtrated on celite and washed with EtOAc (10mL). The organic phase was washed with H_2O (5 mLx2) and brine (5 mLx1). The collected organic phase was dried with anhydrous sodium sulfate and the organic solvent removed under vacuum. The crude was purified by column chromatography (PE:DCM = 3:1), obtaining compound **27** as an orange solid (48.7 mg, 0.07 mmol, 48%).

^1H NMR (200 MHz, $CDCl_3$): δ = 8.28 (s, 2H), 6.64 (s, 2H), 4.00 (d, J = 16.1 Hz, 8H), 1.51-1.39 (m, 8H), 0.91 (t, J = 6.4 Hz, 14H) ppm.

^{13}C NMR (50.3 MHz, $CDCl_3$): δ = 149.9, 147.9, 147.8, 127.6, 124.3, 117.4, 106.2, 43.78, 32.7, 32.0, 22.5, 14.0 ppm.

ESI-MS: m/z = 725.17 $[M+H]^+$.

4,7-bis(8-(9,9-dibutyl-9H-fluoren-2-yl)-3,3-dipentyl-3,4-dihydro-2H-thieno[3,4-b][1,4]dioxepin-6-yl)benzo[c][1,2,5]thiadiazole: LSCA2

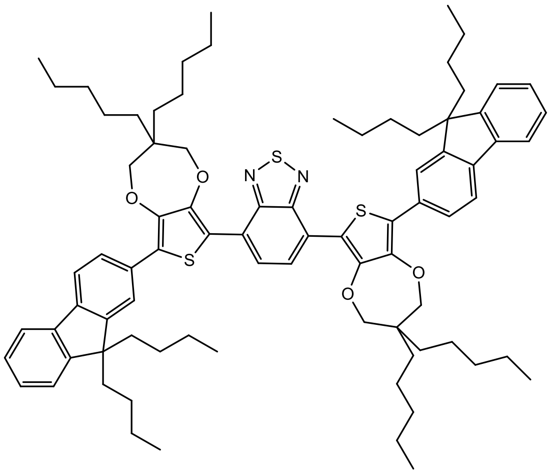

LSCA2

In a schlenk tube, under N_2 atmosphere, **27**, (40.0 mg, 0.14 mmol, 1.0 eq), **25**, (110.0 mg, 0.31 mmol, 2.2 eq), $Pd(OAc)_2$ (2.5 mg, 0.012 mmol, 0.08 eq), PivOH (1.7 mg, 0.017 mmol, 0.12 eq) and K_2CO_3 (29.0 mg, 0.21 mmol, 1.5 eq) were solubilized in anhydrous *N,N*-DMF ([S]=0.14M). The mixture was heated at 95°C for 14 h. Then the mixture was cooled at room temperature, filtrated on celite and washed with EtOAc (10mL). The organic phase was washed with H_2O (5 mLx2) and brine (5 mLx1). The collected organic phase was dried with anhydrous sodium sulfate and the solvent removed under vacuum. The crude was purified by column chromatography (PE:DCM = 3:1), obtaining **LSCA2** as a purple solid (44.7 mg, 0.04 mmol, 25%).

^{1}H NMR (400 MHz, $CDCl_3$): δ = 8.51 (s, 2H), 7.87 (dd, J = 7.8, 2.0 Hz, 2H), 7.83 (s, 2H), 7.78-7.73 (m, 4H), 7.42-7.38 (m, 2H), 7.37-7.31 (m, 4H), 4.17 (d, J = 18.2 Hz, 8H), 2.10-2.00 (m, 8H), 1.60-1.52 (m, 8H), 1.18-1.10 (m, 8H), 1.00-0.93 (m, 12H), 0.77-.65 (m, 19H) ppm.

^{13}C NMR (100.0 MHz, $CDCl_3$): δ = 152.6, 151.0, 149.0, 146.1, 140.7, 140.2, 132.0, 127.2, 126.8, 125.6, 123.8, 123.5, 122.9, 121.1, 119.7, 119.6, 114.8, 77.5, 55.0, 43.7, 40.1, 32.7, 32.0, 26.1, 23.1, 22.7, 22.6, 13.9, 13.7 ppm.

ESI-MS: m/z = 1276.41 $[M\cdot]^+$.

CHAPTER 6

SOME APPLICATIONS OF DEEP EUTECTIC SOLVENTS IN COUPLING REACTIONS

6 GREEN CHEMISTRY

The major part of organic reactions takes place in a liquid medium. The solvent plays a crucial role in the organic synthesis: disperses and dissolves reactants, increases the impacts through reagents, homogenizes solution, controls mass and temperature, influences selective on products and makes work-up and purification easier.
The common volatiles organic solvents (VOCs) are the most used media in organic synthesis due to their compatible properties with the typical organic reactants ("like dissolves like"). However, VOCs show many intrinsic drawbacks, such as low boiling point, flammability, high toxicity and low biodegradability, increasing their high environmental impact[223].
The solvent is a common medium that generally at room temperature and atmospheric pressure should be liquid to well-dissolve all reaction components. Moreover, the solvent should be tunable in presence of co-solvent, available at commercial quantities, inexpensive and inert in the reaction conditions used.
Recently, bio renewability, recycling and safety became other important features. Today's society is looking for new technologies for environmentally sustainable development. The concept of sustainability is at the base of modern chemistry and it is supported by the concept of "Green Chemistry" that is "the design of chemical products and processes to reduce or eliminate the use and the generation of hazardous substances"[224]. The "design" of the Green Chemistry is based on 12 principals, which can be condensed in the word PRODUCTIVELY[225] (Fig. 94).

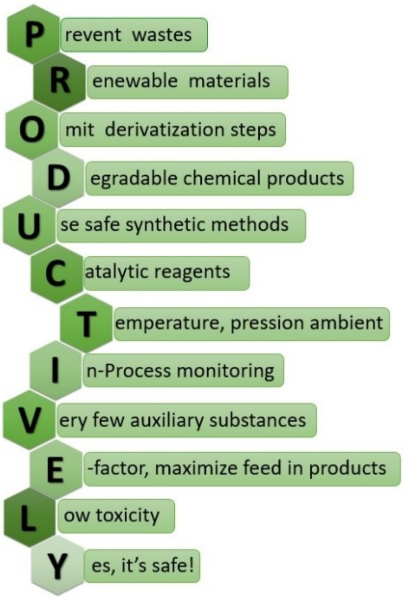

***Fig. 94:** 12 principles of Green Chemistry.*

---

[223] D.A. Alonso, A. Baeza, R. Chinchilla, G. Guillena, I.M. Pastor, D.J. Ramón, *Eur. J. Org. Chem*. **2016**, 612–632.

[224] a) *Green Chemistry: Theory and Practice*; Oxford University Press: New York, **1998**; b) Green Chemistry and Catalysis; Wiley-VHC: Weinheim, 2007; c) P. Anastas, N. Eghbali, *Chem. Soc. Rev*. **2010**, *39*, 301-312; d) R.A. Sheldon, *Chem. Soc. Rev*. **2012**, *41*, 1437-51.

[225] S.Y. Tang, R.A. Bourne, R.L. Smith, M. Poliakoff, *Green. Chem*., **2008**, *10*, 268-269.

From Green Chemistry definition, the comparison among different processes is based on the evaluation of their greenness. There is no ideal greenest process; there are processes greener than others. Therefore, appropriate green parameters are necessary for a meaningful comparison. The two principal metrics are *E-factor* and *Atom Economy* (or *Atom Efficiency*, AE).
E-factor is defined as the mass ratio of waste produced to obtain the desired product[226]; while AE is the molecular weight of product divided into the sum of the molecular weight of all substances involved in processes, in exactly stoichiometric amounts[227].
E-factor, or Environmental Impact Factor, was for the first time by Roger Sheldon in 1992[228]. This metric quantifies the amount of waste, produced during a process, generated per kilogram of product. It takes into consideration all the raw materials and wastes of a process, and is a reply to the first principle of Green Chemistry. The prevention of waste is the primary pollution control. Any material and energy unutilized or not realized are wastes. High *E-factor* means a large amount of wastes and a higher environmental impact. The ideal *E-factor* is zero. The design of new processes with low *E-factor* needs to eliminate or minimize raw materials. In the case of by-product, which cannot be avoided, an innovative eco-friendly approach provides that waste will become an alternative material with higher value, involved again in life-cycle.
If *E-factor* measures the economic and environmental impact of processes, Atom Economy defines theoretically their efficiencies.
The concept of Atom Economy was introduced in 1990 by Barry Trost, referring to the possibility of maximizing the use of raw materials and to involve them in the final product. High AE means that the product contains a higher number of atoms from reactants. The ideal AE is 100%: in this case, all atoms of reagents are involved in the formation of products. Reactions with high AE use catalytic amount of metal reactants and favours one-pot or multi-component reactions.
Clearly Solvents play a significant role to affect these parameters and plan a “green” process.
In the last part of this work we focalized our attention in the use of greener solvent in catalytic reaction especially those processes which might be of interest for synthesis of materials for optoelectronic application.
This study has been carried out in collaboration with the research group of D.J. Ramón Dangla, from the Institute of Organic Synthesis (ISO) of the University of Alicante.
Different solvents have been used to replace common organic solvent: ionic liquid[229],

---

[226] a) P. Anastas, N. Eghbali, *Chem. Soc. Rev.* **2010**, *39*, 301-312; b) D. Prat *et al.*, *Green Chem.*, **2015,** *18*, 288-296; c) R.A. Sheldon, *Chem. Soc. Rev.* **2012**, *41*, 1437-51.

[227] B.M. Trost, *Angew. Chem., Int. Ed. Engl.*, **1995**, *34*, 259-281

[228] R.A. Sheldon, *Green Chem.*, **2007**, *9*, 1273-83.

[229] a) P. Wasserscheid, T. Welton, *Ionic liquids in Synthesis*: *Second Edition,* **2008**; b) P. Wasserscheid, W. Keim, *Angew. Chem. Int. Ed.* **2000**, *39*, 3772–89; c) J.P. Hallett, T. Welton, *Chem. Rev.* **2011**, *111*, 3508–76; e) T. Welton, *Green Chem.* **2011**, *13*, 225; f) M.A.P. Martins, C.P. Frizzo, A.Z. Tier, D.N. Moreira, N. Zanatta, H.G. Bonacorso, *Chem. Rev.* **2014**, *114*, PR1–PR70; g) Organic synthesis using an ionic liquid as reaction media, in: *Environmentally Friendly Synthesis Using Ionic Liquids*, Eds.: J. Dupont, T. Itoh, P. Lozano, S. V. Mahotra, CRC Press, Boca Raton, **2014**, p. 9–30 and p.109-138; h) E. García-Verdugo, B. Altava, M.I. Burguete, P. Lozano, S.V. Luis, *Green Chem.* **2015**, *17*, 2693–2713.

supercritical fluids[230], fluorurate compounds[231], water[232] and deep eutectic solvent (DES)[233] are the principals. In the following chapter, our results in using eutectic solvent for C-H activation processes and Suzuki reaction will be reported.

6.1 GREEN SOLVENTS IN ORGANIC SYNTHESIS

6.1.1 Deep eutectic solvents (DESs)

Deep eutectic solvents (DESs) are two or more phase-immiscible solid component mixtures, with a low melting point, in comparison with the single melting points of its pure components[234]. Their melting point is lower than 100°C and called “eutectic point”, as showed in figure 95.

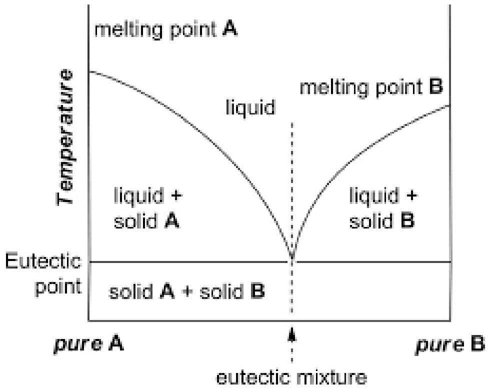

Fig. 95: *Phase diagram of a general deep eutectic solvent, with the corresponding eutectic point*[235].

DESs show large ionic conductivity and immiscibility with solvents incapable of donating hydrogen bond, forming immiscible biphasic liquid. These solvents exhibit a wide range of polarity to the dissolution of many organic and inorganic reactants and catalysts. Moreover, simple and easy work-up conditions, low price and easy preparation for industrial applications are significant advantages. Furthermore, DESs show low toxicity and high biodegradability. Their atom economy is higher than that of other green solvents.

However, low manageable viscosity and their high density limit their applications and make DESs unsuitable for scale-up industrial processes and continuous-flow applications[13].

DES are normally composed by a mixture of hydrogen bond acceptor (HBA), commonly quaternary ammonium salts such as choline chloride, and by hydrogen bond donor (HBD), such as alcohols, amides and carboxylic acids[13] (Fig. 96).

---

[230] a) J.R. Hyde, P. Licence, D. Carter, M. Poliakoff, *Appl. Catal., A*, **2001**, *222*, 119-131; b) N. Budisa, D. Schulze-Makuch, *Life*, **2014**, *4,* 331-340.

[231] a) T. Kitazume, *Journal of Fluorine Chemistry*, **2000**, *105*(2), 265-278; b) S.J. Tavener, J.H. Clark, *Journal of Fluorine Chemistry*, **2003**, *123*, 31–36; c) J. Iskra, S.S. Murphree, *Tetrahedron Letters*, **2017**, *58*, 645–648.

[232] a) U.M. Lindström, *Chem. Rev.*, **2002**, *102*, 2751-72; b) C.J. Li, *Chem. Rev.* **2005**, *105*, 3095–3165.

[233] a) A.P. Abbott, G. Capper, D.L. Davies, R.K. Rasheed, V. Tambyrajah, *Chem. Commun.*, **2003**, 70-71; b) D.A. Alonso, A. Baeza, R. Chinchilla, G. Guillena, I.M. Pastor, D.J. Ramón, *Eur. J. Org. Chem.* **2016**, 612–632.

[234] A.P. Abbott, G. Capper, D.L. Davies, R.K. Rasheed, V. Tambyrajah, *Chem. Commun.*, **2003**, 70-71.

[235] D.A. Alonso, A. Baeza, R. Chinchilla, G. Guillena, I.M. Pastor, D.J. Ramón, *Eur. J. Org. Chem.* **2016**, 612–632.

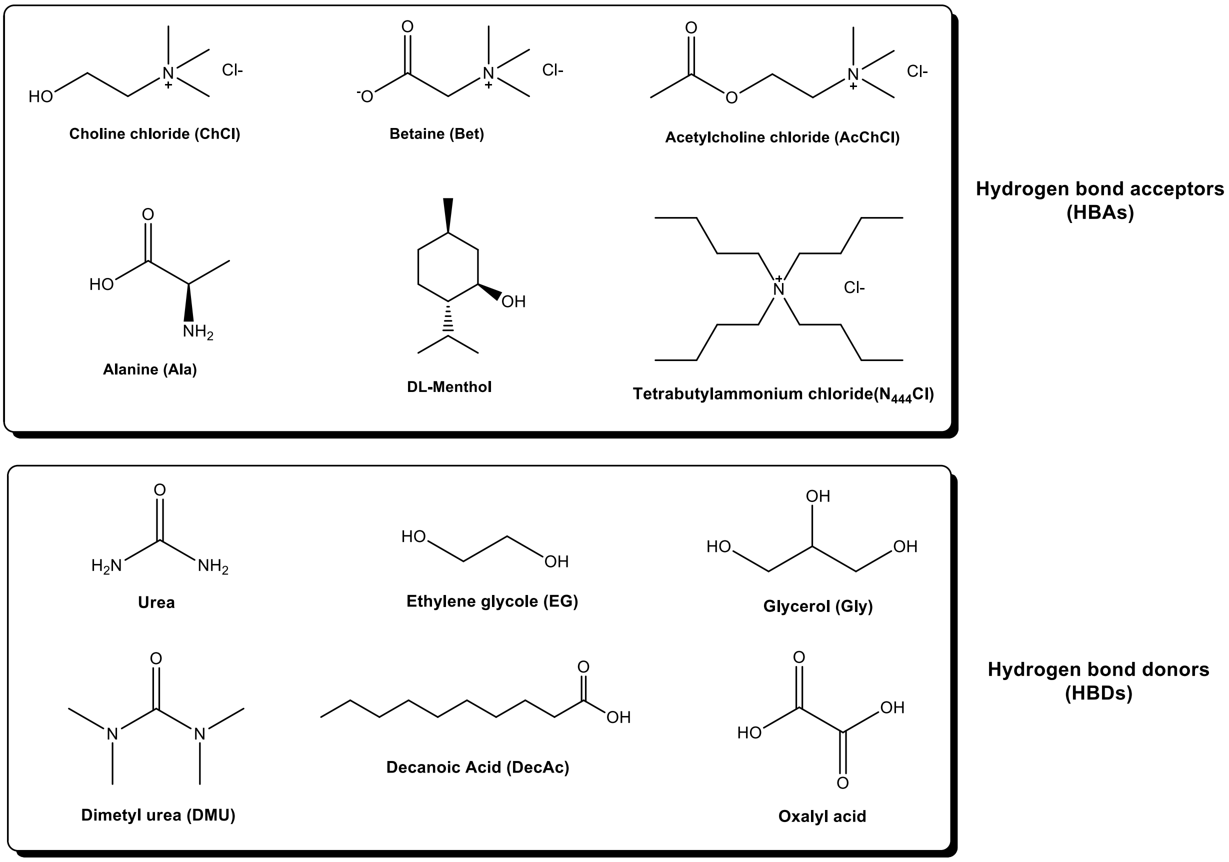

Fig. 96: *Structures of common Hydrogen Bond Acceptor (HBAs) and Donors (HBDs), employed in deep eutectic solvents.*

The mixture is characterized by a specific temperature where the immiscible components give rise to a change of phase. They show peculiar characteristics, such as lower melting point than the single components and at a specific molar ratio of HBD and HBA, the decrease of electrostatic forces of the ionic network and consequently low freezing point. This phenomenon occurs especially when small molecules interact with the larger molecule of the other components, disrupting the crystalline ionic pattern (Fig. 97). For these reasons, the DES mixtures are liquid close to the room temperature.

The composition is usually established by Lewis or Brønsted acid (HBD) and base (HBA), ionic and non-ionic species.

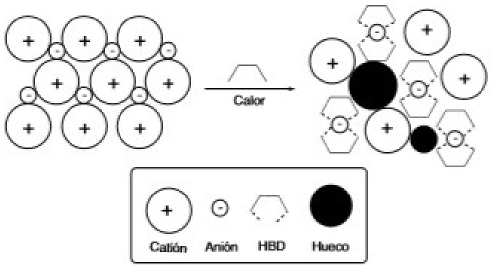

Fig. 97: *Ionic general interactions of deep eutectic solvent components*[236].

The most used DESs are based on choline chloride (ChCl), a bifunctional organic compound composed by a quaternary ammonium salt and an alcohol. Described for the first time by Abbott and co-workers[237], ChCl is typically used as an additive in feedstocks for chickens: it is safe, cheap, biocompatible, non-toxic and high biodegradable. Its principal drawback is high hygroscopicity, showing water contents in its DES compositions. However, its chemical inactivity with water did not limit its application as a component of deep eutectic solvent. Indeed, water could participate as a mixture component and give peculiar properties to DES[238]. However, ChCl could be easily recrystallized by ethanol if we want to remove water from it.

On the other hand, common HBD are alcohols, amines, amides, natural carboxylic acids and polyalcohol.

The preparation of DES requires heating all the components of the mixture in a range between 80°-100°C, under a vigorous stirring, in a determinate molar ratio, till a homogenous transparent liquid is obtained. The molar ratio influences physical and chemical features of green solvent, with a distinctive eutectic point. This typical temperature is recorded by differential scanner calorimetry (DSC) analysis. Selecting a specific range of temperature, near the melting point of the mixture, the thermogram shows an endothermic peak, which indicates the melting point and the corresponding enthalpy. During the cooling of the molten mixture, an exothermic peak is registered, which corresponds to freezing point[239]. Different molar ratio corresponds to different DSC trend and specific melting/freezing point. Some DES compositions could show two or more eutectic points, in which the mixture could behave differently. The most common DES is called Reline, a mixture of choline chloride and urea in a molar ratio 1:2. Its melting point is 12°C with a biodegradability of about 97%[240]. Other typical choline chloride-based DESs are shown in table 22.

---

[236] D. Alonso *et al.*, *An. Quím.* **2018**, *114* (2), 79-87.

[237] A.P. Abbott, G. Capper, D.L. Davies, R.K. Rasheed, V. Tambyrajah, *Chem. Commun*., **2003**, 70-71.

[238] a) X. Meng, K. Ballerat-Busserolles, P. Husson, J.M. Andanson, ***New J. Chem***., **2016**, ***40***, 4492-99; b) O.S. Hammond, D.T. Bowron, K.J. Edler, *Angew. Chem*. **2017**, *129*, 9914 –17.

[239] H.G. Morrison, C.C. Sun, S. Neervannan, *Int. J. Pharm.*, **2009**, *378*, 136–139.

[240] B.Y. Zhao, P. Xu, F.X. Yang, H. Wu, M.H. Zong, W.Y. Lou, *ACS Sustainable Chem. Eng*. **2015**, *3*, 2746–55.

***Table 22:** Some common deep eutectic solvents Choline chloride-based, with their corresponding chemical and physic characteristics.*

DES	***Molar ratio***	***T(°C)***	***Density (g cm^{-3})***	***Viscosity (cP)***	***Conducibility (mS cm^{-1})***	***Biodegradability***	***T$_{prep}$ (°C)***
ChCl:Urea	1:2	12	1.25	750	0.199 (40°C)	97.1	75
ChCl:Gly	1:2	-40	1.18	376 (20°C)	1.05 (20°C)	95.9	100
ChCl:MA	1:2	10	1.25	1124	0.36	76.3	100
ChCL:TA	1:2	47	1.27 (30°C)	66441 (30°C)	0.014 (30°C)	84.6	100
ChCL:CA	1:2	69	1.33 (30°C)	289	0.018 (30°C)	81.6	100
ChCL:Glucose	1:2	14	1.21 (85°C)	8045.1	-	82.0	80

For their chemical characteristics, deep eutectic solvents were divided into three classes, based on their compositions and synthetic applications:

- Hydrophilic: deep eutectic solvents composed by hydrophilic components, such as choline chloride, betaine, (carbamoylmethyl)trimethyl ammonium chloride, as HBAs, and urea, DMU, glycol, ethylene glycol, as HBDs. In this group, natural deep eutectic solvents (NADESs) are embedded, which present one component from natural origin at least, such as D-glucose, D-fructose or amino acid, such as glycine, L-proline, L-arginine;
- Neutral lipophilic: deep eutectic solvents which show non-ionic lipophilic components, usually characterized by an alcohol, as HBD, and a long alkyl chain carboxylic acid, as HBA;
- Ionic lipophilic: deep eutectic solvents in which at least one component is ionic and both of them are lipophilic, such as carboxylic acid with a long alkyl chain, as HBD, and quaternary ammonium salt with alkyl chains, as HBA.

6.1.2 DES in organic reactions: state of art

The singularity of DESs is the possibility to use them as an active or innocent component in an organic reaction.

Active DESs are mixtures, which participate in the reaction and they can be employed as reagent or catalyst. The single components have intrinsic reactivity; therefore, DES could participate as starting material (Fig. 98) or as a component in the catalytic cycle (Fig. 99). At the same time, DES could work as the reaction medium.

Urea-based DES was employed in the production of diurea derivatives, in the presence of aldehydes[241].

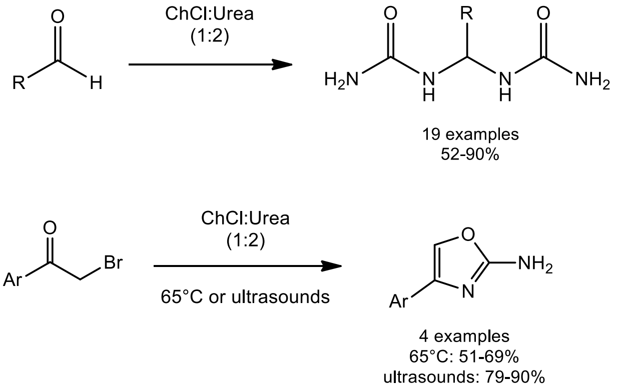

Fig. 98: *Employment of urea in organic reactions as an active component of DES.*

Urea found interesting application in the cyclization of heterocyclic compounds[242]; the same application was found for DMU as a precursor for the synthesis of many heterocyclic derivatives, in presence of the corresponding aldehydes and/or ketones[243].

Carbohydrates are one of the principal components of NADESs; on the other hand, sugars are important building blocks for the production of expensive industrial chemicals. Therefore, 5-(hydroxymethyl)furfural (HMF) is a potentially more sustainable building block than petroleum-based one. In a recent study, HMF could be prepared starting from carbohydrate/ChCl deep eutectic solvent (in a ratio from 2:3 to 1:1) in presence of an acidic catalyst, such as $CrCl_2$ or *p*-toluenesulfonic acid (*p*-TsOH)[244]. Another recent work showed catalytic activity of a tungostophosphoric acid ($H_3PW_{12}O_{40}$) in presence of lysine, which improved the production of HMF with a conversion of 93% in 1 min, starting from NADES fructose based[245].

Moreover, deep eutectic solvents were involved in reactions to participate as a catalytic specie, such as in redox reactions. In these cases, the catalyst was immobilized in DES, which participated as coordinating specie of oxidant catalyst and, at the same time, as the solvent[246].

---

[241] N. Azizi, M. Alipour, *J. Mol. Liq.* **2015**, *206,* 268–271.

[242] B.S. Singh, H.R. Lobo, D.V. Pinjari, K.J. Jarag, A.B. Pandit, G.S. Shankarling, *Ultrason. Sonochem.* **2013**, *20*, 633–639.

[243] S. Gore, S. Baskaran, B. Koenig, *Green Chem.* **2011**, *13*, 1009–13.

[244] F. Ilgen, D. Ott, D. Kralisch, C. Reil, A. Palmberger, B. König, *Green Chem.* **2009**, *11*, 1948–54.

[245] Q. Zhao, Z. Sun, S. Wang, G. Huang, X. Wang, Z. Jiang, *RSC Adv.* **2014**, *4*, 63055–61.

[246] Y. Zhang, F. Lü, X. Cao, J. Zhao, *RSC Adv.* **2014**, *4*, 40161–69.

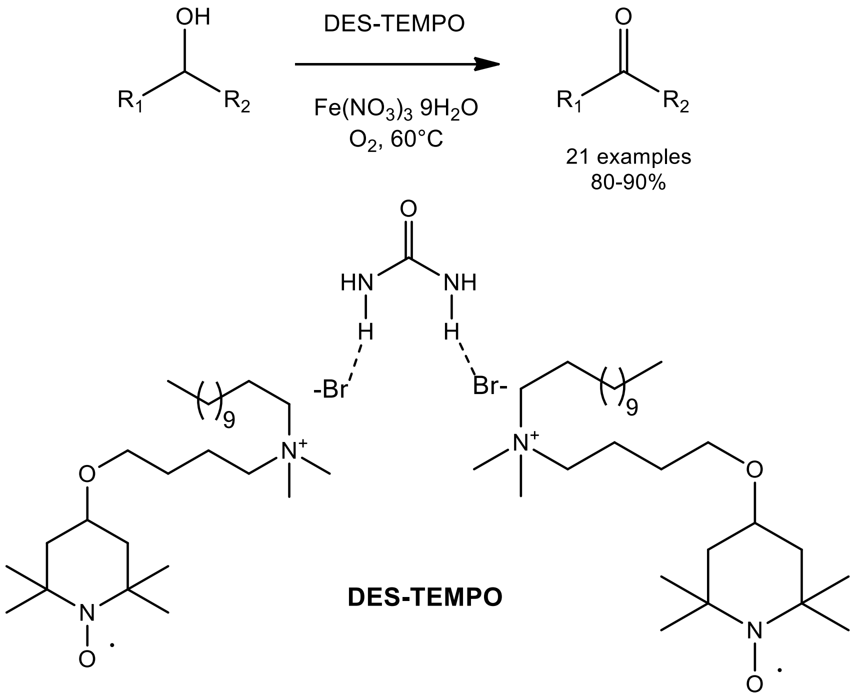

Fig. 99: DES employed as catalytic specie in redox reactions.

One of the most interesting use of DESs was in cross-coupling reactions. In the last years, Suzuki-Miyaura, Stille, Heck and Sonogashira reactions were investigated in presence of DESs[247] (Scheme 12).

The first pioneer of cross-coupling reactions in DES were König and co-workers, in 2006[248]. A three components mixture of D-mannithol-DMU-NH_4Cl was designed to be employed in two metalorganic reactions, Rh-catalyzed hydrogenation and Pd-catalyzed Suzuki-Miyaura cross-coupling reaction for the synthesis of biaryls. While hydrogenation resulted highly sensitive to deep eutectic solvent, Suzuki-Miyaura reactions proceeded cleanly, rapidly and quantitatively in all reaction test.

Furthermore, they applied the liquid mixture sugar-urea as a solvent for Stille, Sonogashira and Heck reactions[249]. In Stille reaction, in particular, faster and more efficient Pd-catalyzed reactions were promoted by high polarity and nucleophilic character of green solvent. Very low catalyst loading (around 0.001 mol%) remained active after several reaction cycles[250].

---

[247] a) B. Saavedra, N. González-Gallardo, A. Meli, D.J. Ramón, *Adv. Synth. Catal.* **2019**, *361*; b) S.E. Hooshmand, R. Afshari, D.J. Ramón, R.S. Varma, *Green Chem.*, **2020**, *22*, 3668-92.

[248] Green Chem. 2006, 8, 1051–1055.

[249] G. Imperato, S. Höger, D. Lenoir, B. König, *Green Chem.* **2006**, *8*, 1051–55.

[250] G. Imperato, R. Vasold, B. König, *Adv. Synth. Catal.* **2006**, *348*, 2243–47.

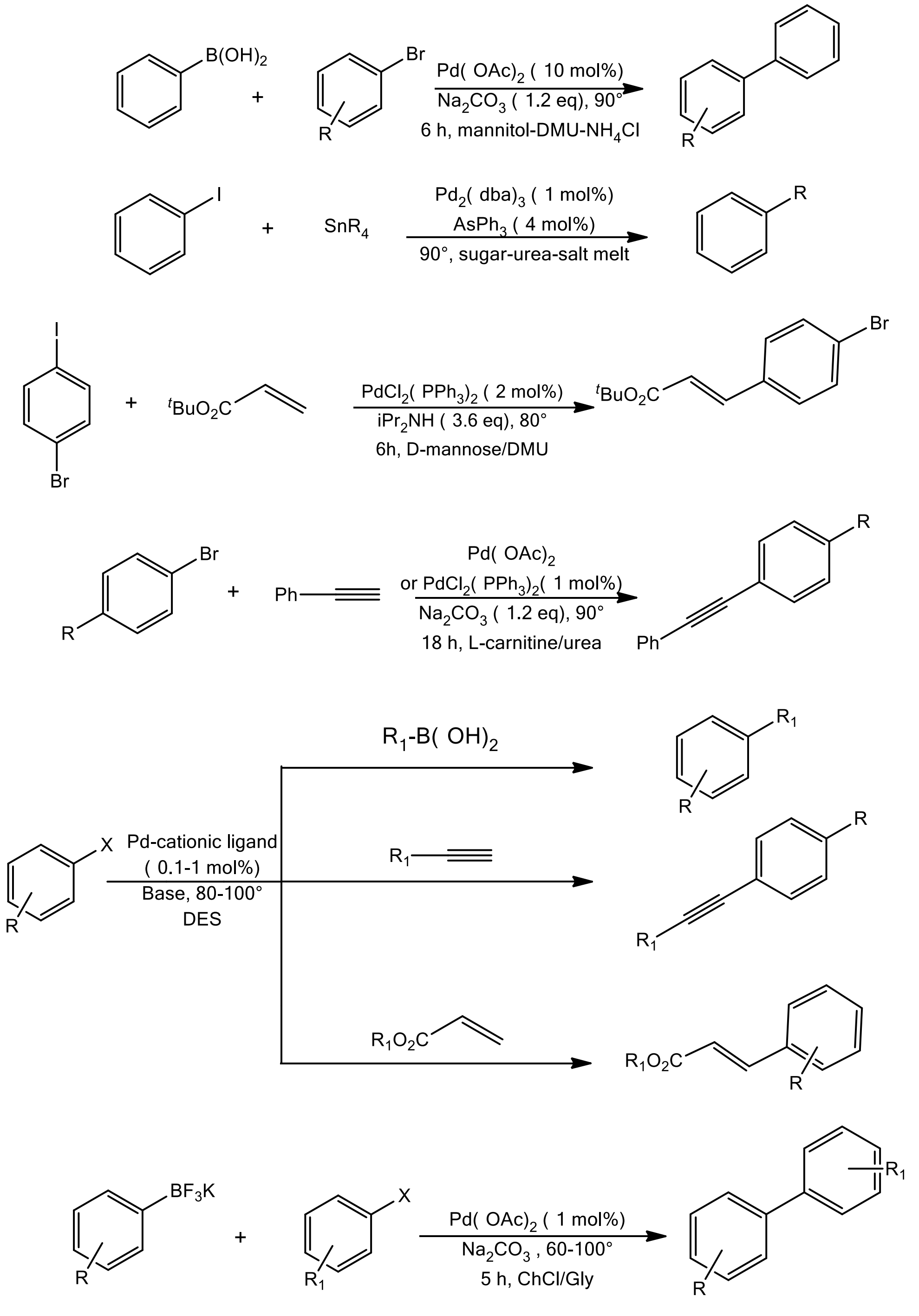

***Scheme 12:** Recent cross coupling reactions in deep eutectic solvents, reported by D.J. Ramón Dangla research group, from Institute of Organic Synthesis (ISO) of University of Alicante.*

Ramón Dangla and co-workers reported Pd-catalyzed cross-coupling examples[251] using cationic pyridiniophosphine ligands **2a-c**, developed to increase the compatibility of the catalyst with typical DESs. This catalytic system was employed in Suzuki-Miyaura, Heck and Sonogashira reactions, in combination with low loaded $PdCl_2$ (Scheme 13).

---

[251] X. Marset, A. Khoshnood, L. Sotorríos, E. Gómez-Bengoa, D.A. Alonso, D.J. Ramón, *ChemCatChem*. **2017,** *9*, 1269–75.

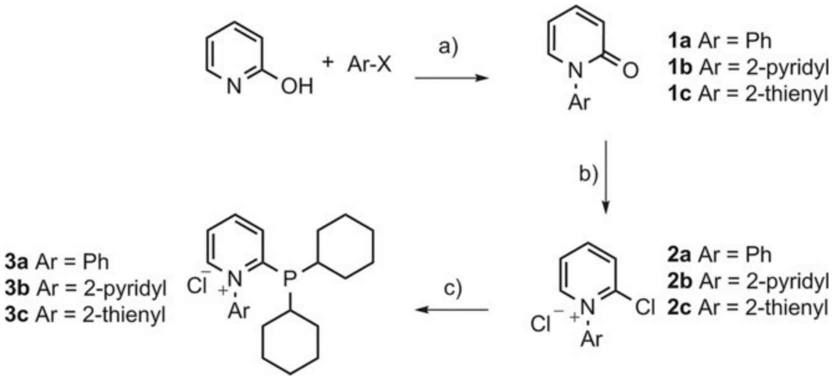

Scheme 13: *Synthetic procedure of cationic pirydiniophosphine ligand: a) CuI (10 mol %), K_2CO_3 (2.1 eq.), DMSO; b) oxalyl chloride (2 eq.), 1,2-dichloroethane, 60 °C; c) $HPCy_2$ (2 equiv), MeCN (dry) reflux.*

While in typical VOCs Pd-catalyzed reactions failed, in DES mixtures this cationic phosphine **3a** improved catalytic activity, with high recyclability, more than its derivatives **3b** and **3c**.

Recently, Capriati et al. developed a new synthetic strategy for Suzuki-Miyaura cross coupling reactions in DES, employing mono or bifunctional aryltrifluoroborates[252]. In this case, the nucleophilic partner was the functional group of trifluoroborate, which favoured oxidative addition in ChCl:Gly solvent, in presence of $Pd(OAc)_2$ and absence of ligands.

In 2019, Ramón Dangla et al. designed a novel and versatile amino –pyridine complex, **4a,** as Pd pre-catalyst (Scheme 14).

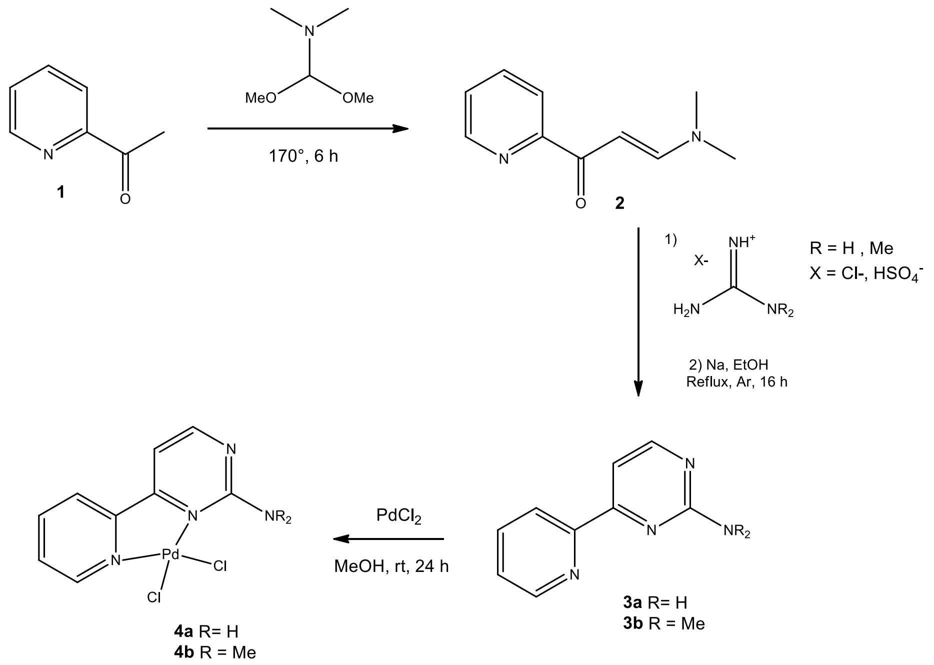

Scheme 14: *Bipyridine-palladium catalyst preparation.*

---

[252] G. Dilauro, S.M. García, D. Tagarelli, P. Vitale, F.M. Perna, V. Capriati, *ChemSusChem* **2018**, *11*, 3495–3501.

Pd-precatalyst **4a** was largely employed in several common cross-coupling reactions (Fig. 100) showing catalytic activity in when reactions were performed in DES, under air conditions, with a catalyst recycling up to 3-5 times[253].

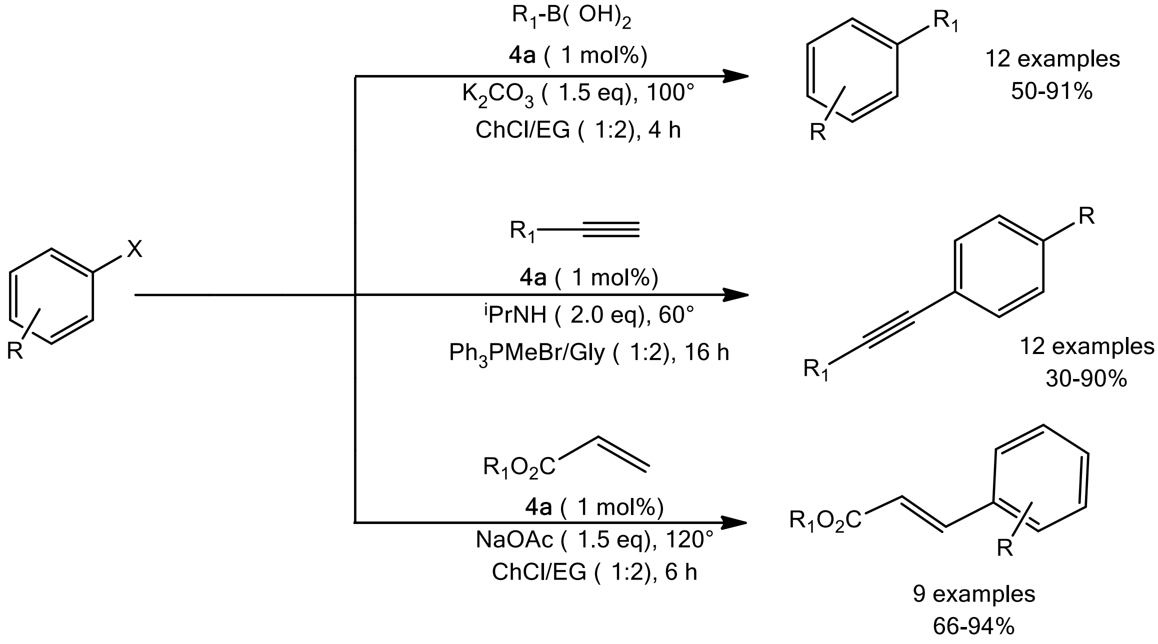

Fig. 100: *Some cross-coupling reactions where **4a** was employed as Pd-catalyst.*

6.2 MIYAURA REACTION IN DES

Suzuki-Miyaura cross-coupling is known and efficient reaction, widely employed for the formation of C-C bond. Generally, aryl halydes are reacted with a boronated intermediate, through Pd-catalyzed reaction. Suzuki-Miyaura cross-coupling is largely applied for C-C *sp*^{2} bond formation, due to its efficient and easy reaction conditions.

Accordingly, arylboronates are very versatile building blocks, so methods for their synthesis are highly demanded.

One of the most used method to prepare arylboronates is the Miyaura borylation reaction which allows preparing boronates starting from aryl or vinyl halides and bis(pinacolate)diboron, through a palladium catalyzed cross coupling reaction. In common organic solvents, such as toluene or *N,N*-DMF, Miyaura reaction of aryl arene evolves in presence of Pd(dppf)Cl_2 and of KOAc as catalyst and base respectively, following catalytic the cycle shown in figure 101.

---

[253] B. Saavedra, N. González-Gallardo, A. Meli, D.J. Ramón, *Adv. Synth. Catal.* **2019**, *361*.

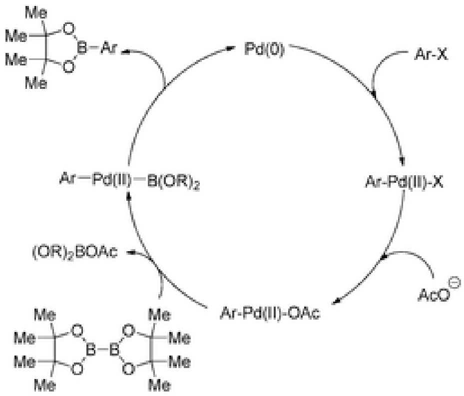

Fig. 101: *Catalytic cycle of generic borylation reaction on haloarene, in presence of bis(pinacolato)diboron as boron source*[254].

Depending on halide substrate, reaction conditions could change, but normally Very mild conditions can be used.

During our studies in the synthesis of fluorophores for LSC application, borilate intermediates had played a crucial role. The major part of final products, designed and synthesized, were obtained through Suzuki-Miyaura cross-coupling reactions using an aryl boronate as reaction partner.

Looking for alternative synthetic methods of their preparation, the development of DES approach captured our attention to study the Miyaura borylation reaction, starting from haloarenes compounds.

To perform Miyaura borylation in DES, our investigations started from the commercially available bromobenzene. Aryl bromide are commonly employed as starting materials due to their low costs, commercial availability and high reactivity with organometallic catalysis.

Tthe common synthetic approach employed in borylation reaction ias based on $Pd(dppf)Cl_2$ catalysis, in presence of KOAc as base using toluene, DMSO or DMF as solvents.

Pd catalyst was also used with alternative medium like PEG-600, for coupling reaction of aryl halide in presence of *bis*(pinacolato)diboron. $Pd(PPh_3)_2Cl_2$ exhibited a good conversion of bromobenzene in its corresponding boronate, in presence of NaOAc and very low catalyst loading[255] (Scheme 15).

Starting from these results, we decided to test the same reaction conditions using a DES, ChCl:Urea (1:2). Initially we investigated the effect of using different amount of bromobenzene (Table 23).

---

[254] W.K. Chow *et al.*, ***RSC Adv.***, **2013**, ***3***, 12518-39.

[255] J. Lu, Z.Z. Guan, J.W. Gao, Z.H. Zhang, *Appl. Organometal. Chem.* **2011**, *25*, 537–541.

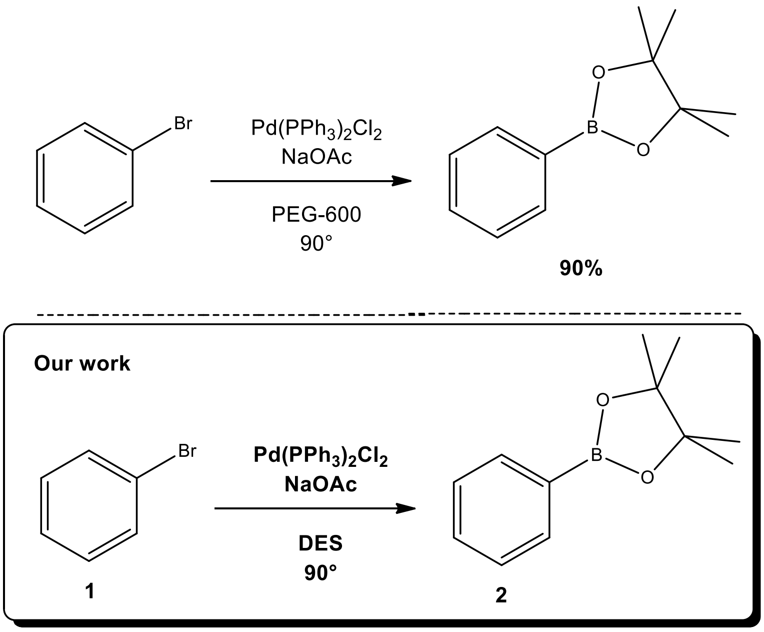

Scheme 15: *Pd-catalized Miyaura reaction in PEG-600 and our first synthetic approach, employed in DES.*

Table 23: *Pd-catalized Miyaura borylation of bromobenzene in ChCl:Urea (1:2), working in different amount of bromobenzene.*

Entry[a]	PhBr (eq)	B_2pin_2 (eq)	[Pd] (mol%)	Base (eq)	DES	Yield of 2 (%)[b]
1	1.0	1.4	$Pd(PPh_3)_2Cl_2$ (5)	NaOAc (4.0)	ChCl:Urea (1:2)	12/-/8[c]
2	3.0	1.0	$Pd(PPh_3)_2Cl_2$ (3.5)	NaOAc (2.85)	ChCl:Urea (1:2)	30/-/50[c]
3	5.0	1.0	$Pd(PPh_3)_2Cl_2$ (3.5)	NaOAc (2.85)	ChCl:Urea (1:2)	30/-/69
4	7.0	1.0	$Pd(PPh_3)_2Cl_2$ (3.5)	NaOAc (2.85)	ChCl:Urea (1:2)	22/-/76

[a] Reaction conditions: in 1 mL of DES, at 90°C for 20 hours.

[b] GC yield measured with GC-MS, relative to product (PhBpin), homocoupling (Ph-Ph), starting material (PhBr), respectively.

[c] amount of B_2pin_2.

The result obtained are reported in table 23. Importantly at the end of the reaction, we observed a low amount of product **2** and starting material **1**, while the main compound founded was B_2pin_2. This fact suggested that the oxidative addition was indeed favoured, while the transmetallation and the consequent reductive elimination were slow and not easily promoted. Working with an excess of bromobenzene a low increase of boronate was observed.

Moving on more polar deep eutectic solvent, such as ChCl:Gly (1:2) and ChCl:EG (1:2), comparable reaction trend with ChCl:Urea (1:2) was observed as reported in table 24).

Table 24: *Pd-catalyzed Miyaura borylation of bromobenezene in ChCl:Urea (1:2), working with large excess of bromobenzene.*

Entry[a]	PhBr (eq)	B_2pin_2 (eq)	[Pd] (mol%)	Base (eq)	DES	Yield (%)[b]
1	7.0	1.0	$Pd(PPh_3)_2Cl_2$ (3.5)	NaOAc (2.85)	ChCl:Urea (1:2)	30/-/69
2	7.0	1.0	$Pd(PPh_3)_2Cl_2$ (3.5)	NaOAc (2.85)	ChCl:EG (1:2)	18/8/74
3	7.0	1.0	$Pd(PPh_3)_2Cl_2$ (3.5)	NaOAc (2.85)	ChCl:Gly (1:2)	17/7/76

[a] Reaction conditions: in 1 mL of DES, at 90°C for 20 hours.

[b] GC yield measured with GC-MS, relative to product (PhBpin), homocoupling (Ph-Ph), starting material (PhBr), respectively.

Disappointingly, a low percentage of homocoupling **Ph-Ph** was observed in the GC analysis when using these more polar DESs, that was not the case using ChCl:Urea (1:2) mixture.

Recently, Cu(I)-catalyzed Miyaura reaction has been proposed. In this case, the catalytic cycle was based on one-electron transfer process, in contrast with two-electron transfer mechanism of Pd catalysis[256] (Fig. 102). According to this catalytic mechanism, the oxidative addition was due to Cu(I) precursor addition on boron source. The formation of Cu-B specie was favoured in presence of phosphine and imidazolium ligands.

Moreover, comparing the energy profile calculated for copper-catalysed borylation of iodobenzene, the energy band gap of the transition state of copper complex is lower for phosphine than imidazolium ligand. Thus, reductive elimination and the formation of C-B bond were favoured in presence of phosphine[257].

---

[256] H. Yoshida, S. Kamio, I. Osaka, *Chem. Lett.* **2018**, *47*, 957-959.

[257] C. Kleeberg, L. Dang, Z. Lin, T.B. Marder, *Angew. Chem. Int. Ed.* **2009**, *48*, 5350 –54.

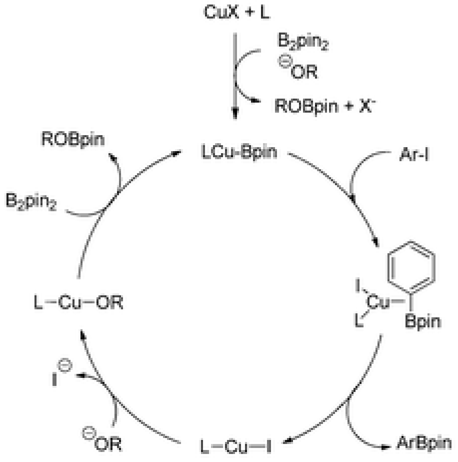

Fig. 102: *Catalytic cycle of Cu(I)-catalyzed borylation.*

For iodobenzene, the best conditions involved a Cu(I) salt, such as CuI or CuCl, in presence of alkyl phosphine such as nBu$_3$P or PCy$_3$, with a small excess of KOtBu as base.

Hence, a series of different reaction conditions based on Cu(I) catalysis were evaluated for studying the aryl halides borylation in DES.

Three different hydrophilic DESs were tested, to evaluate the effect of polarity on reactants (Table 25).

Table 254: *Cu(I)-catalized Miyaura borylation of bromobenzene in ChCl:Urea (1:2), working in presence of Cu(I) catalyst, in different principal hydrophilic choline chloride-based DESs.*

Entry[a]	**CuI**	**L (mol%)**	**DES**	**Yield (%)**[b]
1	10 mol%	PCy$_3$ (20)	ChCl:Urea (1:2)	44/-/55
2	10 mol%	PCy$_3$ (20)	ChCl:EG (1:2)	21/-/78
3	10 mol%	PCy$_3$ (20)	ChCl:Gly (1:2)	20/-/80

[a] Reaction conditions: PhBr (1.0 eq), B$_2$pin$_2$ (2.0 eq), KOtBu (1.2 eq), 1 mL of DES, heating at 90°C for 20 hours.

[b] GC yield measured with GC-MS, relative to product (PhBpin), homocoupling (Ph-Ph), starting material (PhBr), respectively.

ChCl:Urea showed the best result in the same reaction conditions; thus, less polar environment favoured borylation on PhBr. However, the loading of catalyst and ligand was very high, therefore, different loading of catalyst and phosphine were investigated, decreasing CuI amount from 10 mol% to 5 mol% and phosphine from 20 mol% to 10 mol%; unfortunately, no significant variation was observed (35% of PhBpin).

Diferrent halydes sources were then considered such as PhI and PhCl. In the same reaction conditions, while PhCl showed similar behaviour of PhBr (40% to 44% of PhBpin), with PhI no borylation product was observed despite all the starting material was consumed.

In the proposed Cu(I)-catalized approach reported by Marder and co-workers[258], nBu_3P and CuCl as phosphine and Cu(I) precursor were used. We tried to use different phosphines and Cu(I) precursors and the result obtained are reported in table 26.

Table 26: *Miyaura borylation Cu(I)-catalized, with different Cu(I) source and different phosphines.*

Entry[a]	**CuX (mol%)**	**L (mol%)**	**Yield (%)[b]**
1	CuCl (10)	PCy_3 (20)	16/-/78
2	CuI (10)	nBu_3P (20)	10/-/85[c]
3	CuI (10)	$P(tBu)_3$ (20)	9/-/19[d]
4	CuI (10)	PPh_3 (20)	23/-/67[c]
5	CuI (10)	XPhos (20)	13/-/87
6	CuI (10)	MePhos (20)	23/-/44[c]
7	CuI (10)	CyJohnPhos (20)	51/-/32[c]

[a] Reaction conditions: PhBr (1.0 eq), B_2pin_2 (2.0 eq), KOtBu (1.2 eq), 1 mL of ChCl:Urea (1:2), heating at 90°C for 20 hours.

[b] GC yield measured with GC-MS, relative to product (PhBpin), homocoupling (Ph-Ph), starting material (PhBr), respectively.

[c] Presence of B_2pin_2 peak.

[d] No complete solubilisation, during work-up.

The best results were obtained in presence of CyJohnphos ligand, which gave a clear improvement of conversion. However, the increase in yield of borilated product was not satisfactory enough to overcome commercial limits and high costs of CyJohnphos, compared to PCy_3.

Finally, we evaluate the effect of water content. Indeed, choline chloride is highly hygroscopic and, in several studies, the water content exhibited a heavy impact on reagents interactions, controlling selectivity of products and affecting catalytic activity[259].

Six different composition were evaluated by adding specific amounts of water to the ChCl:Urea

---

[258] C. Kleeberg, L. Dang, Z. Lin, T.B. Marder, *Angew. Chem. Int. Ed.* **2009**, *48*, 5350 –54.

[259] a) X. Meng, K. Ballerat-Busserolles, P. Husson, J.M. Andanson, ***New J. Chem.***, **2016, *40***, 4492-99; b) O.S. Hammond, D.T. Bowron, K.J. Edler, *Angew. Chem*. **2017**, *129*, 9914 –17.

(1:2) mixture, prepared from previous crystallization of choline chloride.

Again, no evident improvement was found, thus, for the moment the Miyaura borylation reaction in DES remain a difficult task.

6.3 DIRECT C-H ARYLATION: PRELIMINARY STUDY IN GREEN SOLVENTS

Another interesting process to be tested in DES is the direct arylation, a reaction which has been recently developed and found a great interest for the green chemistry approach due to its atom economy and reduced *E-factor*, compared to other typical organic cross coupling reactions.

For its recent history, direct arylation in green solvents is based on some limited cases.

Deep eutectic solvent have been involved in thiophene-aryl direct C-H coupling where 5-octylthieno[3,4-c]pyrrole-4,6-dione was reacted with a serie of functionalized aryl iodides in ChCl:Urea (1:2) mixture (Scheme 16)[260].

In this case, $Pd_2(dba)_3$ was selected as the more efficient Pd source, in presence of poor electron-rich phosphine P(*o*-MeOPh)$_3$, in presence of Cs_2CO_3 and PivOH as base and additive. The reaction was performed in mild non-anhydrous conditions and under air exposure.

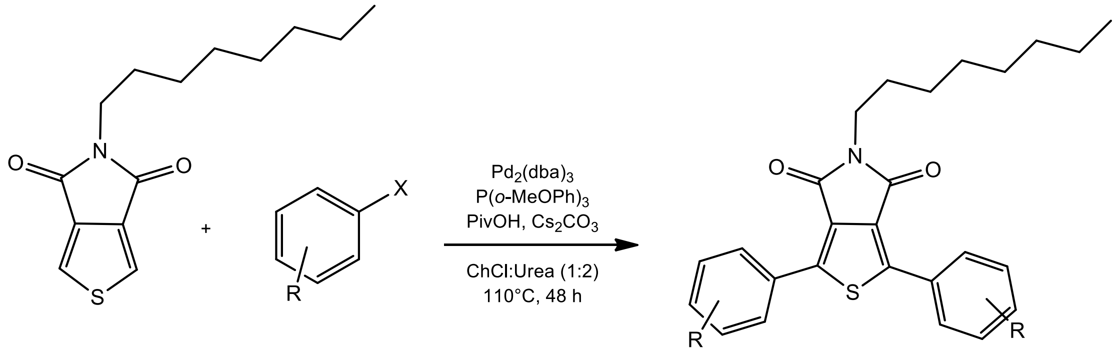

Scheme 16: *Synthetic conditions of direct arylation employed in DES.*

We tried to employ deep eutectic solvents as green alternative medium for the synthesis of **LSCA1** chromophores, which has been indeed prepared by direct arylation reaction (see chapter 5).

As we have already shown**, LSCA1** synthetic method was based on two direct arylation steps. The first one was a double direct arylation between BTD and EDOT, in large excess of donor moiety. $Pd(OAc)_2$ was involved as catalytic specie, employed with 8 mol% loading, in absence of ligand. *N,N*-DMF was choosen as organic solvent, due to its high boiling point and the possibility of working at high temperature (Scheme 17).

For this step, we decided to study the possibility of using a deep eutectic solvent. As we have already found that temperature was not a negligible parameter for the improvement of product yield, which increased at high temperature we decided to evaluate the reaction at different temperatures. Table 27 summarized the different conditions tested.

---

[260] A. Punzi *et al., Org. Lett.* **2017**, *19*, 4754–57.

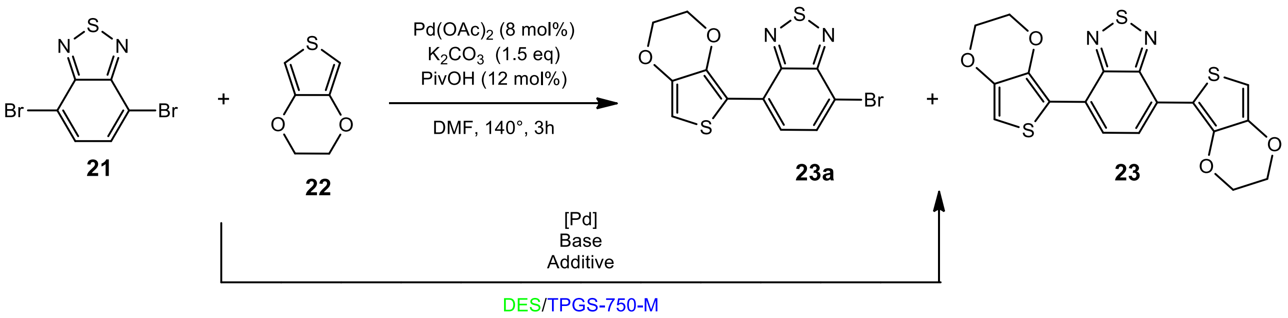

Scheme 17: *Direct arylation performed in organic solvent and generic Pd-catalyzed reaction conditions in green solvents.*

The relative yields were obtained after chromatography purification as GC-MS analysis was not suitable due to the low solubility of the final compound
In general, direct arylation on these substrates was significantly sluggish, in particular at low temperature. From room temperature to around 80°C, the final product was observed in traces. With the increase of temperature, reactions were faster. However, the long-time reaction and the presence of starting material and mono coupling product confirmed worst performances in DES. Moreover, in all cases some oligomers, already observed during traditional **LSCA1** synthesis, started to form in the reaction environment.

Nonetheless, it is interesting to evaluate the effect of different DES. Increasing polarity of solvent (from urea to glycerol), the yield improved (from 19% in ChCl:Urea to 40% in ChCl:Gly) and no starting material was isolated after purification. Moreover, while in ChCl:EG monocoupling intermediate **23a** was isolated in high amount in comparison with the final product, in ChCl:Gly the amount of **23a** was lower. Therefore, it is possible that the more polar interactions and the hydrogen bonds of glycerol-based deep eutectic solvent were less saturated by monocoupling intermediate and improved final product.
We also tested $Pd_2(dba)_3$ as catalyst using the reaction conditions reported by Farinola and co-workers[261] and ChCl:Urea (1:2) as DES. No reaction product was observed in this case and only starting material were recovered. Increasing polarity of DES (from urea to glycerol), traces of product were observed. Finally, changing the electron-rich phosphine with a less donating one, such as the corresponding P(*o*-MePh)$_3$, and using the ChCl:Gly mixture, double coupling product was isolated in 35% yield.

---

[261] A. Punzi *et al.*, *Org. Lett.* **2017**, *19*, 4754–57.

Table 27: *Direct arylation conditions employed in DESs and TPGS-750-M(2 wt%) in water.*

Entry	EDOT (eq)	[Pd] (mol%)	L (mol%)	Base (eq)	Additive (mol%)	Slv	T(°C)/t (h)	Yield (%)^a
1	5.0	Pd(OAc)$_2$ (8)	-	K$_2$CO$_3$ (1.5)	PivOH (12)	ChCl:Urea (1:2)	120/20	19 22 25
2	5.0	Pd(OAc)$_2$ (8)	-	K$_2$CO$_3$ (1.5)	PivOH (12)	ChCl:EG (1:2)	120/20	29 41 -
3	5.0	Pd(OAc)$_2$ (8)	-	K$_2$CO$_3$ (1.5)	PivOH (12)	ChCl:Gly (1:2)	120/20	40 15 -
4	5.0	Pd(OAc)$_2$ (8)	-	K$_2$CO$_3$ (1.5)	PivOH (12)	TPGS-750-M	Reflux/20	19 27 Traces
5	2.0	Pd$_2$(dba)$_3$ (5)	P(*o*-OMePh)$_3$ (10)	Cs$_2$CO$_3$ (1.5)	PivOH (30)	ChCl:Gly (1:2)	110°/20	7 10 70
6	2.0	Pd$_2$(dba)$_3$ (5)	P(*o*-MePh)$_3$ (10)	Cs$_2$CO$_3$ (1.5)	PivOH (30)	ChCl:Gly (1:2)	110°/20	35 13 Traces
7	2.0	Pd$_2$(dba)$_3$ (5)	P(*o*-MePh)$_3$ (10)	Cs$_2$CO$_3$ (1.5)	PivOH (30)	TPGS-750-M	100°/20	17 30 Traces

[a] Isolated yields, after chromatography, respectively of double coupling **23,** monocoupling **23a**, starting material **21** (**BTD**). In all reactions were observed the formation of oligomers.

These preliminary studies showed that there are wide possibilities for the optimization of C-H activation reaction in DES. Different deep eutectic solvents, ligand contribution and different bases and catalysts effect could induce a major reaction control and improve final product. On the other hand, reaction parameters could be controlled to increase product selectivity, favouring mono or di coupling compounds. Remarkably a selective de-symmetrisation can be achieved via mono activation which is not very easy to obtain, but can be very useful for the preparation of asymmetrical moiety which are often employed in organic optoelectronic materials (OPVs, OFETs, DSSCs).

6.4 EXPERIMENTAL PROCEDURE: CHAPTER 6

Deep eutectic solvents preparation: General procedure

In a bottom flask, HBD and HBA were added following the molar ratio of the relative deep eutectic solvents. The solid components were heated at 80°C for 1 h, under inert atmosphere and vigorous stirring. When all the solid components were fused, the liquid transparent mixture was cooled at room temperature.

Purification of choline chloride (ChCl)

In a bottom flask under inert atmosphere, ChCl was solubilized in the minimum amount of EtOH at 80°C under vigorous stirring. Cooling at 0°C, the white solid obtained was filtrated with Buckner filter and the solid recovered maintained under an inert atmosphere in desiccator.

MIYAURA BORYLATION

Pd-catalyzed procedure:

In a schlenk tube, aryl halide (7.0 eq), B_2pin_2 (1.0 eq), Pd catalyst (5 mol%) and NaOAc (2.85 eq) were added. 1 mL of DES was added and heating at 90°C, under vigorous stirring. After 20 h, the mixture was cooled. H_2O and EtOAc were added and the solution was shaken, till the break of DES. A portion of 0.5 mL of the organic phase was added to a GC-MS vial and diluted with 1 mL of EtOAc.

Cu-catalyzed procedure:

In a schlenk tube, aryl halide (1.0 eq), B_2pin_2 (2.0 eq), Cu(I) catalyst (5 mol%), L (10 mol%) and KO^{t}Bu (1.5 eq) were added. 1 mL of DES was added and heating at 90°C, under vigorous stirring. After 20 h, the mixture was cooled. H_2O and EtOAc were added and the solution was shaken, till the break of DES. 0.5 mL of organic phase was added to a GC-MS vial and diluted with 1 mL of EtOAc.

DIRECT C-H ARYLATION

4,7-bis(2,3-dihydrothieno[3,4-b][1,4]dioxin-5-yl)benzo[c][1,2,5]thiadiazole

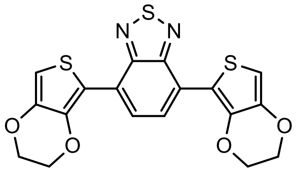

23

$Pd(OAc)_2$ general procedure in DES:

In a vial, BTD, **21** (40 mg, 0.14 mmol, 1.0 eq), EDOT, **22** (722 µL, 0.68 mmol, 5.0 eq), $Pd(OAc)_2$ (2.5 mg, 0.012 mmol, 0.08 eq), PivOH (1.7 mg, 0.017 mmol, 0.12 eq) and K_2CO_3 (29.0 mg, 0.21 mmol, 1.5 eq) were mixed with 1 mL of DES. The mixture was heated at 120°C for 20 h, then cooled at room temperature. Finally, water (3 mL) was added and the organic phase was extracted with EtOAc (3 mLx3).

The organic phase was washed with H_2O (3 mLx2) and dried with Na_2SO_4. The organic solvents were evaporated under vacuum and the crude was purified with flash chromatography PE:DCM = (1:1).

$Pd(OAc)_2$ general procedure in TPGS-750-M (2 wt%) in H_2O:

In a vial were mixed BTD **21** (40 mg, 0.14 mmol, 1.0 eq), EDOT **22** (722 µL, 0.68 mmol, 5.0 eq), $Pd(OAc)_2$ (2.5 mg, 0.012 mmol, 0.08 eq), PivOH (1.7 mg, 0.017 mmol, 0.12 eq) and K_2CO_3 (29.0 mg, 0.21 mmol, 1.5 eq). Then 1 mL of TPGS-750-M (2 wt%) and H_2O were added. The mixture was heated under reflux, for 20 h and then cooled at room temperature. The mixture was washed, under vigorous stirring, with EtOAc (3 mLx4). The organic phase was dried with Na_2SO_4 and the organic solvents were evaporated under vacuum. The crude was purified with flash chromatography PE:DCM = (1:1).

$Pd_2(dba)_3$ general procedure in DES:

In a vial, BTD **21** (40 mg, 0.14 mmol, 1.0 eq), EDOT **22** (330 µL, 0.31 mmol, 2.2 eq), $Pd_2(dba)_3$ (1.2 mg, 0.006 mmol, 0.05 eq), ligand (0.014 mmol, 0.1 eq), PivOH (4.3 mg, 0.042 mmol, 0.30 eq) and Cs_2CO_3 (74.3 mg, 0.21 mmol, 1.5 eq) were mixed. Then 1 mL of DES was added. The mixture was heated at 110°C for 20 h and then cooled at room temperature. H_2O (3 mL) was added and the organic phase was extracted with EtOAc (3 mLx3).

The organic phase was washed with H_2O (3 mLx2) and dried with Na_2SO_4. The organic solvents were evaporated under vacuum and the crude was purified with flash chromatography PE:DCM = (1:1).

$Pd_2(dba)_3$ general procedure in TPGS-750-M (2 wt%) in H_2O:

In a vial, BTD, **21** (40 mg, 0.14 mmol, 1.0 eq), EDOT, **22** (330 µL, 0.31 mmol, 2.2 eq), $Pd_2(dba)_3$ (1.2 mg, 0.006 mmol, 0.05 eq), L (0.014 mmol, 0.1 eq), PivOH (4.3 mg, 0.042 mmol, 0.30 eq) and Cs_2CO_3 (74.3 mg, 0.21 mmol, 1.5 eq) were mixed. Then 1 mL of TPGS-750-M (2 wt%) in H_2O was added. The mixture was heated at 100°C for 20 h and then cooled at room temperature. The mixture was washed, under vigorous stirring, with EtOAc (3 mLx4). The organic phase was dried with Na_2SO_4 and the organic solvents evaporated under vacuum. The crude was purified with flash chromatography PE:DCM = (1:1).

CHAPTER 7

CONCLUSIONS

7 CONCLUSIONS

This Ph.D. thesis has been focused on the synthesis and characterization of organic fluorophores for LSC applications. The fluorophores investigated are based on the general structure donor-acceptor-donor D-A-D. Thanks to intramolecular charge transfer (ICT) during the excitation process, such fluorophores are characterized by absorption in the visible region and high Stokes shift.

All the new organic chromophores we prepared showed broad UV-visible light absorption ranges (400-550 nm), with emission spectra extended between 515 nm and 670 nm in solution. All molecules were synthesized with straightforward procedures that were optimized in order to allow large-scale preparation of materials, as an easy preparation and low cost of fluorophores are essential to promote their subsequent use in LSC technology.

The new compounds were spectroscopically characterized in solution, at different concentrations (from 2 10^{-6} M to 10^{-5}M). For some of them, light concentration efficiency were investigated.

Two main class of compound were prepared.

The first class was based on the benzobisthiazole (BBT) core (chapter 3). Three new fluorophores were prepared, starting from a common intermediate **5,** which was in turn obtained from commercially available precursors. Compound **5** was obtained in 3 reaction steps with an overall yield of 52% without needing a chromatographic purification. The target fluorophores were then prepared from intermediate **5** by Buchwald-Hartwig (**BBT2**) or Suzuki-Miyaura (**BBT3-4**) reactions in good yields. The three molecules showed an intense emission spectrum between 460-550 nm, overlapping the light-absorption spectrum of a Si-based photovoltaic cell, thus, down-converting the blue part of the solar spectrum where the efficiency of Si-cells is usually very low. Furthermore, in all cases, Stokes shifts were large enough to minimize the self-absorption effects.

Computational analysis showed that the main transition involves a charge separation process that causes a planarization of the molecule in the excited state. In particular, **BBT2** and **BBT3** behave very similarly and exhibit a rather low fluorescence quantum yield (approx. 16% and 31% respectively), which is probably due to non-radiative relaxation phenomena, while $\boldsymbol{\Phi_f}$ values up to 73% were recorded for **BBT4** in toluene solution.

Fluorophore were dispersed in PMMA polymeric matrix were only **BBT3** and **BBT4** gave homogenous and transparent films at any concentration, while, **BBT2** generated aggregated system, with phase separation at concentrations higher than 1.4wt%. A different and less polar matrix was also used, in which compounds **BBT2** and **BBT3** showed poor compatibility while **BBT4** was well dispersed, even at a high concentration (1.8 wt%)

Spectroscopic analysis of the films showed that in a more polar environments, such as in PMMA, a lowering of the quantum yield is observed probably due a more twisted charge-separated excited state geometry. This was confirmed by the results of the TAS studies, showing that in PMMA the excited state absorption of **BBT4** decayed more rapidly than in toluene and was characterized by a lower residual intensity. In the case of **BBT4**, this phenomenon could be mitigated by dispersion in less polar matrices such as PCMA, where an increase in $\boldsymbol{\Phi_f}$ was indeed observed.

In agreement with theoretical predictions, ultrafast time-resolved spectroscopy confirmed the charge transfer nature of the low-lying excited state, and showed that no dark states are involved in the excited state relaxation process. Furthermore, the measured pump-probe spectra suggested that the inhibition of a large excited-state conformational relaxation, as it happens in the polymeric matrix, results in increased fluorescence quantum yields and improved LSC performances.

Although **Φ_f** values for compound **BBT2** and **BBT3** were rather low, satisfactory optical efficiencies were measured for the devices built with **BBT2**/PMMA and **BBT3**/PMMA films (5.8% and 6.5% respectively). These results might be possibly due to the beneficial effects granted by the large Stokes shift. More interesting was the optical efficiency measured in the case of **BBT4**, with a value of 7.5 % in PMMA, which was increased to 8.5% and 9.0% using the less polar matrices of PCMA. This was in agreement with the indications of the computational and TAS investigation. Comparison of such results whith those of the reference luminophore **LR305**, measured at the same conditions**,** highlights that latter value is very similar to that found for **LR305** in the same matrix (9.1%) and only 1.2% lower than the best result obtained with **LR305** in PMMA. Furthermore, the large Stokes shifts and the consequent low self-absorption of **BBT-**series fluorophores compared with those reported for **LR305** suggest that better optical efficiencies might be obtained employng these compounds on large surface area LSC devices.

The second class of fluorophores investigated was based on quinoxaline (DQ) core as acceptor unit. Five new DQ-based fluorophores were designed and synthesized. Three of them (**DQ1-3**) were based on the 2,3-diphenylquinoxaline scaffold (**16**) and two of them (**DQ4-5**) on the 2,3-dihexylquinoxaline core (**17**). Differently substituted triarylamines and phenothiazine were used as donor groups. The idea was that of evaluating the effect of different substituents on optoelectronic properties of final compounds and to establish a possible correlation between structure and properties.

The final compounds were obtained through Suzuki-Miyaura cross-coupling, starting from the suitable quinoxalyne dibromide, in good to moderate yields.

Spectroscopic analysis in solution showed for DQs fluorophores broad absorption spectra in the visible region, between 400 nm and 460 nm. Moreover, they showed a large Stoke shift with a low overlapping between absorption and emission spectra.

All the new compounds were dispersed in polymeric matrix PMMA, PCMA and exhibited good optical efficiencies in both of them at different concentrations. The best values were observed for the samples of **DQ1**/PMMA (11.0% at 1.4 wt%) and **DQ2**/PCMA (10.5% at 1.0 wt%). Probably in these two cases the interaction with the host material and the fluorophore were better matched. In other words, the presence of alkyl chains on donor groups as in **DQ2** allow a better dispersion in a less polar matrix as PCMA, than in the more polar PMMA, while the less hydrophobic **DQ1**, was best performing in more polar PMMA films.

Remarkably, the value of optical efficiencies, when compared with those of the reference luminophore **LR305** measured at the same conditions**,** resulted higher (11.0%) than the reference (10.1%) in the case of **DQ1** in PMMA. In this matrix all the other dyes efficiency were around 7-8%, thus lower than the reference, but still good. In the case of PCMA matrix, all the new compounds showed an efficiency comparable or even higher than that found for **LR305**, with the highest value found **DQ2** (10.5% at 1.0 wt%) which performed better than **LR305** (9.1 at 1.0 wt%).

In the third part of the work, two new luminophores with a π-D-A-D-π structure were synthesized. The compounds were designed for application in microalgae photobioreactors and, for this reason, they required to have a specific absorption range between 460 nm and 630 nm, in order to avoid to overlap with the typical absorption bands of Chlorophyll (430 nm and 660 nm) which would hamper photosynthetic process.

The dyes were designed inspired by the previously reported fluorescent probe *FEB-2000*, due to its interesting optoelectronic characteristics. The molecular structure was based on benzo-2,1,3-thiadiazole (BTD) acceptor, 3,4-ethoxylene dioxythiophene (EDOT) donor and fluorene π moieties.

Thus **LSCA1** and **LSCA2** were prepared using a synthetic approach based on direct C-H arylation, involving only two synthetic steps and commercially available reagents, which allowed to obtain the final products with moderate to good yields, after C-H arylation conditions optimization.

The two compounds were characterized spectroscopically in solution. Both of them showed two absorption bands with high **ε**, centered at 385 nm and 550 nm (**LSCA1)**, and at 372 nm and 530 nm (**LSCA2)**, which are completely compatible with the absorption range of Chlorophyll. Emission spectra showed a maximum at 670 nm for **LSCA1** and at 662 nm for **LSCA2** in DCM solutions. The high fluorescence intensity in solution and no evident quenching impact on the emission spectra suggested high fluorescence quantum yields. Such results are very promising for the exploitation of such dyes for the application in algae photobioreactors.

In the last part of the work a preliminary study concerning the possible use of green solvent in catalytic reaction has been carried out, keeping in mind those processes which might be of interest for synthesis of materials for optoelectronic application.

This study has been carried out during a short time stage in the research group of D.J. Ramón Dangla, from the Institute of Organic Synthesis (ISO) of the University of Alicante.

Deep eutectic solvents (DES) were employed in two typical and common organic reactions: Miyaura borylation and direct C-H arylation.

Miyaura reaction was investigated using aryl halides and bis(pinacolate)diboron in presence of different catalytic species. Several reaction conditions were considered, halide, solvent, catalyst, temperature.

Bromobenzene was identified as the best aryl halide having a good compatibility with the common and more involved DES, ChCl:Urea (1:2). $Pd(PPh_3)_2Cl_2$ and CuI/PCy_3 resulted to be the best catalytic systems for borylation. Water, which can play a crucial role in deep eutectic solvents, did not show evident effect. Despite some interesting suggestion might be found from this screening, no optimal condition for borylation reaction could be recovered in this study.

The direct C-H arylation employed for the synthesis for the D-A-D core of **LSCA1**, was tested using deep eutectic solvents. In this case, it was possible to identify suitable conditions to carry out the coupling in DES. Despite the yield were lower than those observed in the traditional approach, and interesting effect of the reaction condition on selectivity was observed. Thus these preliminary studies showed that there are wide possibilities for the optimization of C-H activation reaction in DES

8 GENERAL EXPERIMENTAL REMARKS

All air-sensitive reactions were performed under inert atmosphere in a flame- or oven-dried apparatus using Schlenk technique. Solvents used in cross-coupling reactions were previously degassed by means of the "*freeze-pump-thaw*" method. Petroleum ether was the 40-60 °C boiling fraction. Microwave-assisted transformations were carried out using *Discovery SP – CEM* reactor at fixed temperature (surface sensor monitoring) and variable power (max 300 W). Tetrahydrofuran (THF) was distilled over metallic sodium in the presence of benzophenone. Toluene and N,N–dimethylformamide (DMF) were dried on a resin exchange Solvent Purification System (*MBraun*).

Thin-layer chromatography was carried out on aluminum-supported Merck 60 F254 plates; detection was carried out using UV light (λ = 254 and 365 nm). Flash column chromatography was performed using Merck Kieselgel 60 (300-400 mesh) as the stationary phase. ^{1}H-NMR spectra were recorded at 200 or 400 MHz, and ^{13}C-NMR spectra were recorded at 50.3 or 100.6 MHz, respectively, on *Varian* Oxford 200 Gemini, *Varian* 400 INOVA or *Varian* 400 Mercury series instruments. Chemical shifts were referenced to the residual solvent peak ($CDCl_3$, δ 7.26 ppm for ^{1}H-NMR and δ 77.16 ppm for ^{13}C-NMR; CD_2Cl_2, δ 5.32 ppm for ^{1}H-NMR and δ 54.00 ppm for ^{13}C-NMR; Toluene-d_6, δ 7.09, 7.00, 6.98 and 2.09 ppm for ^{1}H-NMR and δ 137.86, 129.24, 128.33, 125.49 and 20.4 ppm for ^{13}C-NMR; THF-d_8 δ 1.72 and 3.58 ppm for ^{1}H-NMR, δ 67.21 and 25.31 ppm for ^{13}C-NMR; Trifluoroacetic acid, δ 11.50 ppm for ^{1}H-NMR, δ 164.2 and 116.6 ppm for ^{13}C-NMR). GC-MS spectra were measured with a *Shimadzu* gas-chromatograph (*GC-17A* or *GC-2010*) connected to a *Shimadzu* mass spectrometer (*MS-QP2010S* or *MS-QP5050a*) and are reported in the form *m/z* (intensity relative to base = 100). ESI-MS spectra were obtained by direct injection of the sample solution using a *Thermo Scientific* LCQ-FLEET instrument. UV-Vis spectra were recorded with a *Varian Cary* 400 spectrometer and a *Shimadzu* 2600 series spectrometer, and fluorescence spectra were recorded with a FP-8200 Spectrofluorometer-JASCO, irradiating the sample at the wavelength corresponding to maximum absorption in the UV spectrum.

9 ABBREVIATIONS

LSC	Luminescent Solar Concentrator
Bcm	Billion cubic meters
Mtce	Million tons of coal equivalent
RE	Renewable Energy
PV	Photovoltaic
Nd	Neodynium
Yb	Ytterbium
Eu	Europium
Rh6G	Rhodamina 6G
C6	Coumarin 6
NZEB	Nearly Zero Energy Building
PMMA	Polymethylmethacrylate
PCMA	Polycyclhexylmetacrylate
SAN	Styrene-acrilonitrile resin
HOMO	Highest Occupied Molecular Orbital
LUMO	Lowest Occupied Molecular Orbital
LR305	Lumogen F Red 305
QD	Quantum dot
Ln	Lanthanide
BIPV	Building-Integrated Photovoltaic
VOC	Volatile Organic Compounds
DES	Deep Eutectic Solvents
HBA	Hydrogen-Bond Acceptor
HBD	Hydrogen-Bond Donor
AE	Atom Economy
TPGS	D-α-Tocopherol polyethylene glycol succinate